Doctoral theses at NTNU, 2022:280

Vilde Bråten

Fundamental Aspects of Thermodynamics of Small Systems Investigated Through Molecular Simulations and Theoretical Descriptions

Doctoral thesis

NTNU
Norwegian University of Science and Technology
Thesis for the Degree of
Philosophiae Doctor
Faculty of Natural Sciences
Department of Materials Science and Engineering

NTNU
Norwegian University of
Science and Technology

Vilde Bråten

Fundamental Aspects of Thermodynamics of Small Systems Investigated Through Molecular Simulations and Theoretical Descriptions

Thesis for the Degree of Philosophiae Doctor

Trondheim, September 2022

Norwegian University of Science and Technology
Faculty of Natural Sciences
Department of Materials Science and Engineering

NTNU

Norwegian University of
Science and Technology

NTNU
Norwegian University of Science and Technology

Thesis for the Degree of Philosophiae Doctor

Faculty of Natural Sciences
Department of Materials Science and Engineering

ISBN 978-82-326-5357-7 (printed ver.)
ISBN 978-82-326-6749-9 (electronic ver.)
ISSN 1503-8181 (printed ver.)
ISSN 2703-8084 (online ver.)

Doctoral theses at NTNU, 2022:280

Printed by NTNU Grafisk senter

Preface

This thesis is submitted to the Department of Materials Science and Engineering at the Norwegian University of Science and Technology (NTNU) as a partial fulfillment of the requirements for the degree of Philosophiae Doctor (PhD). The PhD period lasted from September 2018 to September 2022, and included the equivalent of one year teaching duties and 30 ECTS of coursework, corresponding to approximately six months.

The work was supported by the Research Council of Norway (Grant No. 275754). Computational resources were provided by UNINETT Sigma2 - The National Infrastructure for High Performance Computing and Data Storage in Norway (Grant No. NN9414k). The main supervisor was Ass. Prof. Sondre Kvalvåg Schnell (NTNU) and the co-supervisor was Prof. Øivind Wilhelmsen (NTNU, SINTEF Energy Research).

Dissemination of the work

Articles included in this thesis

All articles included in this thesis have published in international peer-reviewed journals as listed below. All contributions have been formulated and discussed with the co-authors, who have contributed to the analysis of the results and subsequent improvement of the papers before dissemination of the work. Vilde Bråten has performed most of the work presented in the thesis and written the first version of all contributions. Article III was published in the "2022 JCP Emerging Investigators Special Collection" of *The Journal of Chemical Physics*. It was also selected by the Editor to be promoted as a "Featured Article" and to be featured in a "Scilight" article by *AIP Publishing Journals*.

I. **V. Bråten**, Ø. Wilhelmsen and S. K. Schnell,

Chemical Potential Differences in the Macroscopic Limit from Fluctuations in Small Systems,

Journal of Chemical Information Modeling **61**:2 840-855 (2021).
DOI: 10.1021/acs.jcim.0c01367

Contribution: MD and MC simulations — data analysis — paper drafting, review and editing

II. **V. Bråten**, D. Bedeaux Ø. Wilhelmsen and S. K. Schnell,

Small size effects in open and closed systems: What can we learn from ideal gases about systems with interacting particles?,

The Journal of Chemical Physics **155**:24 244504 (2021).
DOI: 10.1063/5.0076684

Contribution: MC simulations — derivation of theoretical descriptions — data analysis — paper drafting, review and editing

III. **V. Bråten**, D. T. Zhang, M. Hammer, A. Aasen, S. K. Schnell and Ø. Wilhelmsen,

Equation of state for confined fluids,

The Journal of Chemical Physics **156**:24 244504 (2022).
DOI: 10.1063/5.0096875

Contribution: MD simulations — derivation of theoretical descriptions — data analysis — paper drafting, review and editing

Other contributions

The work has been communicated to the scientific community through presentations at international conferences and workshops as listed below. Contributions VIII and VI were in the form of poster presentations, while the remaining contributions were in form of oral presentations.

I. **V. Bråten**, D. T. Zhang, M. Hammer, A. Aasen, S. K. Schnell and Ø. Wilhelmsen,

Equation of State for Nanosystems,

Norsk Kjemisk Selskap - Functional Inorganic Materials (01.11.2021-02.11.2021)

II. **V. Bråten**, Ø. Wilhelmsen and S. K. Schnell,

Chemical Potential Differences from Fluctuations in Small Systems,

Recent progress in the statistical mechanics of solutions through Kirkwood-Buff integrals and related approaches (20.09.2021-22.09.2021)

III. **V. Bråten**, D. T. Zhang, M. Hammer, A. Aasen, S. K. Schnell and Ø. Wilhelmsen,

Perturbation Theory Based Equation of State for Small Systems under Confinement,

Twenty-First Symposium on Thermophysical Properties (20.06.2021-26.06.2021)

IV. **V. Bråten**, D. T. Zhang, M. Hammer, A. Aasen, S. K. Schnell and Ø. Wilhelmsen,

Perturbation Theory for Fluids under Confinement,

InterPore 2021 (31.05.2021-04.06.2021)

V. **V. Bråten**, Ø. Wilhelmsen and S. K. Schnell,

Chemical Potential Differences in Small Systems,

Materials Research Society Fall Meeting (27.11.2020-04.12.2020)

VI. **V. Bråten**, Ø. Wilhelmsen and S. K. Schnell,
Thermodynamic Properties of Small Systems,
7th National Meeting on Inorganic and Materials Chemistry (13.02.2020)

VII. **V. Bråten**, Ø. Wilhelmsen and S. K. Schnell,
Physical Validation of Properties of Small Grand Canonical Systems,
International Workshop on Non-Equilibrium Thermodynamics in Porous Media-SK70 (29.08.2019-30.08.2019)

VIII. **V. Bråten**, Ø. Wilhelmsen and S. K. Schnell,
Thermodynamic Properties of Small Systems,
Workshop for Atomistic Modeling (16.08.2019)

Vilde Bråten has also been active in communicating the work to the general public. In 2020, she finished as runners-up in the science communication competition *Researcher's Grand Prix*. After qualifying from the local competition, she represented NTNU in the national finale, where she competed against candidates from the leading universities in Norway and got second place. Both rounds were later broadcasted on national television. She has presented the scientific work through the popular scientific contributions listed below.

I. Popular science presentation titled *Nanosystems: the outlaws of nature* at the international science festival *Pint of Science Trondheim: Hot news from Nanoworld* (20.05.2021)

II. Popular science presentation titled *Lovløse nanosystemer* at *Realfagkonferansen 2021*, which is a conference for teachers in natural science in Norway. (11.05.2021)

III. Five visits to schools all over Norway, presenting the research and what a day as a PhD candidate looks like. (2021)

IV. Recruitment video for the Materials science study program. The video is still distributed to potential NTNU students through Snapchat and YouTube. (10.12.2020)

V. Story takeover on the official Instagram page of the Faculty of Natural Science, showing the followers what a day as a PhD candidate looks like. (14.11.2020)

VI. Interview titled *På kant med naturlovene* in the student newspaper *Under Dusken*, about research on nanosystems and the importance of public outreach. (27.10.2020)

VII. Popular science blog post titled *Hvordan skal vi forske på naturens regelbrytere?* published on the web pages of the Faculty of Natural Science *NTNU TekNat.* (03.10.2020)

VIII. Popular science presentation titled *Lovløse nanosystem* in the national science communication competition *Researcher's Grand Prix.* (26.09.2020)

IX. Popular science presentation titled *Opprørske nanopartikler krever sin egen fysikk* at *PhD Grand Prix*, which is a mini-version of *Researcher's Grand Prix*, hosted by the student organization for chemistry students. (20.03.2019)

Acknowledgments

First of all, thanks to my supervisors Sondre and Øivind for excellent supervision. It has been a great pleasure working with you these four years, especially because of your dedication, ambition, enthusiasm and your infallible ability to come up with ideas for exciting projects. I feel extremely privileged for the opportunity to spend four years doing the two things I enjoy most: learning new things and telling people about the new things I learned.

Thanks to all my colleagues and friends at the Department of Materials Science, especially to the amazing people of the K2 lunch crowd. I am particularly grateful for the FACET group's admirable dedication to creating a welcoming and including work environment. To Frida and Jacob, for your enthusiasm associated with the quartet of *Grand Prix*-events (*PhD, Chemie, Forsker* and *Melodi*).

Thanks to all my colleagues and friends at PoreLab. You are an outstanding and inspirational group of people. Thanks to Øivind for including me in the group. A special thanks to Marie-Laure for the delicious cakes every Monday (especially the banana cakes) and for facilitating a very positive work environment. To Ailo, for opening my eyes to the wonderful world of ideal gases.

To my two long-time office mates, Harald and Michael. Harald, I appreciate your incomparable kindness, you were greatly missed during your visit to Sweden. Michael, I appreciate the feedback on my memes to a great extent, and I appreciate the scientific discussions to a lesser extent.

To my family. My sister and brother, Synne and Håkon, for all our amazing trips and adventures. When the three of us are together, there is always a good chance that the day will turn into a *drømmedag*. My parents, May and Trond, for always supporting and celebrating me. Thank you for posting my achievements on Facebook, which I am too embarrassed to do myself.

To David, for being the constant support, master of jokes and extremely talented organic chemist that you are. You are the wind beneath my wigs.

You have all contributed to making the last four years memorable and enjoyable. Great work can not be achieved without great breaks, and I believe the recipe for a healthy work-life balance is best summarized by the words of Norway's most talented rapper: "Ha det tidig og cool e viktig. Rekke Vinmonopol e viktig." (Linni, *Viktig*, 2021).

Summary

Systems on the nanoscale can show behaviour that is strikingly different from the behaviour we expect for systems on the macroscopic scale. As a consequence, we can in general not assume that macroscopic theories of matter can be used to describe the properties of small systems. Thermodynamics was initially derived for systems with number of molecules on the order of Avogadro's number. In this work, we explore the elements needed to apply thermodynamics to small systems, containing a much smaller number of molecules. We utilize molecular simulations combined with theoretical descriptions for direct investigations of the systems. We focus on three central questions: (1) How are thermodynamic properties affected by system size? (2) Can we define a consistent thermodynamic framework for small systems? (3) Which computational tools and techniques can be applied to study small systems?

For the first question, we investigate two features of small systems: size- and shape-dependent properties and ensemble in-equivalence. We show how thermodynamic properties can be conveniently described by scaling laws, and discuss the implications of ensemble in-equivalence. For the second question, we compare two theoretical descriptions that provide thermodynamic frameworks for small systems: Gibbs' surface thermodynamics and Hill's nanothermodynamics. We discuss the advantages and limitations of both methods, and give examples of systems where one framework is favored over the other. For the third question, we show how some statistical mechanical identities derived for macroscopic systems do not provide accurate predictions for systems with a small number of molecules. We also discuss some tools and techniques that can be trusted to provide accurate predictions of properties for small systems.

In Article I, we present a new method for computation of chemical potential differences. The method is based on a sampling technique that computes grand canonical particle fluctuations from sub-systems embedded in a larger reservoir. This sampling technique is combined with an overlapping distribution method that extracts chemical potential differences from the overlap between distributions of particle numbers from two systems at different densities. The small sub-systems are non-periodic, which means that their properties deviate from the classical thermodynamic description. We therefore utilize scaling laws to calculate the size dependence of chemical potential differences and eventually extract the value in the thermodynamic limit. In addition

to computing chemical potential differences in the macroscopic limit directly from molecular dynamics simulation, the new method allows for investigation of the size dependence of intensive thermodynamic properties of small systems.

In Article II, we investigate how a small number of particles can induce an ensemble dependence to the properties of grand canonical (open) and canonical (closed) systems. We investigate cubic boxes with a surface energy, containing ideal gases or particles interacting through interatomic potentials. For all the investigated small systems, we find clear differences between the properties in open and closed systems. Through analytical derivation, we find that the properties of the ideal gases are affected by two types of small-size effects. The first type arises from the surfaces, edges and corners of the system, while the second type arises from avoiding assumptions about the magnitude of the number of particles. We utilize the insight gained from investigating the ideal gases to analyze ensemble dependence of systems with interacting particles. For the systems with interacting particles, the difference in chemical potential is qualitatively described by the analytic formula derived for the ideal gas system, while the difference in pressure is not captured by the ideal gas model. The work presented in this paper gives insight into the mechanisms behind ensemble inequivalence in small systems, and illustrates how simple statistical mechanical models can provide useful information.

In Article III, we present a thermodynamic framework that represents an equation of state for pure fluids confined in small geometries. The total system consists of a bulk phase in equilibrium with a surface phase. We base the equation of state on an existing, accurate description of the bulk fluid, and use Gibbs' framework for surface excess properties to consistently incorporate contributions from the surface. We demonstrate the equation of state for a Lennard-Jones spline fluid confined by a spherical surface with a Weeks-Chandler-Andersen wall-potential. The pressure and internal energy predicted from the equation of state are nearly within the accuracy of the properties computed directly from molecular dynamics simulations. We also investigate how the properties of the surface phase depend on the location of the dividing surface, and find that when the location is chosen appropriately, the properties of highly curved surfaces can be predicted from those of a planar surface. A possible application of the equation of state for confined fluids is prediction of thermodynamic properties in porous media.

Populærvitenskapelig sammendrag

Nanosystem er små samlinger av atomer som til sammen ikke er større enn en hundretusendel av et sandkorn. Disse små systemene oppfører seg veldig annerledes enn store system. Dette skjer fordi molekyler i nærheten av en overflate oppfører seg annerledes enn molekylene i midten av systemet, i den delen vi kaller bulken. I store system kan vi ofte se bort ifra bidraget til molekylene i nærheten av overflaten siden de utgjør en så liten andel av det totale systemet. Mens i små system befinner mange av molekylene seg ved overflaten til systemet, som gjør at de i mye større grad bidrar til hvordan systemet oppfører seg.

De helt spesielle egenskapene til små system åpner en ny dimensjon av muligheter for utvikling av teknologi. Nanoteknologi brukes for eksempel til å lage materialer med stort overflateareal, slik som porøse materialer som brukes i solceller, batterier og rensing av vann. Vi kan også spesialdesigne små nanopartikler med spesifikke egenskaper. Nanopartikler av gull kan blant annet brukes som katalysatorer, som får reaksjoner til å gå raskere, mens gull i bulk-form har ingen katalysatoregenskaper. Nanopartikler har også en helt unik evne til å passere gjennom biologiske barriærer i kroppen. De kan brukes til å transportere og levere medisin inni kroppen på en mer målrettet måte vi gjør i dag. Men små system eksisterer ikke bare fordi mennesker har laget de på en lab. Mange viruspartikler er under 100 nm i diameter. Noen av disse består av en genetisk del plassert inni et beskyttene skall, og inni skallet kan trykket bli tjue ganger høyere enn i et vanlig sykkeldekk. Viruset bruker det høye trykket til å skyte den genetiske delen ut av skallet og inn i en celle. På den måten utnytter viruset størrelsen sin til å lage de egenskapene det trenger.

Uansett om de små systemene er laget på laben eller i naturen så trenger vi mer kunnskap om hvordan de fungerer. Gjennom arbeidet med denne doktoravhandlingen har vi jobbet med å forstå små system bedre ved å undersøke de gjennom simuleringer. Simuleringene regner ut hvordan atomene inni nanosystemet oppfører seg. Det gjør at vi kan se forskjellen mellom molekylene som er i bulken og de som er i nærheten av overflaten. Vi kan tenke på simuleringene som et teoretisk mikroskop som brukes til å se på atomene inni de små systemene. På den måten kan vi få svar på hvordan og hvorfor små system oppfører seg sånn som de gjør, slik at vi kan utnytte de spennende egenskapene i fremtidens teknologi.

Contents

1 What are small systems?

A typical dimension for a nanosystem ranges from sub-nanometer to several hundred nanometers. Systems on this size scale often behave in a way that is drastically different from macroscopic systems. This can be utilized to produce nanoparticles with highly specific properties. For instance, gold nanoparticles are excellent low temperature catalysts, while macroscopic gold does not exhibit any catalytic properties.[1] Nanoparticles are also being developed for treatment of diseases, where they are used as delivery vehicles for pharmaceutical agents, due to their unique ability to cross biological barriers.[2] Another category of nanosystems are fluids confined in small spaces. Understanding of these systems is particularly important in porous media science, which has a wide range of applications such as dye-sensitized solar cells,[3] perovskite solar cells,[4] clean water production,[5–7] CO_2 capture[8,9] and production of lithium-ion batteries.[10,11] Due to the small size of the pores, fluids confined inside the porous media often behave differently than fluids in bulk systems. For instance, capillary condensation can lead to the formation of a liquid phase at pressures below the saturation pressure.[12–15] Naturally occurring nanosystems also exist. Most virus particles are on the nanometer scale, and amongst them are several that measure below 100 nm in diameter.[16,17] For virus particles that consist of a virial genome encapsulated by a nanometre-sized capsid, the genome is often so tightly packed that it exerts a high internal pressure on the capsid. By utilizing atomic force microscopy, internal pressures as high as 60 atm have been measured.[18] It has therefore been suggested that the pressure is a crucial part of the mechanism that drives the genome into the host.[16]

From the above examples, it is clear that the nanoscopic scale is not simply a miniaturization of the macroscopic scale. However, there exist no overall accepted *size limit* for when a system is regarded as "small".[1] Instead, systems are often regarded as small when they show deviations from the description in the macroscopic limit that can be attributed to their size. One feature of small systems that often receives specific attention is their non-extensivity. This arises when properties that are regarded as extensive in the macroscopic limit are influenced by the size such that they are no longer Euler homogeneous functions of degree one. However, non-extensivity can also occur for macroscopic, long-range systems, i.e. systems where the range of interactions is comparable with the size of the system.[19–24] Examples of systems that are governed by long-range interactions are two-dimensional fluids,[25,26] plasmas[27] or

self-gravitating systems.[28] Regardless of the cause of non-extensivity, it is clear that non-extensive systems can display remarkable properties. In this work, we focus on systems that are non-extensive due to their smallness. Gaining further insight into the behaviour of such systems is important, both in understanding the role of the naturally occurring small systems and in order to utilize small systems in nanotechnological developments.

The aim of this thesis is to increase the general understanding of small systems through investigations of their thermodynamic properties. We employ molecular dynamics (MD) and Monte Carlo (MC) simulations combined with theoretical descriptions to shed light on how and why the properties deviate from the description in the macroscopic limit. We also investigate different frameworks that can provide consistent thermodynamic descriptions of the systems' properties. One important criteria for such a framework is that it should be applicable in predictive models such as equations of state (EoS).

The thesis is structured as a collection of articles, where the upcoming chapters provide a general background to the work presented in the articles. Chapter 2 gives a short introduction to thermodynamics of small systems, and contains three sections that each are dedicated to a specific area of focus. In Chapter 3, we present the conclusions made from this work together with perspectives and future work. Then follows the scientific articles included in the thesis.

2 Thermodynamics of small systems

Thermodynamics describes the behaviour of energy conversion in nature through relations between energy, work and heat.[29] It is a self-consistent framework of general applicability and makes no reference to the microscopic constituents of the system. A rationalization of thermodynamics based on microscopic mechanical laws is provided by statistical mechanics.[30] Statistical mechanics is a theoretical framework that connects observable properties such as pressure, temperature, heat capacity and compressibility of a many-body system to its microscopic constituents and their interactions.

Thermodynamics was originally derived for systems in the macroscopic limit, where the number of molecules is on the order of Avogadro's number, i.e. 10^{24}. Consequently, the convenient description that thermodynamics provides for large scale systems does not apply to small scale systems. Two immediate questions therefore arise: How can we build a systematic thermodynamic theory that works for small systems? And how should this thermodynamic theory be related to other theoretical descriptions of matter, such as statistical mechanics?

The work presented in this thesis focuses on three topics that can aid the development of a thermodynamic theory for small systems. In Sec. 2.1, we discuss how the behaviour of small systems and their thermodynamic properties depend on system size. In Sec. 2.2, we discuss the definition of a consistent theoretical framework that provides a connection between the thermodynamic properties. In Sec. 2.3 we investigate which computational tools and techniques can be applied to study systems on the small-size scale.

2.1 How are thermodynamic properties affected by system size?

Macroscopic systems containing multiple molecules can be split into a bulk region and a surface region. A molecule close to a surface will experience a different environment than a molecule located in the bulk. Take as an example a fluid in a container. In this system, a molecule in the bulk region will be surrounded by other fluid molecules, while a molecule close to the surface will interact with the container walls as well. Consequently, the behaviour of the molecules in vicinity of the surface often deviates from the behavior of the molecules in the bulk. In macroscopic systems, the ratio of surface

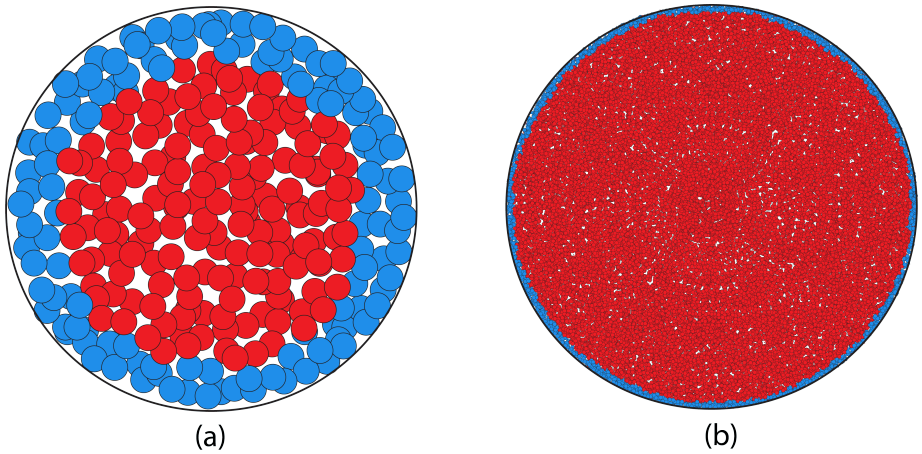

Figure 2.1: A comparison of the influence of the surface region in (a) a small and (b) a large system. The blue particles are interacting with the surface while the red particles feel no energetic contribution from the surface. In the small system, the size of the region in which the molecules are affected by the surface is of the same order as the system size. In the large system, the number of molecules in the surface region is negligible compared to the number of molecules in the bulk region.

molecules to bulk molecules is usually small. The influence of the surface molecules on the total properties of the fluid is therefore often neglected in macroscopic systems. Small systems, however, have much higher ratio of surface molecules to bulk molecules. This difference is illustrated in Fig. 2.1. As a consequence, the thermodynamic properties of small systems depend on the features of the surface, which results in a deviation from the macroscopic description.

In this section, we focus on two topics that are central in the understanding of the size dependence of thermodynamic properties. The first is the use of scaling laws to characterize the different size effects, and the second is how these size effects depend on the ensemble of the system.

2.1.1 Size-scaling

The high surface area-to-volume ratio is considered a characteristic feature of small systems since the leading order small-size effects usually come from the surface area. This means that including a description of how the properties depend on the surface area often provides a sufficient description of the size dependence.[31] However, for non-planar surfaces, higher-order terms such as contributions from the curvature, lines or edges of the system can have an additional impact on the thermodynamic properties.[32] For instance, prediction of nucleation rates of droplets from classical nucleation theory has been shown to significantly improve after including curvature corrections to the planar-wall surface energy.[33]

The different contributions to the size dependence of a thermodynamic property can be conveniently summarized by a scaling law.[34] One example of a scaling law for the general property, A, is the expansion of its density, $a = A/V$, in the system's inverse characteristic size.[32,35,36] The criteria for this scaling law is that the property A is an extensive thermodynamic property, i.e. Euler homogeneous of first-order, in the macroscopic limit. For a three-dimensional system, the inverse size can be defined as $L \equiv \sqrt[3]{V}$, such that a can be written as

$$a = \frac{A}{V} = a_0 + \frac{a_1}{L} + \frac{a_2}{L^2} + \frac{a_3}{L^3} + \cdots, \tag{2.1}$$

where a_0 corresponds to the value of a in the macroscopic limit, a_1 is the first-order size-scaling coefficient, a_2 the second-order size-scaling coefficient, etc. In the scaling law given by Eq. (2.1), all size-scaling coefficients depend on the shape of the system, while the value in the macroscopic limit does not.

Scaling laws are central in the framework of *morphometric thermodynamics*.[37] Instead of the general scaling law in Eq. (2.1), morphometric thermodynamics is based on the more specific scaling law provided by Hadwiger's theorem.[38,39] This theorem is valid for any functional that is translationally invariant, additive, and a continuous functional of the shape. According to Hadwiger's theorem, these functionals can be written as a linear combination of the four Mikowski functionals: volume $V = \int \mathrm{d}V$, surface area $\Omega = \int \mathrm{d}\Omega$, the integral of the total curvature $C = \int J\mathrm{d}\Omega$ and the integral of the Gaussian curvature $X = \int K\mathrm{d}\Omega$. The total curvature is $J = 1/R_1 + 1/R_2$ and the Gaussian curvature is $K = 1/(R_1R_2)$ where R_1 and R_2 are the principal radii of curvature at a certain point on the surface. For a general property A that fulfills Hadwiger's criteria, the linear combination is

$$A = a_V V + a_\Omega \Omega + a_C C + a_X X. \tag{2.2}$$

In this expression, the geometric measurements V, Ω, C and X, depend on the shape of the bounding container of the system, while the scaling coefficients a_V, a_Ω, a_C and a_X, do not. This means that the scaling coefficients computed from a simple geometry can be used to predict values of A for complex geometries as long as V, Ω, C and X can be computed. Another difference between the scaling law based on Hadwiger's theorem and one given in Eq. (2.1) is that Hadwiger's theorem states that there exists a finite number of size-scaling coefficients.

To understand the implications of morphometric thermodynamics, we take as an example the scaling law for the grand potential, $\Upsilon = U - TS - \mu N$. U is the internal energy, T is the temperature, S is the entropy, μ is the chemical potential and N is the number of particles. We consider surfaces with constant J and K, such that $C = J$ and $X = K$. According to morphometric thermodynamics, the grand potential can then be expressed as

$$\Upsilon_{\text{Hadwiger}} = -pV + \gamma_0\Omega + \upsilon_C J + \upsilon_X K, \tag{2.3}$$

where p is the pressure and γ_0 is the surface energy of a planar wall. The terms υ_C and υ_X are often referred to as rigidities.[37] More details on thermodynamics for sur-

faces and the significance of the surface energy are presented in Sec. 2.2.1. In descriptions of thermodynamics for curved surfaces, the Helfrich[40] expansion can be used to express the surface energy of a non-planar surface as the surface energy of a planar wall plus additional curvature corrections.[41–45] The first-order curvature correction was discussed by Tolman,[46] and second-order corrections were included by Helfrich.[40] Applying the Helfrich expansion for the surface energy in the expression for the grand potential gives

$$\Upsilon_{\text{Helfrich}} = -pV + \gamma_0\Omega - \delta\gamma_0 J + \frac{k}{2}J^2 + \bar{k}K + \cdots, \tag{2.4}$$

where δ is the Tolman length, k is the bending rigidity and $\bar{k}$ is the Gaussian-curvature rigidity. Comparing Eq. (2.3) to Eq. (2.4) shows that the bending rigidity is zero in the framework of morphometric thermodynamics.

The validity of morphometric thermodynamics has been investigated for fluids of hard spheres in contact with a hard, curved wall. König et al.[37] investigated the systems using Rosenfeld's *fundamental measure theory* (FMT)[47,48] and concluded that the four morphometric measures in Eq. (2.3) were sufficient to describe the influence of an arbitrarily shaped container on the fluid. However, Blokhuis[49] came to the opposite conclusion, i.e. the bending rigidity is not zero, by comparing the results from three different approaches: (i) applying the same theoretical model as applied by König et al.[37] (ii) using an expansion of the FMT free energy to second order in the curvature for the spherical and cylindrical interface and (iii) investigating results from MD simulations by Laird et al.[50,51] Blokhuis[49] attributed the non-zero bending rigidity to the restructuring of the molecules which occurs when the curvature changes. Urrutia[52] also found non-zero values of k from exact analytical expressions based on cluster integrals. Blokhuis[49] and Urrutia[52] both point out that the magnitude of k is small, and that it can be hard to distinguish it from zero. This challenge was also reported by Laird et al.[50] in their investigations of hard spheres at low packing fractions through MD simulations, which showed that deviations from morphometric thermodynamics were not resolvable within the statistical error. The system of hard spheres confined by a hard wall at low packing fractions was later revisited by Davidchack and Laird[53] and they were able to conclude from high-resolution MD simulations that the grand potential of a cylindrical wall deviates from the morphometric thermodynamic description. For a spherical wall, the high-precision results were still insufficient to resolve deviations from morphometric thermodynamics. These examples show that size-scaling is a useful tool that can facilitate determination of thermodynamic properties across different length scales. However, extraction of size-scaling coefficients beyond the first order in a consistent manner from simulations can be challenging.

In naturally occurring small systems, the small-size effects is an inherent part of the system. When particle-wall interactions are included in simulations, they work as models for the interfaces we can observe in real life systems. However, even when no particle-wall interactions are explicitly included in the simulations, size effects can still be present due to the finite size of the simulations box. When the goal is to extract bulk

properties, this size effect is unwanted. A substantial amount of the research done on size effects has therefore been focused on finding corrections for them. Scaling laws in this setting are therefore often referred to as *finite-size corrections*. In addition to the numerous theoretical descriptions,[54–60] finite-size corrections have been investigated to a large extent through simulations for both simple model fluids and for complex molecular fluids.[31,32,35,61–68]

Sub-sampling techniques are a category of computational techniques that utilize size-scaling to analyze thermodynamic properties. In these methods, sub-systems are sampled from a periodic simulation box of finite size. By sampling the sub-systems at different locations in the simulation box and throughout the simulation run, one gets access to ensemble averages of grand canonical fluctuations in the number of particles and the energy. Since the sub-systems are non-periodic, the fluctuations are affected by a significant contribution from the surface. By sampling differently sized sub-systems, scaling-laws can be used to analyze the size- and shape-dependence of the fluctuations. This sub-sampling technique is illustrated in Fig. 2.2. For the sub-sampled volumes, another type of finite-size effect, not captured by Eqs.(2.1)-(2.2) can influence the fluctuations. This finite-size effect is an artefact that arises from the finite size of the simulation box. For a closed simulation box, a density change in the sub-system can not occur without a corresponding density change in the reservoir. This affects the fluctuations of the largest embedded small systems, since the simulation box is not functioning properly as a grand canonical reservoir at this point. Including a correction for this finite-size effect in the scaling relations has been shown to improve the accuracy of the extrapolation to the macroscopic limit.[31,32,66,67,69–71]

Fluctuations are interesting because they have a direct relation to a number of thermodynamic properties. The origin of these connections is the coupling between the second moments of the probability distribution of the grand canonical ensemble and the fluctuations in the number of particles,

$$(k_B T)^2 \left(\frac{\partial^2 \ln \Xi(\mu, V, T)}{\partial \mu^2} \right)_{T,V} = \langle N^2 \rangle - \langle N \rangle^2, \tag{2.5}$$

where Ξ is the partition function of the grand canonical ensemble and k_B is the Boltzmann constant. The brackets denote ensemble averages. The second moments are in turn connected to a large variety of thermodynamic quantities. Consequently, sub-sampling techniques have been used to calculate values in the macroscopic limit for the magnetic susceptibility,[63,72] the thermodynamic factor,[35] partial molar properties,[36] the isothermal compressibility,[31] and chemical potential.[66–68,73] Extraction of the critical temperature and the critical exponents from particle fluctuations has also been explored.[63,64,74,75]

In addition to extraction of properties in the macroscopic limit, sub-sampling methods have provided insight into the scaling relations for different thermodynamic properties. Strøm et al.[31] presented a close inspection of which fluctuation-based properties can be described by Hadwiger's theorem. The authors showed how properties that do not fulfill the criteria of Hadwiger's theorem can be expressed as combinations

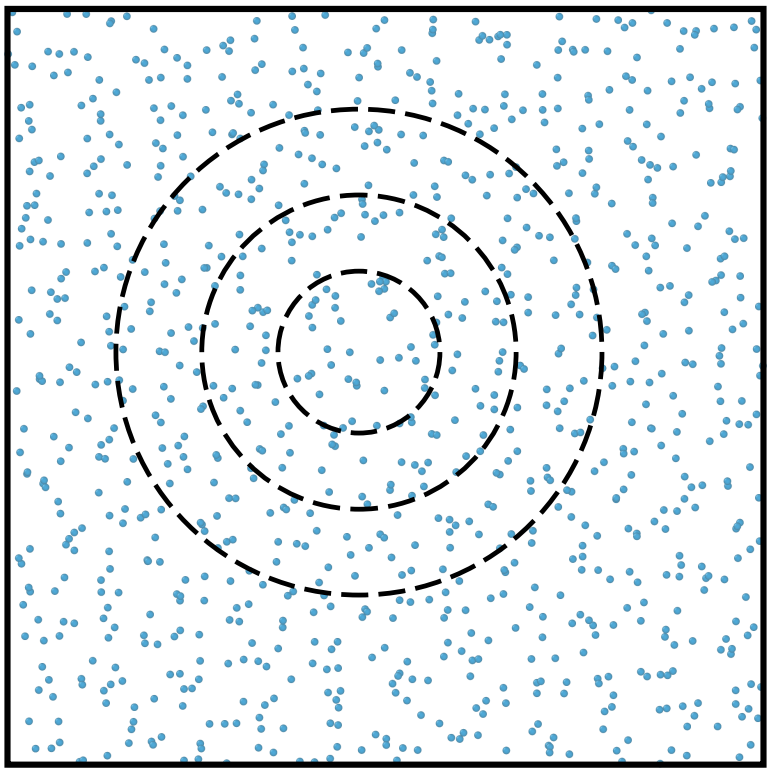

Figure 2.2: Illustration of the sub-sampling procedure where particle fluctuations are calculated in spherical sub-systems inside the total simulation box. Differently sized sub-systems are sampled in order to investigate how the fluctuations change when the size of the system changes. From Bråten et. al. *J. Chem. Inf.* 2021 61 (2), 840-855.

of the ones that do. In their investigations of the size effects for the thermodynamic properties of water, Strøm et al.[31] focused on the scaling law based on the theorem by Hadwiger truncated after the first-order size-scaling coefficient. For the density of A, this compact scaling law is

$$a = a_V + \frac{\Omega}{V} a_\Omega. \tag{2.6}$$

By investigating the fluctuations computed from sub-sampled volumes of different shapes (tetrahedron, cube, dodecahedron and sphere), Strøm et al.[31] found that the size-scaling coefficients in Eq. (2.6) are independent of shape. Holovko et al.[76] showed that Eq. (2.6) also can be used for more complex geometries through investigations of thermodynamic properties of hard sphere fluids confined in random porous media. They found that two different types of porous media have the same chemical potential when they have the same porosity (corresponding to volume) and equal surface areas.

2.1.2 Ensemble dependence

A system's ensemble refers to how the system is connected to its surroundings. Some of the common ensembles are the micro canonical ensemble, canonical ensemble, grand canonical ensemble and the isobaric-isothermal ensemble.[77] The micro canonical ensemble (NVE) represents a system that is closed and isolated, such that it can not exchange energy or particles with the surroundings. The canonical ensemble (NVT) represents a closed system connected to a heat bath, which means that it can exchange energy with the surroundings. The grand canonical ensemble (μVT) represents an open system connected to both a heat bath and a particle reservoir, such that it can exchange energy and particles with the surroundings. The isobaric-isothermal ensemble (NpT) represents a closed system, connected to a heat bath, with a non-constant volume.

In classical thermodynamics, it is well known that ensemble equivalence holds for macroscopic systems with short-range interactions. This means that different ensembles predict compatible or equivalent equilibrium states for a given system.[19,22] However, ensemble *in-equivalence* can occur when properties that normally are regarded as extensive in macroscopic systems are influenced by the small size such that they become higher-order functions of size and shape. As a consequence, properties such as the internal energy or other energy state functions such as the Helmholtz energy, Gibbs energy and the grand potential are no longer Euler homogeneous of degree one.[34] As we have seen in Sec. 2.1.1, this is often the case for small systems.

Occurrences of ensemble dependence have been investigated analytically, theoretically and through simulations. Miranda[78] investigated analytical expressions for small clusters of harmonic oscillators and for two level systems, and found differences between the properties in the canonical, micro canonical and grand canonical ensembles. Rubi et al.[79] showed by theoretical investigations that the properties of a single molecule under stretching are ensemble dependent. They compared the properties a of molecule under isomeric conditions, where the end-to-end distance of the molecule is controlled, and isotensional conditions, where the applied external force is controlled. Bering et al.[80] later showed that the in-equivalence between these two ensembles can be detected from simulations of polymer chains. Ensemble in-equivalence is not restricted to small systems. Deviations from Euler homogeneity have also been observed for systems with long-range interactions.[19–22,24]

The Legendre transform is used in classical thermodynamics since it relates the energy state function of one ensemble to that of another ensemble.[30] The requirements for applying the Legendre transform are that the function is differentiable and convex. Since ensemble in-equivalence occurs when a set of equilibrium states in one ensemble can not be realized for another ensemble, it can give rise to convexity anomalies in the energy state functions.[19–22] For such systems, the energy state functions of different ensembles are no longer connected through Legendre transforms. The Legendre-Fenchel transform is a generalization of the Legendre transform that reduces to the latter when the function is differentiable and convex. The Legendre-

Fenchel transform has therefore been used to transform between different stretching energies in investigations polymer chains,[81] and to transform the Gibbs energy of a deformable slit pore into the Helmholtz energy of a non-deformable slit pore.[82]

2.2 Can we define a consistent thermodynamic framework for small systems?

It is clear that the behavior of small systems can deviate from the behavior of large, macroscopic systems, and that we can in general not assume that the usual classical thermodynamic equations provide valid descriptions for such systems. With increased interest in small systems in fields such as atmospheric science,[83] biology[16,17] and porous media science,[84,85] there is a need for a consistent thermodynamic description that is not restricted to a particular type of small system. Such a description will be crucial in the development of models with predictive abilities for the thermodynamic properties of small systems, such as an EoS.

In this section we present two different formalisms that provide frameworks for handling thermodynamic properties of systems influenced by small-size effects. The first is the framework for surface excess properties derived by Gibbs.[86] The second is the framework developed by Hill,[87] which is a consistent extension of classical thermodynamics that can be applied to small systems. We consider the properties for systems of one component, but extension to mixtures is possible.

2.2.1 Gibbs' surface thermodynamics

The foundations of the thermodynamic theory of interfaces was formulated by Gibbs.[86] His theory describes the thermodynamics of a macroscopic system containing two isotropic phases, α and β, separated by a heterogeneous interface region. Gibbs introduced the concept of a dividing surface, which is a hypothetical sharp surface in the region of heterogeneity between the two phases. The dividing surface provides a geometrical separation of the two homogeneous phases, and has therefore no thickness.

Figure 2.3 shows an illustration of a real, heterogeneous interface region and the geometrical dividing surface introduced by Gibbs. The energetic contribution from the surface to the thermodynamic properties of the total system are described as *surface excess*. The values of the surface excess properties are obtained by assigning to the bulk phases the values they would have if the bulk phases continued uniformly up to the dividing surface. Extensive properties of the total system are therefore expressed as the sum of the bulk values on each side of the dividing surface plus a surface excess.

The properties of the two bulk phases are denoted by superscript "α" or "β", while the surface excess properties are denoted by superscript "s". Since the dividing surface is only a geometrical surface with no thickness and therefore has no volume, $V^{\mathrm{s}} = 0$, the total volume of the system becomes

$$V = V^{\alpha} + V^{\beta}. \tag{2.7}$$

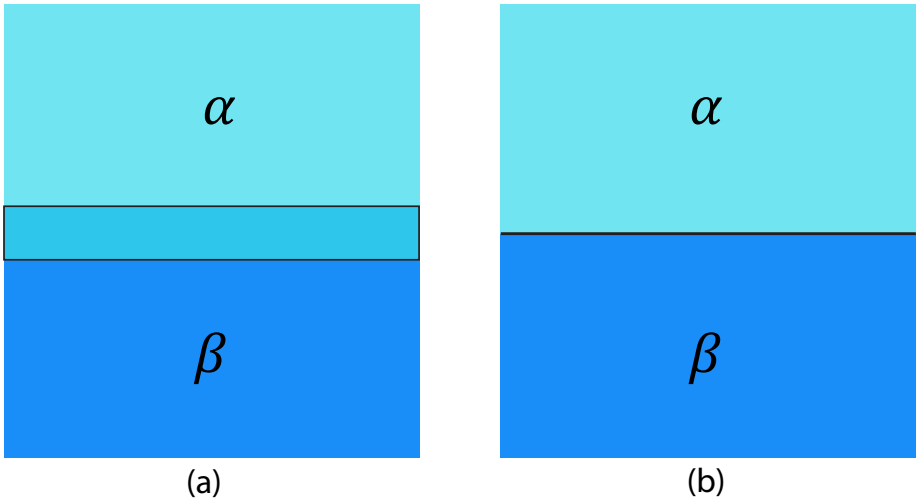

Figure 2.3: An illustration of the two phases α and β separated by (a) a real, heterogeneous interface region and (b) the geometrical dividing surface introduced by Gibbs.

The total number of particles, the total entropy and the total internal energy are

$$N = N^{\alpha} + N^{\beta} + N^{\mathrm{s}}, \tag{2.8}$$

$$S = S^{\alpha} + S^{\beta} + S^{\mathrm{s}}, \tag{2.9}$$

$$U = U^{\alpha} + U^{\beta} + U^{\mathrm{s}}. \tag{2.10}$$

The excess number of particles divided by the surface area is often referred to as adsorption, $\Gamma = N^{\mathrm{s}}/\Omega$, while the excess entropy per area is $\eta = S^{\mathrm{s}}/\Omega$.

A central quantity in Gibbs' surface thermodynamics is the surface energy, γ. The surface energy equals the excess grand potential per area of the dividing surface.[43] For equilibrium systems, the temperature and the chemical potential must be the same everywhere in the system, i.e. $T = T^{\alpha} = T^{\beta} = T^{\mathrm{s}}$ and $\mu = \mu^{\alpha} = \mu^{\beta} = \mu^{\mathrm{s}}$. The pressure, however, can be different in each phase. Hence, the internal energy of the total system, consisting of the two phases separated by the dividing surface, becomes

$$U = TS - p^{\alpha}V^{\alpha} - p^{\beta}V^{\beta} + \mu N + \gamma\Omega. \tag{2.11}$$

For planar surfaces, the term $\gamma\Omega$ is proportional to the surface area. For non-planar surfaces, the surface energy can be expressed as the planar-wall surface energy plus higher-order correction terms that account for the curvature dependence. The scaling law based on Hadwiger's theorem (Eq. (2.3)) and the Helfrich expansion (Eq. (2.4)) are examples of such expressions. As discussed in Sec. 2.1.1, extraction of the size-scaling coefficients that account for the curvature can be challenging. This is further complicated by the fact that both the contribution of a planar wall and the higher-order correction terms can depend on the location of the dividing surface. Aasen et al.[43] applied the Helfrich expansion to investigate the interface between a spherical droplet

and the surrounding vapor, and found that the Tolman length is independent of the choice of dividing surface while the rigidity constants are not. Reindl et al.[88] investigated several model fluids in contact with a curved wall and found that the accuracy of Hadwiger's depends on the location of the dividing surface.

An advantage of Gibbs' surface thermodynamics is that it allows for splitting of the total description of the system into a bulk phase and a surface phase. From Eqs. (2.7)-(2.11), one can derive the Gibbs adsorption equation, which conveniently connects the surface excess properties to the intensive properties of the total system.[86,89] For a given choice of dividing surface at a fixed position relative to the total volume, the Gibbs adsorption equation is

$$\mathrm{d}\gamma = -\Gamma \mathrm{d}\mu - \eta \mathrm{d}T. \tag{2.12}$$

This connection makes Gibbs' surface thermodynamics an attractive framework for description of the properties of confined fluids. For such systems, one must keep in mind that the volume depends on the location of the dividing surface, which means that care should be taken to ensure that it is chosen appropriately.[50,53,90] It is also clear that choosing a suitable scaling law for the surface excess properties is crucial in order to obtain accurate predictions.

One limitation associated with using Gibbs' surface thermodynamics as a thermodynamic framework for small systems is that it is ensemble independent. It therefore does not provide the tools for analyzing systems that are ensemble dependent. Another limitation is that all size effects incorporated in the description are associated with geometric features of the system. This means that small-size contributions that can not be directly associated with a contribution from the system's geometry are not captured by Gibbs' surface thermodynamics. Gibbs' thermodynamics of surfaces is therefore not suitable as a thermodynamic framework for single macro-molecules such as polymers or DNA-chains.

2.2.2 Hill's nanothermodynamics

Hill's description of thermodynamics for small systems was initiated by the work published in 1962.[91] He later published further elaborations and examples of applications in text books.[87] The framework is often referred to as *nanothermodynamics*.[34]

The derivation of Hill's nanothermodynamics starts with a firm macroscopic foundation by considering a collection of $\mathcal{N}$ equivalent, distinguishable, independent small systems. All the small systems have a fixed center of mass and are described by a set of three parameters corresponding to a thermodynamic ensemble. The small systems are too small to be described by classical thermodynamics, but the properties of the *total* collection they make up together can be described by classical thermodynamics. For the collection of small systems, the total energy is a function of the total entropy, the total volume, the total number of particles and the number of small system replicas, $U_\mathrm{t} = U_\mathrm{t}(S_\mathrm{t}, V_\mathrm{t}, N_\mathrm{t}, \mathcal{N})$. Here, the subscript "t" is included in order to indicate properties of the total collection of small systems. The exact differential of the total energy

is found by considering small changes in all the independent variables of the system as follows:

$$\begin{aligned} \mathrm{d}U_\mathrm{t} = \quad & \left(\frac{\partial U_\mathrm{t}}{\partial S_\mathrm{t}}\right)_{V_\mathrm{t},N_\mathrm{t},\mathscr{N}} \mathrm{d}S_\mathrm{t} + \left(\frac{\partial U_\mathrm{t}}{\partial V_\mathrm{t}}\right)_{S_\mathrm{t},N_\mathrm{t},\mathscr{N}} \mathrm{d}V_\mathrm{t} \\ & + \left(\frac{\partial U_\mathrm{t}}{\partial N_\mathrm{t}}\right)_{S_\mathrm{t},V_\mathrm{t},\mathscr{N}} \mathrm{d}N_\mathrm{t} + \left(\frac{\partial U_\mathrm{t}}{\partial \mathscr{N}}\right)_{S_\mathrm{t},V_\mathrm{t},N_\mathrm{t}} \mathrm{d}\mathscr{N}, \end{aligned} \tag{2.13}$$

where the temperature, pressure and chemical potential are defined similarly as in macroscopic thermodynamics:

$$T \equiv \left(\frac{\partial U_\mathrm{t}}{\partial S_\mathrm{t}}\right)_{V_\mathrm{t},N_\mathrm{t},\mathscr{N}}, \tag{2.14}$$

$$p \equiv -\left(\frac{\partial U_\mathrm{t}}{\partial V_\mathrm{t}}\right)_{S_\mathrm{t},N_\mathrm{t},\mathscr{N}}, \tag{2.15}$$

$$\mu \equiv \left(\frac{\partial U_\mathrm{t}}{\partial N_\mathrm{t}}\right)_{S_\mathrm{t},V_\mathrm{t},\mathscr{N}}, \tag{2.16}$$

while the fourth differential is particular for the collection of small systems. The introduction of the number of replicas as a variable gives rise to the conjugate variable $\mathscr{E}$, which Hill named the *subdivision potential*.[87] The subdivision potential is defined as

$$\mathscr{E} \equiv \left(\frac{\partial U_\mathrm{t}}{\partial \mathscr{N}}\right)_{S_\mathrm{t},V_\mathrm{t},N_\mathrm{t}}, \tag{2.17}$$

and describes the change in internal energy of the total system as the number of replicas is changed while the total entropy, the total volume and the total number of particles are kept constant. The subdivision potential therefore corresponds to the energy associated with dividing the total collection of small systems into smaller pieces. This subdivision process is illustrated in Fig. 2.4. Combining the above definitions (Eqs. (2.14)-(2.17)) with Eq. (2.13) yields

$$\mathrm{d}U_\mathrm{t} = T\mathrm{d}S_\mathrm{t} - p\mathrm{d}V_\mathrm{t} + \mu\mathrm{d}N_\mathrm{t} + \mathscr{E}\mathrm{d}\mathscr{N}. \tag{2.18}$$

Since the internal energy of the total collection of small systems is an Euler homogeneous function of degree one, we get

$$U_t = TS_t - pV_t + \mu N_t + \mathscr{E}\mathscr{N}. \tag{2.19}$$

Hill named the term $\mathscr{E}\mathrm{d}\mathscr{N}$ the *subdivision energy*.[87] The introduction of this conjugate pair of variables reinstates the extensivity of the total collection of small system replicas, but the internal energy of one small system can still be non-extensive. Hill showed this by retrieving the properties of a single small system by computing the averages of the total collection of small system replicas. The average properties of the small systems can be expressed by dividing the total properties by the number of replicas, which gives

$$U = \frac{U_\mathrm{t}}{\mathscr{N}}, \quad S = \frac{S_\mathrm{t}}{\mathscr{N}}, \quad V = \frac{V_\mathrm{t}}{\mathscr{N}}, \quad N = \frac{N_\mathrm{t}}{\mathscr{N}}. \tag{2.20}$$

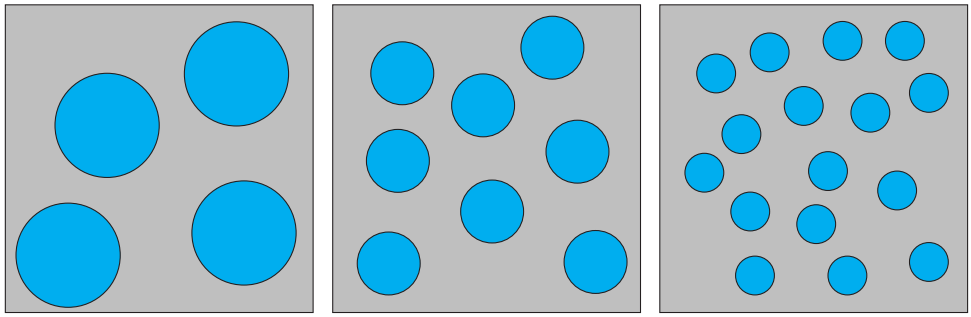

Figure 2.4: Three ensembles of small systems, where each blue circle is considered a small system. The number of small systems increases from left to right, while keeping the total entropy S_t, total volume V_t and total number of particles N_t constant.

These are average quantities per small system, but since all the small systems are equivalent, they can also be viewed as ensemble averages for a single small system. Inserting the identities in Eq. (2.20) in Eq. (2.19) yields the average internal energy of one small system

$$U = TS - pV + \mu N + \mathscr{E}. \tag{2.21}$$

From Eqs. (2.18)-(2.21), it can be deduced that

$$\mathrm{d}U = T\mathrm{d}S - p\mathrm{d}V + \mu\mathrm{d}N, \tag{2.22}$$

$$\mathrm{d}\mathscr{E} = -S\mathrm{d}T + V\mathrm{d}p - N\mathrm{d}\mu, \tag{2.23}$$

which shows that when $\mathscr{E}$ is non-zero, the internal energy of the small system is not an Euler homogeneous function of degree one.

The energy state functions of the various thermodynamic ensembles can also be obtained from Eqs. (2.18)-(2.21). Similarly to the internal energy, the energy state functions of the total collection of small systems become Euler homogeneous functions of degree one, while the energy state functions for each small system do not. Hill also showed that the fundamental connection between the energy state functions and the partition functions remains valid for small systems. More details on the derivation of these functions are found in the books by Hill[87] or the extended explanations presented by Bedeaux et al.[34] A key part of the derivation of these functions is that each thermodynamic ensemble is considered separately, such that the thermodynamic properties always are ensemble specific. As a consequence, the subdivision potential takes different forms for the different ensembles and new, ensemble specific properties arise. Nanothermodynamics has therefore become an important tool in research on ensemble in-equivalence.[79–82]

The advantage of the subdivision potential lies in its generality. It can describe all types of contributions to the internal energy, without explicitly defining contributions

from the system's geometry, such as surface area, curvature, corners, edges, etc. Hill therefore envisioned that his framework would be relevant for research on colloidal particles, polymers, macro-molecules or in statistical mechanical descriptions of any kind of finite system.[87] Hill was to a large extent correct in these predictions. Nanothermodynamics has been used in research on polymer chains, both in the form of theoretical descriptions[79] and in simulation based investigations.[80,81] Is has also been used in theoretical investigations of the statistical mechanical description of an ideal gas adsorbed on a spherical adsorbent.[92] In addition, nanothermodynamics has supported the analysis of size-scaling of thermodynamic properties,[31,36] and it has been particularly important in investigations of transport in porous media.[93–95] In fact, a system does not even need to be small in order to apply Hill's nanothermodynamics. The subdivision potential can be used to describe any contribution to the internal energy that is not captured by the natural variables of the system's thermodynamic ensemble. For instance, Campa et al.[24] showed how Hill's nanothermodynamics can be applied to macroscopic, non-additive systems.

Hill also introduced the concept of excess properties to his framework by distinguishing between contributions that are of macroscopic order and those that are of small order. The goal of this was to extract equations that only contain the small-order terms, and in that way obtain a pure *thermodynamics of smallness*. A general property, A, which is extensive in the macroscopic limit, is in Hill's framework expressed as the sum of a macroscopic contribution plus an excess contribution

$$A = A^{(0)} + A^{(x)}. \tag{2.24}$$

Hill discussed how the density of the excess contribution, $A^{(x)}/V$, can be expanded according to a scaling law that contains terms proportional to the inverse size, but he also considered terms that are not connected to any geometrical feature of the systems, such as $\ln L$. In contrast to the work by Gibbs, the excess properties in Hill's framework are not directly coupled to a surface. Hill showed how his framework can be applied to spherical droplets in vapor in a way that does not require a dividing surface. By introducing a dividing surface, the formalism by Hill becomes equivalent to Gibbs' description.[87]

Nanothermodynamics provides a firm theoretical framework for treatment of properties that are influenced by size effects. However, there are some challenges related to application of Hill's framework for computation of thermodynamic properties. A consequence of the generality of $\mathscr{E}$ is that some insight into the origin of the small-size effects is sacrificed. Since the subdivision potential is not coupled to a specific feature of the system, computation of $\mathscr{E}$ from experiments or simulations can be difficult. For most systems, computation of the subdivision potential directly from the definition given in Eq. (2.17) is not realistic. An alternative route to $\mathscr{E}$ is via the energy state function. For systems such as ideal gases, where the energy state function can be computed exactly from analytical expressions, the subdivision potential can also be computed exactly.[92,96] For systems containing interacting particles, thermodynamic integration is a popular tool that has been used to compute the Helmholtz and Gibbs

energies for slit pores[82] and polymer chains.[80,81] Another approach, often used in investigations of porous media, is the assumption that the energy state function can be expressed as a sum of energy contributions that are attributed to different bulk phases, surfaces and lines in the porous media.[93–95,97]

There have been efforts to connect the properties Hill's framework to mechanical properties, such as the mechanical pressure tensor. In the derivation of Hill's framework for a grand canonical system, a new pressure, $\widehat{p}$, arises. The new pressure is called the *integral pressure*, and differs from the *differential pressure*, p. The subdivision potential in the grand canonical ensemble is a function of the difference between these two pressures

$$\mathscr{E} = (p - \widehat{p})V. \tag{2.25}$$

Rauter et al.[94] investigated a bulk fluid in a slit pore at mechanical equilibrium and computed the values of $\widehat{p}$ from the sum of a pressure contribution from the bulk fluid and a contribution proportional to the fluid-solid surface energy. For this description of the system, the authors showed analytically that $\widehat{p}$ equals the average tangential pressure, while p equals the average of the trace of the mechanical pressure tensor. Numerical investigations of fluid flow through a porous matrix have also resulted in the same conclusion.[97] However, the analytical analysis for the porous matrix has so far been inconclusive.

2.3 Which computational tools and techniques can be applied to study small systems?

In Sec. 2.1 we have seen that properties of small systems deviate from those of large systems, and in Sec. 2.2 we have seen that it is possible to obtain a meaningful thermodynamic description of these properties. In this section, we will discuss the *computation* of thermodynamic properties of small system. We present examples of identities that are normally applied to systems in the macroscopic limit, which are not accurate for small systems. We also discuss some computational and analytical tools that can be trusted to provide accurate predictions of properties for small systems. The discussion presented here is not a complete list of methods that can be utilized for computation of properties of small systems. It is intended as suggestions to what one should consider when evaluating whether a method is appropriate for investigations of small systems.

Some ingrained definitions and relations from statistical mechanics have been derived for the purpose of application in the macroscopic limit. They can therefore include approximations based on the assumptions that $N \to \infty$, which not necessarily are valid for systems containing a small number of particles. One example is the classical virial theorem. For a system with Hamiltonian $\mathscr{H}(\mathbf{x})$, where $\mathbf{x}$ is the phase space vector while x_i and x_j are specific components of the phase space vector, the classical

virial theorem states that

$$\left\langle x_i \frac{\partial \mathcal{H}}{\partial x_j} \right\rangle = \delta_{ij} k_{\mathrm{B}} T, \tag{2.26}$$

where δ_{ij} is the Kronecker delta.[30] Tuckerman[30] derived the above relation by computing the ensemble average in Eq. (2.26) in the micro canonical ensemble. In this derivation, the partition function of the uniform ensemble appears. In the partition function of the micro canonical ensemble, the phase space integral is performed over the constant-energy hypersurface, while for the uniform ensemble, the phase space integral is performed over the volume enclosed by the constant-energy hypersurface. Tuckerman[30] points out that even though this means that the uniform and micro canonical ensembles are associated with different numbers of microstates, the difference becomes vanishingly small in the macroscopic limit. Hence, for a micro canonical ensemble, the classical virial theorem presented in Eq. (2.26) is only true for systems is in the macroscopic limit. The implications of this restriction was further investigated by Uline et al.,[98] who investigated the validity of the generalized equipartition theorem for small systems. The generalized equipartition theorem represents a specific application of the classical virial theorem. They found that the expressions for the equipartiton theorems for the canonical and micro canonical ensemble are different, but that the expressions become equivalent in the macroscopic limit. A consequence of the violation of the generalized equipartition theorem is that while the kinetic energy is proportional to the temperature in the canonical ensemble, this is no longer true in the micro canonical ensemble. Violations of the generalized equipartition theorem have also been investigated by simulations.[99,100]

Approximations based on the assumption that $N \to \infty$ are also used in the classical derivation of the bulk properties of the ideal gas. In Tuckerman's[30] derivation of these properties, he meticulously points out every time such an approximation is used and provides the exact expressions before presenting relations based on approximations. Ensemble in-equivalence of several system types, such as ideal gas systems,[96] harmonic oscillators and two-level systems,[78] has been shown to occur as a result of avoiding assumptions about the magnitude of N.

When approximations that only apply in the macroscopic limit are avoided, statistical mechanics provides a valuable tool for investigation of small-size effects. Hill showed that the connection between the energy state functions and the partition functions remains valid in his framework.[87] Methods that utilize this connection are therefore attractive for analyzing small systems. Examples of methods that have a firm basis in statistical mechanics are methods based on fluctuations, such as the one presented in Sec. 2.1.1. Another category of fluctuation based methods are overlapping distribution methods, which can extract thermodynamic properties from the overlap between probability distributions of two different systems.[101–103] In the canonical ensemble, the Helmholtz energy can be computed from the overlap of two energy distributions sampled from two systems at different temperatures. In the grand canonical ensemble, the grand potential can be computed from the overlap of two distributions in number of particles sampled from two systems at two different chemical potentials.

These relations remain valid for small systems when Hill's description for the energy state function of the small system is applied.

3 Conclusion and perspectives

This work set out to advance our understanding of thermodynamics of small systems. Theoretical investigations have been used in combination with molecular simulations to gain further insight into how and why the behavior of small systems deviates from that of large systems. Three topics have been central in these investigations: (1) how thermodynamic properties change with system size, (2) theoretical frameworks that can consistently describe these effects and (3) which computational tools and techniques can be trusted in investigations of small systems. The results of these investigations have been published in three independent articles in peer-reviewed journals. In this chapter, we recapitulate the main conclusions of the work by explaining how the three main topics are relevant to each article. We also suggest directions for future work.

3.1 Application to the articles

In Article I, we tested the application of a fluctuation-based, overlapping distribution method for extraction of thermodynamic properties of small systems. The main focus was to investigate how properties that are normally regarded as intensive in the macroscopic limit can become size dependent in small systems. From the overlap between distributions of particle numbers from two systems at different densities, one can extract the difference in grand potential and the difference in chemical potential between the two systems. In Article I, we utilized this to investigated the difference in chemical potential of sub-systems sampled from a larger simulation box containing particles interacting through the Lennard-Jones potential. The sizes of the subsystems ranged from three particle diameters to the size of the simulation box. The sub-systems do not have periodic boundaries, which means that the particle fluctuations are influenced by a significant contribution from the small size. Since the small-size effects are not coupled to any specific feature of the system, a suitable thermodynamic framework for the sub-systems is Hill's nanothermodynamics. Hill's framework also ensures consistent treatment of the statistical mechanical connection that relates the fluctuations to the thermodynamic properties of the small systems. Before applying the overlapping distribution method to the sub-systems, we tested its performance for small, grand canonical MC systems. A system with periodic boundaries was used

as a reference. We found that the overlapping distribution method is equally reliable for the small and large systems investigated in Article I.

Applying the overlapping distribution to differently sized sub-systems gives access to how the difference in chemical potential is changing with size. From this, we identified a size-scaling relation that can be utilized to extract the chemical potential difference in the macroscopic limit. Hence, the method for computation of macroscopic chemical potential differences presented in Article I provides an alternative to methods based on insertion of particles, which are known to become inefficient at higher densities.

In Article II, we investigated the ensemble dependence of systems with a small number of particles. The main goal was to gain insight into the mechanisms behind ensemble in-equivalence by comparing the thermodynamic properties of open (grand canonical) and closed (canonical) systems. We investigated cubic boxes with a surface energy that contained ideal gases or particles interacting through interatomic potentials. The properties of the ideal gases were derived analytically. By avoiding assumptions that are only valid in the macroscopic limit, i.e. $N \to \infty$, we identified two types of small-size effects to the properties of the ideal gases. The first type arises from the surfaces, edges and corners of the system, while the second type arises from avoiding assumptions about the magnitude of the number of particles. The latter effect is only present for the properties in the closed system. The nanothermodynamic framework by Hill is a suitable framework for the systems investigated in Article II since it provides tools for analyzing ensemble dependence and for description of small-size effects that are not connected to a specific geometrical feature of the system. For the ideal gas systems, we fond that the differential pressure is not ensemble dependent while the chemical potential is ensemble dependent.

We utilized the insight gained from investigating the ideal gases to analyze ensemble dependence of small systems containing particles interacting through the Lennard-Jones or the Weeks-Chandler-Andersen potential. We applied MC simulations to compute the pressure and the chemical potential in these systems. We found that the ensemble dependence of the chemical potential in the systems with the interacting particles is qualitatively described by the analytic formula derived for an ideal gas system. However, in contrast to the predictions of the ideal gas systems, the differential pressure is ensemble dependent in the systems with interacting particles. This shows that while some contributions to the ensemble dependence of systems with interacting particles are captured by the ideal gas model, there are also some contributions arising from inter-particle interactions. This was further investigated by analysing the effect of increased excluded volume per particles and increased repulsive forces on the system walls. We found that these two modifications of the system resulted in similar responses in the ensemble dependent properties. This indicates that the magnitude of the difference between the properties in open and closed systems is likely to be related to the restricted movement of the particles in the system. The work presented in Article II illustrates the usefulness of models based on statistical mechanics and how

they can provide insight into the mechanisms behind ensemble in-equivalence.

In Article III, we presented a consistent thermodynamic framework that represents an EoS for pure, confined fluids. We applied MD simulations to investigate systems of a Lennard-Jones spline fluid confined by a spherical surface with a Weeks-Chandler-Andersen wall-potential. The EoS is based on a theoretical description in which the total system is decomposed into a bulk phase in equilibrium with a surface phase. Since the small-size effects are connected to a specific geometric feature, Gibbs' framework for surface excess properties provides a suitable description of the systems investigated in Article III. We used an existing, accurate description of the bulk fluid, and utilized Gibbs' framework to consistently incorporate contributions from the surface. In the low-density limit, the properties of fluids with interacting particles can be approximated by the properties of an ideal gas. In order to ensure a consistent extrapolation to low densities, we therefore included exact analytical expressions for the surface excess properties of a confined ideal gas in the EoS-predictions. We found that the pressure and internal energy predicted from the EoS are nearly within the accuracy of properties obtained directly from MD simulations.

The curvature dependencies of the thermodynamic properties of the surface phase were analysed by the use of scaling laws. This allowed us to investigate how the curvature corrections depended on the choice of dividing surface. We found that the choice of dividing surface affects the magnitude of the planar-wall contribution and the first-order size-scaling coefficient. We also showed how the surface properties of one dividing surface are related to those of another dividing surface.

We refer to the framework presented in Article III as Nano-EoS. Due to its ability to efficiently and accurately capture the effect of confinement, a possible application of the Nano-EoS is prediction of thermodynamic properties of fluids in porous media. We expect the Nano-EoS to facilitate development of thermodynamic models for confined fluids in general, and to shed new light on yet unresolved physical phenomena in confined systems, such as changes in dynamic behavior and phase transitions of e.g. confined water.

3.2 Future work

In this section, we present suggestions for future work within the topics: computation of chemical potential differences, size-scaling, choice of dividing surface and choice of thermodynamic framework for small systems.

In Article I, we demonstrated the method for computation of chemical potential differences for pure Lennard-Jones fluids. Application of this method to multicomponent systems and molecular systems has yet to be investigated. It is also possible to compute the partial derivative of chemical potential with respect to density from fluctuations in the number of particles. This can give access to chemical potential differences through numerical integration.[66–68] A comparison of the overlapping dis-

tribution method presented in Article I and the methods based on computation of the differential chemical potentials could illuminate the merits and drawbacks of the two methods.

In Gibbs's framework, we usually express surface properties of non-planar surfaces as the surface properties of a planar wall plus additional curvature corrections, line contributions and edge contributions. In Article III, we focused on Lennard-Jones spline particles in contact with a spherical Weeks-Chandler-Andersen wall. Consequently, we only investigated higher-order corrections to the surface excess properties arising from the curvature. Including higher-order corrections from e.g. lines and edges would make the EoS applicable to a larger variety of shapes and sizes.

For the confined fluid investigated in Article III, both the planar-wall contribution and the higher-order corrections depend on the choice of dividing surface. Choosing a dividing surface that minimizes the higher-order corrections is convenient since surface properties of a planar wall can then be used to describe properties of highly curved surfaces. Tools for optimizing the choice of dividing surface would therefore be useful.

We have seen that the theoretical frameworks by Hill and Gibbs are both good candidates for thermodynamic descriptions of small systems. For some systems, one of the frameworks has clear advantages over the other. For instance, Hill's framework provides a useful description for single macro-molecules, while Gibbs' framework is often chosen in systems where properties can be clearly attributed to the presence of a surface. However, in some systems, such as porous media, the choice might not be as obvious. A comparison of the two methods applied to the same system could provide further insight that could lead to a more robust thermodynamic description of small systems.

References

[1] C. Guozhong. *Nanostructures And Nanomaterials: Synthesis, Properties, And Applications*. London: Imperial College Press; Illustrated edition, 2004.

[2] B. Pelaz, C. Alexiou, R. A. Alvarez-Puebla, F. Alves, A. M. Andrews, S. Ashraf, L. P. Balogh, L. Ballerini, A. Bestetti, C. Brendel, et al. "Diverse applications of nanomedicine". *ACS Nano.* **11** (2017), 2313–2381.

[3] B. O'Regan and M. Grätzel. "A low-cost, high-efficiency solar cell based on dye-sensitized colloidal TiO2 films". *Nature.* **353** (1991), 737–740.

[4] H.-S. Kim, C.-R. Lee, J.-H. Im, K.-B. Lee, T. Moehl, A. Marchioro, S.-J. Moon, R. Humphry-Baker, J.-H. Yum, J. E. Moser, et al. "Lead iodide perovskite sensitized all-solid-state submicron thin film mesoscopic solar cell with efficiency exceeding 9%". *Sci. Rep.* **2** (2012), 1–7.

[5] M. Qasim, M. Badrelzaman, N. N. Darwish, N. A. Darwish, and N. Hilal. "Reverse osmosis desalination: A state-of-the-art review". *Desalination.* **459** (2019), 59–104.

[6] M. T. Rauter, S. K. Schnell, B. Hafskjold, and S. Kjelstrup. "Thermo-osmotic pressure and resistance to mass transport in a vapor-gap membrane". *Phys. Chem. Chem. Phys.* **23** (2021), 12988–13000.

[7] M. T. Rauter, S. K. Schnell, and S. Kjelstrup. "Cassie–Baxter and Wenzel States and the Effect of Interfaces on Transport Properties across Membranes". *J. Phys. Chem. B.* **125** (2021), 12730–12740.

[8] H. Li, J. P. Jakobsen, Ø. Wilhelmsen, and J. Yan. "PVTxy properties of CO2 mixtures relevant for CO2 capture, transport and storage: Review of available experimental data and theoretical models". *Appl. Energy.* **88** (2011), 3567–3579.

[9] A. Aasen, M. Hammer, G. Skaugen, J. P. Jakobsen, and Ø. Wilhelmsen. "Thermodynamic models to accurately describe the PVTxy-behavior of water / carbon dioxide mixtures". *Fluid Phase Equilib.* **442** (2017), 125–139.

[10] Y. Zhao, P. Stein, Y. Bai, M. Al-Siraj, Y. Yang, and B.-X. Xu. "A review on modeling of electro-chemo-mechanics in lithium-ion batteries". *J. Power Sources.* **413** (2019), 259–283.

[11] A. F. Gunnarshaug, S. Kjelstrup, D. Bedeaux, F. Richter, and O. S. Burheim. "The reversible heat effects at lithium iron phosphate-and graphite electrodes". *Electrochim. Acta.* **337** (2020), 135567.

[12] A. V. Neimark and K. G. Kornev. "Classification of equilibrium configurations of wetting films on planar substrates". *Langmuir.* **16** (2000), 5526–5529.

[13] A. V. Neimark, P. I. Ravikovitch, and A. Vishnyakov. "Inside the hysteresis loop: Multiplicity of internal states in confined fluids". *Phys. Rev. E.* **65** (2002), 031505.

[14] T. Horikawa, D. D. Do, and D. Nicholson. "Capillary condensation of adsorbates in porous materials". *Adv. Colloid Interface Sci.* **169** (2011), 40–58.

[15] T. Hiratsuka, H. Tanaka, and M. T. Miyahara. "Comprehensive modeling of capillary condensation in open-ended nanopores: Equilibrium, metastability, and spinodal". *J. Phys. Chem. C.* **121** (2017), 26877–26886.

[16] W. H. Roos, I. L. Ivanovska, A. Evilevitch, and G. J. L. Wuite. "Viral capsids: Mechanical characteristics, genome packaging and delivery mechanisms". *Cell. Mol. Life Sci.* **64** (2007), 1484.

[17] N. P. Stone, G. Demo, E. Agnello, and B. A. Kelch. "Principles for enhancing virus capsid capacity and stability from a thermophilic virus capsid structure". *Nat. Commun.* **10** (2019), 4471.

[18] D. E. Smith, S. J. Tans, S. B. Smith, S. Grimes, D. L. Anderson, and C. Bustamante. "The bacteriophage φ29 portal motor can package DNA against a large internal force". *Nature.* **413** (2001), 748–752.

[19] A. Campa, T. Dauxois, and S. Ruffo. "Statistical mechanics and dynamics of solvable models with long-range interactions". *Phys. Rep.* **480** (2009), 57–159.

[20] H. Touchette, R. S. Ellis, and B. Turkington. "An introduction to the thermodynamic and macrostate levels of nonequivalent ensembles". *Phys. A: Stat. Mech. Appl.* **340** (2004), 138–146.

[21] H. Touchette. "Ensemble equivalence for general many-body systems". *EPL.* **96** (2011), 50010.

[22] D. F. A. Campa T. Dauxois and S. Ruffo. *Physics of Long-Range Interacting Systems.* Oxford: Oxford University Press, 2014.

[23] I. Latella, A. Pérez-Madrid, A. Campa, L. Casetti, and S. Ruffo. "Long-range interacting systems in the unconstrained ensemble". *Phys. Rev. E.* **95** (2017), 012140.

[24] A. Campa, L. Casetti, I. Latella, A. Pérez-Madrid, and S. Ruffo. "Concavity, response functions and replica energy". *Entropy.* **20** (2018), 907.

[25] J. Miller. "Statistical mechanics of Euler equations in two dimensions". *Phys. Rev. Lett.* **65** (1990), 2137.

[26] R. Robert and J. Sommeria. “Statistical equilibrium states for two-dimensional flows”. *J. Fluid Mech.* **229** (1991), 291–310.

[27] M. K.-H. Kiessling and T. Neukirch. “Negative specific heat of a magnetically self-confined plasma torus”. *Proc. Natl. Acad. Sci.* **100** (2003), 1510–1514.

[28] H. De Vega and N. Sanchez. “Statistical mechanics of the self-gravitating gas: I. Thermodynamic limit and phase diagrams”. *Nucl. Phys. B.* **625** (2002), 409–459.

[29] M. Helbæk and S. Kjelstrup. *Fysikalsk kjemi*. Bergen: Fagbokforlaget Vigmostad & Bjørke AS, 2009.

[30] M. E. Tuckerman. *Statistical Mechanics: Theory and Molecular Simulation*. New York: Oxford University Press Inc., 2010.

[31] B. A. Strøm, J.-M. Simon, S. K. Schnell, S. Kjelstrup, J. He, and D. Bedeaux. “Size and shape effects on the thermodynamic properties of nanoscale volumes of water”. *Phys. Chem. Chem. Phys.* **19** (2017), 9016–9027.

[32] S. K. Schnell, T. J. H. Vlugt, J.-M. Simon, D. Bedeaux, and S. Kjelstrup. “Thermodynamics of small systems embedded in a reservoir: a detailed analysis of finite size effects”. *Mol. Phys.* **110** (2012), 1069–1079.

[33] A. Aasen, D. Reguera, and Ø. Wilhelmsen. “Curvature corrections remove the inconsistencies of binary classical nucleation theory”. *Phys. Rev. Lett.* **124** (2020), 045701.

[34] D. Bedeaux, S. Kjelstrup, and S. K. Schnell. *Nanothermodynamics. General theory*. Porelab publisher, 2020.

[35] S. K. Schnell, T. J. H. Vlugt, J.-M. Simon, D. Bedeaux, and S. Kjelstrup. “Thermodynamics of a small system in a μT reservoir”. *Chem. Phys. Lett.* **504** (2011), 199–201.

[36] S. K. Schnell, R. Skorpa, D. Bedeaux, S. Kjelstrup, T. J. H. Vlugt, and J.-M. Simon. “Partial molar enthalpies and reaction enthalpies from equilibrium molecular dynamics simulation”. *J. Chem. Phys.* **141** (2014), 144501.

[37] P.-M. König, R. Roth, and K. R. Mecke. “Morphological Thermodynamics of Fluids: Shape Dependence of Free Energies”. *Phys. Rev. Lett.* **93** (2004), 160601.

[38] H. Hadwiger. *Vorlesungen Über Inhalt, Oberfläche und Isoperimetrie*. Springer, 1957.

[39] K. R. Mecke. “Integral Geometry in Statistical Physics”. *Int. J. Mod. Phys. B.* **12** (1998), 861–899.

[40] W. Helfrich. “Elastic Properties of Lipid Bilayers: Theory and Possible Experiments”. *Zeitschrift für Naturforschung C.* **28** (1973), 693–703.

[41] E. M. Blokhuis and A. E. Van Giessen. “Density functional theory of a curved liquid–vapour interface: evaluation of the rigidity constants”. *J. Phys. Condens. Matter.* **25** (2013), 225003.

[42] Ø. Wilhelmsen, D. Bedeaux, and D. Reguera. “Tolman length and rigidity constants of the Lennard-Jones fluid”. *J. Chem. Phys.* **142** (2015), 064706.

[43] A. Aasen, E. M. Blokhuis, and Ø. Wilhelmsen. “Tolman lengths and rigidity constants of multicomponent fluids: Fundamental theory and numerical examples”. *J. Chem. Phys.* **148** (2018), 204702.

[44] P. Rehner and J. Gross. “Surface tension of droplets and Tolman lengths of real substances and mixtures from density functional theory”. *J. Chem. Phys.* **148** (2018), 164703.

[45] P. Rehner, A. Aasen, and Ø. Wilhelmsen. “Tolman lengths and rigidity constants from free-energy functionals—General expressions and comparison of theories”. *J. Chem. Phys.* **151** (2019), 244710.

[46] R. C. Tolman. “The Effect of Droplet Size on Surface Tension”. *J. Chem. Phys.* **17** (1949), 333–337.

[47] Y. Rosenfeld. “Free-energy model for the inhomogeneous hard-sphere fluid mixture and density-functional theory of freezing”. *Phys. Rev. Lett.* **63** (1989), 980–983.

[48] R. Roth. “Fundamental measure theory for hard-sphere mixtures: a review”. *J. Phys. Condens. Matter.* **22** (2010), 063102.

[49] E. M. Blokhuis. “Existence of a bending rigidity for a hard-sphere liquid near a curved hard wall: Validity of the Hadwiger theorem”. *Phys. Rev. E.* **87** (2013), 022401.

[50] B. B. Laird, A. Hunter, and R. L. Davidchack. “Interfacial free energy of a hard-sphere fluid in contact with curved hard surfaces”. *Phys. Rev. E.* **86** (2012), 060602.

[51] B. B. Laird and R. L. Davidchack. “Calculation of the interfacial free energy of a fluid at a static wall by Gibbs–Cahn integration”. *J. Chem. Phys.* **132** (2010), 204101.

[52] I. Urrutia. “Bending rigidity and higher-order curvature terms for the hard-sphere fluid near a curved wall”. *Phys. Rev. E.* **89** (2014), 032122.

[53] R. L. Davidchack and B. B. Laird. “Surface free energy of a hard-sphere fluid at curved walls: Deviations from morphometric thermodynamics”. *J. Chem. Phys.* **149** (2018), 174706.

[54] I. Oppenheim and P. Mazur. “Density expansions of distribution functions. I.: Virial expansion for finite closed systems: Canonical esemble”. *Physica.* **23** (1957), 197–215.

[55] J. L. Lebowitz and J. K. Percus. “Long-Range Correlations in a Closed System with Applications to Nonuniform Fluids”. *Phys. Rev.* **122** (1961), 1675–1691.

[56] J. L. Lebowitz and J. K. Percus. “Thermodynamic Properties of Small Systems”. *Phys. Rev.* **124** (1961), 1673–1681.

[57] J. I. Siepmann, I. R. McDonald, and D. Frenkel. “Finite-size corrections to the chemical potential”. *J. Phys. Condens. Matter.* **4** (1992), 679–691.

[58] P. Krüger, S. K. Schnell, D. Bedeaux, S. Kjelstrup, T. J. H. Vlugt, and J.-M. Simon. “Kirkwood–Buff Integrals for Finite Volumes”. *J. Phys. Chem. Lett.* **4** (2013), 235–238.

[59] J. Milzetti, D. Nayar, and N. F. A. van der Vegt. “Convergence of Kirkwood–Buff Integrals of Ideal and Nonideal Aqueous Solutions Using Molecular Dynamics Simulations”. *J. Phys. Chem. B.* **122** (2018), 5515–5526.

[60] N. Dawass, P. Krüger, S. K. Schnell, J.-M. Simon, and T. J. H. Vlugt. “Kirkwood-Buff integrals from molecular simulation”. *Fluid Ph. Equilibria.* **486** (2019), 21–36.

[61] W. W. Wood, F. R. Parker, and J. D. Jacobson. “Recent monte carlo calculations of the equation of state of Lenard-Jones and hard sphere molecules”. *Il Nuovo Cimento.* **9** (1958), 133–143.

[62] B. J. Alder and T. E. Wainwright. “Studies in Molecular Dynamics. II. Behavior of a Small Number of Elastic Spheres”. *J. Chem. Phys.* **33** (1960), 1439–1451.

[63] K. Binder. “Finite size scaling analysis of ising model block distribution functions”. *Z. Phys.* **43** (1981), 119–140.

[64] M. Rovere, P. Nielaba, and K. Binder. “Simulation studies of gas-liquid transitions in two dimensions via a subsystem-block-density distribution analysis”. *Z. Phys.* **90** (1993), 215–228.

[65] P. Ganguly and N. F. A. van der Vegt. “Convergence of Sampling Kirkwood–Buff Integrals of Aqueous Solutions with Molecular Dynamics Simulations”. *J. Chem. Theory Comput.* **9** (2013), 1347–1355.

[66] R. Cortes-Huerto, K. Kremer, and R. Potestio. “Communication: Kirkwood-Buff integrals in the thermodynamic limit from small-sized molecular dynamics simulations”. *J. Chem. Phys.* **145** (2016), 141103.

[67] M. Heidari, K. Kremer, R. Potestio, and R. Cortes-Huerto. “Fluctuations, Finite-Size Effects and the Thermodynamic Limit in Computer Simulations: Revisiting the Spatial Block Analysis Method”. *Entropy.* **20** (2018), 222.

[68] M. Heidari, K. Kremer, R. Potestio, and R. Cortes-Huerto. “Finite-size integral equations in the theory of liquids and the thermodynamic limit in computer simulations”. *Mol. Phys.* **116** (2018), 3301–3310.

[69] F. L. Román, J. A. White, and S. Velasco. “Fluctuations in an equilibrium hard-disk fluid: Explicit size effects”. *J. Chem. Phys.* **107** (1997), 4635–4641.

[70] J. J. Salacuse. “Particle fluctuations within sub-regions of an N-particle, two-dimensional fluid: Finite-size effects and compressibility”. *Physica A.* **379** (2007), 372–388.

[71] J. J. Salacuse. “Particle fluctuations within sub-regions of an N-particle, three-dimensional fluid: Finite-size effects and compressibility”. *Physica A.* **387** (2008), 3073–3083.

[72] K. Binder. “Critical Properties from Monte Carlo Coarse Graining and Renormalization”. *Phys. Rev. Lett.* **47** (1981), 693–696.

[73] V. Bråten, Ø. Wilhelmsen, and S. K. Schnell. “Chemical Potential Differences in the Macroscopic Limit from Fluctuations in Small Systems”. *J. Chem. Inf. Model.* **61** (2021), 840–855.

[74] M. Rovere, D. W. Hermann, and K. Binder. “Block Density Distribution Function Analysis of Two-Dimensional Lennard-Jones Fluids”. *EPL.* **6** (1988), 585–590.

[75] M. Rovere, D. W. Heermann, and K. Binder. “The gas-liquid transition of the two-dimensional Lennard-Jones fluid”. *J. Phys. Condens. Matter.* **2** (1990), 7009–7032.

[76] M. Holovko, T. Patsahan, and W. Dong. “Fluids in random porous media: Scaled particle theory”. *Pure Appl. Chem.* **85** (2012), 115–133.

[77] J.-P. Hansen and I. R. McDonald. *Theory of simple liquids: with applications to soft matter*. Academic press, 2013.

[78] E. N. Miranda. “Statistical mechanics of few-particle systems: exact results for two useful models”. *Eur. J. Phys.* **38** (2017), 065101.

[79] J. M. Rubi, D. Bedeaux, and S. Kjelstrup. “Thermodynamics for Single-Molecule Stretching Experiments”. *J. Phys. Chem. B.* **110** (2006), 12733–12737.

[80] E. Bering, S. Kjelstrup, D. Bedeaux, J. M. Rubi, and A. S. de Wijn. “Entropy Production beyond the Thermodynamic Limit from Single-Molecule Stretching Simulations”. *J. Phys. Chem. B.* **124** (2020), 8909–8917.

[81] E. Bering, D. Bedeaux, S. Kjelstrup, A. S. de Wijn, I. Latella, and J. M. Rubi. “A Legendre–Fenchel Transform for Molecular Stretching Energies”. *Nanomaterials.* **10** (2020), 2355.

[82] O. Galteland, E. Bering, K. Kristiansen, D. Bedeaux, and S. Kjelstrup. “Legendre-Fenchel transforms capture layering transitions in porous media”. *Nanoscale Adv.* (2022).

[83] M. Kulmala, H. Vehkamäki, T. Petäjä, M. Dal Maso, A. Lauri, V.-M. Kerminen, W. Birmili, and P. McMurry. “Formation and growth rates of ultrafine atmospheric particles: a review of observations”. *J. Aerosol Sci.* **35** (2004), 143–176.

[84] H. Singh and R. S. Myong. “Critical Review of Fluid Flow Physics at Micro- to Nano-scale Porous Media Applications in the Energy Sector”. *Adv. Mater. Sci. Eng.* **2018** (2018), 9565240.

[85] P. Sudarsanam, E. Peeters, E. V. Makshina, V. I. Parvulescu, and B. F. Sels. "Advances in porous and nanoscale catalysts for viable biomass conversion". *Chem. Soc. Rev.* **48** (2019), 2366–2421.

[86] J. W. Gibbs. *The Scientific Papers of J. Willard Gibbs*. London: Ox Bow Press, 1993.

[87] T. L. Hill. *Thermodynamics of Small Systems*. New York: Dover Publications, 1994.

[88] A. Reindl, M. Bier, and S. Dietrich. "Implications of interface conventions for morphometric thermodynamics". *Phys. Rev. E.* **91** (2015), 022406.

[89] S. Stølen, T. Grande, and N. L. Allan. *Chemical Thermodynamics of Materials - Macroscopic and Microscopic Aspects*. Chichester: John Wiley Sons Ltd., 2004.

[90] I. E. Paganini, R. L. Davidchack, B. B. Laird, and I. Urrutia. "Properties of the hard-sphere fluid at a planar wall using virial series and molecular-dynamics simulation". *J. Chem. Phys.* **149** (2018), 014704.

[91] T. L. Hill. "Thermodynamics of Small Systems". *J. Chem. Phys.* **36** (1962), 3182–3197.

[92] B. A. Strøm, D. Bedeaux, and S. K. Schnell. "Adsorption of an ideal gas on a small spherical adsorbent". *Nanomaterials.* **11** (2021), 431.

[93] O. Galteland, D. Bedeaux, B. Hafskjold, and S. Kjelstrup. "Pressures Inside a Nano-Porous Medium. The Case of a Single Phase Fluid". *Front. Phys.* **7** (2019), 60.

[94] M. T. Rauter, O. Galteland, M. Erdős, O. A. Moultos, T. J. Vlugt, S. K. Schnell, D. Bedeaux, and S. Kjelstrup. "Two-phase equilibrium conditions in nanopores". *Nanomaterials.* **10** (2020), 608.

[95] O. Galteland, D. Bedeaux, and S. Kjelstrup. "Nanothermodynamic description and molecular simulation of a single-phase fluid in a slit pore". *Nanomaterials.* **11** (2021), 165.

[96] V. Bråten, D. Bedeaux, Ø. Wilhelmsen, and S. K. Schnell. "Small size effects in open and closed systems: What can we learn from ideal gases about systems with interacting particles?" *J. Chem. Phys.* **155** (2021), 244504.

[97] O. Galteland, M. T. Rauter, M. S. Bratvold, T. T. Trinh, D. Bedeaux, and S. Kjelstrup. "Local thermodynamic description of isothermal single-phase flow in porous media". *arXiv preprint arXiv:2203.02334* (2022).

[98] M. J. Uline, D. W. Siderius, and D. S. Corti. "On the generalized equipartition theorem in molecular dynamics ensembles and the microcanonical thermodynamics of small systems". *J. Chem. Phys.* **128** (2008), 124301.

[99] R. B. Shirts, S. R. Burt, and A. M. Johnson. “Periodic boundary condition induced breakdown of the equipartition principle and other kinetic effects of finite sample size in classical hard-sphere molecular dynamics simulation”. *J. Chem. Phys.* **125** (2006), 164102.

[100] T. Niiyama, Y. Shimizu, T. R. Kobayashi, T. Okushima, and K. S. Ikeda. “Effect of translational and angular momentum conservation on energy equipartition in microcanonical equilibrium in small clusters”. *Phys. Rev. E.* **79** (2009), 051101.

[101] D. Frenkel and B. Smit. *Understanding Molecular Simulation*. Second Edition. Academic Press, 2002.

[102] M. R. Shirts, E. Bair, G. Hooker, and V. S. Pande. “Equilibrium Free Energies from Nonequilibrium Measurements Using Maximum-Likelihood Methods”. *Phys. Rev. Lett.* **91** (2003), 140601.

[103] M. R. Shirts. “Simple quantitative tests to validate sampling from thermodynamic ensembles”. *J. Chem. Theory Comput.* **9** (2013), 909–926.

Articles

Article I

V. Bråten, Ø. Wilhelmsen and S. K. Schnell

Chemical Potential Differences in the Macroscopic Limit from Fluctuations in Small Systems,

Journal of Chemical Information Modeling **61**:2 840-855 (2021).
DOI: 10.1021/acs.jcim.0c01367

Article I

Article I

JCIM JOURNAL OF CHEMICAL INFORMATION AND MODELING

ACS AUTHORCHOICE

pubs.acs.org/jcim Article

Chemical Potential Differences in the Macroscopic Limit from Fluctuations in Small Systems

Vilde Bråten, Øivind Wilhelmsen, and Sondre Kvalvåg Schnell*

Cite This: J. Chem. Inf. Model. 2021, 61, 840−855 Read Online

ACCESS | Metrics & More | Article Recommendations | Supporting Information

ABSTRACT: We present a new method for computing chemical potential differences of macroscopic systems by sampling fluctuations in small systems. The small system method, presented by Schnell et al. [Schnell et al., J. Phys. Chem. B, 2011, **115**, 10911], is used to create small embedded systems from molecular dynamics simulations, in which fluctuations of the number of particles are sampled. The sampled fluctuations represent the Boltzmann distributed probability of the number of particles. The overlapping region of two such distributions, sampled from two different systems, is used to compute their chemical potential difference. Since the thermodynamics of small systems is known to deviate from the classical thermodynamic description, the particle distributions will deviate from the macroscopic behavior as well. We show how this can be utilized to calculate the size dependence of chemical potential differences and eventually extract the chemical potential difference in the thermodynamic limit. The macroscopic chemical potential difference is determined with a relative error of 3% in systems containing particles that interact through the truncated and shifted Lennard-Jones potential. In addition to computing chemical potential differences in the macroscopic limit directly from molecular dynamics simulation, the new method provides insights into the size dependency that is introduced to intensive properties in small systems.

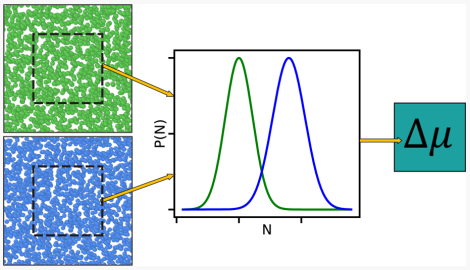

INTRODUCTION

Properties available from molecular simulations (MD) can be sorted in two categories: mechanical properties and thermal properties.[1] The difference between these comes from how they are connected to the partition function. Mechanical properties are related to the derivative of the partition function, while the thermal properties are functions of the partition function itself.[1] Examples of mechanical properties are therefore the internal energy, pressure, and heat capacity, while examples of thermal properties are Gibbs energy, Helmholtz energy, and chemical potential.

The mechanical properties can be expressed as averages of functions of phase space coordinates and can therefore be calculated directly from the simulation trajectory.[2] The thermal properties cannot be expressed as such averages. This is because they are related to the complete volume of phase space accessible to the system, which can normally not be sampled in MD.[3] In order to calculate thermal properties, one must resort to other alternatives than simply analyzing the simulation trajectory. For the Gibbs energy or Helmholtz energy, there are options such as thermodynamic integration[4−8] or umbrella sampling,[9−11] while a common method for computation of chemical potential is Widom's particle insertion method.[2,12,13] Another route to compute chemical potentials is found in the overlapping distribution methods (ODMs).

The term ODM can be used to describe any method that can extract thermodynamic properties from the overlap between probability distributions of two different systems.[2] The distributions represent the Boltzmann distribution of the fluctuating properties of the system, which are ensemble-dependent. In the canonical ensemble, where the number of particles, volume, and temperature are constant, the energy will fluctuate. In the isobaric−isothermal ensemble, where the number of particles, pressure, and temperature are fixed, there will be fluctuations in volume and energy. Grand canonical systems, with constant chemical potential, volume, and temperature will have fluctuations in energy and in the number of particles. Naturally, the properties available from the distributions will depend on the ensemble used in the simulation.

For canonical systems, the Helmholtz energy difference is accessible from the overlapping region of two energy distributions. One version of the ODM that utilizes this is

Received: November 25, 2020
Published: February 10, 2021

https://dx.doi.org/10.1021/acs.jcim.0c01367
J. Chem. Inf. Model. 2021, 61, 840−855

the acceptance ratio method presented by Bennett,[14] who presented strategies for estimating the difference in Helmholtz energy between two canonical systems. Shirts et al.[15] later showed that it was possible to derive the same expressions from maximum likelihood arguments. Frenkel and Smit[2] also illustrated how the method can be used to calculate excess chemical potentials. This is achieved by considering two canonical systems where the first contains N particles, and the second contains $N - 1$ particles and one ideal gas particle. The Helmholtz energy difference between these systems corresponds to the change in Helmholtz energy in the first system when one of its N particles is transformed to an ideal gas particle. Hence, applying the ODM to the energy distributions in these two systems returns the excess chemical potential of the first system.

Even though the most frequent use of the method is calculations of properties in the canonical ensemble,[16,17] it is not restricted to this. Bennett[14] showed that it is possible to develop analogous expressions for other ensembles. Recently, Shirts[18] introduced yet another convenient aspect of the overlapping distributions by using them to determine whether the desired thermodynamic ensemble is properly sampled in the simulations. This ensemble consistency test can be applied to molecular dynamics as well as Monte Carlo (MC) simulations,[19,20] and it can be used to evaluate simulations performed in the canonical ensemble, isobaric−isothermal ensemble, grand canonical ensemble, or the microcanonical ensemble.

Whether the objective is to use the distributions to calculate thermal properties or to test for ensemble consistency, the starting point is the same: the statistical mechanical connection that exists for every ensemble between its corresponding energy state function and the partition function.

In this work, we will show how the ODM can be used to extract the chemical potential difference of two small grand canonical systems, directly from two MD simulations at different densities. These small systems are generated by placing subsystems at random locations inside the total simulation boxes. The total simulation box can be canonical, microcanonical, or isobaric−isothermal and works as a grand canonical reservoir for the small embedded systems. Hence, fluctuations in the number of particles that arise in the subsystems will not depend on the ensemble of the MD simulation box. These fluctuations represent the Boltzmann distributions of the number of particles in small grand canonical systems. The chemical potential difference between two embedded systems is then available from the overlapping region of two such distributions.

It is also possible to utilize the chemical potential differences in the subsystems to obtain the chemical potential difference for the total simulation boxes, that is, in the macroscopic limit. When investigating these distributions, one must keep in mind that they are calculated in small nonperiodic systems, which means that their thermodynamic properties will deviate from the classical macroscopic behavior. We will therefore use the thermodynamics for small systems developed by Hill.[21,22] Combined with the proper scaling laws, we are able to obtain the chemical potential difference in the thermodynamic limit.

The idea of using finite-size scaling analysis to obtain thermodynamic properties was explored already in the eighties by Binder's block analysis method.[23] In his work, Binder investigated how the probability distributions of the Ising lattice model depend on system size, which in turn was utilized to calculate the magnetic susceptibility in the thermodynamic limit.[23,24] Binder also extracted values of root-mean-square magnetization and internal energy and explored the possibility of identifying the critical temperature and the critical exponents. This application was later investigated for the two-dimensional Lennard-Jones (LJ) system for both one- and two-phase systems.[25−27]

The method used to create the subsystems in this work is known as the small system method (SSM), developed by Schnell et al.,[28] and it differs from Binder's block analysis method in the way the subsystems are created. Binder's blocks are created as cubic sections in a grid superimposed on the simulation box, while the SSM creates subsystems by placing them at random locations inside the simulation box. One consequence of this difference is that the shape of the subsystems is not restricted to being cubic.[29]

Binder focused largely on critical phenomena and the method's ability to extract properties in the critical point. Lately, finite-size analysis of subsystems has received more intention in the application to one-phase systems, further from the critical point. It has been used to calculate enthalpies and the thermodynamic factor,[28] partial molar properties,[30] and the isothermal compressibility.[29] For multicomponent systems, the calculation of Kirkwood−Buff integrals[31] has received much attention due to the connection these integrals have to a number of thermodynamic properties.[32−38] One of the properties available through the Kirkwood−Buff integrals is the differential chemical potential, which upon numerical integration can provide insights on how chemical potential change with the density of the system.[34,35] For one-component systems, this can be achieved by investigating the isothermal compressibility.[37,38] The method we propose in this work does not rely on numerical integration since the chemical potential difference is directly available from the two simulations.

To the best of our knowledge, this is the first time an ODM has been used to extract the properties for small systems. We therefore investigate how well it performs for small grand canonical systems with a MC approach before applying it to the systems generated by the SSM.

For macroscopic systems, the chemical potential is known as an intensive property, meaning that it does not depend on the system size. The newly presented method gives insights on how the chemical potential deviates from this intensive behavior when the system becomes small enough. For calculation of chemical potential differences in macroscopic systems, the method will be particularly useful at high densities, where moves that include insertion and deletion of particles become very inefficient.[1,2,39−41] Chemical potentials calculated in finite periodic systems are also known to be rather strongly dependent on size.[13,42,43] This problem is avoided in the method presented here since the macroscopic chemical potential differences are not calculated directly but instead extrapolated to the thermodynamic limit by the use of scaling laws.

THEORY

In the following sections, we present the theoretical background needed for computation of chemical potential differences from fluctuations in small grand canonical systems. The treatment of the thermodynamics of small systems is based on the formalism introduced by Hill.[21] We will explain how it can be used in combination with scaling laws to obtain properties in the thermodynamic limit. We also explain how

https://dx.doi.org/10.1021/acs.jcim.0c01367
J. Chem. Inf. Model. 2021, 61, 840−855

the SSM can be used to extract fluctuation in small systems from molecular dynamics simulations. Lastly, we show how the distributions corresponding to these fluctuations can be used to calculate chemical potential differences.

Thermodynamics for Small Systems. The main difference between small systems and macroscopic systems is usually the surface area-to-volume ratio. Since this ratio is much larger for small systems, the effects of the surface become significant, and the thermodynamic properties can no longer be directly compared to those of macroscopic systems.[21] This becomes clear by studying the system's extensive properties, which for small systems will not be proportional to the volume, but higher-order functions of size and shape. The smallness also introduces a size dependence in the system's intensive properties, which is not present for macroscopic systems. As a result, macroscopic thermodynamic equations cannot be used to describe the properties in small systems.[21,22]

The formalism developed by Hill[21] provides modified versions of the macroscopic thermodynamic equations that can be applied to small systems. In this derivation, Hill[21] considered a collection of $\mathcal{N}$ small systems that are all equivalent, distinguishable, and independent. The ensemble they make up together can therefore be considered macroscopic, and its differential energy can be expressed as

$$\mathrm{d}U = T\,\mathrm{d}S - p\,\mathrm{d}V + \sum_{i=1}^{n} \mu_i \mathrm{d}N_i + \mathcal{E}\,\mathrm{d}\mathcal{N} \tag{1}$$

where U is the system's energy, T is the temperature, S is the entropy, p is the pressure, V is the system's volume, μ_i is the chemical potential of component i, and N_i is the number of particles of component i in the system. The property $\mathcal{E}$ is called the subdivision potential and is represented by different functions for different ensembles. In the grand canonical ensemble, it is given by $\mathcal{E}^{\mathrm{GC}} = (p - \hat{p})V$. The property $\hat{p}$ is known as the integral pressure, which is related to the differential pressure p through the following equation

$$\begin{aligned} p(\mu, V, T) &= \left(\frac{\partial \hat{p}(\mu, V, T)V}{\partial V}\right)_{T,\mu} \\ &= \hat{p}(\mu, V, T) + V\left(\frac{\partial(\hat{p}(\mu, V, T)}{\partial V}\right)_{T,\mu} \end{aligned} \tag{2}$$

The second term in the above equation is only of significant magnitude when the system is small, which means that in the thermodynamic limit, $\hat{p}(\mu,V,T) = p(\mu,V,T)$.

The two pressures are connected to different types of mechanical work that arise from volume change of the total ensemble, but the mechanisms behind these are not equal. The differential pressure, p, is the one associated with the pressure of a macroscopic system. The volume change mechanism connected to p must therefore be equal to that of a macroscopic system. This volume change is defined as the change in total volume when changing the volume of all the small system replicas. This represents the work done on the surroundings by the volume change and will be the same whether the systems in the ensemble are small or macroscopic. The work connected to the integral pressure, $\hat{p}$, however, is unique for small systems. In this volume change, the volumes of the small systems are kept constant, while the volume of the total system is changed by adding one replica to the ensemble of small systems. This is done while keeping the entropy and number of particles in the total collection of small systems constant, which means that these properties must be redistributed over all the small systems, including the added replica.

This explains the significance of the different terms in eq 2, but in order to understand its origin, we must look to the connection between the partition function and the energy state function of the system. For a system in the grand canonical ensemble, this is equal to the contribution to the internal energy from the pressure−volume term. In small grand canonical systems, Hill[21] showed that this relation becomes

$$\hat{p}(\mu, V, T)V = k_{\mathrm{B}} T \ln \Xi(\mu, V, T) \tag{3}$$

where k_{B} represents the Boltzmann constant and Ξ is the grand canonical partition function. The small system version of the familiar equations for the entropy, pressure, and number of particles in a grand canonical ensemble is

$$\begin{aligned} S(\mu, V, T) &= \left(\frac{\partial \hat{p}(\mu, V, T)V}{\partial T}\right)_{V,\mu}, \\ p(\mu, V, T) &= \left(\frac{\partial \hat{p}(\mu, V, T)V}{\partial V}\right)_{T,\mu}, \\ \langle N\rangle(\mu, V, T) &= \left(\frac{\partial \hat{p}(\mu, V, T)V}{\partial \mu}\right)_{T,V} \end{aligned} \tag{4}$$

where the brackets denote average values.

Size- and Shape-Dependent Properties. When investigating properties of small systems, it is convenient to use another aspect introduced by Hill.[21] He argued that a property's small size contribution can be treated as an excess property, meaning that all dependent properties of a system can be split into a macroscopic contribution and the contribution from finite-size effects. A general property, A, can therefore be expressed as

$$A = A^{\infty} + A^{\mathrm{small}} \tag{5}$$

where A^{∞} is the macroscopic contribution and A^{small} is the finite-size contribution to A. In the thermodynamic limit, A^{small} becomes vanishingly small compared to A^{∞}. Consequently, for macroscopic systems, the property A can be regarded as represented by A^{∞} only, and macroscopic thermodynamics is applicable. For small systems, A^{small} becomes significant, which makes A depend on the system's size and shape, and the macroscopic thermodynamic equations are no longer directly applicable.

In Hill's[21] treatment of small systems, only the dependent properties of the system have a finite-size contribution. These are the properties that are not fixed by the system's ensemble. For a grand canonical system, these are given in eq 4 and can be expressed as

$$\begin{aligned} S(\mu, V, T) &= S^{\infty}(\mu, V, T) + S^{\mathrm{small}}(\mu, V, T), \\ p(\mu, V, T) &= p^{\infty}(\mu, V, T) + p^{\mathrm{small}}(\mu, V, T), \\ \langle N\rangle(\mu, V, T) &= \langle N\rangle^{\infty}(\mu, V, T) + \langle N\rangle^{\mathrm{small}}(\mu, V, T) \end{aligned} \tag{6}$$

A theorem presented by Hadwiger[44] provides more insights into the meaning of the different terms in the above equations. According to this theorem, any functional of a system that is translationally invariant, additive, and continuous can be

https://dx.doi.org/10.1021/acs.jcim.0c01367
J. Chem. Inf. Model. 2021, 61, 840−855

written as a sum of four contributions, where one is a constant and the other three are proportional to V, $V^{2/3}$, and $V^{1/3}$, respectively.[45] The property A can therefore be written as

$$A(V) = Va^{\infty} + \alpha V^{2/3}a^{s} + \beta V^{1/3}a^{e} + \gamma a^{c} \quad (7)$$

where α, β, and γ are geometric factors that depend on the shape of the system. In the first term, a^{∞} can be understood as the density of A in the thermodynamic limit $A^{\infty} = Va^{\infty}$, which means that the remaining terms represent A^{small}. Equations showing the same size and shape dependence have been derived independently and shown to apply to fluids of hard disks,[46] LJ particles,[47] and Weeks−Chandler−Anderson particles.[48]

Hadwiger's theorem can only be used if A is extensive, but it is possible to define an alternative equation that applies to intensive properties by dividing eq 7 by the volume

$$a(V) = \frac{A(V)}{V} = a^{\infty} + \frac{\alpha}{L}a^{s} + \frac{\beta}{L^{2}}a^{e} + \frac{\gamma}{L^{3}}a^{c} \quad (8)$$

where we have defined the characteristic length $L = V^{1/3}$.

Small System Method. For both macroscopic systems and systems with finite-size effects, knowledge about the fluctuations in energy and number of particles can give access to a large number of thermodynamic properties. The accessibility of these fluctuations depends on the simulation method. Systems with a fluctuating number of particles can normally not be created with MD simulations. In order to simulate grand canonical systems, one can resort to MC simulations, but these are computationally expensive, especially for systems at higher particle densities. The SSM developed by Schnell et al.[28] offers an alternative way of creating systems with a fluctuating number of particles. In this approach, the grand canonical systems are not simulated directly but instead created by sampling subvolumes from a larger reservoir. The reservoir is typically a large simulation box, which can be simulated using MD or MC. An ensemble average of such a subsampled system is created by placing control volumes of equal size at different locations inside the simulation box.

Some thermodynamic properties have a direct connection to the fluctuations in the number of particles. The origin of these connections is the identity of the second moments of the probability distribution of a grand canonical ensemble

$$(k_{B}T)^{2}\left(\frac{\partial^{2}\ln \Xi(\mu, V, T)}{\partial \mu^{2}}\right)_{T,V} = \langle N^{2}\rangle - \langle N\rangle^{2} \quad (9)$$

These second moments are in turn connected to thermodynamic quantities such as the thermodynamic factor, the isothermal compressibility, the partial enthalpy, and the partial internal energy.[49] The fluctuations sampled from the subsystem can therefore provide access to a variety of thermodynamic properties. However, it must be kept in mind that the subsampled system cannot be regarded as a representation of the bulk due to the nature of its boundaries. The subsampled system is nonperiodic, which means that it will be affected by a significant contribution from the surface. Since the subsystem represents a small system, its statistics will be different from that of an equivalent system with periodic boundaries. Its thermodynamic properties and the connections between them must therefore be treated with the formalism developed by Hill.[21]

Since the subsystems are created from control volumes inside a reservoir, we can create systems for a range of different sizes, as illustrated in Figure 1. By systematically changing the size of the subsystem, one can evaluate how its properties

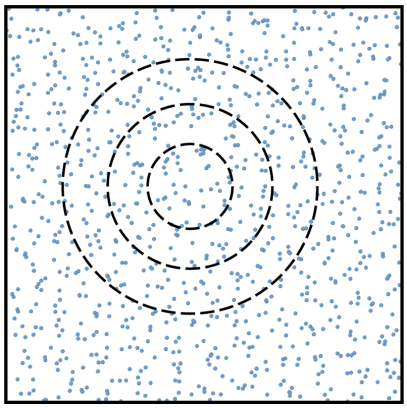

Figure 1. Particle fluctuations are calculated in spherical subsystems inside the total simulation box. The size of the subsystem is gradually increased in order to calculate how the fluctuations change when the size of the system changes.

change with system size. Combined with the equations provided by Hadwiger,[44] the different contributions from the different parts of the system's geometry can be identified (see eq 7). The most popular feature of this method has been its ability to extract the macroscopic contribution, meaning the value of a^{∞}.[28−30,32,48] If the main purpose is to extrapolate the values calculated for the subsystems to the thermodynamic limit, the term corresponding to the contribution from the surface usually provides a sufficient description of the size dependency. As a first approximation, eq 8 can therefore be written as

$$a(V) = a^{\infty} + \frac{\Omega}{V}a^{s} \quad (10)$$

where we have used that $\alpha/L = \Omega/V$ when Ω is the surface of the system. This expression is particularly useful because it is a straight line if $a(V)$ is plotted as a function of the surface area-to-volume ratio of the system it was calculated in. The intersection is then equal to the macroscopic contribution.

When using scaling laws to describe size dependence of thermodynamic properties, it is first important to understand which properties will change with size and how this is affected by the type of the system. One important factor to consider for the subsampled systems in the SSM is that they all have the same average particle density. Equation 6 shows that small grand canonical systems will have a finite-size contribution in the number of particles and therefore also to the particle density. However, if this contribution is nonzero in the subsampled systems, it will not appear in their calculated densities. This is because the sampling approach forces the average density of each subvolume to be equal to the reservoir density. In the following, we will explain that if such a size dependency does exist, it will appear in the values of the chemical potentials of the subsystems.

It is important to point out that even though all subsampled systems of different sizes have the same particle density, each individual subsampled system does not have a constant

https://dx.doi.org/10.1021/acs.jcim.0c01367
J. Chem. Inf. Model. 2021, 61, 840−855

density. The subsampled systems can exchange particles and energy with the surroundings, and they maintain a constant chemical potential due to their connection to the particle reservoir represented by the simulation box. However, the chemical potential does not necessarily remain fixed when the size of the subsystem is changed.

This can be illustrated by considering a general case. We consider two small grand canonical systems with equal average particle density, n, and temperature, but different volumes

$$\langle n_1 \rangle = \langle n_2 \rangle, \qquad T_1 = T_2, \qquad V_1 \neq V_2 \tag{11}$$

Since the systems are grand canonical, their densities can according to eq 5 be written as a sum of the macroscopic contribution and a contribution from the small size

$$n_1^{\infty} + n_1^{\text{small}} = n_2^{\infty} + n_2^{\text{small}} \tag{12}$$

From eq 8, we see that n^{small} should depend on the system size. Since the two systems considered here have different sizes, their small size contribution are likely to differ, giving $n_1^{\text{small}} \neq n_2^{\text{small}}$. According to eq 12, the macroscopic contribution in the two systems will not be equal either, giving $n_1^{\infty} \neq n_2^{\infty}$.

The macroscopic particle densities, n^{∞}, do not depend on size, but they depend on the chemical potential and temperature. Since the temperature is the same in the two systems, a difference in n^{∞} must arise from a difference in chemical potential. This means that since n_1^{∞} and n_2^{∞} are different, the two differently sized systems considered here must also have different chemical potentials, that is, $\mu_1 \neq \mu_2$. Equation 12 is therefore more correctly expressed as

$$\begin{aligned} &n^{\infty}(\mu_1, T) + n^{\text{small}}(\mu_1, V_1, T) \\ &\quad = n^{\infty}(\mu_2, T) + n^{\text{small}}(\mu_2, V_2, T) \end{aligned} \tag{13}$$

This shows that keeping the particle density equal in all the differently sized subvolumes imposes a difference in their chemical potentials.

ODMs for Small Systems. We will now show how combining fluctuations calculated from two independent systems can be used to extract thermodynamic properties.

The fluctuations in the number of particles represent the Boltzmann distributed probability of finding a certain number of particles in the system. In a grand canonical system, this is given by

$$P(N|\mu, V, T) = \frac{Q(N, V, T)\exp(\beta\mu N)}{\Xi(\mu, V, T)} \tag{14}$$

where $\beta = 1/k_B T$ and Q represents the canonical partition function.

This distribution is unique for a given set of chemical potential, volume, and temperature. This means that if one of these is changed, the total distribution will change. This feature is utilized by a number of different methods, which all can be placed in the category of ODMs.[2,14−18] Common for all of these is that they extract thermodynamic properties from the overlapping region of two distributions sampled from two different states. In this region, the ratio of the two probability distributions gives access to thermodynamic properties through the connection between their respective partition functions and their corresponding energy state function.

Following the procedure of Shirts,[18] we derive an expression for the ratio of two probability distributions of the number of particles, corresponding to two different grand canonical systems. Moving forward, it must be kept in mind that the goal is to derive a method that can be applied to small systems. This means that we must use equations that take the small system effects into account. Hill's[21] equations are convenient because they are valid for small systems and for macroscopic systems. This formalism does not require a separate set of equations in the treatment of small systems since all of Hill's equations reduce to the corresponding macroscopic identities when the systems become large enough.

Starting from eq 14, we see that Q is a function of N but not of μ. This means that it is possible to perform two simulations at different chemical potentials but otherwise identical parameters (meaning T and V) and calculate the ratio of their probability distributions as

$$\frac{P(N|\mu_2, V, T)}{P(N|\mu_1, V, T)} = \exp(\beta\mu_2 N - \beta\mu_1 N)\frac{\Xi(\mu_1, V, T)}{\Xi(\mu_2, V, T)} \tag{15}$$

where the canonical partition function cancels because it has no direct dependence on μ. Taking the natural logarithm of this equation and inserting eq 3 gives

$$\ln \frac{P(N|\mu_2, V, T)}{P(N|\mu_1, V, T)} = -\beta\Delta\hat{p}V + \beta\Delta\mu N \tag{16}$$

This expression is in the form of a straight line, $\alpha_0 + \alpha_1 N$, if the logarithm of the ratio of the probability distributions is plotted as a function of the number of particles. The values of $\Delta\mu = \mu_2 - \mu_1$ and $\Delta\hat{p} = \hat{p}_2 - \hat{p}_1$ are then readily available since the slope of this line is $\alpha_1 = \beta\Delta\mu$, while the intersection with the y-axis represents $\alpha_0 = -\beta\Delta\hat{p}V$.

The calculation of the distributions is straightforward since the only required information is the number of particles in the systems throughout the simulations. The probabilities can also easily be visualized by binning the particle numbers in histograms. One can even calculate the ratio of the probability distributions directly from the histograms in order to visually inspect that it forms a straight line. Another alternative which is more robust is to use the maximum likelihood approach.[15] Using this method, the slope can be found from the maximum likelihood expressions for the ratio of the probability distributions. For the grand canonical ensemble, the maximum likelihood expression becomes

$$\begin{aligned} \ln L(\alpha|\text{data}) = &\sum_{i=1}^{N_1} \ln f(-\alpha_0 - \alpha_1 N_i) \\ &+ \sum_{j=1}^{N_2} \ln f(\alpha_0 + \alpha_1 N_j) \end{aligned} \tag{17}$$

where $f(x)$ is the Fermi function $f(x) = [1 - \exp(-x)]^{-1}$. The expression only has one maximum, which means that it will always converge, and it can be solved by any standard technique for multidimensional optimization.[18]

The equations presented above can be used to calculate the difference in pressure and chemical potential for two grand canonical systems with different chemical potentials but identical volume and temperature. The subsystems generated by the SSM are examples of such systems. It is possible to investigate the size dependence of $\Delta\mu$ and $\Delta\hat{p}$by sampling subsystems over the same size range in two reservoirs at different chemical potentials. In addition, eq 10 can be used to

https://dx.doi.org/10.1021/acs.jcim.0c01367
J. Chem. Inf. Model. 2021, 61, 840−855

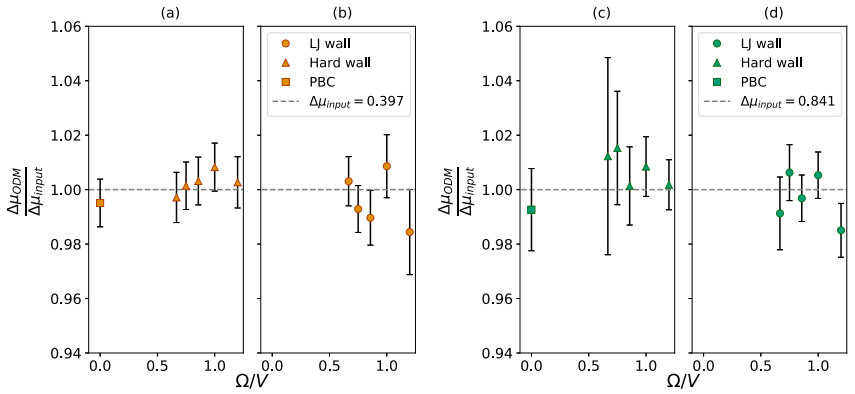

Figure 2. Chemical potential difference calculated from the ODM relative to the input value for different system sizes. Ω/V corresponds to the surface area-to-volume ratio. The input value of $\Delta\mu$ is represented by the dashed line, while the symbols show the results from the ODM. The circles represent systems with LJ potential on the boundaries, while the triangles represent systems enclosed by a hard wall. The squares represent PBCs, which gives the value in the macroscopic limit. (a,b) corresponds to the input $\Delta\mu = 0.397$, while (c,d) corresponds to $\Delta\mu = 0.841$. All error bars denote two standard deviations.

identify the values in the macroscopic limit as $\Delta\hat{p}^{\infty} = \Delta p^{\infty}$ and $\Delta\mu^{\infty}$.

SIMULATION DETAILS

All systems considered in this work consist of LJ particles that interact via the truncated and shifted potential, with the cutoff radius at 2.5. Unless otherwise specified, all values are presented in reduced units. The critical point of the truncated and shifted LJ system is at $T = 1.086$, $p = 0.101$, and $\rho = 0.319$.[50] In all simulations, a temperature of $T = 1.5$ is used.

Four types of systems are investigated:

1. Small grand canonical system with nonperiodic, hard walls. This is simulated using an in-house MC code.
2. Small grand canonical systems with nonperiodic walls, interacting with the particles according to the LJ potential. This is simulated using and in-house MC code.
3. Grand canonical systems with periodic boundary conditions (PBCs). This is simulated using and in-house MC code.
4. Small subsampled systems generated from a large reservoir simulated using the MD code LAMMPS.[51]

The first three system types are used to investigate how well the ODM performs for small systems, compared to systems with periodic boundaries. For these simulations, we use an in-house MC code, with input chemical potentials $\mu = 0.33$, $\mu = 0.73$, and $\mu = 1.2$. For systems of type 3, periodic boundaries are used to remove finite-size effects in order to obtain the system's bulk properties. For the small systems, type 1 and type 2, the boundaries are treated in a way that introduces a significant contribution from finite-size effects. This is achieved by two different approaches. Systems of type 1 have hard walls, which means that there is no explicit interaction between the particles and the wall, but MC moves that attempt to move a particle outside the simulation box are rejected. Systems of type 2 have a LJ potential with a cutoff distance equal to 1 on the boundaries. This means that any particle within a distance $r_c^{wall} = 1$ from one of the boundaries interacts with the wall according to the LJ potential. All grand canonical MC systems are cubic, and five different sizes are considered for the small systems, $L = 5$, $L = 6$, $L = 7$, $L = 8$, and $L = 9$, while the periodic system has a size of $L = 9$.

The fourth system type is used in the combination of the SSM and ODM to calculate how the chemical potential difference changes with the system size. The SSM reservoirs are created from molecular dynamics simulations in the *NVT* ensemble using the open source code LAMMPS.[51] The system's configuration is stored from the trajectory every 50 time steps from a simulation with a total of one million time steps. For each configuration, 100 randomly positioned points are used to position the center of the small subsystems, giving a total of 2×10^6 samples for each small system volume.

The subvolumes investigated are either spherical or cubic and centered at randomly chosen points, $p_c = (x_c, y_c, z_c)$. All particles with position $p_p = (x_p, y_p, z_p)$ satisfying $(x_p - x_c)^2 + (y_p - y_c)^2 + (z_p - z_c)^2 \leq R^2$ are placed inside the sphere of radius R. For the cubic system, the conditions of the particles' position become $(x_p - x_c) \leq L/2$, $(y_p - y_c) \leq L/2$, and $(z_p - z_c) \leq L/2$. All particles satisfying these three conditions are placed inside the cubic small system of box length L. We investigate 200 differently sized small systems with sizes increasing linearly with the reciprocal radius or reciprocal box length.

One of the conditions for the SSM to work properly is that the investigated state is sufficiently far from the critical point. This is because fluctuations become very long ranging close to the critical point and can therefore not be used to calculate properties accurately.[52] The simulations are therefore carried out at a temperature of $T = 1.5$.

A second condition for the SSM to give reliable results is that the differently sized subvolumes display a definitive linear region as a function of inverse system size. This means that the simulation box used as the reservoir must be large enough to sample systems in this region. We therefore use cubic simulation boxes containing 27,000 particles at three different number densities, $\rho = 0.70$, $\rho = 0.72$, and $\rho = 0.74$. For these three densities, the macroscopic chemical potential is calculated with the Widom[12] particle insertion method using

https://dx.doi.org/10.1021/acs.jcim.0c01367
J. Chem. Inf. Model. 2021, 61, 840−855

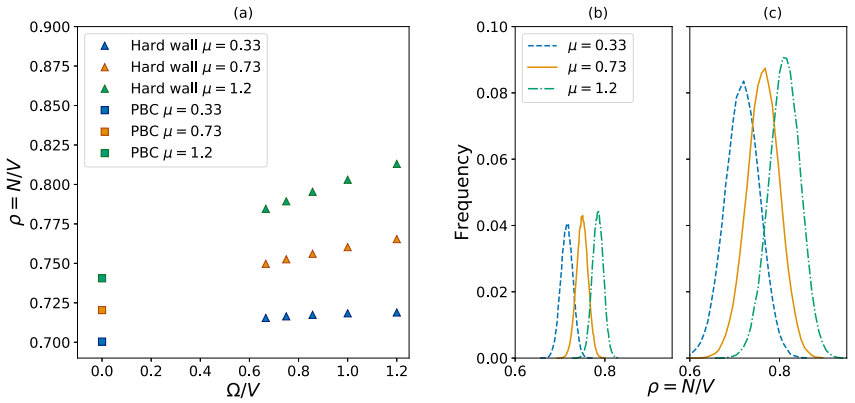

Figure 3. (a) shows how the density in a system enclosed by a hard wall changes with the surface-to-volume ratio when the chemical potential and temperature is kept constant. The triangles represent the hard wall systems, while the squares represent PBCs, which gives the value in the macroscopic limit. (b) shows distributions in density for the largest system, $L = 9$, while (c) shows the one for the smallest system, $L = 5$.

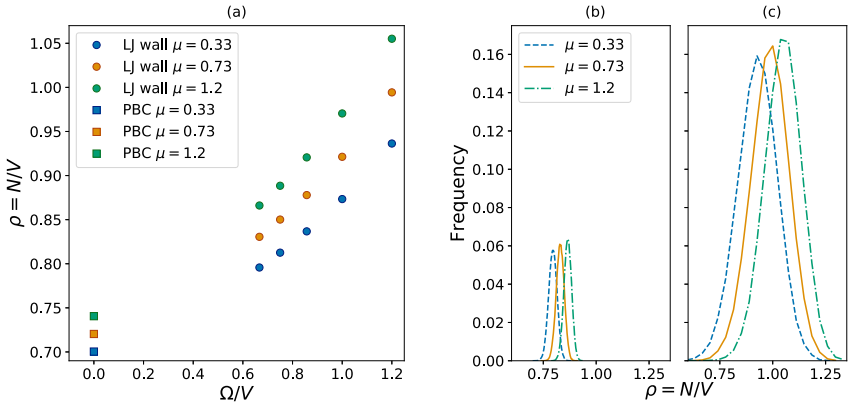

Figure 4. (a) shows how the density in a system enclosed by a wall with a LJ potential changes with the surface-to-volume ratio when the chemical potential and temperature are kept constant. The circles represent the LJ wall systems, while the squares represent PBCs, which gives the value in the macroscopic limit. (b) shows distributions in density for the largest system, $L = 9$, while (c) shows the one for the smallest system, $L = 5$.

an in-house MC code and cross-checked with the TREND equation of state (EOS) provided by Thol et al.[50]

RESULTS

The purpose of the first section of the results is to investigate the performance of the ODM in small systems compared to how well it performs in a periodic system. Two small grand canonical systems with the same size and temperature but different chemical potentials will have different size effects. We shall investigate whether this will influence the results from the ODM. This section also elaborates on how the density should be calculated in small systems.

The second section contains a description on how the SSM is combined with the ODM to compute the size dependence of chemical potential differences. This includes a guide on how to choose the sizes of the subsampled systems in order to achieve an accurate extrapolation to the thermodynamic limit.

ODM for Grand Canonical MC Systems. In order to evaluate how well the combination of the SSM and ODM works, we must first evaluate how well the ODM works for small and large systems. This is performed by using the ODM to calculate the chemical potential difference in different types of grand canonical MC systems. The difference between the system types is determined by the way its boundaries are treated. The values of $\Delta\mu$ are calculated by using the maximum likelihood version of the ODM, meaning that eq 17 is applied to the particle numbers calculated from two simulations of grand canonical MC systems. Since μ is one of the input values of a grand canonical MC simulation, the true value of $\Delta\mu$ corresponds to the difference between these two input values.

From the three absolute values of μ, two values of $\Delta\mu$ are calculated: between the two states with the lowest values of μ and between the lowest and the highest values of μ. The standard deviations are computed from 500 bootstrap samples of the total data set. Figure 2 shows the results from applying the ODM to the system with PBC and to the two types of small systems. Figure 2a,b corresponds to $\Delta\mu = 0.397$, while Figure 2c,d corresponds to $\Delta\mu = 0.841$. The results are shown

https://dx.doi.org/10.1021/acs.jcim.0c01367
J. Chem. Inf. Model. 2021, 61, 840−855

as a function of the surface area-to-volume ratio, which is proportional to the inverse system size. This means that the largest systems are found to the left in the figures. The results from the periodic systems represent the macroscopic values and are therefore placed at $\Omega/V = 0$. The PBC values are only shown in Figure 2a,c since $\Delta\mu$ in both the hard wall system and the LJ wall system approaches the same value in the macroscopic limit.

The values of $\Delta\mu$ calculated from the ODM show no size dependence for any of the systems considered, and the relative error is below 2% for all systems.

A common criterion for evaluating the accuracy of a method is that its mean value should be within two standard deviations of the true value. Nearly all of the mean values are less than two standard deviations from the true input value; the only exception is the smallest LJ wall system for $\Delta\mu = 0.841$ (Figure 2d). Since this evaluation is very much dependent on the magnitude of the standard deviations, we investigate the origin of their varying magnitudes.

In the following, we shall see that the magnitude of the standard deviations can mainly be attributed to the choice of the two states investigated. Shirts[18] pointed out that if the states are far apart, the overlapping region will be small and there will be too few sampled data points, while if the states are too close, the same distribution is essentially sampled from both systems.

The distance between two sampled distributions is determined by the system's particle densities, which can be size-dependent. The consequence is that this distance for small systems is likely to differ from that of the macroscopic systems. The actual width of the distributions is also likely to change with both size and density. At high densities ($\rho \approx 0.7$), small systems usually have larger relative fluctuations than their corresponding macroscopic system.[28,32,48]

Figures 3 and 4 show that both these effects are present for both types of small systems considered here. Figures 3a and 4a show that the density is size-dependent and that the size dependence varies with the value of μ since higher values of μ give steeper slopes. The result is that the distance between the distributions increases when the systems become smaller. The width of the distributions also changes with the system size. Figures 3b and 4b show the density distributions for the largest systems considered, with a size of $L = 9$. Figures 3c and 4c show the density distributions for the smallest systems considered, with a size of $L = 5$. Both types of small systems show wider distributions for smaller systems.

The fact that both the mean value of the densities and the width of the distributions change with size can explain the variation in magnitude of the standard deviations seen in Figure 2. The largest hard wall system shown in Figure 2c is taken as an example. The distributions corresponding to this system are shown in Figure 3b, where the curves corresponding to the highest and lowest values of μ have almost no overlap. This means that there is very little data to calculate $\Delta\mu$ from, which gives this value of $\Delta\mu$ the largest standard deviation in Figure 2c. When the system becomes smaller, as shown in Figure 3c, the distance between the peaks becomes larger, but at the same time, the distributions become wider. This increases the overlap, which reduces the magnitude of the standard deviations.

We conclude that different factors contribute to the magnitude of the standard deviations in different ways and sometimes cancel. Fortunately, the same factors have no significant effect on the mean values since they all have a relative error below 2%. For the systems considered here, the values of $\Delta\mu$ calculated from the ODM are equally reliable for systems with finite-size effects and for systems with periodic boundaries.

Calculation of the Density in Small Systems with a Wall Potential. When calculating properties that include the system's volume, it is common to use the full volume of the simulation box. For a system with periodic boundaries, this is unproblematic. However, if the system is small and has a wall potential, this choice might introduce errors. The reason for this is that the simulation volume is not always equal to the volume available to the center of masses of the particles. This effect has been discussed in a paper by Reiss and Reguera,[53] where they investigate how neglecting the difference between these volumes can lead to errors in pressures calculated by the virial.

They present results from a simple system consisting of hard spheres with radius ξ inside a spherical simulation volume. The particles interact with the wall such that the center of mass of each particle will never be closer to the wall than a distance equal to the particles' radius ξ. As a result, the movement of the particles is restricted to a smaller volume than the total simulation volume. Since the virial refers to the volume available to the center of masses of the particles, it results in incorrectly computed pressures when the total simulation volume is used.

The same principles apply when the density of a system is calculated. To get a proper representation of the density experienced by the particles, the volume available to their center of masses should be used. For the hard wall system considered in this work, no correction is needed since the particles do not actually interact with the wall. The particles are allowed to move around in the total simulation volume, but every MC move that attempts to move the center of mass of a particle outside the simulation box is rejected.

For the systems with the LJ wall, however, such a correction must be incorporated. For the case considered by Reiss and Reguera,[53] finding the volume available to the particles' center of mass is a trivial task. The radius of the spherical simulation box is simply reduced by ξ. The equivalent distance in the system considered here is the collision radius $\sigma^{\text{wall-particle}}$ between the LJ particles and the LJ wall. This distance is not as rigid as the radius of a hard sphere, but it still gives an indicator of the density experienced by the particles. The densities presented in Figure 4a are therefore calculated by using the corrected box length $L_{\text{corr}} = L - 2\sigma^{\text{wall-particle}}$. They are still plotted as a function of the size of the total simulation box volume, meaning that Ω/V is calculated from the noncorrected L. Since the effect a system's wall potential has on its properties is not the main topic of this work, the density calculations will not be discussed further.

Combining the ODM and SSM. When choosing which system sizes to investigate with the SSM, the most important criterion is that the fluctuations in the subvolumes must represent grand canonical fluctuations. For certain subvolume sizes, this criterion has previously been confirmed by comparing the fluctuations sampled in a closed simulation box to ones computed in subvolumes in true grand canonical reservoirs.[47,48] In this region, the properties must display a clear linear behavior as a function of inverse system size. This means that the total simulation box must be large enough to act as a grand canonical reservoir for the relevant system sizes.

https://dx.doi.org/10.1021/acs.jcim.0c01367
J. Chem. Inf. Model. 2021, 61, 840−855

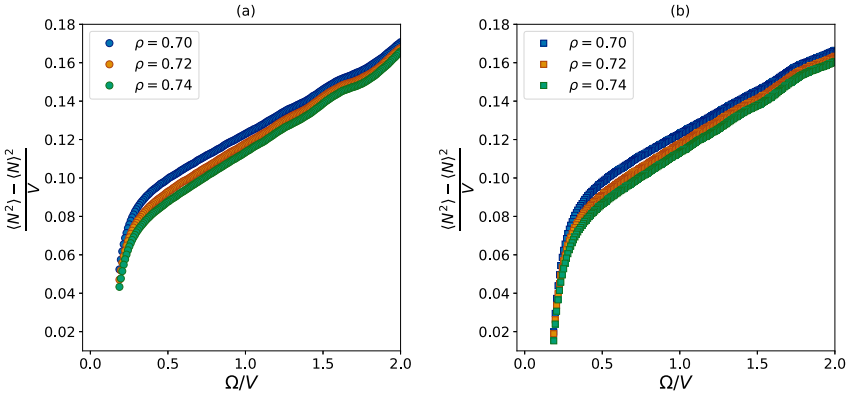

Figure 5. How the value of ν given by eq 18 changes with the surface-to-volume ratio of the subsystem it was calculated in. For the three different curves, the density is constant, equal to that of the reservoir. (a) shows the fluctuations calculated in spherical subvolumes, while (b) shows the fluctuations calculated in cubic subvolumes.

Knowing exactly when the reservoir is large enough is not always a trivial task since this can vary for different types of systems. After calculating the properties, it can also be challenging to identify the linear region. Before evaluating the results of the SSM combined with the ODM, we will therefore present a few tools that can be used to identify the linear region for properties calculated from fluctuations in systems sampled using the SSM. All reported relative errors in the following sections are calculated with respect to the Thol et al.[50] EOS, unless otherwise specified.

How to Identify the Linear Region. Properties in the SSM are calculated from the fluctuations in the number of particles and sometimes also fluctuations in energy.[30] In this work, we will only consider properties calculated from fluctuations in the number of particles.

When the particle fluctuations are affected by size, the properties calculated from these fluctuations share that size dependence. This means that if it is possible to identify the system sizes that display a linear region for the particle fluctuations, other properties are expected to behave linearly within the same region. The fluctuation in the number of particles is represented by the property

$$\nu = \frac{\langle N^2\rangle - \langle N\rangle^2}{V} = \nu^{\infty} + \frac{\Omega}{V}\nu^{s} \tag{18}$$

This scaling law only describes small size contributions proportional to the surface area. This means that size effects originating from other parts of the system's geometry, such as curvature, edges, and corners, are not described. System sizes that have a significant contribution from one of these small size effects should therefore not be included in the extrapolation.

In the other end of the size scale, the fluctuations in the largest subvolumes will be affected by the limited size of the reservoir. A density change in a small subsystem cannot happen without a corresponding density change in the reservoir.[29] This means that as long as the reservoir is closed, it will not act as a proper grand canonical reservoir for the largest subvolumes.[46−48]

In order to identify the linear region, two questions must be answered: (1) What is the smallest volume that is not affected by other finite-size effects than surface area? (2) What is the largest volume that is not affected by the finite size of the reservoir? All volumes in between these limits should be used for extrapolation in combination with scaling laws such as eq 10.

Now, we will show how these questions can be answered for the particle fluctuations calculated in subsystems embedded in simulation boxes at the three different densities considered here ρ = 0.70, ρ = 0.72, and ρ = 0.74. Figure 5 shows the property ν, given by eq 18, as a function of the surface-to-volume ratio.

In order to answer the first of the two questions introduced above, one must look for signs that other finite-size effects than those proportional to the surface area are present.

In Figure 5, the smallest volumes are found at the right side at the highest values of Ω/V. In this region, we observe that the fluctuations display a wavy behavior, which indicates the influence by higher-order terms,[48] as shown in eq 8. Exactly where the wavy region begins depends on the density of the system. This is because higher densities normally cause larger size effects due to a larger number of the particles closer to the surface.[46]

When the aim is to combine the fluctuations in the ODM, a common limit for the linear region should be chosen for the three densities, and it should be based on the behavior of the system with the highest density since this is most influenced by the higher-order terms. The wavy region for the highest density disappears around Ω/V = 1.0 for both spherical and cubic subvolumes, which means that subvolumes with a size corresponding to values of $\Omega/V > 1.0$ should not be included in the extrapolation.

The other end of the linear region, representing the largest subvolumes, can sometimes be more challenging to determine visually. This is because the impact of the closed reservoir is gradually introduced as the systems become larger. Figure 5 shows that the values of the fluctuations all approach zero in this limit because the reservoir is not able to create large enough fluctuations. Visual inspection alone does not give a clear answer to which value of Ω/V the fluctuations start to approach zero. However, it seems to appear at smaller volumes for the system with the lowest density since the fluctuations are

https://dx.doi.org/10.1021/acs.jcim.0c01367
J. Chem. Inf. Model. 2021, 61, 840−855

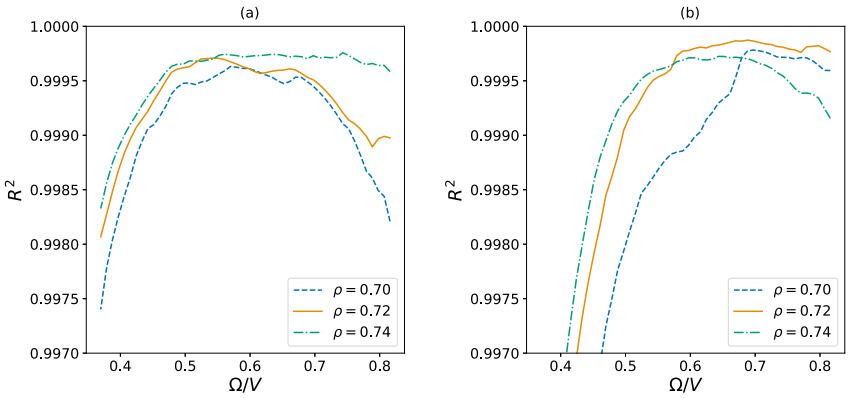

Figure 6. Coefficient of determination, R^2, calculated from a fitted straight line to the data points shown in Figure 5. The values are shown as a function of the surface-to-volume ratio, which means that the value with most included data points is found to the left. The first value of R^2 is calculated based on a linear fit of the data points between $\Omega/V = 1.0$ and $\Omega/V = 0.8$ and then gradually updated as more data points are included in the linear fit. (a) shows the case for spherical subvolumes, while (b) represents cubic subvolumes.

larger here, which might be more challenging for the closed simulation box to satisfy.

Since this limit behaves differently for different types of systems and is less apparent than the wavy region, it is helpful to take advantage of some extra tools to identify it. Some general guidelines for identifying this limit have previously been proposed by Cortes-Huerto et al.[35] and Rovere et al.[27] These limits are based on the size of the subvolumes relative to the volume of the simulation box, V_0, and correspond to $(V/V_0)^{1/3} = 0.3$ and $(V/V_0)^{1/3} = 0.25$, respectively. The most conservative subvolume sizes identified by these suggested limits are based on the system with the highest density ($\rho = 0.74$) since this is the one with the smallest simulation box. For spherical subvolumes, the above limits translate to $\Omega/V \approx 0.49$ and $\Omega/V \approx 0.58$, and for cubic subvolumes, they correspond to $\Omega/V \approx 0.60$ and $\Omega/V \approx 0.72$.

We note that these generalized guidelines do not properly represent the situation investigated here since they allow for larger subvolumes when the simulation box is larger. As explained above, Figure 5 shows that the fluctuations in the largest simulation box are the ones most affected by its finite size. In addition, the suggested limits are based on the behavior of fluctuations in cubic subvolumes. Since it has previously been shown that the location of the linear region is dependent on the shape of the subvolumes,[29,48] it is possible that the predicted limit for a spherical subsystem might not reflect the true location of the linear region. In the following, we therefore investigate two additional tools that can be used directly for the systems under investigation.

One simple option is to fit a straight line to the data points and evaluate at which point the residual, meaning the difference between the fitted line and the actual data points, starts to deviate. The coefficient of determination, also known as R^2, provides an indicator of how well a model describes the data points.[54] If there is complete overlap between the model and the data points, the value of R^2 is equal to 1, while if R^2 is closer to 0, the data points are uncorrelated and cannot be described by the model.

Figure 6 shows how the coefficient of determination changes as a function of data points included in the linear fit. The values of R^2 are shown as functions of the surface area-to-volume ratio, which means that the number of data points included in the linear fit increases to the left in the figure. The first values of R^2 (furthest to the right in Figure 6) are calculated based on a linear fit of the data points between $\Omega/V = 1.0$ and $\Omega/V = 0.8$ in Figure 5. The remaining data points are then included in the fitting one by one, and R^2 is recalculated based on the new linear fit.

We observe that when more data points are included in the fitting, the values of R^2 initially approach 1. However, at one point, the R^2-values start to deviate. This means that we have reached the regime where the simulation box no longer functions as a proper grand canonical reservoir. For systems with the lowest density, this deviating behavior is observed to start for smaller subvolumes, where it is more challenging for reservoirs to satisfy the fluctuations in their subvolumes. We therefore choose the limit based on the curve for the lowest density, which starts to deviate from 1 around $\Omega/V = 0.57$ for the spherical subvolumes and for $\Omega/V = 0.72$ for cubic subvolumes.

A more advanced alternative is to compare the results found by linear fitting to values extracted by an equation that explicitly includes the effect of the finite size of the simulation box. The possibility of including effect in scaling equations has been explored to a large extent in the literature.[35,37,46,48,55,56] One such equation was proposed by Strøm et al.[29] and is given by

$$\nu = \left(1 - \frac{V}{V_0}\right)\nu^{\infty} + \frac{\Omega}{V}\left(1 - \left(\frac{V}{V_0}\right)^{4/3}\right)\nu^{s} \tag{19}$$

This equation is derived by assuming that $\nu = 0$ for $V/V_0 = 1$, which only is valid for subvolumes of the same shape as the reservoir. We apply eq 19 to the fluctuations calculated in the cubic subvolumes with size $0.4 < \Omega/V < 1.0$. The largest subvolumes ($\Omega/V < 0.4$) are not included in the fitting of eq 19 since this resulted decreased accuracy in the values of ν^{∞}. We believe that this can be explained by two factors. The first is that the fluctuations in larger systems usually converge more slowly than their smaller counterparts.[25,26] The second is that fluctuations in subvolumes of a size comparable to the total

https://dx.doi.org/10.1021/acs.jcim.0c01367
J. Chem. Inf. Model. 2021, 61, 840−855

simulation box can become influenced by its periodic boundaries.[47]

The relative errors of ν^{∞} extracted from eq 19 are below 1% for all densities investigated. This means that the values of ν^{∞} obtained from this fit can be compared with the values extracted from the linear fitting and thereby work as a quality check for the limits identified by analyzing R^2. The ν^{∞}-value obtained from eq 19 differs by 4% from the value obtained from linear fitting to spherical volumes in the range $0.57 < \Omega/V < 1.0$ and by 6% from linear fit to cubic subvolumes in the range $0.72 < \Omega/V < 1.0$. It is also possible to systematically vary the limits until we reach the minimum difference between the values extracted from the two types of curve fitting. By changing the lower limit of Ω/V to 0.60 for spherical subvolumes and to 0.78 for cubic subvolumes, this difference is reduced by 1%-point. Changing the limits beyond these values does not decrease the difference further.

We note that an equation similar to eq 19, which also takes the finite size of the simulation box into account, has been developed by Cortes-Huerto et al.[35] and that this equation should work for the same purpose as described above.

Figure 7 shows eq 19 fitted to all fluctuations computed in cubic subvolumes $0.4 < \Omega/V < 1.0$ and the line resulting from linear fitting between $\Omega/V = 0.78$ and $\Omega/V = 1.0$. The two lines show good overlap in the region between the dashed lines, which indicate the region used for the linear fit.

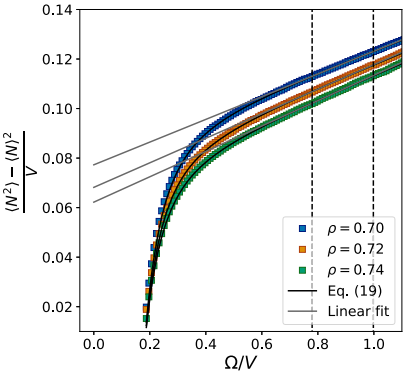

Figure 7. How the value of ν given by eq 18 changes with the surface-to-volume ratio of the cubic subsystem it was calculated in. For the three different curves, the density is constant, equal to that of the reservoir. The full gray line shows the result of linear fitting to the data points between the dashed lines, while the full black curve shows the result of fitting eq 19 to the data points between $0.4 < \Omega/V < 1.0$.

In conclusion, a simple analysis of R^2 based on the linear fit is able provide good estimates for the location of the linear region. These estimates can be further improved by utilizing an equation that explicitly includes the effect of the finite size of the simulation box, but the effect of this additional step was marginal for the systems investigated here. The final limits identified by this method correspond to slightly smaller subvolumes than those of the previously suggested general limits.[27,35] In the following analysis of chemical potential, we therefore analyze the regions $0.60 < \Omega/V < 1.0$ for spherical subvolumes and between $0.78 < \Omega/V < 1.0$ for cubic subvolumes.

Calculating Chemical Potential Differences from the SSM. Now, we will show how the distributions in the subsystems are used to calculate their chemical potential differences. Figure 5 shows the fluctuations that represent the distributions, which we apply the ODM to. Also here we use the maximum likelihood approach, which means that we apply eq 17 to the particle distributions in two subvolumes of equal size, sampled from two reservoirs at different densities. From the three densities available, $\Delta\mu$ is computed for the two systems with the lowest densities and for the systems with the lowest and the highest densities. Standard deviations for each value of $\Delta\mu$ are calculated from 20 bootstrap samples. For some of the largest subvolumes, the distributions become too far apart for the ODM analysis to converge. The 20 largest subvolumes are therefore not included in the following analysis. In the linear region for the cubic subvolumes, $0.78 < \Omega/V < 1.0$, the values calculated in both spherical and cubic subvolumes overlap. The figures presented in this section therefore only contain results from spherical subvolumes, while the corresponding figures for the cubic subvolumes are found in the Supporting Information. Relative errors for the values in the thermodynamic limit are presented for both cubic and spherical subvolumes.

Figure 8 shows that the values of $\Delta\mu$ increase with the subvolume size and that they clearly approach the correct value in the thermodynamic limit ($\Omega/V \to 0$). Accurate estimates of values in the thermodynamic limit are calculated from the EOS by Thol et al.[50] The ones calculated using the Widom particle insertion method show only a 0.6% deviation from these and are therefore not included in the figure. In the following, the reported relative errors are therefore calculated with respect to the values obtained from the EOS by Thol et al.[50]

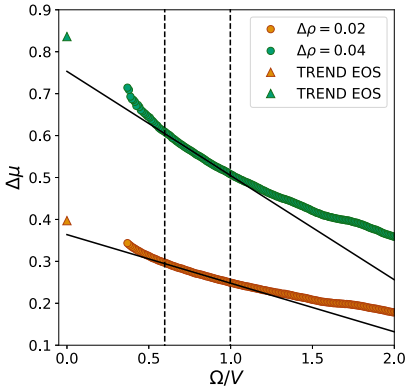

Figure 8. Chemical potential difference as a function of the surface-to-volume ratio. The values of $\Delta\mu$ were calculated by using fluctuations generated from spherical subvolumes in two separate reservoirs with different densities, combined in the maximum likelihood approach of the ODM. Error bars representing two standard deviations are included, but they are smaller than the markers.

Before proceeding to investigate the accuracy of the results, one important question must be answered. How is it possible that the chemical potential inside a subvolume differs from the chemical potential in the particle reservoir to which it is connected?

https://dx.doi.org/10.1021/acs.jcim.0c01367
J. Chem. Inf. Model. 2021, 61, 840−855

The answer to this is that the reservoir and the subsystems have different types of boundaries. The reservoir has periodic boundaries, which make it behave as a macroscopic system. The subsystems, however, do not have periodic boundaries, which introduces a surface effect to their properties. We have already shown that grand canonical systems can have a size-dependent density, and we have explained that if this is the case for the subsystems sampled with the SSM, the size dependence will not appear in the densities. The sampling procedure forces all subsystems to have the same average density, which means that the size dependence instead modifies the values of the chemical potentials. Hence, the chemical potential inside subsystems will be size-dependent and different from the chemical potential of the reservoir.

The dashed lines in Figure 8 show the limits of the linear region, which means that between these lines, we find values of ν that scale linearly with the surface area-to-volume ratio. For the volumes that are too large for this region ($\Omega/V < 0.60$), $\Delta\mu$ displays a more rapid change. While the values of ν in Figure 5 decreased at this point, the values of $\Delta\mu$ in Figure 8 instead increased more rapidly when approaching larger subsystems. This can be attributed to the fact that the fluctuations become too small at this point since too small fluctuations correspond to too narrow distributions, which results in higher values of $\Delta\mu$.[18]

The full black lines in Figure 8 show the straight lines fitted to the data points between the dashed lines. According to eq 10, the intersection of this line corresponds to the value in the thermodynamic limit. The relative errors of $\Delta\mu^{\infty}$ are calculated with respect to the EOS by Thol et al.[50] and correspond to 8 and 10% (10 and 12% for the cubic subvolumes). The relative error is larger than what we can expect when using the ODM separately since it was shown to give relative errors below 2% for different types of small systems.

It is possible to improve the accuracy of the extrapolated value by plotting the data differently. When using the SSM, it has been shown that the quality of the extrapolated value depends mostly on the quality of the linear fit.[48] Some properties have earlier been shown to have a more clear linear region if they are plotted as their inverse. This was the case for the partial enthalpies[30] and for the thermodynamic factor.[32] Common for both of these properties is that they are partial derivatives with respect to the number of particles. Since the chemical potential also is a partial derivative with respect to number of particles, it is interesting to see how its inverse behaves.

This idea can be further substantiated by investigating the connection between the partial derivative of chemical potential with respect to density and the particle fluctuations. The relation comes from combining eqs's 3, 4, and 9 and is given by

$$\left(\frac{\partial\mu}{\partial\rho}\right)_{T,V} = \frac{k_B T}{\nu} \tag{20}$$

which upon integration becomes

$$\Delta\mu = k_B T \int_{\rho_1}^{\rho_2} \frac{1}{\nu^{\infty}(\rho) + \frac{\Omega}{V}\nu^{s}(\rho)} \mathrm{d}\rho \tag{21}$$

It can here be argued that even though the values of ν^{∞} and ν^{s} depend on density, the scaling of ν as a function of Ω/V remains linear. This suggests that $1/\Delta\mu$ also will scale linearly as a function of Ω/V.

Figure 9 shows the values of $1/\Delta\mu$ as a function of the surface-to-volume ratio. This curve shows a more clear linear behavior than the ones in Figure 8. By using the same system sizes in the curve fitting, the relative errors of the extrapolated values of $\Delta\mu$ are reduced to 2 and 3% (3 and 4% for cubic subvolumes). This is closer to the accuracy we can expect from the ODM, and it is similar to previously reported accuracies for other properties calculated by the SSM.[29]

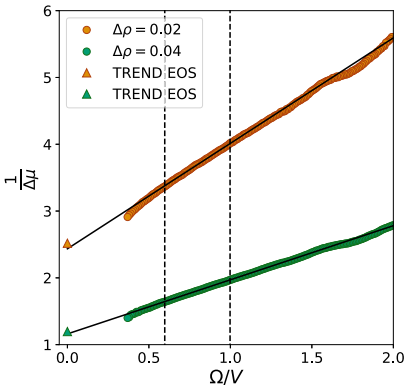

Figure 9. Inverse chemical potential difference as a function of the surface area-to-volume ratio. The values of $\Delta\mu$ were calculated by using fluctuations generated from spherical subvolumes in two separate reservoirs with different densities, combined in the maximum likelihood approach of the ODM. Error bars representing two standard deviations are included, but they are smaller than the markers.

Histogram versus the Maximum Likelihood Approach of the ODM. In early applications of the ODM, histograms were used to calculate the distributions and their overlaps.[2,14,16,17] The maximum likelihood approach by Shirts et al.[15] is able to use the complete set of data of particle numbers instead of reducing these to histograms, which usually provides more precise and accurate results.[18] However, the maximum likelihood approach includes an optimization step that is much more demanding with respect to both computational time and memory, compared to simply sorting the particle numbers in histograms. In this section, we will investigate if it is possible reduce time and computational cost, without loss of accuracy, by replacing the maximum likelihood approach with the original histogram version of the ODM.

Another convenient aspect with histograms is that they make it possible to visually inspect the distributions. Figure 10a shows the distributions in the largest ($\Omega/V = 0.60$) subsystem included in the curve fitting, and Figure 10b shows the smallest ($\Omega/V = 1.0$) subsystem included in the curve fitting. The size of the x- and y-axis ranges is equal in Figure 10a,b for the total, as well as the inset figures. This makes it possible to directly compare the features of the distributions. We observe that the distributions in the smallest subsystem have poorer statistics than the distributions in the largest subsystem. For systems with such a low number of particles, the histograms will deviate more from a smooth curve, which can introduce inaccuracies in the properties calculated from the overlap. There is,

https://dx.doi.org/10.1021/acs.jcim.0c01367
J. Chem. Inf. Model. 2021, 61, 840−855

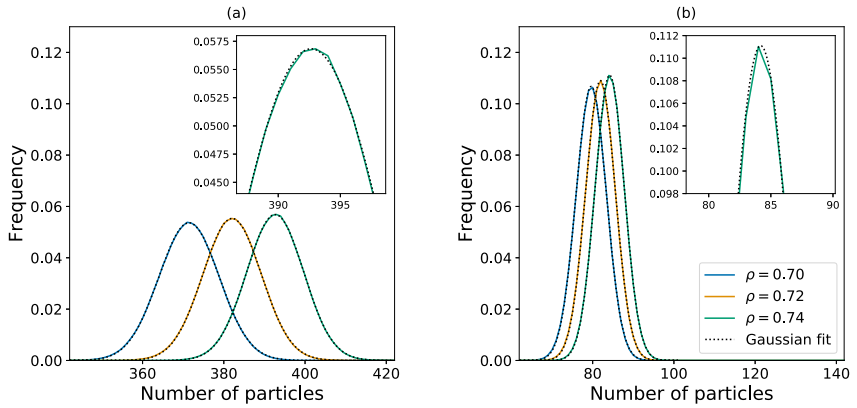

Figure 10. Histograms of particle distributions representing the fluctuations shown in Figure 5. (a) shows the distribution of number of particles in the largest volume in the linear region, corresponding to $\Omega/V = 0.60$, while (b) shows the ones for the smallest volume in the linear region, corresponding to $\Omega/V = 1.0$. The dotted lines represent the Gaussian curves fitted to the histogram data.

however, a simple solution to this problem. As suggested by McDonald and Singer,[16] a Gaussian curve can first be fitted to the distributions before calculating the ratio of the overlap. The fitted Gaussian curves are displayed in Figure 10, together with the histograms calculated directly from the particle numbers.

The results of applying the above described method for calculation of $\Delta\mu$ are shown in Figure 11. By comparing this to

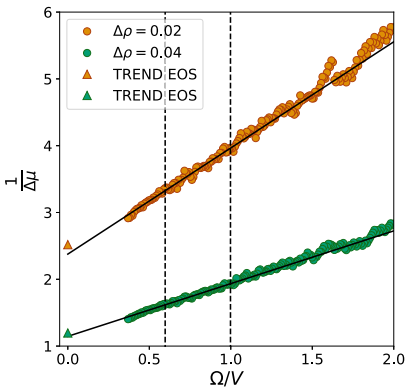

Figure 11. Inverse chemical potential difference as a function of the surface-to-volume ratio. The values of $\Delta\mu$ were calculated by using fluctuations generated from spherical subvolumes in two separate reservoirs with different densities, combined in the histogram approach of the ODM. Error bars representing two standard deviations are included, but they are smaller than the markers.

the results obtained from the maximum likelihood version of the ODM (Figure 9), we can see that the histogram method introduces larger variations in the values of $\Delta\mu$. However, the relative error of the extrapolated value is only increased by 1%-point. This means that even though the accuracy of a single data point calculated from histograms generally is lower than the one obtained from the maximum likelihood approach, it does not have a large effect on the results from the curve fitting. As long as the uncertainties introduced by the histogram approach do not lead to a change in trend of the data, it will act as randomly distributed noise, which eventually is canceled out in the curve fitting.

Consequently, if the goal is to obtain the value of $\Delta\mu$ in the thermodynamic limit, the histogram approach and the maximum likelihood approach works almost equally well for the systems considered here. However, if the main interest is properties for a specific system size, the maximum likelihood method is more likely to determine this value with higher accuracy.

Scope and Limitations. Computational methods for chemical potential differences are a field that is being continuously explored. One of the most popular methods for these investigations is the Widom particle insertion method,[12] which is often used as a benchmark reference when new methods are presented.[39−41,47] It is well known that the steps involving insertion or deletion of particles used in the Widom method become inefficient at higher densities. The same goes for related grand canonical particle insertion schemes such as the Gibbs ensemble MC method which often is used to investigate phase equilibria.[47] The branch of methods that instead compute chemical potential differences from fluctuations sampled from subsystems thus have an advantage at higher densities.

In addition to the relations used to extract $\Delta\mu$ in this work, there also exists a connection between the differential chemical potential and the fluctuations, given by eq 20. Absolute values of chemical potential have previously been successfully extracted from this method for both one-component[38] and multicomponent systems.[35,37] Both the method based on the differentials of μ and the one presented here are able to provide absolute values when used in combination with another method that allows one to calculate the chemical potential at a reference state point.

One important difference between the two methods is that the method based on the differentials of μ involves numerical integration. It is therefore necessary to sample a large enough range of different densities in order to provide accurate values of μ. The method presented here is able to extract values of $\Delta\mu$ directly from two simulations.

https://dx.doi.org/10.1021/acs.jcim.0c01367
J. Chem. Inf. Model. 2021, 61, 840−855

Another important difference is that the method based on the differentials of μ can explicitly include the effect of the finite size of the simulation box in the scaling laws used to extract $(\partial\mu/\partial\rho)_{T,V}$. In contrast, the method presented here is only able to use these scaling laws to identify the subvolumes that are not affected by this feature. We have shown that explicitly including this effect returns a value of ν^{∞} with a relative error below 1%. Based on a similar analysis,[29] this could suggest that even larger simulation box sizes are needed to further decrease the relative error computed by the method presented in this work.

Further work with the method presented here involves extension to multicomponent systems and investigation of its application to molecular fluids.

CONCLUSIONS

We have presented a new method for computation of chemical potential differences, in both small and large systems, from molecular dynamics simulations. The new method can be seen as an extension of the SSM, which uses small subsystems embedded in a larger simulation box to calculate distributions of the number of particles. This method, which until now has been used to calculate enthalpies and the thermodynamic factor,[28] partial molar properties,[30] Kirkwood−Buff integrals,[32,33] and the isothermal compressibility,[29] has been extended to calculate chemical potential differences. This new feature was obtained by combining the SSM with an ODM. As the name suggests, the ODM uses the overlap of distributions from two different simulations to calculate thermodynamic properties. For systems with a fluctuating number of particles, one of the available properties is the chemical potential difference.

Before applying the ODM to the distributions created from the SSM, it was necessary to investigate how well the ODM performs for small systems. This was done by applying the ODM to particle distributions generated by two grand canonical MC simulations with different input values of μ, but otherwise identical parameters. Two different types of small systems were investigated, and a system with periodic boundaries was used as a reference. The values of $\Delta\mu$ calculated from the ODM for all of these systems had a relative error below 2%, which means that the ODM can be regarded as equally reliable for both the small and large systems investigated in this work.

The SSM generates small systems of a range of different sizes, which means that it can give insights on how an intensive property such as the chemical potential starts depending on the system size when the system becomes small enough. As a result of this, the chemical potential difference can be calculated as a function of the system size. Combined with a scaling law based on Hadwiger's[44] theorem, the values of $\Delta\mu$ can be extrapolated from the small systems to the thermodynamic limit. We also have presented tools that will be helpful in determining which system sizes should be included in this extrapolation. Compared to methods based on insertion of particles, the fluctuation-based methods have an advantage when it comes to extracting thermodynamic properties at high densities. The particular method presented here also provides an option that is independent of numerical integration.

When using the ODM, there are two options for extracting information from the overlap of the distributions. The fluctuations in number of particles can either be stored in histograms before the overlap of these is computed, or a maximum likelihood approach can be used on the complete data set. We have shown that these methods work almost equally well for determining the value of $\Delta\mu$ in the thermodynamic limit since they both provide values with a relative error below 4%. The maximum likelihood approach is able to determine this value with 1%-point higher accuracy. The small difference is mainly because random noise is canceled out in the curve fitting. If the main interest is one value of $\Delta\mu$ for a specific system size, the maximum likelihood approach will probably provide a more accurate result.

ASSOCIATED CONTENT

Supporting Information

The Supporting Information is available free of charge at https://pubs.acs.org/doi/10.1021/acs.jcim.0c01367.

Chemical potential difference in cubic subvolumes (PDF)

AUTHOR INFORMATION

Corresponding Author

Sondre Kvalvåg Schnell − *Department of Materials Science and Engineering, Norwegian University of Science and Technology, NTNU, Trondheim N-7491, Norway;* orcid.org/0000-0002-0664-6756; Email: sondre.k.schnell@ntnu.no

Authors

Vilde Bråten − *Department of Materials Science and Engineering, Norwegian University of Science and Technology, NTNU, Trondheim NO-7491, Norway;* orcid.org/0000-0001-6462-6107

Øivind Wilhelmsen − *SINTEF Energy Research, Trondheim NO-7465, Norway; Department of Energy and Process Engineering, Norwegian University of Science and Technology, Trondheim NO-7491, Norway;* orcid.org/0000-0003-4631-0349

Complete contact information is available at: https://pubs.acs.org/10.1021/acs.jcim.0c01367

Notes

The authors declare no competing financial interest.

ACKNOWLEDGMENTS

This work was supported by the Research Council of Norway (275754). Computational resources are provided by the UNINETT Sigma2—The National Infrastructure for High Performance Computing and Data Storage in Norway (NN9414k).

REFERENCES

(1) Leach, A. *Molecular Modelling: Principles and Applications*, 2nd ed.; Pearson Education Limited, 2001.

(2) Frenkel, D.; Smit, B. *Understanding Molecular Simulation*, 2 ed.; Academic Press, 2002.

(3) Allen, M. P.; Tidesely, D. J. *Computer Simulations of Liquids*; Oxford University Press Inc., 1987.

(4) Kirkwood, J. G. Statistical Mechanics of Fluid Mixtures. *J. Chem. Phys.* **1935**, *3*, 300−313.

(5) Mitchell, M. J.; McCammon, J. A. Free energy difference calculations by thermodynamic integration: Difficulties in obtaining a precise value. *J. Comput. Chem.* **1991**, *12*, 271−275.

(6) Straatsma, T. P.; McCammon, J. A. Multiconfiguration thermodynamic integration. *J. Chem. Phys.* **1991**, *95*, 1175−1188.

(7) Hummer, G. Fast-growth thermodynamic integration: Error and efficiency analysis. *J. Chem. Phys.* **2001**, *114*, 7330−7337.
(8) Lartillot, N.; Philippe, H. Computing Bayes Factors Using Thermodynamic Integration. *Syst. Biol.* **2006**, *55*, 195−207.
(9) Torrie, G. M.; Valleau, J. P. Nonphysical sampling distributions in Monte Carlo free-energy estimation: Umbrella sampling. *J. Comput. Phys.* **1977**, *23*, 187−199.
(10) Souaille, M.; Roux, B. Extension to the weighted histogram analysis method: combining umbrella sampling with free energy calculations. *Comput. Phys. Commun.* **2001**, *135*, 40−57.
(11) Kästner, J.; Thiel, W. Bridging the gap between thermodynamic integration and umbrella sampling provides a novel analysis method: "Umbrella integration". *J. Chem. Phys.* **2005**, *123*, 144104.
(12) Widom, B. Some Topics in the Theory of Fluids. *J. Chem. Phys.* **1963**, *39*, 2808−2812.
(13) Heinbuch, U.; Fischer, J. On the Application of Widom's Test Particle Method to Homogeneous and Inhomogeneous Fluids. *Mol. Simul.* **1987**, *1*, 109−120.
(14) Bennett, C. H. Efficient estimation of free energy differences from Monte Carlo data. *J. Comput. Phys.* **1976**, *22*, 245−268.
(15) Shirts, M. R.; Bair, E.; Hooker, G.; Pande, V. S. Equilibrium Free Energies from Nonequilibrium Measurements Using Maximum-Likelihood Methods. *Phys. Rev. Lett.* **2003**, *91*, 140601.
(16) McDonald, I. R.; Singer, K. Machine Calculation of Thermodynamic Properties of a Simple Fluid at Supercritical Temperatures. *J. Chem. Phys.* **1967**, *47*, 4766−4772.
(17) Valleau, J. P.; Card, D. N. Monte Carlo Estimation of the Free Energy by Multistage Sampling. *J. Chem. Phys.* **1972**, *57*, 5457−5462.
(18) Shirts, M. R. Simple quantitative tests to validate sampling from thermodynamic ensembles. *J. Chem. Theory Comput.* **2013**, *9*, 909−926.
(19) Somani, S.; Okamoto, Y.; Ballard, A. J.; Wales, D. J. Equilibrium Molecular Thermodynamics from Kirkwood Sampling. *J. Phys. Chem. B* **2015**, *119*, 6155−6169.
(20) Clavier, G.; Desbiens, N.; Bourasseau, E.; Lachet, V.; Brusselle-Dupend, N.; Rousseau, B. Computation of elastic constants of solids using molecular simulation: comparison of constant volume and constant pressure ensemble methods. *Mol. Simul.* **2017**, *43*, 1413−1422.
(21) Hill, T. L. Thermodynamics of Small Systems. *J. Chem. Phys.* **1962**, *36*, 3182−3197.
(22) Bedeaux, D.; Kjelstrup, S.; Schnell, S. K. *Nanothermodynamics. General Theory*; Porelab Publisher, 2020.
(23) Binder, K. Finite size scaling analysis of ising model block distribution functions. *Z. Phys.* **1981**, *43*, 119−140.
(24) Binder, K. Critical Properties from Monte Carlo Coarse Graining and Renormalization. *Phys. Rev. Lett.* **1981**, *47*, 693−696.
(25) Rovere, M.; Hermann, D. W.; Binder, K. Block Density Distribution Function Analysis of Two-Dimensional Lennard-Jones Fluids. *Europhys. Lett.* **1988**, *6*, 585−590.
(26) Rovere, M.; Heermann, D. W.; Binder, K. The gas-liquid transition of the two-dimensional Lennard-Jones fluid. *J. Phys.: Condens. Matter* **1990**, *2*, 7009−7032.
(27) Rovere, M.; Nielaba, P.; Binder, K. Simulation studies of gas-liquid transitions in two dimensions via a subsystem-block-density distribution analysis. *Z. Phys.* **1993**, *90*, 215−228.
(28) Schnell, S. K.; Vlugt, T. J. H.; Simon, J.-M.; Bedeaux, D.; Kjelstrup, S. Thermodynamics of a small system in a μT reservoir. *Chem. Phys. Lett.* **2011**, *504*, 199−201.
(29) Strøm, B. A.; Simon, J.-M.; Schnell, S. K.; Kjelstrup, S.; He, J.; Bedeaux, D. Size and shape effects on the thermodynamic properties of nanoscale volumes of water. *Phys. Chem. Chem. Phys.* **2017**, *19*, 9016−9027.
(30) Schnell, S. K.; Skorpa, R.; Bedeaux, D.; Kjelstrup, S.; Vlugt, T. J. H.; Simon, J.-M. Partial molar enthalpies and reaction enthalpies from equilibrium molecular dynamics simulation. *J. Chem. Phys.* **2014**, *141*, 144501.
(31) Kirkwood, J. G.; Buff, F. P. The Statistical Mechanical Theory of Solutions. I. *J. Chem. Phys.* **1951**, *19*, 774−777.
(32) Schnell, S. K.; Liu, X.; Simon, J.-M.; Bardow, A.; Bedeaux, D.; Vlugt, T. J. H.; Kjelstrup, S. Calculating Thermodynamic Properties from Fluctuations at Small Scales. *J. Phys. Chem. B* **2011**, *115*, 10911−10918.
(33) Dawass, N.; Krüger, P.; Schnell, S. K.; Simon, J.-M.; Vlugt, T. J. H. Kirkwood-Buff integrals from molecular simulation. *Fluid Phase Equilib.* **2019**, *486*, 21−36.
(34) Ganguly, P.; van der Vegt, N. F. A. Convergence of Sampling Kirkwood-Buff Integrals of Aqueous Solutions with Molecular Dynamics Simulations. *J. Chem. Theory Comput.* **2013**, *9*, 1347−1355.
(35) Cortes-Huerto, R.; Kremer, K.; Potestio, R. Communication: Kirkwood-Buff integrals in the thermodynamic limit from small-sized molecular dynamics simulations. *J. Chem. Phys.* **2016**, *145*, 141103.
(36) Galata, A. A.; Anogiannakis, S. D.; Theodorou, D. N. Thermodynamic analysis of Lennard-Jones binary mixtures using Kirkwood-Buff theory. *Fluid Phase Equilib.* **2018**, *470*, 25−37.
(37) Heidari, M.; Kremer, K.; Potestio, R.; Cortes-Huerto, R. Fluctuations, Finite-Size Effects and the Thermodynamic Limit in Computer Simulations: Revisiting the Spatial Block Analysis Method. *Entropy* **2018**, *20*, 222.
(38) Heidari, M.; Kremer, K.; Potestio, R.; Cortes-Huerto, R. Finite-size integral equations in the theory of liquids and the thermodynamic limit in computer simulations. *Mol. Phys.* **2018**, *116*, 3301−3310.
(39) Nezbeda, I.; Kolafa, J. A New Version of the Insertion Particle Method for Determining the Chemical Potential by Monte Carlo Simulation. *Mol. Simul.* **1991**, *5*, 391−403.
(40) Ding, K.; Valleau, J. P. Umbrella-sampling realization of "Widom" chemical potential estimation. *J. Chem. Phys.* **1993**, *98*, 3306−3312.
(41) Shi, W.; Maginn, E. J. Continuous Fractional Component Monte Carlo: An Adaptive Biasing Method for Open System Atomistic Simulations. *J. Chem. Theory Comput.* **2007**, *3*, 1451−1463.
(42) Adams, D. J. Chemical potential of hard-sphere fluids by Monte Carlo methods. *Mol. Phys.* **1974**, *28*, 1241−1252.
(43) Siepmann, J. I.; McDonald, I. R.; Frenkel, D. Finite-size corrections to the chemical potential. *J. Phys.: Condens. Matter* **1992**, *4*, 679−691.
(44) Hadwiger, H. *Vorlesungen Über Inhalt, Oberfläche und Isoperimetrie*; Springer, 1957.
(45) Klain, D. A. A short proof of Hadwiger's characterization theorem. *Mathematika* **1995**, *42*, 329−339.
(46) Román, F. L.; White, J. A.; Velasco, S. Fluctuations in an equilibrium hard-disk fluid: Explicit size effects. *J. Chem. Phys.* **1997**, *107*, 4635−4641.
(47) Román, F. L.; White, J. A.; Velasco, S. Block analysis method in off-lattice fluids. *Europhys. Lett.* **1998**, *42*, 371−376.
(48) Schnell, S. K.; Vlugt, T. J. H.; Simon, J.-M.; Bedeaux, D.; Kjelstrup, S. Thermodynamics of small systems embedded in a reservoir: a detailed analysis of finite size effects. *Mol. Phys.* **2012**, *110*, 1069−1079.
(49) Ben-Naim, A. *Molecular Theory of Solutions*; OUP Oxford, 2006.
(50) Thol, M.; Rutkai, G.; Span, R.; Vrabec, J.; Lustig, R. Equation of State for the Lennard-Jones Truncated and Shifted Model Fluid. *Int. J. Thermophys.* **2015**, *36*, 25−43.
(51) Plimpton, S. Fast Parallel Algorithms for Short-Range Molecular Dynamics. *J. Comput. Phys.* **1995**, *117*, 1−19.
(52) Hansen, J.-P.; McDonald, I. R. *Theory of Simple Fluids*; Academic Press Inc.: London, 1976.
(53) Reiss, H.; Reguera, D. Understanding the Limitations of the Virial in the Simulation of Nanosystems: A Puzzle That Stimulated the Search for Understanding. *J. Phys. Chem. B* **2004**, *108*, 6555−6563.
(54) Taylor, J. R. *An Introduction to Error Analysis—The Study of Uncertainties in Physical Measurements*, 2nd ed.; University Science Books, 1997.
(55) Salacuse, J. J. Particle fluctuations within sub-regions of an N-particle, two-dimensional fluid: Finite-size effects and compressibility. *Phys. A* **2007**, *379*, 372−388.

(56) Salacuse, J. J. Particle fluctuations within sub-regions of an N-particle, three-dimensional fluid: Finite-size effects and compressibility. *Phys. A* **2008**, *387*, 3073−3083.

https://dx.doi.org/10.1021/acs.jcim.0c01367
J. Chem. Inf. Model. 2021, 61, 840−855

Supporting Information
Chemical Potential Differences in the Macroscopic Limit from Fluctuations in Small Systems

Vilde Bråten,[†] Øivind Wilhelmsen,[‡,¶] and Sondre Kvalvåg Schnell[*,§]

[†]*Department of Materials Science and Engineering, Norwegian University of Science and Technology, NTNU, Trondheim, NO-7491, Norway*

[‡]*SINTEF Energy Research, Trondheim, NO-7465, Norway*

[¶]*Department of Energy and Process Engineering, Norwegian University of Science and Technology, Trondheim, NO-7491, Norway*

[§]*Department of Materials Science and Engineering, Norwegian University of Science and Technology, NTNU, Trondheim, N-7491, Norway*

E-mail: sondre.k.schnell@ntnu.no

The Fig.'s S1, S2 and S3 represent the values of chemical potential difference, $\Delta\mu$, calculated in cubic sub-volumes.

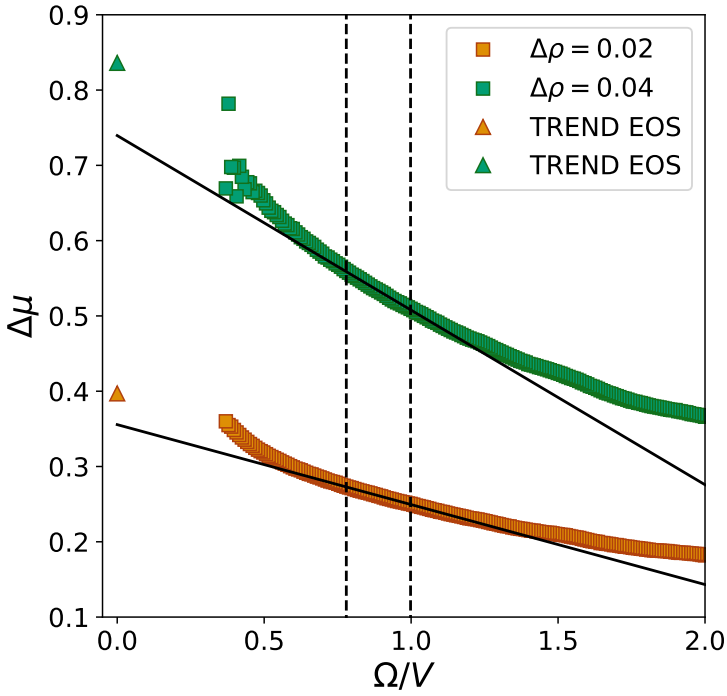

Figure S1: Chemical potential difference as a function of surface to volume ratio. The values of $\Delta\mu$ were calculated by using fluctuations generated from cubic sub-volumes in two separate reservoirs with different density, combined in the maximum likelihood approach of ODM. Error bars representing two standard deviations are included, but they are smaller than the markers.

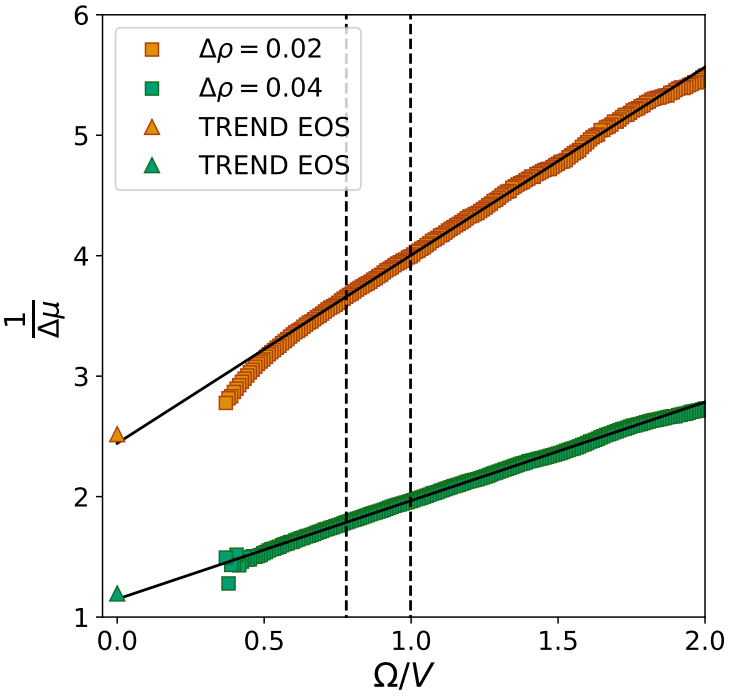

Figure S2: The inverse chemical potential difference as a function of surface area to volume ratio. The values of $\Delta\mu$ were calculated by using fluctuations generated from cubic sub-volumes in two separate reservoirs with different density, combined in the maximum likelihood approach of ODM. Error bars representing two standard deviations are included, but they are smaller than the markers.

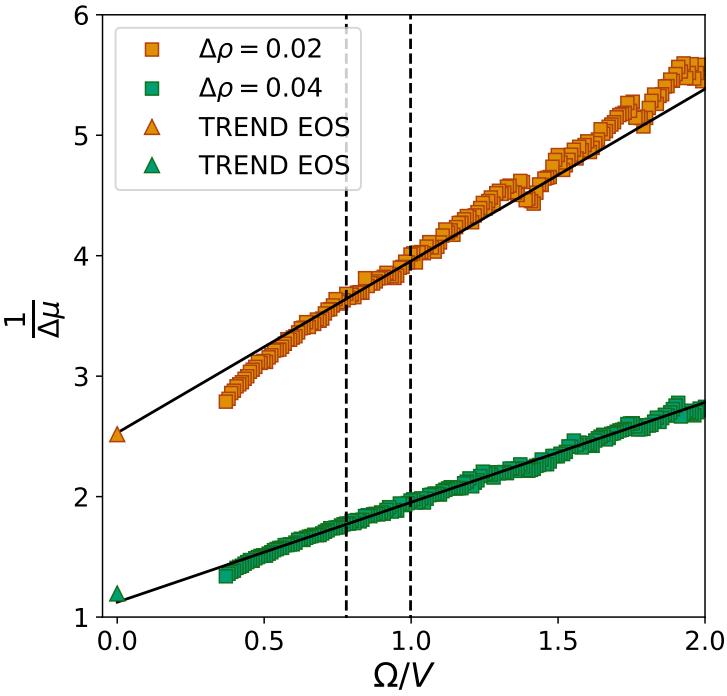

Figure S3: The inverse chemical potential difference as a function of surface to volume ratio. The values of $\Delta\mu$ were calculated by using fluctuations generated from cubic sub-volumes in two separate reservoirs with different density, combined in the histogram approach of ODM. Error bars representing two standard deviations are included, but they are smaller than the markers.

Article II

V. Bråten, D. Bedeaux, Ø. Wilhelmsen and S. K. Schnell

Small size effects in open and closed systems: What can we learn from ideal gases about systems with interacting particles?,

The Journal of Chemical Physics **155**:24 244504 (2021).
DOI: 10.1063/5.0076684

Article II

Article II

The Journal of Chemical Physics ARTICLE scitation.org/journal/jcp

Small size effects in open and closed systems: What can we learn from ideal gases about systems with interacting particles?

Cite as: J. Chem. Phys. 155, 244504 (2021); doi: 10.1063/5.0076684
Submitted: 27 October 2021 • Accepted: 22 November 2021 •
Published Online: 27 December 2021

Vilde Bråten,[1] Dick Bedeaux,[2] Øivind Wilhelmsen,[2] and Sondre Kvalvåg Schnell[1,a)]

AFFILIATIONS

[1] Department of Materials Science and Engineering, Norwegian University of Science and Technology, NTNU, Trondheim NO-7491, Norway
[2] PoreLab, Department of Chemistry, Norwegian University of Science and Technology, NTNU, Trondheim NO-7491, Norway

[a)] Author to whom correspondence should be addressed: sondre.k.schnell@ntnu.no

ABSTRACT

Small systems have higher surface area-to-volume ratios than macroscopic systems. The thermodynamics of small systems therefore deviates from the description of classical thermodynamics. One consequence of this is that properties of small systems can be dependent on the system's ensemble. By comparing the properties in grand canonical (open) and canonical (closed) systems, we investigate how a small number of particles can induce an ensemble dependence. Emphasis is placed on the insight that can be gained by investigating ideal gases. The ensemble equivalence of small ideal gas systems is investigated by deriving the properties analytically, while the ensemble equivalence of small systems with particles interacting via the Lennard-Jones or the Weeks–Chandler–Andersen potential is investigated through Monte Carlo simulations. For all the investigated small systems, we find clear differences between the properties in open and closed systems. For systems with interacting particles, the difference between the pressure contribution to the internal energy, and the difference between the chemical potential contribution to the internal energy, are both increasing with the number density. The difference in chemical potential is, with the exception of the density dependence, qualitatively described by the analytic formula derived for an ideal gas system. The difference in pressure, however, is not captured by the ideal gas model. For the difference between the properties in the open and closed systems, the response of increasing the particles' excluded volume is similar to the response of increasing the repulsive forces on the system walls. This indicates that the magnitude of the difference between the properties in open and closed systems is related to the restricted movement of the particles in the system. The work presented in this paper gives insight into the mechanisms behind ensemble in-equivalence in small systems, and illustrates how a simple statistical mechanical model, such as the ideal gas, can be a useful tool in these investigations.

I. INTRODUCTION

The effect a system's finite size can have on its properties is an important factor to consider when investigating systems through simulations.[1] Initially, finite size effects in simulations were unwanted since the main goal of the simulations was to extract macroscopic properties. Research on finite size effects was therefore mainly focused on finding corrections for them so that the properties in the thermodynamic limit could be extracted. In addition to the numerous theoretical descriptions,[2–8] finite size effects have been investigated to a large extent through simulations for both simple model fluids and for complex molecular fluids.[9–20]

With increased interest in nanosized systems in fields such as biology,[21,22] atmospheric science,[23] and porous media science,[24,25] it becomes important to understand how these finite size effects are not only artifacts in simulations, but also significant contributions to the behavior of small systems. In naturally occurring nanosized systems, the small size effect is an inherent part of the system. To get a complete understanding of the behavior of such systems, we need a proper description of the finite size effects. An essential part of this development is to have a thermodynamic description that applies on a small size scale. This was provided by Hill[26] through an extension of classical thermodynamics that can be applied to small systems, often referred to as nanothermodynamics. Nanothermodynamics has been used in different works to describe small

systems, such as in the description of transport in porous media,[27,28] stretching and breaking of polymer chains,[29,30] and in the use of sub-sampling techniques for computation of macroscopic thermodynamic properties.[14,19,20]

The objective of this paper is to demonstrate how investigations of a simple model system can be used in combinations with Hill's[26] nanothermodynamics to gain more insight into the behavior of small systems. More specifically, we investigate whether small confinement can lead to a difference in the properties of open and closed systems. We consider single-phase systems that are inherently identical except for their boundaries. The open system considered here is in the grand canonical ensemble and can exchange particles and energy with the surroundings, while the closed system is in the canonical ensemble and can exchange only energy with the surroundings.

If the two ensembles predict compatible or equivalent equilibrium states for a given system, we refer to this system as ensemble equivalent.[31,32] In classical thermodynamics, it is well known that ensemble equivalence holds for macroscopic systems with short range interactions. However, it is also known that systems with a small number of particles can be ensemble *in-equivalent*. This can occur when properties that are regarded extensive in the thermodynamic limit are influenced by finite size effects and become non-extensive. It is not surprising that Hill's[26] formalism, where the thermodynamic properties have been derived for each ensemble separately, has gained some interest in the research on ensemble in-equivalence. Rubi, Bedeaux, and Kjelstrup[33] used Hill's[26] framework in a theoretical investigation of the properties of a single molecule under isomeric and isotensional conditions.[33] Bering *et al.*[29] later showed that the in-equivalence between these two ensembles can be detected in simulations of polymer chains.

Systems with a large number of particles can also be ensemble in-equivalent. A substantial amount of the research carried out on ensemble in-equivalence has focused on systems with long-range interactions.[31,32,34–36] The main interest of these studies has been the non-additive rather than the non-extensive nature of the system's properties. Additivity is closely related to extensivity, but their definitions are different. A thermodynamic property f is *extensive* if it is Euler homogeneous of degree one with respect to the variable x, meaning that $f(2x) = 2f(x)$. If a property f is *additive*, it means that if the total system is split into i sub-parts, the total property is the sum of all its sub-parts, $f_{\text{tot}} = f_1 + f_2 + \cdots + f_i$. If a property is non-additive, there is an additional contribution from the interaction between the sub-parts, f_{int}. This means that a system can be non-additive and still be extensive if the contribution from the interactions scales with system size.[31] Hence, additive properties are always extensive, and non-extensive properties are non-additive, but not necessarily the other way around. This was used by Campa *et al.*,[36] who showed how Hill's[26] nanothermodynamics can be applied to macroscopic non-additive systems.

Models based on statistical mechanics can provide insight into the mechanisms behind ensemble in-equivalence. In this work, the ideal gas model represents an important case because it has no inter-particle interactions. Studying the ideal gas can possibly reveal ensemble in-equivalence arising from other sources than long-range interactions. Another motivation for studying ideal gases is that previous investigations of their finite size effects have been shown to also apply to systems with interacting particles.[13,37,38]

When investigating model systems with a small number of particles, it is important to keep in mind that some ingrained definitions and relations from statistical mechanics use approximations based on the assumptions that $N \to \infty$, where N is the number of particles. One example is the proof of the virial theorem, for which Tuckerman[39] briefly discussed the necessary assumption made about the number of microstates associated with different ensembles. The equipartition theorem has also been shown to break down for small particle numbers in systems containing hard spheres,[40] and later for particles interacting via intermolecular potentials.[41,42] Miranda[43] showed that avoiding assumptions about the magnitude of N in the derivation of the properties of small clusters of harmonic oscillators, and two-level systems, results in differences between the properties in the canonical, microcanonical, and grand canonical ensembles.

Approximations based on the assumption that $N \to \infty$ are also used in the classical derivation of the bulk properties of the ideal gas. In this paper, we derive the properties of an ideal gas in a small system with a surface energy, without assuming that $N \to \infty$, and investigate how finite size contributions to the thermodynamic properties arise when the system is small. We find that some finite size terms arise from surface effects and some arise from avoiding approximations about the magnitude of the number of particles. Similar models have been used previously to investigate ideal gas mixtures with surface energy,[44] and the adsorbed phase on a spherical adsorbent.[45] Here, we take it one step further by presenting a direct comparison of the properties in an open and closed system. We also compare the results of the ideal gas with the results from Monte Carlo (MC) simulations of the system with Lennard-Jones (LJ) particles and systems with Weeks-Chandler-Andersen (WCA) particles.

II. THERMODYNAMICS OF SMALL SYSTEMS

Finite size effects in small systems are usually a result of surface area-to-volume ratios larger than those of macroscopic systems. For small systems, the effects of the surface can be a significant contribution to the thermodynamic properties. As a consequence of this, properties that normally are regarded as extensive in macroscopic systems can become higher order functions of size and shape in small systems, while properties that are normally regarded as intensive in macroscopic systems can become size dependent if the system is small.[26]

Classical macroscopic thermodynamic equations cannot be used to describe the properties in small systems, but the framework developed by Hill[26] provides an extension of the systematic structure of thermodynamics that applies to small systems. Instead of considering one single small system, Hill[26] investigated a collection of small systems that are all equivalent, distinguishable, and independent. By introducing a new extensive variable $\mathcal{N}$, equal to the number of small system replicas, the differential energy of the collection of small systems can be expressed as

$$\mathrm{d}U_{\mathrm{t}} = T\mathrm{d}S_{\mathrm{t}} - p\mathrm{d}V_{\mathrm{t}} + \sum_{i=1}^{n} \mu_i \mathrm{d}N_{i,\mathrm{t}} + \mathscr{E}\,\mathrm{d}\mathcal{N}, \tag{1}$$

where U_{t} is the energy, T is the temperature, S_{t} is the entropy, p is the pressure, V_{t} is the volume, μ_i is the chemical potential of component i, and $N_{i,\mathrm{t}}$ is the number of particles of component i, where subscript t stands for the total collection of small system replicas. The property

$\mathscr{E}$ is called the subdivision potential and represents the change in U_t as we change the number of replicas at constant S_t, V_t, and $N_{i,t}$. From this starting point, Hill[26] retrieved the properties of a single small system by computing the averages of the total collection of small system replicas.

A key part of this derivation is that each thermodynamic ensemble is considered separately. As a consequence, the expression for the subdivision potential takes different forms for the different ensembles, which, in turn, gives rise to some unique small system properties. In the canonical ensemble, the subdivision potential is

$$\mathscr{E}(N,V,T) = F(N,V,T) + p(N,V,T)V - \mu(N,V,T)N, \quad (2)$$

where F represents the energy state function of the canonical ensemble. The subdivision potential in the grand canonical ensemble is represented by

$$\mathscr{E}(\mu,V,T) = \Upsilon(\mu,V,T) + p(\mu,V,T)V, \quad (3)$$

where υ represents the energy state function of the grand canonical ensemble. The subdivision potential in grand canonical systems is also connected to one of the unique small system properties through $\mathscr{E}(\mu,V,T) = (p-\hat{p})V$, where $\hat{p}$ is known as the integral pressure. For more details on the derivation of these properties, we refer to the books by Hill[46] or the extended explanations presented by Bedeaux, Kjelstrup, and Schnell.[44]

III. IDEAL GAS IN A SMALL SYSTEM WITH SURFACE ENERGY

In this section, we derive the thermodynamic properties of an ideal gas in a small confinement from the partition function of the system. Many steps of the derivation are based on well-known derivations of the properties of an ideal gas.[39] Therefore, only the outlines are provided here, while the full derivation can be found in the supplementary material.

In derivations of properties of macroscopic systems, it is normally assumed that $N \to \infty$, which justifies the use of approximations such as Stirling's approximation, $N! \approx (N/e)^N$. We will here avoid this assumption such that the final equations appropriately describe systems with a small number of particles.

A. The system

The system we consider here is a three-dimensional box with volume equal to L^3. The ideal gas particles do not interact with each other, but they can interact with the boundaries of the system. This means that the energy of the particles will depend on whether they are located close to the boundary of the system or not. When the particles are closer than a distance δ from a wall of the system, they experience a potential energy contribution U^s from that wall. This means that if a particle is close to an edge, it experiences a potential energy of $2U^s$, and if it is close to a corner, it experiences a potential energy of $3U^s$. The system and the different potential energy zones are illustrated in Fig. 1. The potential energy is included in the Hamiltonian through the Heaviside function

$$H(x) = \begin{cases} 0 & \text{if } x < 0, \\ 1 & \text{if } x \geq 0. \end{cases}$$

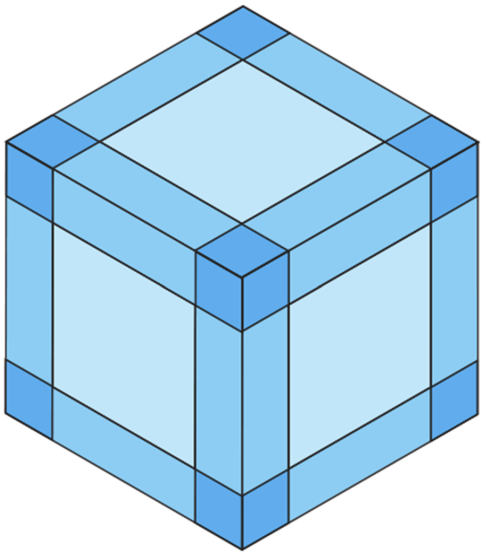

FIG. 1. Illustration of the cubic simulation box with surface energy U^s experienced by particles closer than a distance δ from each wall. Particles close to the sides (light blue regions) experience a potential energy contribution of U^s, while particles close to the edges (medium blue regions) experience a potential energy contribution of $2U^s$, and particles close to the corners (dark blue regions) experience a potential energy contribution of $3U^s$.

The Hamiltonian as a function of the particles' momenta $\mathbf{p}$ and positions $\mathbf{r}$ then becomes

$$\mathscr{H}(\mathbf{p},\mathbf{r}) = \sum_{i=1}^{N}\sum_{\alpha=1}^{3}\left(\frac{p_{\alpha i}^2}{2m_i} + U^s[H(\delta-\alpha_i) + H(\alpha_i-(L-\delta))]\right), \quad (4)$$

where m is the particle mass, $\beta = 1/k_B T$, where k_B is the Boltzmann constant, and $\alpha = (x,y,z)$ are the Cartesian coordinates.

1. Properties of a confined ideal gas in a closed system

The partition function of the closed system (canonical ensemble), computed from the Hamiltonian in Eq. (4), becomes

$$\begin{aligned} Q(N,V,T) &= \frac{1}{N!h^{3N}}\int_{D(V)}\int \mathrm{d}^N\mathbf{r}\mathrm{d}^N\mathbf{p}\,\exp(-\beta\mathscr{H}(\mathbf{p},\mathbf{r})) \\ &= \frac{1}{N!h^{3N}}\int_{D(V)}\mathrm{d}^N\mathbf{r}\,\exp\Bigg(-\beta U^s\sum_{i=1}^{N}\sum_{\alpha=1}^{3}[H(\delta-\alpha_i) \\ &\quad + H(\alpha_i-(L-\delta))]\Bigg) \\ &\quad \times\int\mathrm{d}^N\mathbf{p}\,\exp\Bigg(-\beta\sum_{i=1}^{N}\sum_{\alpha=1}^{3}\frac{p_{\alpha i}^2}{2m_i}\Bigg), \end{aligned} \quad (5)$$

where h is Planck's constant. Since there are no interactions between the particles, the integrals can be split into identical one-dimensional one-particle integrals. The integral over momenta and the integral over spatial coordinates can be solved separately. The integral over momenta becomes $1/\Lambda^3$, where $\Lambda = \sqrt{h^2\beta/2\pi m}$ is the de Broglie wavelength. The one-dimensional one-particle spatial integral can be split in three parts, where two of these integrals represent the regions that are influenced by the wall potential and one is the region that is not affected by U^s.

The final expression for the partition function then becomes

$$Q(N,V,T) = \frac{1}{N!}\left(\frac{L}{\Lambda}\left(1-\frac{2\delta}{L}\left(1-\exp(-\beta U^s)\right)\right)\right)^{3N}. \quad (6)$$

It is convenient to express the canonical partition function in terms of the one-particle canonical partition function, related to the canonical partition function through $Q(N,V,T) = Q(V,T)^N/N!$, where $Q(V,T)$ is given by

$$Q(V,T) = \frac{V}{\Lambda^3}\left(1-\frac{2\delta}{L}\left(1-\exp(-\beta U^s)\right)\right)^3. \quad (7)$$

The properties of a closed system are calculated from the known connection between the partition function and the energy state function. The energy state function of the closed system is the Helmholtz energy, which becomes

$$\begin{aligned} F(N,V,T) &= -k_B T \ln Q(N,V,T) \\ &= k_B T(\ln N! - N \ln Q(V,T)). \end{aligned} \quad (8)$$

The expressions for entropy, pressure, and chemical potential are found by differentiating the Helmholtz energy. By combining these identities, we can also find the expression for the subdivision potential shown in Eq. (2).

The properties in the closed system are split into three parts, where one represents the well-known bulk contribution, another describes the contribution from the surface energy, and the last arises from the exact treatment of the factorial term,

$$\mathscr{A}(N,V,T) = \mathscr{A}(N,V,T)_{\text{bulk}} + \mathscr{A}(N,V,T)_{\text{surf}} + \mathscr{A}(N,V,T)_{\text{fac}}. \quad (9)$$

The different contributions to the thermodynamic properties are presented in Table I, where we assume that the surface energy U^s is independent of N, V, and T such that its partial derivatives become zero. The complete derivation and the expressions for the thermodynamic properties including the partial derivatives are presented in the supplementary material.

The properties presented in Table I show clear characteristics of small systems. The properties that are regarded as intensive in the thermodynamic limit are size dependent, and the properties that are regarded extensive in the thermodynamic limit are not directly proportional to system size. If U^s is non-zero, all properties in the closed system become non-extensive due to the $1/L$ dependence of the surface terms. If $U^s = 0$, only the properties that have non-zero factorial terms $\mathscr{A}(N,V,T)_{\text{fac}} \neq 0$ are influenced by the small number of particles.

2. Properties of a confined ideal gas in an open system

The partition function of an open system (grand canonical ensemble) is

$$\begin{aligned} \Xi(\mu,V,T) &= \sum_{N=0}^{\infty} \exp(\beta\mu N) Q(N,V,T) \\ &= \sum_{N=0}^{\infty} \frac{(\exp(\beta\mu)Q(V,T))^N}{N!}. \end{aligned} \quad (10)$$

By using $\exp(a) = \sum_{N=0}^{\infty} a^N/N!$, we get

$$\Xi(\mu,V,T) = \exp(\exp(\beta\mu)Q(V,T)), \quad (11)$$

and the energy state function of the open system is

$$\begin{aligned} \Upsilon(\mu,V,T) &= -k_B T \ln \Xi(\mu,V,T) \\ &= -k_B T \exp(\beta\mu) Q(V,T). \end{aligned} \quad (12)$$

The entropy, pressure, and number of particles in the open system are calculated from partial derivatives of the energy state function, and the subdivision potential is computed from Eq. (3). From Hill's[26] thermodynamics for small systems, we also have the integral pressure $\hat{p} = -\Upsilon(\mu,V,T)/V$.

The properties of the open system are represented by three contributions, but in contrast to the closed system, none of these arise from factorial terms. The total properties are given as a sum of

TABLE I. Thermodynamic properties of an ideal gas confined in a closed cubic box with surface energy U^s experienced by all particles within a distance δ from each wall.

$\mathscr{A}(N,V,T)$	$\mathscr{A}(N,V,T)_{\text{bulk}}$	$\mathscr{A}(N,V,T)_{\text{surf}}$	$\mathscr{A}(N,V,T)_{\text{fac}}$
$F(N,V,T)$	$Nk_BT\left(\ln\left(\frac{N}{V}\Lambda^3\right)-1\right)$	$-3\,Nk_BT\ln\left(1-\frac{2\delta}{L}\left(1-\exp(-\beta U^s)\right)\right)$	$k_BT\left(\ln N! - N\ln\left(\frac{N}{e}\right)\right)$
$S(N,V,T)$	$Nk_B\left(\ln\left(\frac{V}{N}\frac{1}{\Lambda^3}\right)+\frac{5}{2}\right)$	$Nk_B\left(3\ln\left(1-\frac{2\delta}{L}\left(1-\exp(-\beta U^s)\right)\right)+\frac{2\delta}{L}\frac{3\beta U^s\exp(-\beta U^s)}{1-\frac{2\delta}{L}(1-\exp(-\beta U^s))}\right)$	$-k_B\left(\ln N! - N\ln\left(\frac{N}{e}\right)\right)$
$p(N,V,T)$	$\frac{Nk_BT}{V}$	$\frac{Nk_BT}{V}\left(\frac{2\delta}{L}\frac{1-\exp(-\beta U^s)}{1-\frac{2\delta}{L}(1-\exp(-\beta U^s))}\right)$	$\cdots$
$\mu(N,V,T)$	$k_BT\ln\left(\frac{N}{V}\Lambda^3\right)$	$-3k_BT\ln\left(1-\frac{2\delta}{L}\left(1-\exp(-\beta U^s)\right)\right)$	$k_BT\left(\frac{1}{N!}\frac{\partial N!}{\partial N}-\ln N\right)$
$\mathscr{E}(N,V,T)$	$\cdots$	$Nk_BT\left(\frac{2\delta}{L}\frac{1-\exp(-\beta U^s)}{1-\frac{2\delta}{L}(1-\exp(-\beta U^s))}\right)$	$Nk_BT\left(\frac{\ln N!}{N}+1-\frac{1}{N!}\frac{\partial N!}{\partial N}\right)$

TABLE II. Thermodynamic properties of an ideal gas confined in an open cubic box with surface energy U^s experienced by all particles within a distance δ from each wall.

$\mathscr{B}(\mu,V,T)$	$\mathscr{B}(\mu,V,T)_{\text{bulk}}$	$\mathscr{B}(\mu,V,T)_{\text{surf},1}$
$\Upsilon(\mu,V,T)$	$-k_{\text{B}}T\exp(\beta\mu)\frac{V}{\Lambda^3}$	$\cdots$
$S(\mu,V,T)$	$k_{\text{B}}\exp(\beta\mu)\frac{V}{\Lambda^3}\left(\frac{5}{2}-\beta\mu\right)$	$k_{\text{B}}\exp(\beta\mu)\frac{V}{\Lambda^3}\left(\frac{2\delta}{L}\frac{3\beta U^s\exp(-\beta U^s)}{1-\frac{2\delta}{L}(1-\exp(-\beta U^s))}\right)$
$p(\mu,V,T)$	$k_{\text{B}}T\exp(\beta\mu)\frac{1}{\Lambda^3}$	$k_{\text{B}}T\exp(\beta\mu)\frac{1}{\Lambda^3}\left(\frac{2\delta}{L}\frac{1-\exp(-\beta U^s)}{1-\frac{2\delta}{L}(1-\exp(-\beta U^s))}\right)$
$N(\mu,V,T)$	$\exp(\beta\mu)\frac{V}{\Lambda^3}$	$\cdots$
$\mathscr{E}(\mu,V,T)$	$\cdots$	$k_{\text{B}}T\exp(\beta\mu)\frac{V}{\Lambda^3}\left(\frac{2\delta}{L}\frac{1-\exp(-\beta U^s)}{1-\frac{2\delta}{L}(1-\exp(-\beta U^s))}\right)$
$\hat{p}(\mu,V,T)$	$k_{\text{B}}T\exp(\beta\mu)\frac{1}{\Lambda^3}$	$\cdots$

a bulk contribution and a surface contribution, which is multiplied with an additional surface contribution

$$\mathscr{B}(\mu,V,T)=\left[\mathscr{B}(\mu,V,T)_{\text{bulk}}+\mathscr{B}(\mu,V,T)_{\text{surf},1}\right]\mathscr{B}(\mu,V,T)_{\text{surf},2}, \tag{13}$$

where

$$\mathscr{B}(\mu,V,T)_{\text{surf},2}=\left(1-\frac{2\delta}{L}\left(1-\exp(-\beta U^s)\right)\right)^3. \tag{14}$$

The other two contributions to Eq. (13) are presented in Table II, where we again have assumed that the partial derivatives of U^s are zero.

In contrast to the closed systems, the small size contributions in the open systems are only present if U^s is non-zero. $U^s=0$ means that all size effects vanish and only the bulk contribution remains.

B. Comparing properties of a confined ideal gas in open and closed systems

When $\mathrm{d}U^s=0$, the properties in the open and closed systems can easily be compared at the same density, meaning that

$$\frac{N}{V}=\frac{N(\mu,V,T)}{V}=\exp(\beta\mu)\frac{1}{\Lambda^3}\left(1-\frac{2\delta}{L}\left(1-\exp(-\beta U^s)\right)\right)^3. \tag{15}$$

By inserting this expression into the identities shown in Tables I and II, we can directly compare the energy state functions, entropy, pressure, chemical potential, and subdivision potential of the open and closed systems.

It becomes clear that when the wall potential is independent of the ensemble variables ($\mathrm{d}U^s=0$), the difference between the properties of an ideal gas in the open and closed systems arises from the factorial terms given in the last column of Table I. This means that this difference is simply an effect of a small number of particles and not an effect of the surface. The surface effect does change the thermodynamic properties in both systems, meaning that they have different values than they would have in a bulk system, but this surface effect is the same in the open and the closed systems.

The surface energy, U^s, can in theory depend on temperature, system size, the number of particles and chemical potential. Strøm, Bedeaux, and Schnell[45] showed how it is possible to define U^s such that it depends on the surface area of an adsorbed phase. Since systems with this type of behavior is beyond the scope of this paper, we will not investigate this further here.

All factorial terms in the last column of Table I can be solved in an exact manner using the gamma function and the polygamma function, but approximations can be helpful to get insight into the form and magnitude of these terms. If we evaluate these terms with the regular Stirling's approximation, $N!\approx(N/e)^N$, which is normally used to derive properties in the thermodynamic limit, all factorial terms become zero. We therefore use a more accurate version of Stirling's approximation

$$N!\approx\sqrt{2\pi N}\left(\frac{N}{e}\right)^N, \tag{16}$$

which we refer to as "Stirling enhanced." Figure 2 shows that when the number of particles becomes small, it is crucial to compute factorials with a more accurate expression than the regular Stirling's approximation. The gamma function is exact for discrete numbers, but Stirling enhanced is a good representation, as long as the average number of particles is larger than one.

Using Eq. (16) results in the approximations for the factorial terms for the entropy,

$$S(N,V,T)_{\text{fac}}=-k_{\text{B}}\left(\ln N!-N\ln\left(\frac{N}{e}\right)\right)\approx-k_{\text{B}}\left(\frac{1}{2}\ln(2\pi N)\right), \tag{17}$$

and the chemical potential,

$$\mu(N,V,T)_{\text{fac}}=k_{\text{B}}T\left(\frac{1}{N!}\frac{\partial N!}{\partial N}-\ln N\right)\approx k_{\text{B}}T\left(\frac{1}{2}\frac{1}{N}\right). \tag{18}$$

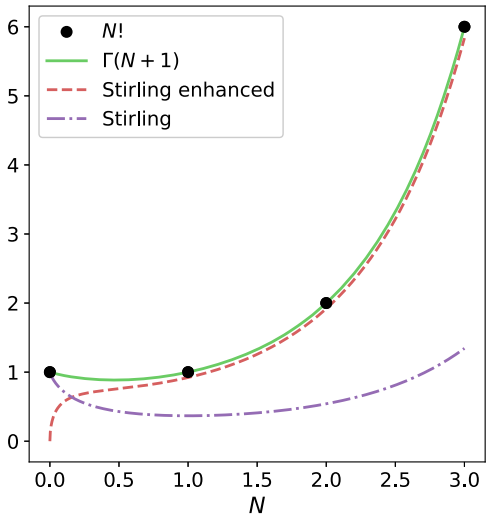

FIG. 2. The factorial computed from exact expressions and approximations. $\Gamma(N+1)$ represents the gamma function, which gives exact values of the factorial for discrete numbers.

The factorial contribution to the entropy is clearly increasing with the number of particles, while the factorial contribution to the chemical potential is decreasing with the number of particles.

IV. SIMULATION DETAILS

We use an in-house MC code, and all the presented values and results are given in reduced LJ units. We investigate systems with particles interacting via two types of potentials:

1. LJ particles interacting via the truncated and shifted potential with the cutoff radius at $r_c = 2.5$.
2. Particles interacting through the WCA potential,[47] which is the LJ potential truncated and shifted at $r_c = 2^{1/6}\sigma$.

The simulation boxes are cubic, and we investigate three types of boundary conditions:

1. The particles are confined by a hard wall. This means that the particles do not interact with the walls, but moves attempting to displace a particle outside the walls are rejected.
2. The wall is hard, and the particles closer than a distance $\delta = 1$ from each wall experience an additional potential energy of (a) $U^s = 1$ or (b) $U^s = 3$.
3. Periodic boundary conditions (PBCs). In order to compare to bulk properties.

The different combinations of simulation settings are presented in Table III.

TABLE III. Simulation settings for different boundary conditions (BCs) and interaction potentials (IPs) investigated. L is the simulation box length, T represents the temperature, n represents the number density, and μ is the chemical potential.

BC	IP	L	T	n	μ
1	LJ	3, 5, 7, 9	3	0.025–0.750	−7.0–7.5
1	WCA	3, 5, 7, 9	3	0.025–0.750	−7.0–13.5
2 (a)	LJ	3, 5, 7, 9	3	0.025–0.750	−7.0–7.5
2 (b)	LJ	3, 5, 7, 9	3	0.025–0.750	−4.0–10.5
3	LJ	15	3	0.025–0.750	−7.0–7.5

We run all simulations in five parallels for 10^6 cycles after equilibration. The number of trial moves (i.e., attempts to modify the system) carried out in each cycle has a lower limit of 20 but is otherwise equal to the number of particles. In the closed system, the chemical potential is computed using Widom's[48] test particle insertion method, which is sampled ten times the number of particles in the system, every cycle of the simulation. The pressure in both the open and the closed system is computed using the virial equation, which is sampled every cycle of the simulation.

V. RESULTS AND DISCUSSION

In this section, we present predictions for the ideal gas systems and the results from the MC simulations of systems with interacting particles.

A. Ideal gas

For the ideal gas, the results are computed in systems with $U^s = 1$ and $\delta = 1$ in order to analyze the small size contribution from both the surface terms and the factorial terms. We discuss in detail the ideal gas predictions for system sizes corresponding to the two smallest systems investigated by simulations. Figure 3 shows the energy state functions, entropy, pressure, and chemical potential as functions of density, n, for a system with size $L = 3$. For the presented densities, a system size of $L = 3$ corresponds to particle numbers between ~3 and 20. Entropy, pressure, and chemical potential show clear deviations from macroscopic values in both the open and the closed systems. The Helmholtz energy in the closed system also shows clear deviations from bulk values. Interestingly, we see that the relationship between Y and n is the same in a small system and in a macroscopic system. In addition, the relationship between $\hat{p}$ and n in a small system is equal to the relationship between p and n in a macroscopic system. A similar result was found for the integral and differential surface tensions of the adsorbed phase investigated by Strøm, Bedeaux, and Schnell.[45] The entropy in the open system is larger than the entropy in the closed system. This was also the case for the properties of the harmonic oscillators and the two-level systems presented by Miranda,[43] who found a higher entropy for the grand canonical systems than the canonical systems.

Figures 3(b) and 3(d) also clearly show the predictions of Eqs. (18) and (17) since the difference between the entropies in the two systems is increasing with density, while the difference between their chemical potentials is decreasing with density. This difference,

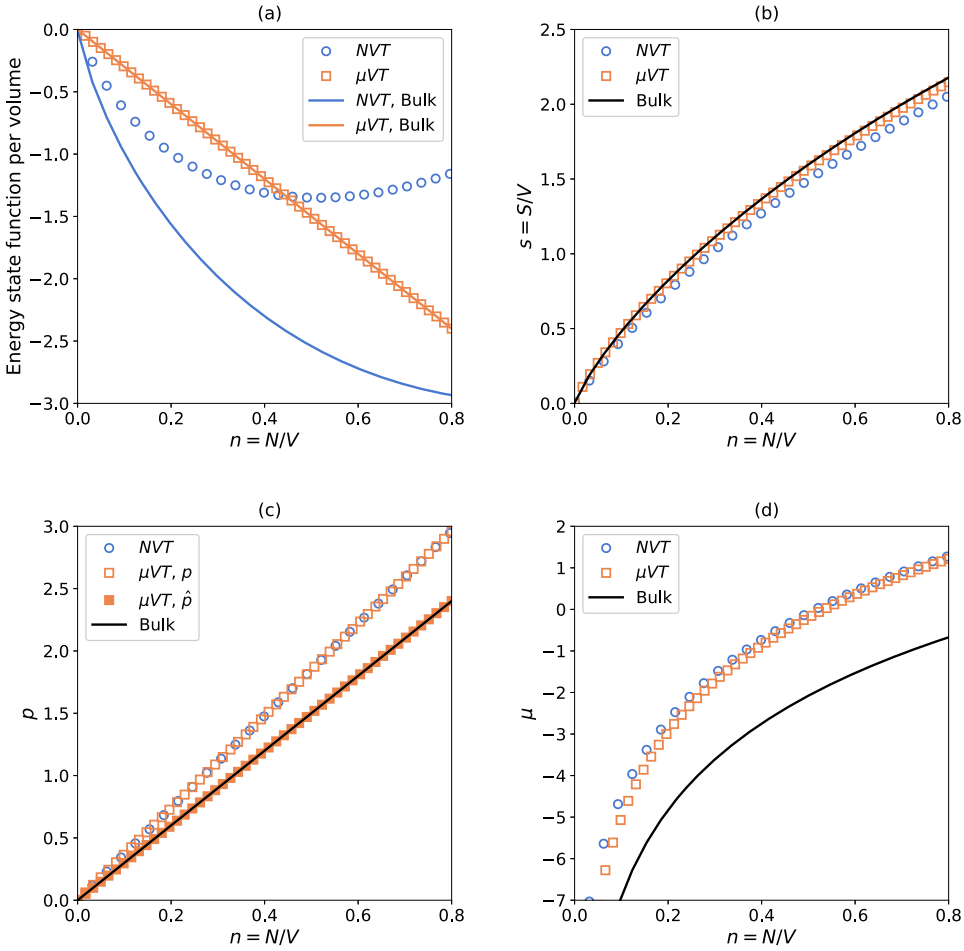

FIG. 3. (a)–(d) Energy state functions, entropy, pressure, and chemical potential as functions of number density of an ideal gas in a small cubic box with sides $L = 3$. The surface energy is $U^s = 1$ and is experienced by all particles within a distance $\delta = 1$ from each wall.

for both the entropy and the chemical potential, is decreasing as the system becomes larger. Figure 4 shows the energy state functions, entropy, pressure, and chemical potential for an ideal gas system with size $L = 5$. For the presented densities, this corresponds to particle numbers between ~12 and 100. We see that already at this size, the difference between the properties in the two ensembles is barely visible. Further increasing the size of the system gives properties that are visually indistinguishable for the ranges on the y axis considered here.

The subdivision potential is a central property of the nanothermodynamic description presented by Hill.[26] Equations (1)–(3) show that when the subdivision potential is zero, the nanothermodynamic description reduces to the macroscopic thermodynamic equations. The concept of the subdivision potential has received much attention in attempts to describe the thermodynamics of small systems.[28,44,45] However, with the exception of the work on spherical adsorbents by Strøm, Bedeaux, and Schnell,[45] its numerical values are usually not presented. For the ideal gas systems with sizes $L = 3$ and $L = 5$, the subdivision potential is shown in Fig. 5, where we can see that this property is also ensemble dependent.

The equations presented in Tables I and II, and the visualization of these in Figs. 3 and 4 show that an ideal gas in a cubic

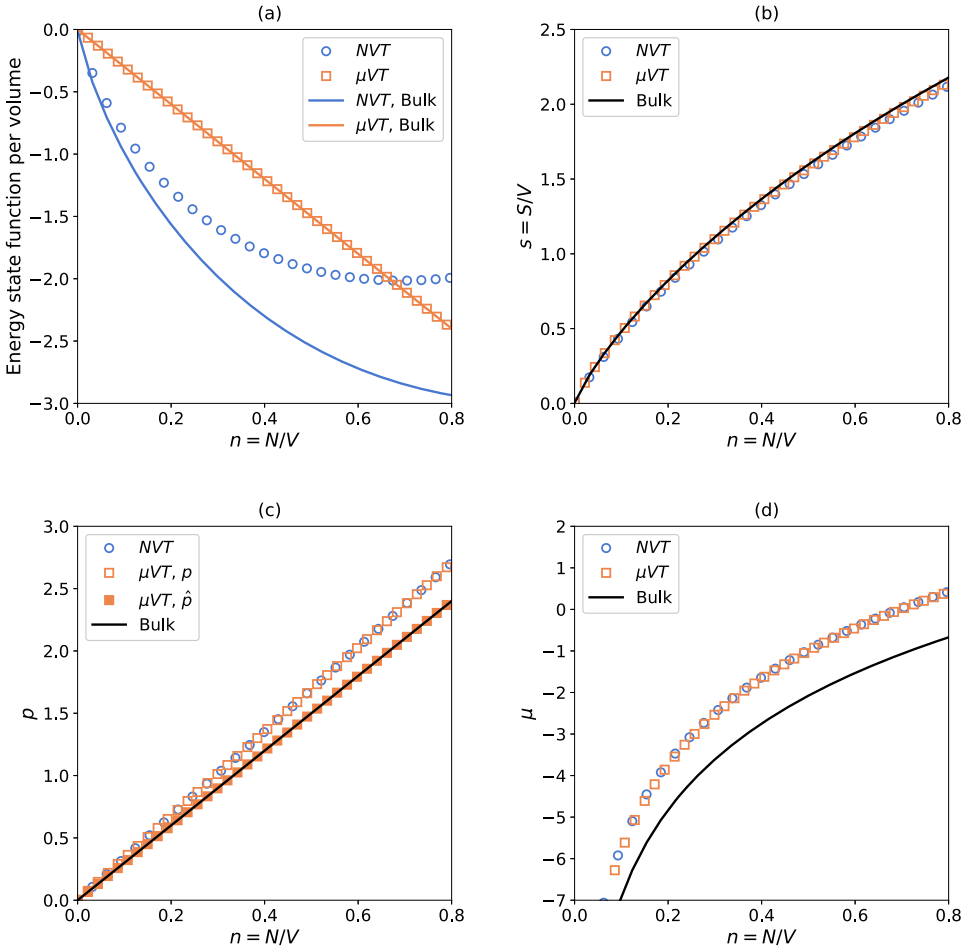

FIG. 4. (a)–(d) Energy state functions, entropy, pressure, and chemical potential as functions of number density of an ideal gas in a small cubic box with sides $L = 5$. The surface energy is $U^s = 1$ and is experienced by all particles within a distance $\delta = 1$ from each wall.

box is ensemble in-equivalent when the number of particles is small enough. It is, in general, not possible to give a universal limit for when N is small enough for these differences to become significant. The model presented here is one example of an ideal gas system that can be used to investigate finite size effects of this kind. Similar models can be derived for other geometries and dimensions, which can affect the magnitude of the surface terms and thereby change the relative importance of the factorial terms. The magnitude of the surface terms depends on the number of particles, the size and shape, U^s and δ, while the magnitude of the factorial terms only depends on the number of particles. However, the relative influence of the factorial terms will, of course, depend on the size and shape, U^s and δ.

Some general remarks that can be made are that the ensemble in-equivalence of the ideal gases does not depend on the surface energy as long as this surface energy does not depend on N, μ, V, or T. It is also not a result of long-range interactions since the ideal gas particles have no inter-particle interactions. In Sec. V B, we investigate how the results for the ideal gases can be used to gain insight into the ensemble equivalence for open and closed small systems with interacting particles.

B. Interacting particles

In this section, we investigate the properties of open and closed systems computed from MC simulations. Before we compare these

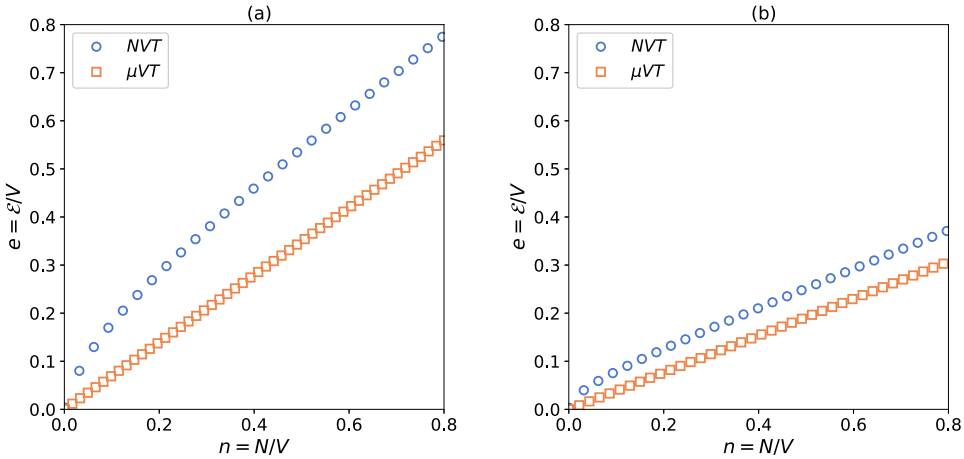

FIG. 5. Subdivision potential as a function of number density of an ideal gas in a small cubic box with sides (a) $L = 3$ and (b) $L = 5$. The surface energy is $U^s = 1$ and is experienced by all particles within a distance $\delta = 1$ from each wall.

results with those predicted by the ideal gas model, we discuss different methods for computation of average values in small systems. Error bars corresponding to two standard deviations are included in all figures with markers, but they are smaller than the marker size.

1. Computing averages in small systems

The macroscopic definitions used for computation of thermodynamic properties from simulations do not always apply to small systems.[44] One of the reasons for this is that the volume is often not uniquely defined for systems with significant surface effects. For homogeneous systems with periodic boundary conditions, the volume available to the center of masses of the molecules is equal to the full volume of the simulation box. For small confined systems, these two volumes often differ, which can affect the computation of the properties that depend on the system's volume. How to get a proper representation of volume dependent properties has been widely discussed, and new methods have been proposed for computation of both the pressure and the density of small systems.[20,27,28,49] The definition of system volume will also clearly affect the properties presented in this work. However, it should not affect the comparison between the properties in open and closed systems as long as their volumes are equally defined.

Something that can affect this comparison is the method used for computation of mean values. For the open system, two ways of computing the mean density are compared. The first is the *arithmetic mean*, which is the sum of all the sampled values, divided by the number of sampled values. This is also referred to as the average or the sample mean. Another alternative is the *population mean* or expected value, which is the number that is most likely to be observed during the simulations. For large systems, these two ways of computing the mean value should be equivalent. For small systems, however, the density distributions of the open system will have a cutoff at low densities since we cannot have a number of particles below zero.

In order to investigate how this influences the comparison of the properties in open and closed systems, we compare the two methods for the open LJ systems with $U^s = 1$. Figure 6, which displays some selected density distributions for this system with size $L = 3$, illustrates this effect. The population mean is extracted from the dashed lines, which are computed by fitting a Gaussian curve to

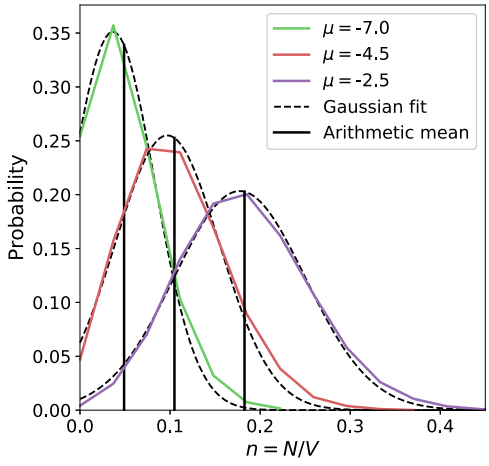

FIG. 6. Distribution of the number density for an open system with LJ particles for a few selected chemical potentials in a system with $L = 3$. The surface energy is $U^s = 1$ and is experienced by all particles within a distance $\delta = 1$ from each wall.

the distributions. For extracting the population mean, two different methods of curve fitting are tested. In the first method, all data points from the density distributions are included in the fit, while in the second approach, we only include the data points that are available symmetrically around the maximum value of each distribution. The two methods are found to give the same results within the statistical accuracies, and we therefore only present the population mean densities extracted from the symmetrical fit.

The black solid lines in Fig. 6 represent the arithmetic mean, which clearly do not fit the peaks of the distributions for low densities. It is also clear that the Gaussian curves do not fit the distributions perfectly but, instead, are shifted toward lower densities. The population mean density becomes lower than the arithmetic mean density, and the comparison of the properties in the open and closed systems is clearly influenced by the method used to compute the mean density.

This also becomes clear from Fig. 7, which shows the pressure and the chemical potential as functions of the density for small open and closed LJ systems with sizes $L = 3$ and $U^s = 1$. In the low density region, the difference between the densities computed from the arithmetic mean and the ones computed from the population mean is visible. For high densities, the two methods give overlapping densities.

Both methods still show that there is a difference between the chemical potentials in open and closed systems and that the trend is similar to that predicted by the ideal gas model in Fig. 3. Figure 7(a) also shows a slight difference between the pressures at higher densities, which is a feature not described by the ideal gas model. Since the main focus of this section is to investigate the differences between the arithmetic mean and the population mean, we discuss the deviations from the ideal gas model in more detail in Sec. V B 2.

Figure 8 shows the pressure and the chemical potential as functions of density in open and closed systems with size $L = 5$. Already at this size, the mean densities are close to indistinguishable.

For better visualization of the difference between the properties in open and closed systems, we fit a quadratic spline function to the data points displayed in Figs. 7 and 8 and the other investigated system sizes ($L = 7, 9$), as well as the system with PBCs. Since the spacing between the data points on the y axis is increasing in the high density region for the pressure and in the low density region for the chemical potential, we fit the spline functions only to the densities between $n = 0.1$–0.7 in order to reduce the chance of overfitting. The differences between the properties in the open and closed systems, based on these spline functions, are shown in Fig. 9 for the pressure and in Figs. 9 and 10 for the chemical potential. The predictions of the ideal gas model, shown in Tables I and II, are also included in the figure.

Also here we see a clear difference between the mean density computed by the arithmetic mean and the one computed by the population mean, as they give different trends as functions of the density. For both properties, the population mean gives less systematic results and displays larger fluctuations than those found by using the arithmetic mean. As shown in Fig. 6, neither of the methods perfectly describes the expected number of particles. The arithmetic mean does not fit the peak of the distribution, and the Gaussian curve, used to extract the population mean, does not fit the tails of the distribution. Due to the additional curve fitting step, the population mean becomes the less convenient method among the two. When we have such a low number of data points available, curve fitting can quickly induce errors. In the following, we therefore consider only the results represented by the arithmetic mean density.

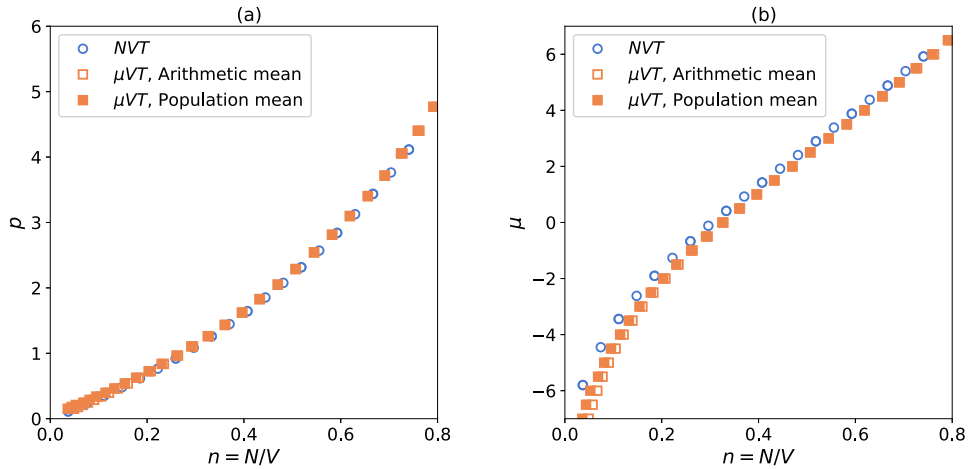

FIG. 7. (a) Pressure and (b) chemical potential as functions of number density of a LJ fluid in a small cubic box with sides $L = 3$, computed from MC simulations. The surface energy is $U^s = 1$ and is experienced by all particles within a distance $\delta = 1$ from each wall.

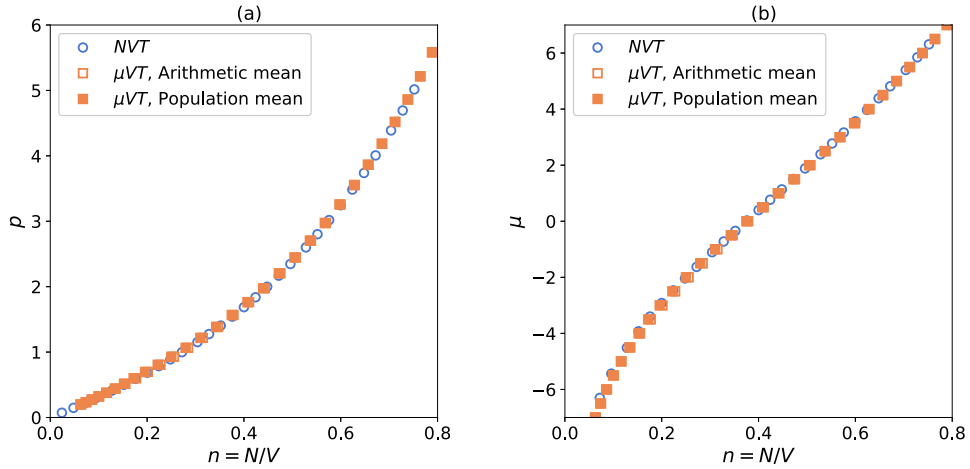

FIG. 8. (a) Pressure and (b) chemical potential as functions of number density of a LJ fluid in a small cubic box with sides $L = 5$, computed from MC simulations. The surface energy is $U^s = 1$ and is experienced by all particles within a distance $\delta = 1$ from each wall.

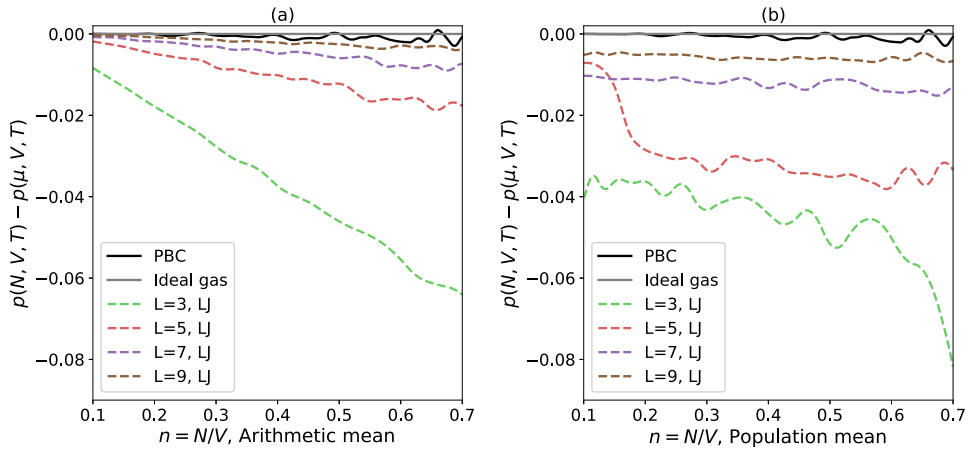

FIG. 9. How the difference in pressure of a LJ fluid in open and closed systems varies with arithmetic mean density (a) and population mean density (b) for differently sized small cubic boxes. The surface energy is $U^s = 1$ and is experienced by all particles within a distance $\delta = 1$ from each wall.

2. Properties in open and closed systems with interacting particles

In this section, we investigate how the pressure and the chemical potential differ in open and closed systems for different boundary conditions and particle types investigated by simulations. The results presented in Sec. VI already show that the properties in open and closed systems are different when the systems are small enough. Comparing Figs. 3(c) and 3(d) to Fig. 7 for size $L = 3$ and Figs. 4(c) and 4(d) to Fig. 8 for size $L = 5$ shows that in the low density region, the pressure and chemical potential of the interacting systems are similar to the values predicted by the ideal gas model. For the more dense systems, where the effects of crowding and cooperativity become important, we see larger differences. Figures showing computed values for all systems sizes, types of boundary conditions, and particle interactions are found in the supplementary material.

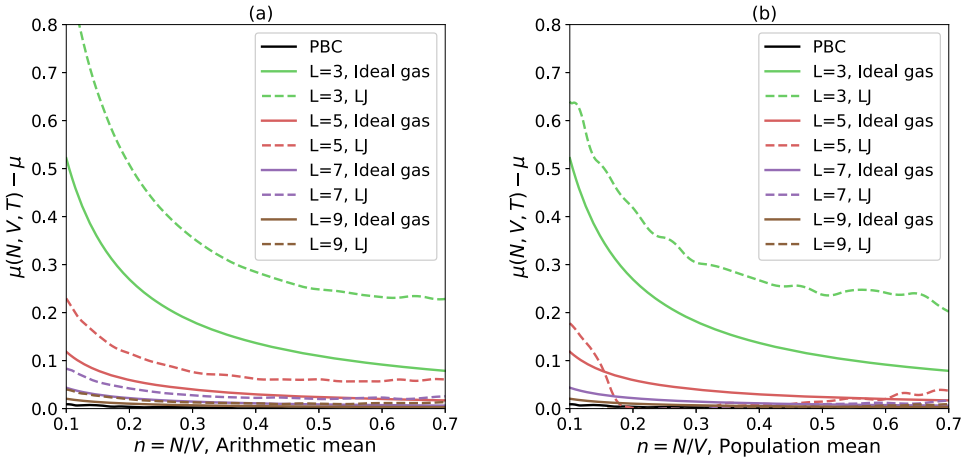

FIG. 10. How the difference in chemical potential of a LJ fluid in open and closed systems varies with arithmetic mean density (a) and population mean density (b) for differently sized small cubic boxes. The surface energy is $U^s = 1$ and is experienced by all particles within a distance $\delta = 1$ from each wall.

Figures 9 and 10 show that the differences between the properties in the open and closed systems cannot be fully explained by the ideal gas model. For the chemical potential difference, the trend of the interacting particles is very similar to the one predicted by the ideal gas model, which could indicate that this difference is partly described by the factorial terms. The contributions from the interactions between the particles can be investigated separately by subtracting the ideal gas prediction from the total property computed from simulations. To directly compare the magnitude of this contribution for the pressure and the chemical potential, the properties need to be evaluated for the same units. We therefore consider the conjugate pairs in the expression for the internal energy of the system, divided by the volume

$$u = sT - p + \mu n, \tag{19}$$

where $u = U/V$ and $s = S/V$.

The differences investigated are

$$\begin{aligned}\Delta(-p) &= \Delta(-p)_{\mathrm{IG}} + \Delta(-p)_{\mathrm{int}} \\ &= \left[(-p(N,V,T)) - (-p(\mu,V,T))\right]_{\mathrm{IG}} \\ &\quad + \left[(-p(N,V,T)) - (-p(\mu,V,T))\right]_{\mathrm{int}}\end{aligned} \tag{20}$$

and

$$\begin{aligned}\Delta(\mu n) &= \Delta(\mu n)_{\mathrm{IG}} + \Delta(\mu n)_{\mathrm{int}} \\ &= \left[\mu(N,V,T)n - \mu n(\mu,V,T)\right]_{\mathrm{IG}} \\ &\quad + \left[\mu(N,V,T)n - \mu n(\mu,V,T)\right]_{\mathrm{int}},\end{aligned} \tag{21}$$

where the subscript "IG" refers to the ideal gas contribution and "int" refers to the contribution from particle interactions. This is also often referred to as the residual contribution.

Figure 11 shows $\Delta(-p)$ and $\Delta(\mu n)$ for the four different sizes investigated for the system with LJ particles and $U^s = 1$. The values of $\Delta(-p)$ show clear linear trends for all system sizes, while the values of $\Delta(\mu n)$ are almost constant for low densities, with an increasing slope at higher densities. The ideal gas contribution to these properties shows very little dependence on density: $\Delta(-p)_{\mathrm{IG}} = 0$, while Eq. (18) shows that $\Delta(\mu n)_{\mathrm{IG}}$ is approximately constant for different densities when the volume is constant. The density dependence shown in Fig. 11 must therefore be related to contribution from the particle interactions, $\Delta(-p)_{\mathrm{int}}$ and $\Delta(\mu n)_{\mathrm{int}}$.

This contribution becomes more important at higher densities, which could indicate that it is related to the particles' excluded volume. The excluded volume of a particle is the volume that is inaccessible to other particles in the system due to the presence of the first particle. At higher densities, a larger portion of the system will be occupied by the particles' excluded volume. At higher densities, a larger portion of the system's volume will be occupied by the particles' excluded volume. This is similar to the results found from simulations of stretching of polymer chains performed by Bering *et al.*[29] In the comparison between isomeric stretching and isotensional stretching they find that for small forces, the molecules are in what they call an entropic regime. In this regime, the molecule has numerous degrees of freedom for movements, and the system is ensemble equivalent. As the molecule becomes more stretched out, the properties computed in the isomeric and the isotensional ensembles start to differ. This could indicate that restricted movement of particles causes related to ensemble in-equivalence. We further explore this by investigating the effect of changing the interactions between the particles and the wall and the effect of changing the interparticle interactions.

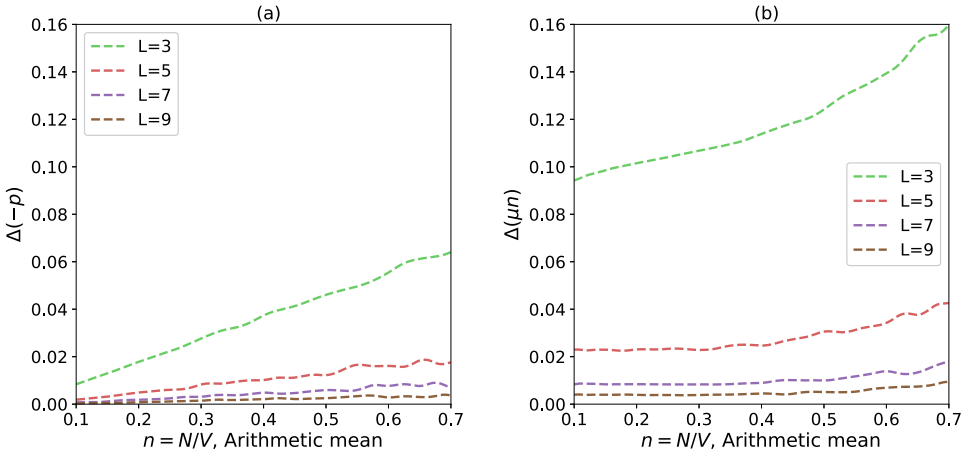

FIG. 11. How the difference in pressure (a) and the chemical potential (b), in open and closed systems varies with density. The simulation box sizes are $L = 3, 5, 7, 9$. The particles are interacting through the truncated and shifted LJ potential, and the surface energy is $U^s = 1$, which is experienced by all particles within a distance $\delta = 1$ from each wall.

First, we investigate how the value of the surface energy, U^s, influences the difference between the properties in the open and closed systems. Higher values of U^s means that the particles are less likely to be positioned close to the system walls. For better readability, the following figures (Figs. 12 and 13) only show the results of the two smallest systems. Figure 12 shows how $\Delta(-p)$ and $\Delta(\mu n)$ depend on the density for $U^s = 0$, $U^s = 1$, and $U^s = 3$. As the surface energy is increasing, the values of $\Delta(\mu n)$ become larger. For the pressure, however, the difference still shows a linear trend, but it is not increasing with U^s. As U^s becomes larger, these lines, instead, show a slight decrease in the slope and an increase in the intersection with the y axis.

By changing the interparticle interactions, the excluded volume also changes. The WCA potential is a purely repulsive potential,

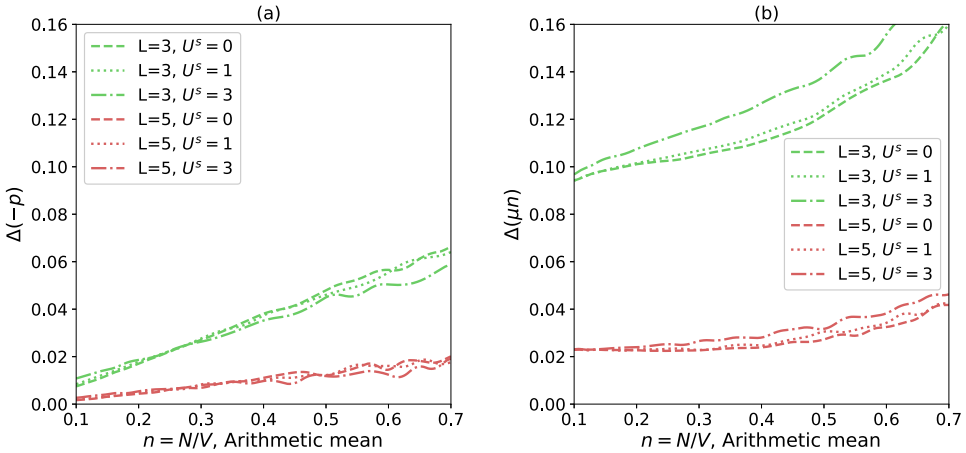

FIG. 12. How the difference between pressure (a) and the chemical potential (b) in open and closed systems varies with density. The simulation box sizes are $L = 3, 5$. The particles are interacting through the truncated and shifted LJ potential, and the surface energies are $U^s = 0$ (dashed lines), $U^s = 1$ (dotted lines), or $U^s = 3$ (dashed-dotted lines), which is experienced by all particles within a distance $\delta = 1$ from each wall.

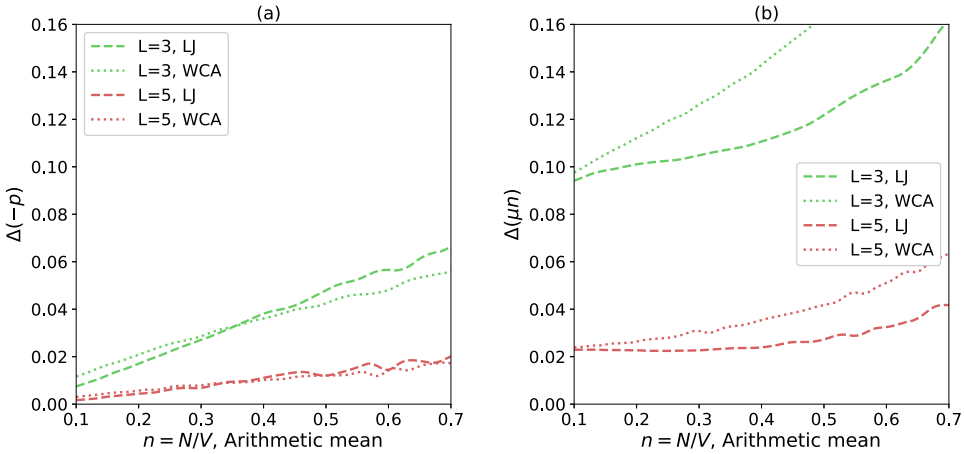

FIG. 13. How the difference between pressure (a) and the chemical potential (b) in open and closed systems varies with density. The particles are interacting through the truncated and shifted LJ potential (dashed lines) or the WCA potential (dotted lines). The simulation box sizes are $L = 3, 5$. There is no surface energy ($U^s = 0$).

and since it consists of the LJ potential truncated and shifted at its minimum, it has a larger excluded volume than the LJ potential. Figure 13 compares the values of $\Delta(-p)$ and $\Delta(\mu n)$ for the LJ systems and the WCA systems with $U^s = 0$. Figure 13 shows that similar to a larger excluded volume is similar to increased repulsive forces close to the walls. The values of $\Delta(\mu n)$ are larger for the WCA systems than they are for the LJ systems, and the change in the slope of $\Delta(-p)$ is more visible in this plot.

This indicates that, for the systems investigated here, the contribution from particle interactions to the difference between the properties in open and closed systems is related to restrictions in the movement of particles. As the movements of the particles become more restricted, the difference in the chemical potential shows a stronger dependence on density. The pressure, on the other hand, becomes less dependent on density and is, instead, approaching a constant value. At this stage, it is unclear why $\Delta(-p)$ and $\Delta(\mu n)$ respond differently to these changes. It is possible that the pressure difference is affected by crowding and cooperativity in a way that is not described by the restriction in movement of the particles alone. Or, it could be related to the fact that N is a canonical variable and μ is a grand canonical variable, while p is neither a canonical nor a grand canonical variable. This can be further studied by investigating the effect of restrictions in particle movement for pairs of ensemble variables of other dual statistical ensembles, such as U and T in the microcanonical and canonical ensemble or V and p in the canonical and the isobaric–isothermal ensemble. However, this falls beyond the scope of the present work.

VI. CONCLUSION

The thermodynamics of small systems is known to deviate from that of bulk systems. One consequence of this is that the properties can become ensemble dependent. We investigate the ensemble equivalence of open (grand canonical) and closed (canonical) ensembles for small systems containing ideal gas particles and for systems containing particles interacting via either the LJ or the WCA potentials.

Ideal gas systems are investigated analytically by deriving the properties from the respective partition functions. A surface contribution is introduced to the ideal gas particles' potential energy through a surface energy U^s experienced by particles closer than a distance δ from each wall. The purpose of this is to investigate whether the behavior of a simple model system can provide insight into the ensemble in-equivalence of more complex systems with interacting particles. For the ideal gas, we find that the properties in open and closed ensembles are not equivalent. The ensemble in-equivalence is not a consequence of the surface energy since the surface contribution to the ideal gas properties is equivalent in the open and closed systems. The difference between the properties of the ideal gas in the open and closed systems is, instead, a result of factorial terms that appear in the properties of the closed system. These terms only depend on the number of particles and are direct consequences of avoiding assumptions about $N \to \infty$, such as Stirling's approximation.

The systems with interacting particles are investigated through MC simulations. With a small number of particles, the systems investigated through simulations have different pressures and chemical potentials in the open and closed systems. We find that the magnitude of the difference between the properties in the open and closed systems of a given volume depends on the surface energy U^s, the interatomic interactions, and the density. This deviates from the prediction of the difference between the properties in the open and closed systems of the ideal gas, which for a given volume is independent of U^s and approximately independent of density. For the interacting particles, we also find that increasing the particles' excluded volume, and increasing the repulsive forces close to the

walls, results in similar responses in the differences between properties in open and closed systems. This indicates that the contribution to ensemble in-equivalence, which is not explained by the ideal gas model, is connected to the restricted movement of particles in the systems and that system features that increase this restriction can lead to larger differences between the properties in the open and closed systems.

SUPPLEMENTARY MATERIAL

See the supplementary material for the full derivation of the properties of the ideal gases and the computed thermodynamic properties for all systems investigated through simulations.

ACKNOWLEDGMENTS

This work was supported by the Research Council of Norway (Grant No. 275754). Thanks to the Center of Excellence funding scheme of the Research Council of Norway, (Grant No. 262644), PoreLab. Computational resources are provided by UNINETT Sigma2—The National Infrastructure for High Performance Computing and Data Storage in Norway (Grant No. NN9414k).

AUTHOR DECLARATIONS

Conflict of Interest

The authors have no conflicts to disclose.

DATA AVAILABILITY

The data that support the findings of this study are available from the corresponding author upon reasonable request.

REFERENCES

[1] D. Frenkel and B. Smit, *Understanding Molecular Simulation*, 2nd ed. (Academic Press, 2002).
[2] I. Oppenheim and P. Mazur, "Density expansions of distribution functions. I.: Virial expansion for finite closed systems: Canonical esemble," Physica **23**, 197–215 (1957).
[3] J. L. Lebowitz and J. K. Percus, "Long-range correlations in a closed system with applications to nonuniform fluids," Phys. Rev. **122**, 1675–1691 (1961).
[4] J. L. Lebowitz and J. K. Percus, "Thermodynamic properties of small systems," Phys. Rev. **124**, 1673–1681 (1961).
[5] J. I. Siepmann, I. R. McDonald, and D. Frenkel, "Finite-size corrections to the chemical potential," J. Phys.: Condens. Matter **4**, 679–691 (1992).
[6] P. Krüger, S. K. Schnell, D. Bedeaux, S. Kjelstrup, T. J. H. Vlugt, and J.-M. Simon, "Kirkwood–Buff integrals for finite volumes," J. Phys. Chem. Lett. **4**, 235–238 (2013).
[7] J. Milzetti, D. Nayar, and N. F. A. van der Vegt, "Convergence of Kirkwood–Buff integrals of ideal and nonideal aqueous solutions using molecular dynamics simulations," J. Phys. Chem. B **122**, 5515–5526 (2018).
[8] N. Dawass, P. Krüger, S. K. Schnell, J.-M. Simon, and T. J. H. Vlugt, "Kirkwood-Buff integrals from molecular simulation," Fluid Phase Equilib. **486**, 21–36 (2019).
[9] W. W. Wood, F. R. Parker, and J. D. Jacobson, "Recent Monte Carlo calculations of the equation of state of Lenard-Jones and hard sphere molecules," Nuovo Cimento **9**, 133–143 (1958).
[10] B. J. Alder and T. E. Wainwright, "Studies in molecular dynamics. II. Behavior of a small number of elastic spheres," J. Chem. Phys. **33**, 1439–1451 (1960).
[11] K. Binder, "Finite size scaling analysis of ising model block distribution functions," Z. Phys. B: Condens. Matter **43**, 119–140 (1981).
[12] M. Rovere, P. Nielaba, and K. Binder, "Simulation studies of gas-liquid transitions in two dimensions via a subsystem-block-density distribution analysis," Z. Phys. B: Condens. Matter **90**, 215–228 (1993).
[13] S. K. Schnell, T. J. H. Vlugt, J.-M. Simon, D. Bedeaux, and S. Kjelstrup, "Thermodynamics of a small system in a μT reservoir," Chem. Phys. Lett. **504**, 199–201 (2011).
[14] S. K. Schnell, T. J. H. Vlugt, J.-M. Simon, D. Bedeaux, and S. Kjelstrup, "Thermodynamics of small systems embedded in a reservoir: A detailed analysis of finite size effects," Mol. Phys. **110**, 1069–1079 (2012).
[15] P. Ganguly and N. F. A. van der Vegt, "Convergence of sampling Kirkwood–Buff integrals of aqueous solutions with molecular dynamics simulations," J. Chem. Theory Comput. **9**, 1347–1355 (2013).
[16] R. Cortes-Huerto, K. Kremer, and R. Potestio, "Communication: Kirkwood-Buff integrals in the thermodynamic limit from small-sized molecular dynamics simulations," J. Chem. Phys. **145**, 141103 (2016).
[17] M. Heidari, K. Kremer, R. Potestio, and R. Cortes-Huerto, "Fluctuations, finite-size effects and the thermodynamic limit in computer simulations: Revisiting the spatial block analysis method," Entropy **20**, 222 (2018).
[18] M. Heidari, K. Kremer, R. Potestio, and R. Cortes-Huerto, "Finite-size integral equations in the theory of liquids and the thermodynamic limit in computer simulations," Mol. Phys. **116**, 3301–3310 (2018).
[19] B. A. Strøm, J.-M. Simon, S. K. Schnell, S. Kjelstrup, J. He, and D. Bedeaux, "Size and shape effects on the thermodynamic properties of nanoscale volumes of water," Phys. Chem. Chem. Phys. **19**, 9016–9027 (2017).
[20] V. Bråten, Ø. Wilhelmsen, and S. K. Schnell, "Chemical potential differences in the macroscopic limit from fluctuations in small systems," J. Chem. Inf. Model. **61**, 840–855 (2021).
[21] W. H. Roos, I. L. Ivanovska, A. Evilevitch, and G. J. L. Wuite, "Viral capsids: Mechanical characteristics, genome packaging and delivery mechanisms," Cell. Mol. Life Sci. **64**, 1484 (2007).
[22] N. P. Stone, G. Demo, E. Agnello, and B. A. Kelch, "Principles for enhancing virus capsid capacity and stability from a thermophilic virus capsid structure," Nat. Commun. **10**, 4471 (2019).
[23] M. Kulmala, H. Vehkamäki, T. Petäjä, M. Dal Maso, A. Lauri, V. M. Kerminen, W. Birmili, and P. H. McMurry, "Formation and growth rates of ultrafine atmospheric particles: A review of observations," J. Aerosol Sci. **35**, 143–176 (2004).
[24] H. Singh and R. S. Myong, "Critical review of fluid flow physics at micro- to nano-scale porous media applications in the energy sector," Adv. Mater. Sci. Eng. **2018**, 9565240.
[25] P. Sudarsanam, E. Peeters, E. V. Makshina, V. I. Parvulescu, and B. F. Sels, "Advances in porous and nanoscale catalysts for viable biomass conversion," Chem. Soc. Rev. **48**, 2366–2421 (2019).
[26] T. L. Hill, "Thermodynamics of small systems," J. Chem. Phys. **36**, 3182–3197 (1962).
[27] O. Galteland, D. Bedeaux, B. Hafskjold, and S. Kjelstrup, "Pressures inside a nano-porous medium. The case of a single phase fluid," Front. Phys. **7**, 60 (2019).
[28] M. T. Rauter, O. Galteland, M. Erdős, O. A. Moultos, T. J. H. Vlugt, S. K. Schnell, D. Bedeaux, and S. Kjelstrup, "Two-phase equilibrium conditions in nanopores," Nanomaterials **10**, 608 (2020).
[29] E. Bering, S. Kjelstrup, D. Bedeaux, J. M. Rubi, and A. S. de Wijn, "Entropy production beyond the thermodynamic limit from single-molecule stretching simulations," J. Phys. Chem. B **124**, 8909–8917 (2020).
[30] E. Bering, D. Bedeaux, S. Kjelstrup, A. S. de Wijn, I. Latella, and J. M. Rubi, "A Legendre-Fenchel transform for molecular stretching energies," Nanomaterials **10**, 2355 (2020).
[31] A. Campa, T. Dauxois, and S. Ruffo, "Statistical mechanics and dynamics of solvable models with long-range interactions," Phys. Rep. **480**, 57–159 (2009).
[32] D. F. A. Campa, T. Dauxois, and S. Ruffo, *Physics of Long-Range Interacting Systems* (Oxford University Press, 2014).
[33] J. M. Rubi, D. Bedeaux, and S. Kjelstrup, "Thermodynamics for single-molecule stretching experiments," J. Phys. Chem. B **110**, 12733–12737 (2006).

[34]H. Touchette, R. S. Ellis, and B. Turkington, "An introduction to the thermodynamic and macrostate levels of nonequivalent ensembles," Physica A **340**, 138–146 (2004).
[35]H. Touchette, "Ensemble equivalence for general many-body systems," Europhys. Lett. **96**, 50010 (2011).
[36]A. Campa, L. Casetti, I. Latella, A. Pérez-Madrid, and S. Ruffo, "Concavity, response functions and replica energy," Entropy **20**, 907 (2018).
[37]F. L. Román, A. González, J. A. White, and S. Velasco, "Fluctuations in the number of particles of the ideal gas: A simple example of explicit finite-size effects," Am. J. Phys. **67**, 1149–1151 (1999).
[38]D. Villamaina and E. Trizac, "Thinking outside the box: Fluctuations and finite size effects," Eur. J. Phys. **35**, 035011 (2014).
[39]M. E. Tuckerman, *Statistical Mechanics: Theory and Molecular Simulation* (Oxford University Press, Inc., New York, 2010).
[40]R. B. Shirts, S. R. Burt, and A. M. Johnson, "Periodic boundary condition induced breakdown of the equipartition principle and other kinetic effects of finite sample size in classical hard-sphere molecular dynamics simulation," J. Chem. Phys. **125**, 164102 (2006).
[41]M. J. Uline, D. W. Siderius, and D. S. Corti, "On the generalized equipartition theorem in molecular dynamics ensembles and the microcanonical thermodynamics of small systems," J. Chem. Phys. **128**, 124301 (2008).
[42]T. Niiyama, Y. Shimizu, T. R. Kobayashi, T. Okushima, and K. S. Ikeda, "Effect of translational and angular momentum conservation on energy equipartition in microcanonical equilibrium in small clusters," Phys. Rev. E **79**, 051101 (2009).
[43]E. N. Miranda, "Statistical mechanics of few-particle systems: Exact results for two useful models," Eur. J. Phys. **38**, 065101 (2017).
[44]D. Bedeaux, S. Kjelstrup, and S. K. Schnell, *Nanothermodynamics. General Theory* (PoreLab Publisher, 2020).
[45]B. A. Strøm, D. Bedeaux, and S. K. Schnell, "Adsorption of an ideal gas on a small spherical adsorbent," Nanomaterials **11**, 431 (2021).
[46]T. L. Hill, *Thermodynamics of Small Systems* (Dover Publications, New York, 1994).
[47]J. D. Weeks, D. Chandler, and H. C. Andersen, "Role of repulsive forces in determining the equilibrium structure of simple liquids," J. Chem. Phys. **54**, 5237–5247 (1971).
[48]B. Widom, "Some topics in the theory of fluids," J. Chem. Phys. **39**, 2808–2812 (1963).
[49]H. Reiss and D. Reguera, "Understanding the limitations of the virial in the simulation of nanosystems: A puzzle that stimulated the search for understanding," J. Phys. Chem. B **108**, 6555–6563 (2004).

Supporting Information for "Small Size Effects in Open and Closed Systems: What Can We Learn from Ideal Gases about Systems with Interacting Particles?"

Vilde Bråten,[1] Dick Bedeaux,[2] Øivind Wilhelmsen,[2] and Sondre Kvalvåg Schnell[1, a)]

[1)]*Department of Materials Science and Engineering, Norwegian University of Science and Technology, NTNU, Trondheim, NO-7491, Norway*

[2)]*PoreLab, Department of Chemistry, Norwegian University of Science and Technology, NTNU, Trondheim, NO-7491, Norway*

(Dated: 20 October 2021)

[a)]Electronic mail: sondre.k.schnell@ntnu.no

I. FULL DERIVATION OF IDEAL GAS IN A SMALL SYSTEM WITH SURFACE ENERGY

A. Partition function

We derive the thermodynamic properties of an ideal gas in a small confinement from the partition function of the system. In contrast to the derivation for macroscopic systems, where we safely can assume that $N \to \infty$, where N is the number of particles, we here avoid such assumptions in order for the equations to apply to systems with small number of particles. One example of such an assumption is Stirling's approximation. We consider the canonical and grand canonical ensembles. The particles in the ideal gas will not interact with each other, but they will interact with the boundaries of the system. This means that the energy of these particles will depend on whether they are located close to the boundary of the system or not.

The system is a three dimensional canonical system of size equal to L^3. When the particles are closer than a distance δ from the walls of the system, they experience a potential energy contribution U^s from that wall. This potential energy is therefore included in the Hamiltonian through the Heaviside function

$$H(x) = \begin{cases} 0, & \text{if } x < 0 \\ 1, & \text{if } x \geq 0 \end{cases}$$

The Hamiltonian as a function of the particle's momenta $\mathbf{p}$ and position $\mathbf{r}$ then becomes

$$\mathscr{H}(\mathbf{p},\mathbf{r}) = \sum_{i=1}^{N}\sum_{\alpha=1}^{3}\left(\frac{p_{\alpha i}^2}{2m_i} + U^s\left[H(\delta-\alpha_i)+H(\alpha_i-(L-\delta))\right]\right), \tag{1}$$

where m is the particle mass, $\beta = 1/k_{\mathrm{B}}T$, where T is the temperaure, and $\alpha = (x,y,z)$. The partition function becomes

$$\begin{aligned} Q(N,V,T) &= \frac{1}{N!h^{3N}}\int_{D(V)}\int \mathrm{d}^N\mathbf{r}\mathrm{d}^N\mathbf{p}\exp\left(-\beta\mathscr{H}(\mathbf{p},\mathbf{r})\right) \\ &= \frac{1}{N!h^{3N}}\int_{D(V)}\mathrm{d}^N\mathbf{r}\exp\left(-\beta U^s\sum_{i=1}^{N}\sum_{\alpha=1}^{3}\left[H(\delta-\alpha_i)+H(\alpha_i-(L-\delta))\right]\right) \\ &\times\int\mathrm{d}^N\mathbf{p}\exp\left(-\beta\sum_{i=1}^{N}\sum_{\alpha=1}^{3}\frac{p_{\alpha i}^2}{2m_i}\right) \end{aligned} \tag{2}$$

where h is Planck's constant. The integrals can be split into identical one-particle integrals since there are no interactions between the particles.

$$
\begin{aligned}
Q(N,V,T) = \frac{1}{N!}\Bigg(\Bigg[\int_{D(V)} \mathrm{d}\mathbf{r}_1 \exp\Bigg(-\beta U^s \sum_{\alpha=1}^{3}\big[H(\delta-\alpha_1)+H(\alpha_1-(L-\delta))\big]\Bigg)\Bigg] \\
\times \Bigg[\int_{D(V)} \mathrm{d}\mathbf{r}_2 \exp\Bigg(-\beta U^s \sum_{\alpha=1}^{3}\big[H(\delta-\alpha_2)+H(\alpha_2-(L-\delta))\big]\Bigg)\Bigg]\ldots \\
\Bigg[\int_{D(V)} \mathrm{d}\mathbf{r}_N \exp\Bigg(-\beta U^s \sum_{\alpha=1}^{3}\big[H(\delta-\alpha_N)+H(\alpha_N-(L-\delta))\big]\Bigg)\Bigg]\Bigg) \\
\times \Bigg(\Bigg[\frac{1}{h^3}\int \mathrm{d}\mathbf{p}_1 \exp\Bigg(-\beta \sum_{\alpha=1}^{3}\frac{p_{\alpha 1}^2}{2m_1}\Bigg)\Bigg]\Bigg[\frac{1}{h^3}\int \mathrm{d}\mathbf{p}_2 \exp\Bigg(-\beta \sum_{\alpha=1}^{3}\frac{p_{\alpha 2}^2}{2m_2}\Bigg)\Bigg]\ldots \\
\Bigg[\frac{1}{h^3}\int \mathrm{d}\mathbf{p}_N \exp\Bigg(-\beta \sum_{\alpha=1}^{3}\frac{p_{\alpha N}^2}{2m_N}\Bigg)\Bigg]\Bigg)
\end{aligned}
\tag{3}
$$

$$
\begin{aligned}
= \frac{1}{N!}\Bigg[\int_{D(V)} \mathrm{d}\mathbf{r} \exp\Bigg(-\beta U^s \sum_{\alpha=1}^{3}\big[H(\delta-\alpha)+H(\alpha-(L-\delta))\big]\Bigg)\Bigg]^N \\
\times \Bigg[\frac{1}{h^3}\int \mathrm{d}\mathbf{p} \exp\Bigg(-\beta \sum_{\alpha=1}^{3}\frac{p_\alpha^2}{2m}\Bigg)\Bigg]^N
\end{aligned}
$$

Each of the integrals inside the square brackets can be split in three dimensions. First we rewrite the integral over momenta as

$$
\begin{aligned}
\frac{1}{h^3}\int \mathrm{d}\mathbf{p} \exp\Bigg(-\beta\frac{\mathbf{p}^2}{2m}\Bigg) &= \frac{1}{h^3}\int_{-\infty}^{\infty}\mathrm{d}p_x \exp\Bigg(-\beta\frac{p_x^2}{2m}\Bigg)\int_{-\infty}^{\infty}\mathrm{d}p_y \exp\Bigg(-\beta\frac{p_y^2}{2m}\Bigg)\int_{-\infty}^{\infty}\mathrm{d}p_z \exp\Bigg(-\beta\frac{p_z^2}{2m}\Bigg) \\
&= \Bigg[\frac{1}{h}\int_{-\infty}^{\infty}\mathrm{d}p \exp\Bigg(-\beta\frac{p^2}{2m}\Bigg)\Bigg]^3
\end{aligned}
\tag{4}
$$

This can be solved by using

$$
\int_{-\infty}^{\infty}\mathrm{d}y \exp\left(-\alpha y^2\right) = \sqrt{\frac{\pi}{\alpha}} \tag{5}
$$

which gives

$$\left[\frac{1}{h}\int \mathrm{d}p \exp\left(-\beta\frac{p^2}{2m}\right)\right]^3 = \left[\sqrt{\frac{2\pi m}{\beta h^2}}\right]^3 = \frac{1}{\Lambda^3} \tag{6}$$

where $\Lambda = \sqrt{h^2\beta/2\pi m}$ is the de Broglie wavelength.

The spatial integral can be rewritten as

$$\begin{aligned}
&\int_{D(V)} \mathbf{dr} \exp\left(-\beta U^s \sum_{\alpha=1}^{3}\left[H(\delta-\alpha)+H(\alpha-(L-\delta))\right]\right) = \\
&\int_0^L \mathrm{d}x \exp\left(-\beta U^s\left[H(\delta-x)+H(x-(L-\delta))\right]\right) \\
&\times \int_0^L \mathrm{d}y \exp\left(-\beta U^s\left[H(\delta-y)+H(y-(L-\delta))\right]\right) \\
&\times \int_0^L \mathrm{d}z \exp\left(-\beta U^s\left[H(\delta-z)+H(z-(L-\delta))\right]\right)
\end{aligned} \tag{7}$$

$$= \left[\int_0^L \mathrm{d}x \exp\left(-\beta U^s\left[H(\delta-x)+H(x-(L-\delta))\right]\right)\right]^3$$

This can be solved by splitting it in three parts

$$\begin{aligned}
&\int_0^L \mathrm{d}x \exp\left(-\beta U^s\left[H(\delta-x)+H(x-(L-\delta))\right]\right) \\
&= \int_0^\delta \mathrm{d}x \exp\left(-\beta U^s\right) + \int_\delta^{L-\delta} \mathrm{d}x \exp\left(0\right) + \int_{L-\delta}^{L} \mathrm{d}x \exp\left(-\beta U^s\right) \\
&= L - 2\delta + 2\delta\exp\left(-\beta U^s\right) \\
&= L - 2\delta\left(1-\exp(-\beta U^s)\right) \\
&= L\left(1-\frac{2\delta}{L}\left(1-\exp(-\beta U^s)\right)\right)
\end{aligned} \tag{8}$$

The final expression for the partition function then becomes

$$Q(N,V,T) = \frac{1}{N!}\left(\frac{L}{\Lambda}\left(1-\frac{2\delta}{L}\left(1-\exp(-\beta U^s)\right)\right)\right)^{3N} \tag{9}$$

It is convenient to express the canonical partition function in terms of the one particle canonical partition function $Q(N,V,T) = Q(V,T)^N/N!$, where $Q(V,T)$ is

$$Q(V,T) = \frac{V}{\Lambda^3}\left(1-\frac{2\delta}{L}\left(1-\exp(-\beta U^s)\right)\right)^3 \tag{10}$$

B. Properties in the canonical ensemble

We calculate the properties in the canonical ensemble from their known connection to the partition function and free energy.

The Helmholtz energy becomes

$$\begin{aligned}
F(N,V,T) &= -k_{\mathrm{B}}T\ln Q(N,V,T) = k_{\mathrm{B}}T\left(\ln N! - N\ln Q(V,T)\right) \\
&= k_{\mathrm{B}}T\left\{\ln N! - N\ln\frac{V}{\Lambda^3} - 3N\ln\left(1-\frac{2\delta}{L}\left(1-\exp(-\beta U^s)\right)\right)\right\} \\
&= k_{\mathrm{B}}T\left\{N\ln\left(\frac{N}{e}\right) - N\ln\frac{V}{\Lambda^3} - 3N\ln\left(1-\frac{2\delta}{L}\left(1-\exp(-\beta U^s)\right)\right)\right. \\
&\left. - N\ln(\frac{N}{e}) + \ln N!\right\} \\
&= Nk_{\mathrm{B}}T\left\{\ln\left(\frac{N}{V}\Lambda^3\right) - 1 - 3\ln\left(1-\frac{2\delta}{L}\left(1-\exp(-\beta U^s)\right)\right)\right\} \\
&+ k_{\mathrm{B}}T\left(\ln N! - N\ln\left(\frac{N}{e}\right)\right)
\end{aligned} \tag{11}$$

We find expressions for entropy, pressure and chemical potential by differentiating the equation for Helmholtz free energy.

$$\begin{aligned}
S(N,V,T) &= -\left(\frac{\partial F(N,V,T)}{\partial T}\right)_{N,V} \\
&= Nk_{\mathrm{B}}\left\{\ln\left(\frac{V}{N}\frac{1}{\Lambda^3}\right) + \frac{5}{2} + 3\ln\left(1-\frac{2\delta}{L}\left(1-\exp(-\beta U^s)\right)\right)\right. \\
&\left. + \frac{2\delta}{L}\frac{3\left(\beta U^s - \frac{1}{k_{\mathrm{B}}}\left(\frac{\partial U^s}{\partial T}\right)_{N,V}\right)\exp(-\beta U^s)}{1-\frac{2\delta}{L}\left(1-\exp(-\beta U^s)\right)}\right\} - k_{\mathrm{B}}\left(\ln N! - N\ln\left(\frac{N}{e}\right)\right)
\end{aligned} \tag{12}$$

$$\begin{aligned}
p(N,V,T) &= -\left(\frac{\partial F(N,V,T)}{\partial V}\right)_{N,T} \\
&= \frac{Nk_{\mathrm{B}}T}{V}\left\{1 + \frac{2\delta}{L}\frac{1-\left(1+3\beta V\left(\frac{\partial U^s}{\partial V}\right)_{N,T}\right)\exp(-\beta U^s)}{1-\frac{2\delta}{L}\left(1-\exp(-\beta U^s)\right)}\right\}
\end{aligned} \tag{13}$$

$$\begin{aligned}\mu(N,V,T) &= \left(\frac{\partial F(N,V,T)}{\partial N}\right)_{V,T} \\ &= k_{\mathrm{B}}T\left\{\ln\left(\frac{N}{V}\Lambda^3\right) - 3\ln\left(1-\frac{2\delta}{L}\left(1-\exp(-\beta U^s)\right)\right)\right. \\ &\left. + \frac{2\delta}{L}\frac{3\beta N\left(\frac{\partial U^s}{\partial N}\right)_{V,T}\exp(-\beta U^s)}{1-\frac{2\delta}{L}\left(1-\exp(-\beta U^s)\right)}\right\} \\ &+ k_{\mathrm{B}}T\left(\frac{1}{N!}\frac{\partial N!}{\partial N} - \ln N\right)\end{aligned} \tag{14}$$

By combining the above identities we can also find an expression for the subdivision potential, which in the canonical ensemble is expressed as

$$\begin{aligned}\mathscr{E}(N,V,T) &= F(N,V,T) + p(N,V,T)V - \mu(N,V,T)N \\ &= Nk_{\mathrm{B}}T\left\{\frac{2\delta}{L}\frac{1-\left(1+3\beta\left(V\left(\frac{\partial U^s}{\partial V}\right)_{N,T} + N\left(\frac{\partial U^s}{\partial N}\right)_{V,T}\right)\right)\exp(-\beta U^s)}{1-\frac{2\delta}{L}\left(1-\exp(-\beta U^s)\right)}\right\} \\ &+ Nk_{\mathrm{B}}T\left(\frac{\ln N!}{N} + 1 - \frac{1}{N!}\frac{\partial N!}{\partial N}\right)\end{aligned} \tag{15}$$

1. *Constant U^s in the canonical ensemble*

If we assume that the energy U^s is constant and that its partial derivatives are zero, we get

$$\begin{aligned}S(N,V,T) &= -\left(\frac{\partial F(N,V,T)}{\partial T}\right)_{N,V} \\ &= Nk_{\mathrm{B}}\left\{\ln\left(\frac{V}{N}\frac{1}{\Lambda^3}\right) + \frac{5}{2} + 3\ln\left(1-\frac{2\delta}{L}\left(1-\exp(-\beta U^s)\right)\right)\right. \\ &\left. + \frac{2\delta}{L}\frac{3\beta U^s\exp(-\beta U^s)}{1-\frac{2\delta}{L}\left(1-\exp(-\beta U^s)\right)}\right\} - k_{\mathrm{B}}\left(\ln N! - N\ln\left(\frac{N}{e}\right)\right)\end{aligned} \tag{16}$$

$$\begin{aligned}p(N,V,T) &= -\left(\frac{\partial F(N,V,T)}{\partial V}\right)_{N,T} \\ &= \frac{Nk_{\mathrm{B}}T}{V}\left\{1 + \frac{2\delta}{L}\frac{1-\exp(-\beta U^s)}{1-\frac{2\delta}{L}\left(1-\exp(-\beta U^s)\right)}\right\}\end{aligned} \tag{17}$$

$$\begin{aligned}\mu(N,V,T) &= \left(\frac{\partial F(N,V,T)}{\partial N}\right)_{V,T} \\ &= k_{\mathrm{B}}T\left\{\ln\left(\frac{N}{V}\Lambda^3\right) - 3\ln\left(1-\frac{2\delta}{L}\left(1-\exp(-\beta U^s)\right)\right)\right\} \\ &+ k_{\mathrm{B}}T\left(\frac{1}{N!}\frac{\partial N!}{\partial N} - \ln N\right)\end{aligned} \tag{18}$$

$$\begin{aligned}\mathscr{E}(N,V,T) &= F(N,V,T) + p(N,V,T)V - \mu(N,V,T)N \\ &= Nk_{\mathrm{B}}T\left\{\frac{2\delta}{L}\frac{1-\exp(-\beta U^s)}{1-\frac{2\delta}{L}\left(1-\exp(-\beta U^s)\right)}\right\} \\ &+ Nk_{\mathrm{B}}T\left(\frac{\ln N!}{N} + 1 - \frac{1}{N!}\frac{\partial N!}{\partial N}\right)\end{aligned} \tag{19}$$

C. Macroscopic properties in the canonical ensemble

In the thermodynamic limit $N \to \infty$ and $1/L \to 0$, the expressions returns the macroscopic identities for all the thermodynamic properties properties.

$$Q(N,V,T) = \frac{1}{N!}\left(\frac{V}{\Lambda^3}\right)^N \tag{20}$$

$$F(N,V,T) = Nk_{\mathrm{B}}T\left(\ln\left(\frac{N}{V}\Lambda^3\right) - 1\right) \tag{21}$$

$$S(N,V,T) = Nk_{\mathrm{B}}\left(\ln\left(\frac{V}{N}\frac{1}{\Lambda^3}\right) + \frac{5}{2}\right) \tag{22}$$

$$p(N,V,T) = \frac{Nk_{\mathrm{B}}T}{V} \tag{23}$$

$$\mu(N,V,T) = k_{\mathrm{B}}T\ln\left(\frac{N}{V}\Lambda^3\right) \tag{24}$$

D. Properties in the grand canonical ensemble

We now consider the fluctuating properties in the grand canonical ensemble, where the chemical potential, volume and temperature is controlled.

The partition function for the grand canonical ensemble is given by

$$\Xi(\mu,V,T) = \sum_{N=0}^{\infty} \exp(\beta\mu N) Q(N,V,T) = \sum_{N=0}^{\infty} \frac{(\exp(\beta\mu)Q(V,T))^N}{N!} \tag{25}$$

By using

$$\exp(a) = \sum_{N=0}^{\infty} \frac{a^N}{N!} \tag{26}$$

we get

$$\begin{aligned} \Xi(\mu,V,T) &= \exp\left(\exp(\beta\mu)Q(V,T)\right) \\ &= \exp\left(\exp(\beta\mu)\frac{V}{\Lambda^3}\left(1-\frac{2\delta}{L}\left(1-\exp(-\beta U^s)\right)\right)^3\right) \end{aligned} \tag{27}$$

The free energy of the grand canonical ensemble is given by the grand potential which becomes

$$\begin{aligned} \Upsilon(\mu,V,T) &= -k_{\mathrm{B}}T\ln\Xi(\mu,V,T) \\ &= -k_{\mathrm{B}}T\exp(\beta\mu)\frac{V}{\Lambda^3}\left(1-\frac{2\delta}{L}\left(1-\exp(-\beta U^s)\right)\right)^3 \end{aligned} \tag{28}$$

We can calculate entropy, pressure and number of particles from partial derivatives of the free energy

$$\begin{aligned} S(\mu,V,T) &= -\left(\frac{\partial\Upsilon}{\partial T}\right)_{\mu,V} \\ &= k_{\mathrm{B}}\exp\left(\beta\mu\right)\frac{V}{\Lambda^3}\left(1-\frac{2\delta}{L}\left(1-\exp(-\beta U^s)\right)\right)^3 \\ &\times\left\{\frac{5}{2}-\beta\mu+\frac{2\delta}{L}\frac{3\left(\beta U^s-\frac{1}{k_{\mathrm{B}}}\left(\frac{\partial U^s}{\partial T}\right)_{\mu,V}\right)\exp(-\beta U^s)}{1-\frac{2\delta}{L}\left(1-\exp(-\beta U^s)\right)}\right\} \end{aligned} \tag{29}$$

$$
\begin{aligned}
p(\mu,V,T) &= -\left(\frac{\partial \Upsilon}{\partial V}\right)_{\mu,T} \\
&= k_{\mathrm{B}}T\exp(\beta\mu)\frac{1}{\Lambda^3}\left(1-\frac{2\delta}{L}\big(1-\exp(-\beta U^s)\big)\right)^3 \\
&\times\left\{1+\frac{2\delta}{L}\frac{1-\big(1+3\beta V\left(\frac{\partial U^s}{\partial V}\right)_{\mu,T}\big)\exp(-\beta U^s)}{1-\frac{2\delta}{L}\big(1-\exp(-\beta U^s)\big)}\right\}
\end{aligned}
\tag{30}
$$

$$
\begin{aligned}
N(\mu,V,T) &= -\left(\frac{\partial \Upsilon}{\partial \mu}\right)_{V,T} \\
&= \exp(\beta\mu)\frac{V}{\Lambda^3}\left(1-\frac{2\delta}{L}\big(1-\exp(-\beta U^s)\big)\right)^3 \\
&\times\left\{1-\frac{2\delta}{L}\frac{3\left(\frac{\partial U^s}{\partial \mu}\right)_{V,T}\exp(-\beta U^s)}{1-\frac{2\delta}{L}\big(1-\exp(-\beta U^s)\big)}\right\}
\end{aligned}
\tag{31}
$$

By combining the above identities we can also find an expression for the subdivision potential, which in the canonical ensemble is expressed as

$$
\begin{aligned}
\mathscr{E}(\mu,V,T) &= \Upsilon(\mu,V,T)+p(\mu,V,T)V \\
&= k_{\mathrm{B}}T\exp(\beta\mu)\frac{V}{\Lambda^3}\left(1-\frac{2\delta}{L}\big(1-\exp(-\beta U^s)\big)\right)^3 \\
&\times\left\{\frac{2\delta}{L}\frac{1-\big(1+3\beta V\left(\frac{\partial U^s}{\partial V}\right)_{\mu,T}\big)\exp(-\beta U^s)}{1-\frac{2\delta}{L}\big(1-\exp(-\beta U^s)\big)}\right\}
\end{aligned}
\tag{32}
$$

1. Constant U^s in the grand canonical ensemble

If we assume that the energy U^s is constant and that its partial derivatives are zero, we get

$$
\begin{aligned}
S(\mu,V,T) &= -\left(\frac{\partial \Upsilon}{\partial T}\right)_{\mu,V} \\
&= k_{\mathrm{B}}\exp(\beta\mu)\frac{V}{\Lambda^3}\left(1-\frac{2\delta}{L}\big(1-\exp(-\beta U^s)\big)\right)^3 \\
&\times\left\{\frac{5}{2}-\beta\mu+\frac{2\delta}{L}\frac{3\beta U^s\exp(-\beta U^s)}{1-\frac{2\delta}{L}\big(1-\exp(-\beta U^s)\big)}\right\}
\end{aligned}
\tag{33}
$$

$$
\begin{aligned}
p(\mu,V,T) &= -\left(\frac{\partial \Upsilon}{\partial V}\right)_{\mu,T} \\
&= k_{\mathrm{B}}T\exp(\beta\mu)\frac{1}{\Lambda^3}\left(1-\frac{2\delta}{L}\big(1-\exp(-\beta U^s)\big)\right)^3 \\
&\times\left\{1+\frac{2\delta}{L}\frac{1-\exp(-\beta U^s)}{1-\frac{2\delta}{L}\big(1-\exp(-\beta U^s)\big)}\right\}
\end{aligned}
\tag{34}
$$

$$
\begin{aligned}
N(\mu,V,T) &= -\left(\frac{\partial \Upsilon}{\partial \mu}\right)_{V,T} \\
&= \exp(\beta\mu)\frac{V}{\Lambda^3}\left(1-\frac{2\delta}{L}\big(1-\exp(-\beta U^s)\big)\right)^3
\end{aligned}
\tag{35}
$$

$$
\begin{aligned}
\mathscr{E}(\mu,V,T) &= \Upsilon(\mu,V,T)+p(\mu,V,T)V \\
&= k_{\mathrm{B}}T\exp(\beta\mu)\frac{V}{\Lambda^3}\left(1-\frac{2\delta}{L}\big(1-\exp(-\beta U^s)\big)\right)^3 \\
&\times\left\{\frac{2\delta}{L}\frac{1-\exp(-\beta U^s)}{1-\frac{2\delta}{L}\big(1-\exp(-\beta U^s)\big)}\right\}
\end{aligned}
\tag{36}
$$

E. Macroscopic properties in the grand canonical ensemble

In the thermodynamic limit $N\to\infty$ and $1/L\to 0$, the expressions returns the macroscopic identities for all the thermodynamic properties properties.

$$
\Xi(\mu,V,T) = \exp\left(\exp(\beta\mu)\frac{V}{\Lambda^3}\right) \tag{37}
$$

$$
\Upsilon(\mu,V,T) = -k_{\mathrm{B}}T\exp(\beta\mu)\frac{V}{\Lambda^3} \tag{38}
$$

$$
S(\mu,V,T) = k_{\mathrm{B}}\exp(\beta\mu)\frac{V}{\Lambda^d}\left(\frac{5}{2}-\beta\mu\right) \tag{39}
$$

$$
p(\mu,V,T) = k_{\mathrm{B}}T\exp(\beta\mu)\frac{1}{\Lambda^3} \tag{40}
$$

$$
N(\mu,V,T) = \exp(\beta\mu)\frac{V}{\Lambda^3} \tag{41}
$$

F. Comparing properties

Properties in the canonical and grand canonical ensemble can easily be compared for the case of $dU^s = 0$ if we investigate the properties at the same density, meaning that N/V in the canonical ensemble is equal to the $N(\mu,V,T)/V$ in the grand canonical ensemble.

1. Number of particles

$$N(\mu,V,T) = \exp(\beta\mu)\frac{V}{\Lambda^3}\left(1-\frac{2\delta}{L}\left(1-\exp(-\beta U^s)\right)\right)^3 \tag{42}$$

Rewritten as an expression for chemical potential in the grand canonical ensemble gives

$$\mu = k_\mathrm{B}T\left\{\ln\left(\frac{N(\mu,V,T)}{V}\Lambda^3\right) - 3\ln\left(1-\frac{2\delta}{L}\left(1-\exp(-\beta U^s)\right)\right)\right\} \tag{43}$$

2. Chemical potential

$$\begin{aligned}\mu(N,V,T) &= k_\mathrm{B}T\left\{\ln\left(\frac{N}{V}\Lambda^3\right) - 3\ln\left(1-\frac{2\delta}{L}\left(1-\exp(-\beta U^s)\right)\right)\right\} \\ &\quad + k_\mathrm{B}T\left(\frac{1}{N!}\frac{\partial N!}{\partial N} - \ln N\right) \\ &= \mu + k_\mathrm{B}T\left(\frac{1}{N!}\frac{\partial N!}{\partial N} - \ln N\right)\end{aligned} \tag{44}$$

3. Free energy

$$\begin{aligned}F(N,V,T) &= Nk_\mathrm{B}T\left\{\ln\left(\frac{N}{V}\Lambda^3\right) - 1 - 3\ln\left(1-\frac{2\delta}{L}\left(1-\exp(-\beta U^s)\right)\right)\right\} \\ &\quad + k_\mathrm{B}T\left(\ln N! - N\ln\left(\frac{N}{e}\right)\right) \\ &= Nk_\mathrm{B}T\left\{\beta\mu(N,V,T) - \left(\frac{1}{N!}\frac{\partial N!}{\partial N} - \ln N\right) - 1\right\} + k_\mathrm{B}T\left(\ln N! - N\ln\left(\frac{N}{e}\right)\right) \\ &= \mu(N,V,T)N - Nk_\mathrm{B}T + Nk_\mathrm{B}T\left(\frac{\ln N!}{N} + 1 - \frac{1}{N!}\frac{\partial N!}{\partial N}\right)\end{aligned} \tag{45}$$

$$
\begin{aligned}
\Upsilon(\mu,V,T) &= -k_{\mathrm{B}}T\exp(\beta\mu)\frac{V}{\Lambda^3}\left(1-\frac{2\delta}{L}\big(1-\exp(-\beta U^s)\big)\right)^3 \\
&= -N(\mu,V,T)k_{\mathrm{B}}T \\
&= -Nk_{\mathrm{B}}T \\
&= F(N,V,T)-\mu(N,V,T)N-Nk_{\mathrm{B}}T\left(\frac{\ln N!}{N}+1-\frac{1}{N!}\frac{\partial N!}{\partial N}\right)
\end{aligned}
\tag{46}
$$

4. Entropy

$$
\begin{aligned}
S(N,V,T) = Nk_{\mathrm{B}}\Bigg\{ &\ln\left(\frac{V}{N}\frac{1}{\Lambda^3}\right)+\frac{5}{2}+3\ln\left(1-\frac{2\delta}{L}\big(1-\exp(-\beta U^s)\big)\right) \\
&+\frac{2\delta}{L}\frac{3\beta U^s\exp(-\beta U^s)}{1-\frac{2\delta}{L}\big(1-\exp(-\beta U^s)\big)}\Bigg\}-k_{\mathrm{B}}\left(\ln N!-N\ln\left(\frac{N}{e}\right)\right)
\end{aligned}
\tag{47}
$$

$$
\begin{aligned}
S(\mu,V,T) &= k_{\mathrm{B}}\exp(\beta\mu)\frac{V}{\Lambda^3}\left(1-\frac{2\delta}{L}\big(1-\exp(-\beta U^s)\big)\right)^3 \\
&\times\left\{\frac{5}{2}-\beta\mu+\frac{2\delta}{L}\frac{3\beta U^s\exp(-\beta U^s)}{1-\frac{2\delta}{L}\big(1-\exp(-\beta U^s)\big)}\right\} \\
&= N(\mu,V,T)k_{\mathrm{B}}\Bigg\{\ln\left(\frac{V}{N(\mu,V,T)}\frac{1}{\Lambda^3}\right)+\frac{5}{2}+3\ln\left(1-\frac{2\delta}{L}\big(1-\exp(-\beta U^s)\big)\right) \\
&+\frac{2\delta}{L}\frac{3\beta U^s\exp(-\beta U^s)}{1-\frac{2\delta}{L}\big(1-\exp(-\beta U^s)\big)}\Bigg\} \\
&= Nk_{\mathrm{B}}\Bigg\{\ln\left(\frac{V}{N}\frac{1}{\Lambda^3}\right)+\frac{5}{2}+3\ln\left(1-\frac{2\delta}{L}\big(1-\exp(-\beta U^s)\big)\right) \\
&+\frac{2\delta}{L}\frac{3\beta U^s\exp(-\beta U^s)}{1-\frac{2\delta}{L}\big(1-\exp(-\beta U^s)\big)}\Bigg\} \\
&= S(N,V,T)+k_{\mathrm{B}}\left(\ln N!-N\ln\left(\frac{N}{e}\right)\right)
\end{aligned}
\tag{48}
$$

5. Pressure

$$
p(N,V,T) = \frac{Nk_{\mathrm{B}}T}{V}\left\{1+\frac{2\delta}{L}\frac{1-\exp(-\beta U^s)}{1-\frac{2\delta}{L}\big(1-\exp(-\beta U^s)\big)}\right\}
\tag{49}
$$

$$
\begin{aligned}
p(\mu,V,T) &= k_{\mathrm{B}}T\exp(\beta\mu)\frac{1}{\Lambda^3}\left(1-\frac{2\delta}{L}\big(1-\exp(-\beta U^s)\big)\right)^3 \\
&\times\left\{1+\frac{2\delta}{L}\frac{1-\exp(-\beta U^s)}{1-\frac{2\delta}{L}\big(1-\exp(-\beta U^s)\big)}\right\} \\
&= k_{\mathrm{B}}T\frac{N(\mu,V,T)}{V}\left\{1+\frac{2\delta}{L}\frac{1-\exp(-\beta U^s)}{1-\frac{2\delta}{L}\big(1-\exp(-\beta U^s)\big)}\right\} \\
&= \frac{Nk_{\mathrm{B}}T}{V}\left\{1+\frac{2\delta}{L}\frac{1-\exp(-\beta U^s)}{1-\frac{2\delta}{L}\big(1-\exp(-\beta U^s)\big)}\right\} \\
&= p(N,V,T)
\end{aligned}
\tag{50}
$$

6. Subdivision potential

$$
\begin{aligned}
\mathscr{E}(N,V,T) &= Nk_{\mathrm{B}}T\left\{\frac{2\delta}{L}\frac{1-\exp(-\beta U^s)}{1-\frac{2\delta}{L}\big(1-\exp(-\beta U^s)\big)}\right\} \\
&+ Nk_{\mathrm{B}}T\left(\frac{\ln N!}{N}+1-\frac{1}{N!}\frac{\partial N!}{\partial N}\right)
\end{aligned}
\tag{51}
$$

$$
\begin{aligned}
\mathscr{E}(\mu,V,T) &= k_{\mathrm{B}}T\exp(\beta\mu)\frac{V}{\Lambda^3}\left(1-\frac{2\delta}{L}\big(1-\exp(-\beta U^s)\big)\right)^3 \\
&\times\left\{\frac{2\delta}{L}\frac{1-\exp(-\beta U^s)}{1-\frac{2\delta}{L}\big(1-\exp(-\beta U^s)\big)}\right\} \\
&= N(\mu,V,T)k_{\mathrm{B}}T\left\{\frac{2\delta}{L}\frac{1-\exp(-\beta U^s)}{1-\frac{2\delta}{L}\big(1-\exp(-\beta U^s)\big)}\right\} \\
&= Nk_{\mathrm{B}}T\left\{\frac{2\delta}{L}\frac{1-\exp(-\beta U^s)}{1-\frac{2\delta}{L}\big(1-\exp(-\beta U^s)\big)}\right\} \\
&= \mathscr{E}(N,V,T)-Nk_{\mathrm{B}}T\left(\frac{\ln N!}{N}+1-\frac{1}{N!}\frac{\partial N!}{\partial N}\right)
\end{aligned}
\tag{52}
$$

7. Energy

$$
E(N,V,T) = TS(N,V,T)-p(N,V,T)V+\mu(N,V,T)N+\mathscr{E}(N,V,T) \tag{53}
$$

$$
\begin{aligned}
E(\mu,V,T) &= TS(\mu,V,T) - p(\mu,V,T)V + \mu N(\mu,V,T) + \mathscr{E}(\mu,V,T) \\
&= TS(N,V,T) + k_{\mathrm{B}}T\left(\ln N! - N\ln\left(\frac{N}{e}\right)\right) - p(N,V,T)V \\
&+ \mu(N,V,T) - k_{\mathrm{B}}T\left(N\frac{1}{N!}\frac{\partial N!}{\partial N} - N\ln N\right) \\
&+ \mathscr{E}(N,V,T) - k_{\mathrm{B}}T\left(\ln N! + N - N\frac{1}{N!}\frac{\partial N!}{\partial N}\right) \\
&= E(N,V,T)
\end{aligned}
\tag{54}
$$

II. ADDITIONAL FIGURES

A. Results of LJ Simulations

1. *With surface energy* $U^s = 1$

Figures 1-4 show the pressure and chemical potential for LJ particles in systems with surface energy $U^s = 1$ experienced by all particles within a distance $\delta = 1$ from any wall, for system sizes $L = 3, 5, 7, 9$. Figure 5 shows the potential energies of these systems.

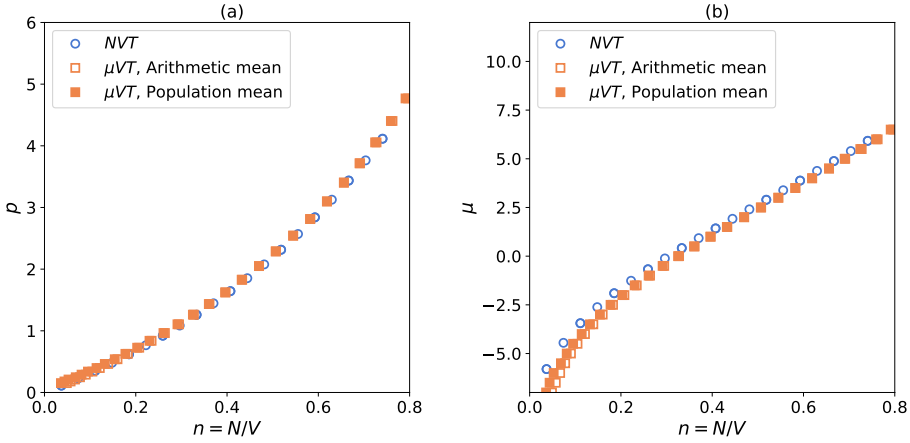

FIG. 1. Pressure and chemical potential as a function of number density of a LJ fluid in a small cubic box with sides $L = 3$, computed from MC simulations. The surface energy is $U^s = 1$ and is experienced by all particles within a distance $\delta = 1$ from any wall. The temperature is $T = 3$.

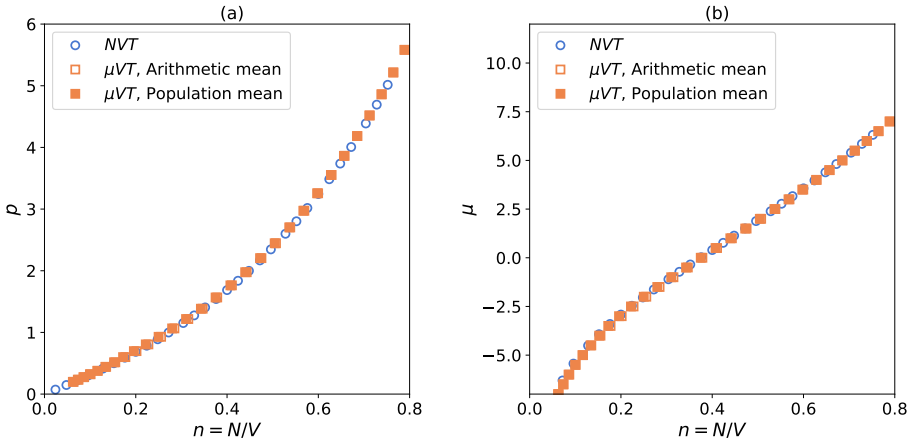

FIG. 2. Pressure and chemical potential as a function of number density of a LJ fluid in a small cubic box with sides $L = 5$, computed from MC simulations. The surface energy is $U^s = 1$ and is experienced by all particles within a distance $\delta = 1$ from any wall. The temperature is $T = 3$.

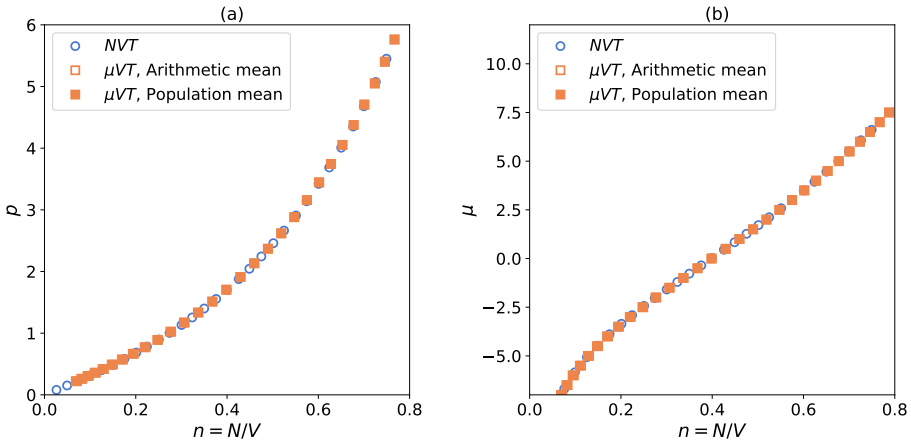

FIG. 3. Pressure and chemical potential as a function of number density of a LJ fluid in a small cubic box with sides $L = 7$, computed from MC simulations. The surface energy is $U^s = 1$ and is experienced by all particles within a distance $\delta = 1$ from any wall. The temperature is $T = 3$.

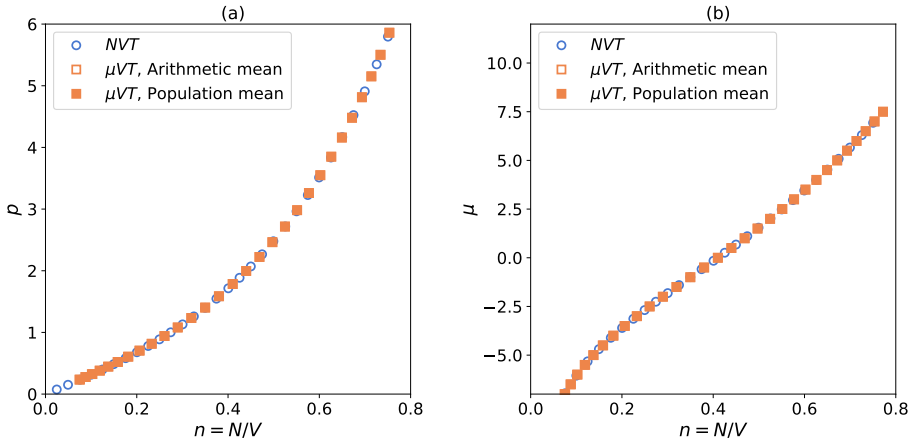

FIG. 4. Pressure and chemical potential as a function of number density of a LJ fluid in a small cubic box with sides $L = 9$, computed from MC simulations. The surface energy is $U^s = 1$ and is experienced by all particles within a distance $\delta = 1$ from any wall. The temperature is $T = 3$.

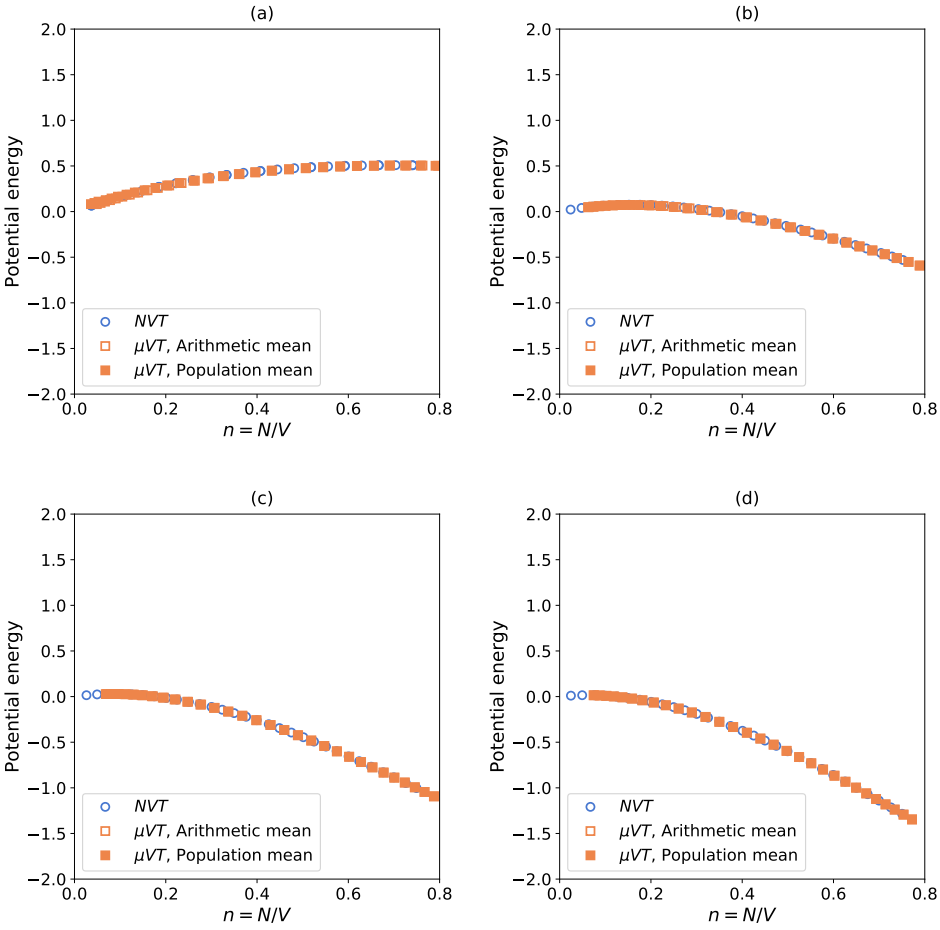

FIG. 5. Potential energy as a function of number density of a LJ fluid in a small cubic box with sides $L = 3$ (a), $L = 5$ (b), $L = 7$ (c) and $L = 9$ (d), computed from MC simulations. The surface energy is $U^s = 1$ and is experienced by all particles within a distance $\delta = 1$ from any wall. The temperature is $T = 3$.

2. *With surface energy* $U^s = 3$

Figures 11-14 show the pressure and chemical potential for LJ particles in systems with surface energy $U^s = 3$ experienced by all particles within a distance $\delta = 1$ from any wall, for system sizes $L = 3, 5, 7, 9$. Figure 15 shows the potential energies of these systems.

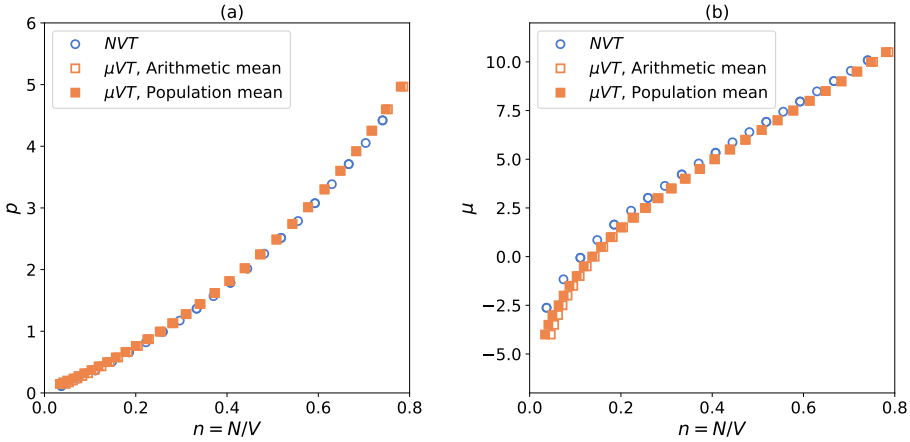

FIG. 6. Pressure and chemical potential as a function of number density of a LJ fluid in a small cubic box with sides $L = 3$, computed from MC simulations. The surface energy is $U^s = 3$ and is experienced by all particles within a distance $\delta = 1$ from any wall. The temperature is $T = 3$.

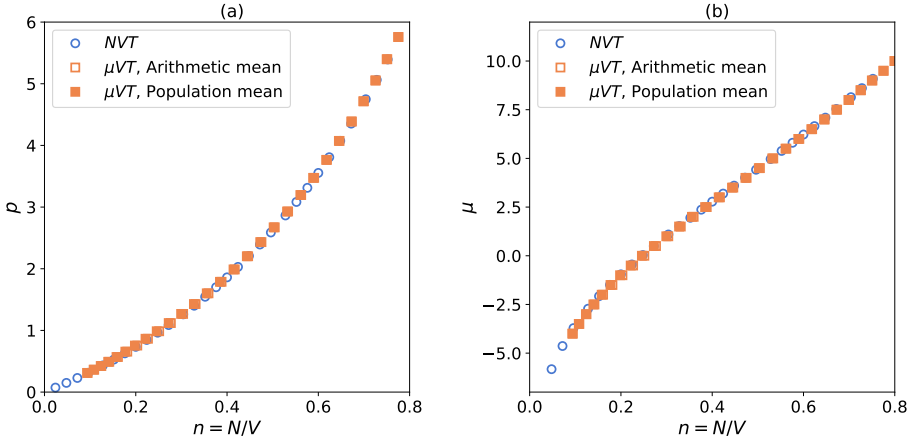

FIG. 7. Pressure and chemical potential as a function of number density of a LJ fluid in a small cubic box with sides $L = 5$, computed from MC simulations. The surface energy is $U^s = 3$ and is experienced by all particles within a distance $\delta = 1$ from any wall. The temperature is $T = 3$.

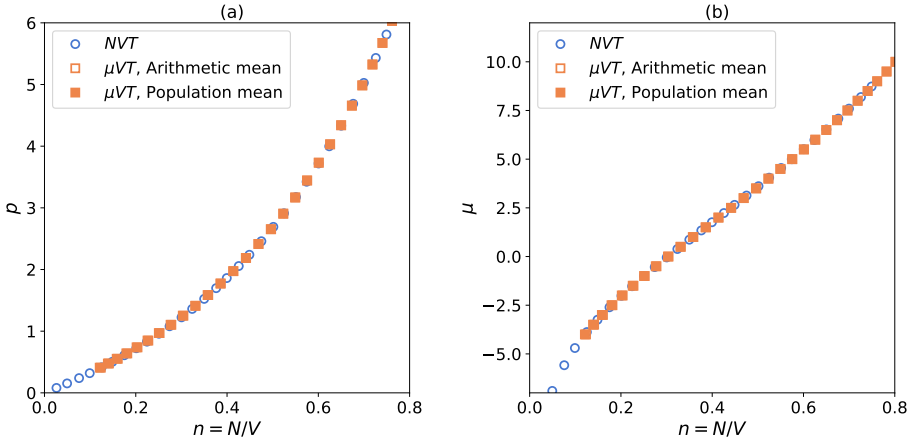

FIG. 8. Pressure and chemical potential as a function of number density of a LJ fluid in a small cubic box with sides $L = 7$, computed from MC simulations. The surface energy is $U^s = 3$ and is experienced by all particles within a distance $\delta = 1$ from any wall. The temperature is $T = 3$.

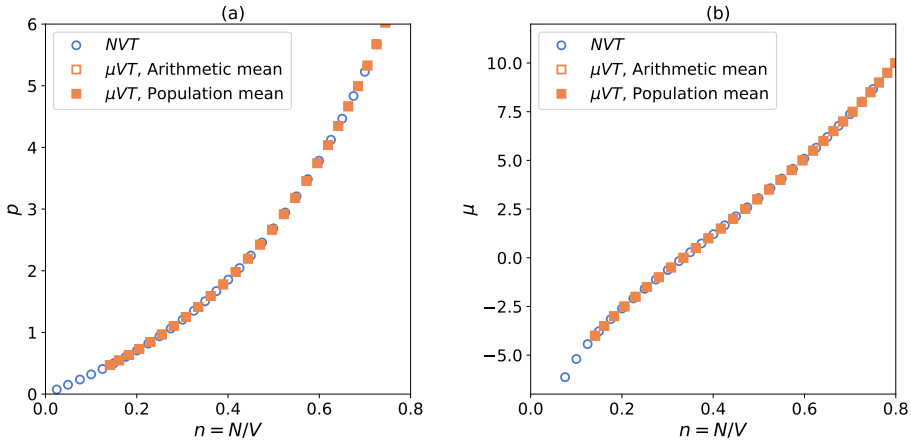

FIG. 9. Pressure and chemical potential as a function of number density of a LJ fluid in a small cubic box with sides $L = 9$, computed from MC simulations. The surface energy is $U^s = 5$ and is experienced by all particles within a distance $\delta = 1$ from any wall. The temperature is $T = 3$.

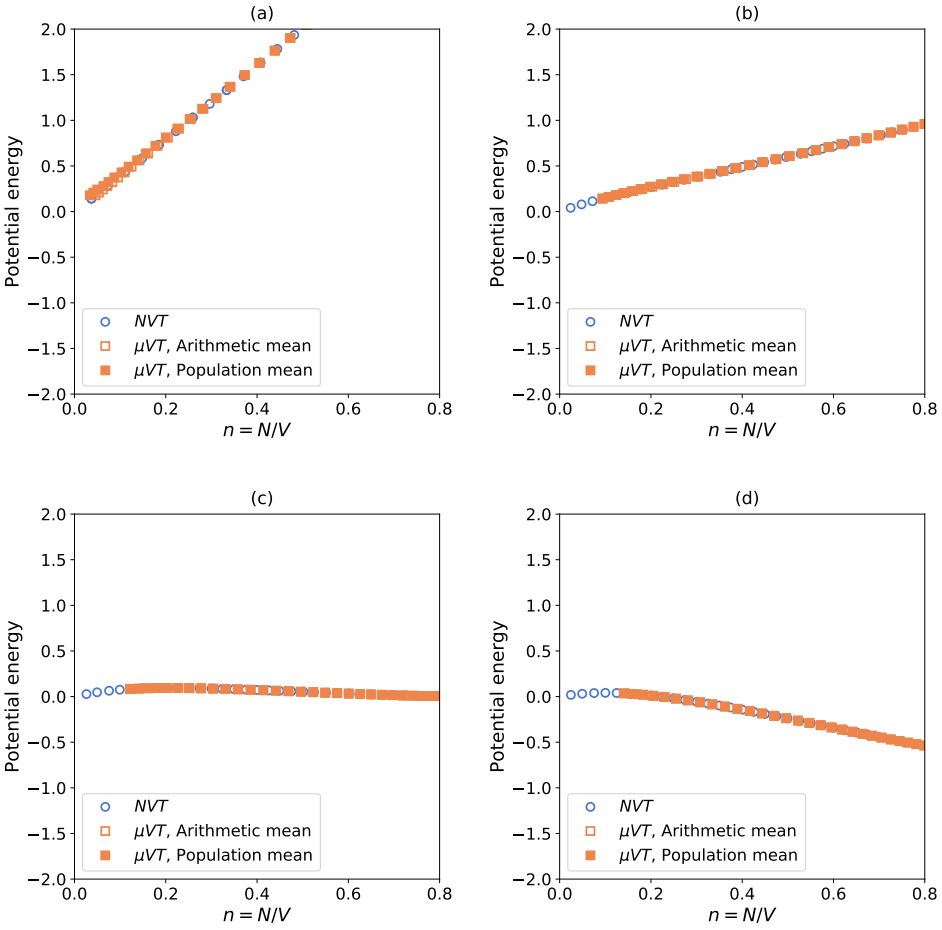

FIG. 10. Potential energy as a function of number density of a LJ fluid in a small cubic box with sides $L = 3$ (a), $L = 5$ (b), $L = 7$ (c) and $L = 9$ (d), computed from MC simulations. The surface energy is $U^s = 3$ and is experienced by all particles within a distance $\delta = 1$ from any wall. The temperature is $T = 3$.

3. *With no surface energy*

Figures 1-4 show the pressure and chemical potential for LJ particles in systems with no surface energy, $U^s = 0$, for system sizes $L = 3, 5, 7, 9$. Figure 5 shows the potential energies of these systems.

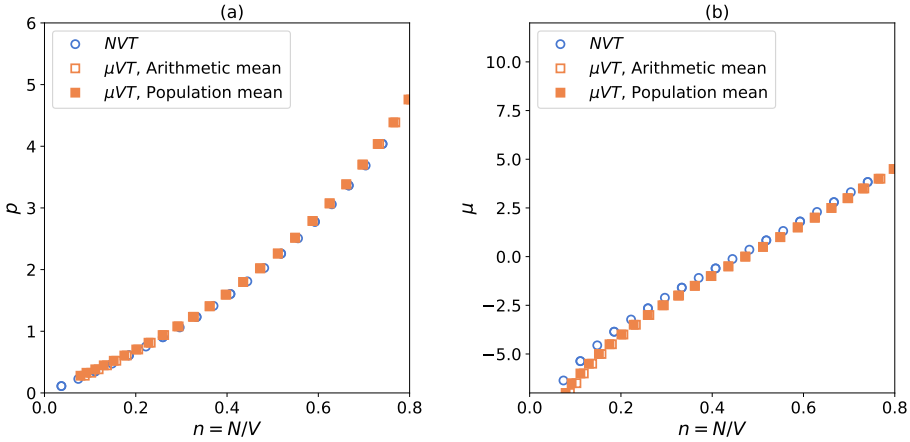

FIG. 11. Pressure and chemical potential as a function of number density of a LJ fluid in a small cubic box with sides $L = 3$, computed from MC simulations. The surface energy is $U^s = 0$ and, the temperature is $T = 3$.

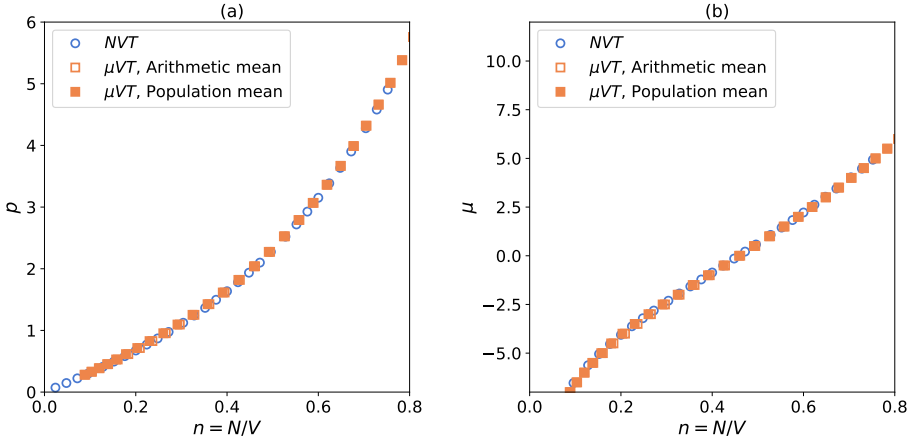

FIG. 12. Pressure and chemical potential as a function of number density of a LJ fluid in a small cubic box with sides $L = 5$, computed from MC simulations. The surface energy is $U^s = 0$ and, the temperature is $T = 3$.

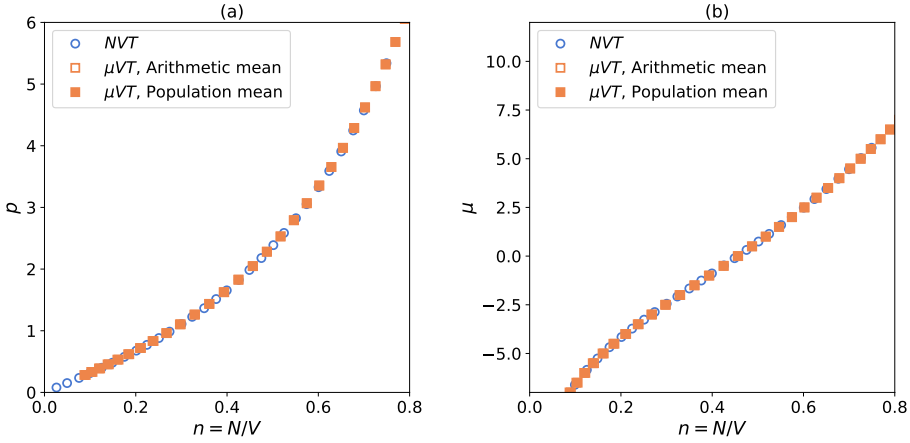

FIG. 13. Pressure and chemical potential as a function of number density of a LJ fluid in a small cubic box with sides $L = 7$, computed from MC simulations. The surface energy is $U^s = 0$ and, the temperature is $T = 3$.

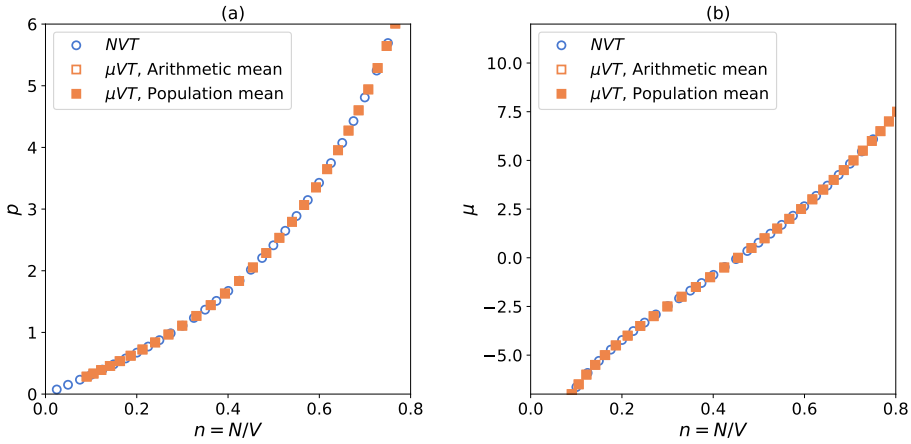

FIG. 14. Pressure and chemical potential as a function of number density of a LJ fluid in a small cubic box with sides $L = 9$, computed from MC simulations. The surface energy is $U^s = 0$ and, the temperature is $T = 3$.

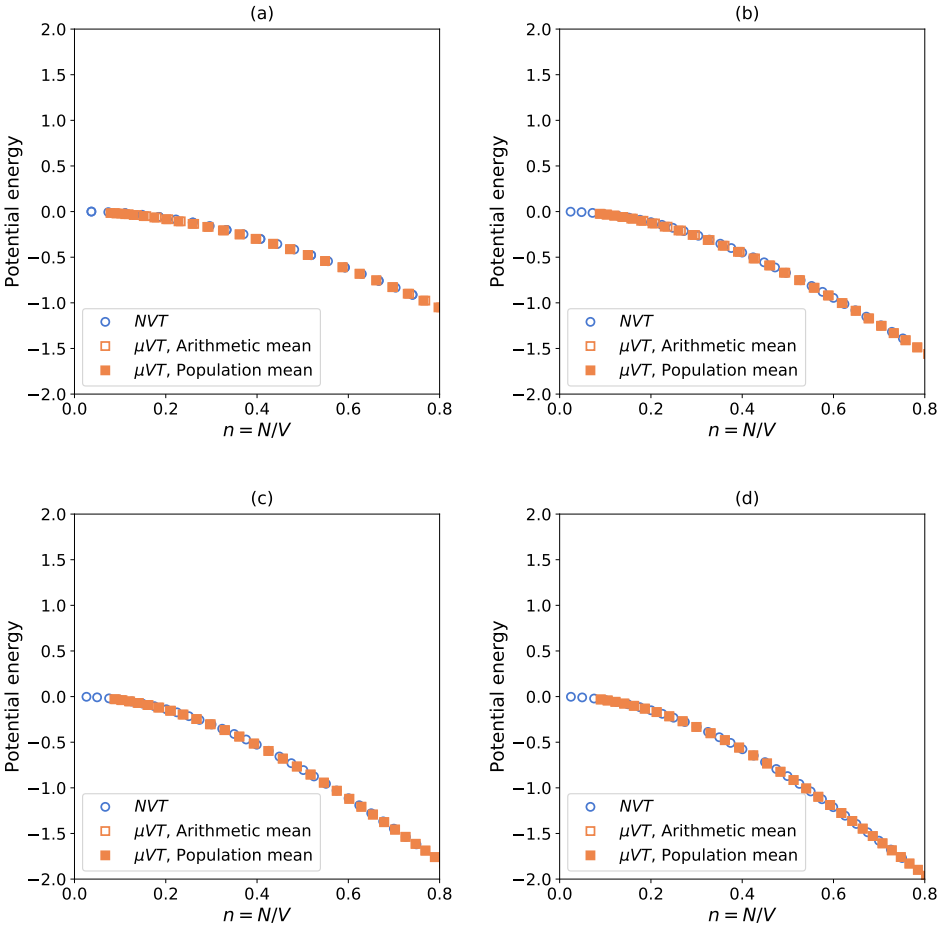

FIG. 15. Potential energy as a function of number density of a LJ fluid in a small cubic box with sides $L = 3$ (a), $L = 5$ (b), $L = 7$ (c) and $L = 9$ (d), computed from MC simulations. The surface energy is $U^s = 0$ and, the temperature is $T = 3$.

B. Results of WCA Simulations

1. With no surface energy.

Figures 16-19 show the pressure and chemical potential for WCA particles in systems with no surface energy, $U^s = 0$, for system sizes $L = 3, 5, 7, 9$. Figure 20 shows the potential energies of these systems.

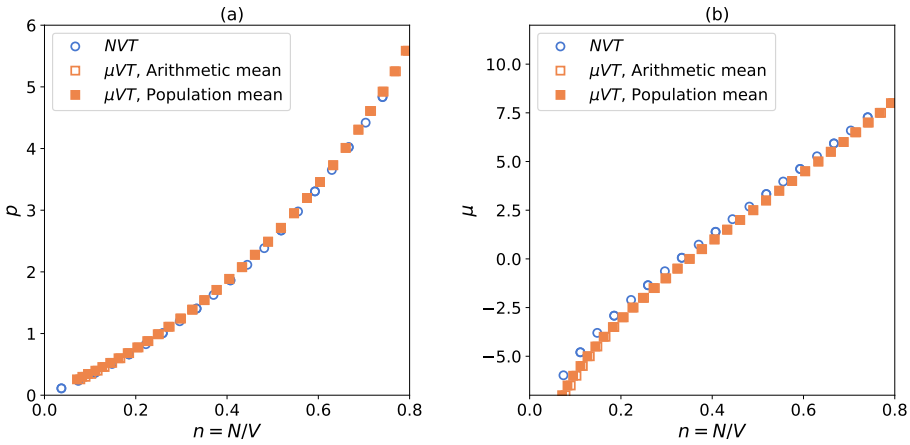

FIG. 16. Pressure and chemical potential as a function of number density of a WCA fluid in a small cubic box with sides $L = 3$, computed from MC simulations. The surface energy is $U^s = 0$ and, the temperature is $T = 3$.

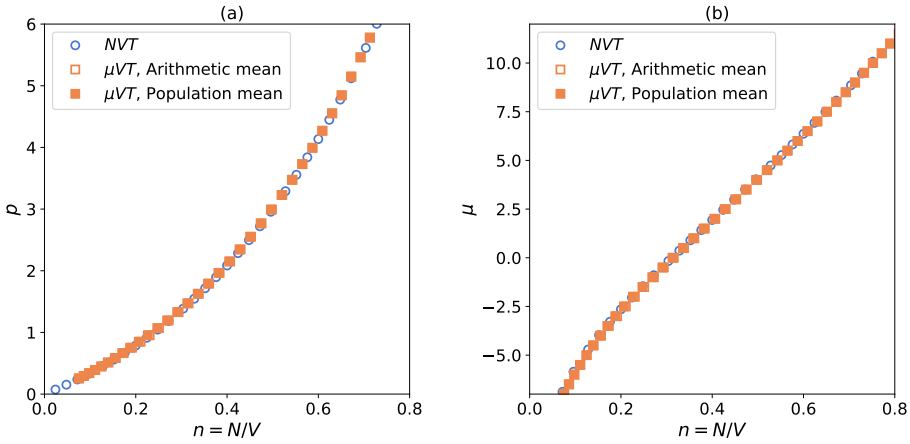

FIG. 17. Pressure and chemical potential as a function of number density of a WCA fluid in a small cubic box with sides $L = 5$, computed from MC simulations. The surface energy is $U^s = 0$ and, the temperature is $T = 3$.

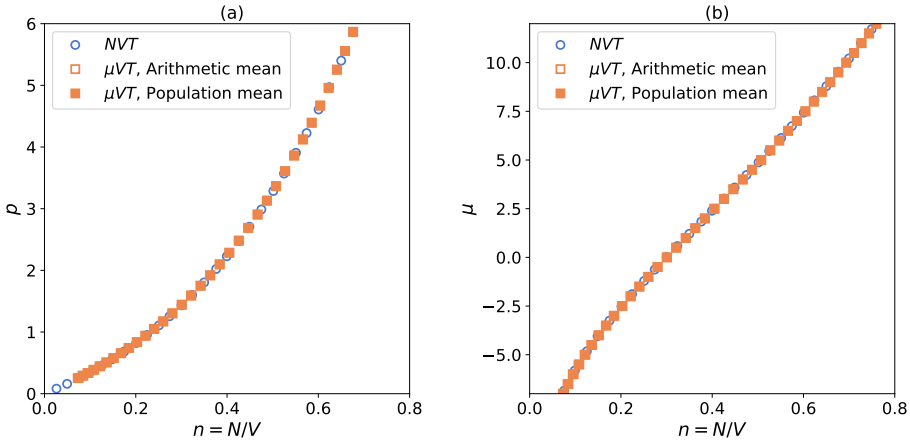

FIG. 18. Pressure and chemical potential as a function of number density of a WCA fluid in a small cubic box with sides $L = 7$, computed from MC simulations. The surface energy is $U^s = 0$ and, the temperature is $T = 3$.

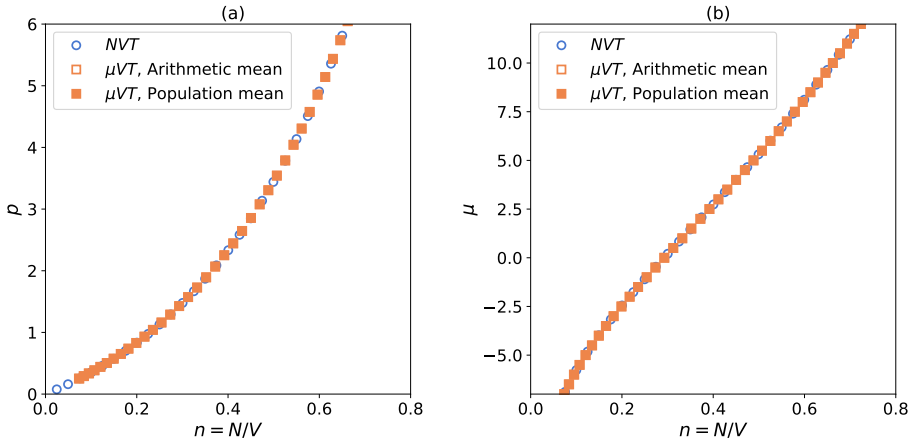

FIG. 19. Pressure and chemical potential as a function of number density of a WCA fluid in a small cubic box with sides $L = 9$, computed from MC simulations. The surface energy is $U^s = 0$ and, the temperature is $T = 3$.

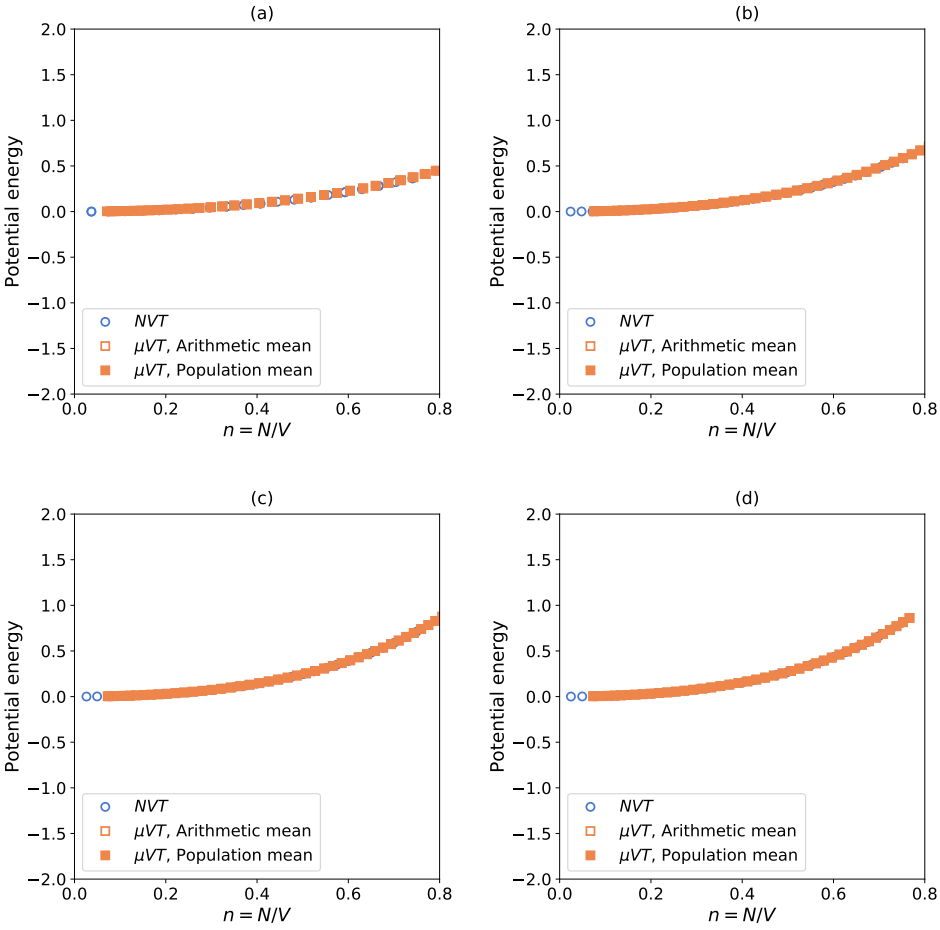

FIG. 20. Potential energy as a function of number density of a WCA fluid in a small cubic box with sides $L = 3$ (a), $L = 5$ (b), $L = 7$ (c) and $L = 9$ (d), computed from MC simulations. The surface energy is $U^s = 0$ and, the temperature is $T = 3$.

Article III

V. Bråten, D. T. Zhang, M. Hammer, A. Aasen, S. K. Schnell and Ø. Wilhelmsen

Equation of state for confined fluids,

The Journal of Chemical Physics **156**:24 244504 (2022).
DOI: 10.1063/5.0096875

Article III

Article III

The Journal of Chemical Physics ARTICLE scitation.org/journal/jcp

Equation of state for confined fluids

Cite as: J. Chem. Phys. 156, 244504 (2022); doi: 10.1063/5.0096875
Submitted: 22 April 2022 • Accepted: 3 June 2022 •
Published Online: 28 June 2022

Vilde Bråten,[1] Daniel Tianhou Zhang,[2] Morten Hammer,[3,4] Ailo Aasen,[4] Sondre Kvalvåg Schnell,[1] and Øivind Wilhelmsen[3,4,a)]

AFFILIATIONS

[1] Department of Materials Science and Engineering, Norwegian University of Science and Technology, NTNU, Trondheim NO-7491, Norway
[2] Department of Chemistry, Norwegian University of Science and Technology, NTNU, Trondheim NO-7491, Norway
[3] PoreLab, Department of Chemistry, Norwegian University of Science and Technology, NTNU, Trondheim NO-7491, Norway
[4] Gas Technology, PoreLab, SINTEF Energy Research, Trondheim NO-7465, Norway

Note: This paper is part of the 2022 JCP Emerging Investigators Special Collection.
[a)] Author to whom correspondence should be addressed: oivind.wilhelmsen@ntnu.no

ABSTRACT

Fluids confined in small volumes behave differently than fluids in bulk systems. For bulk systems, a compact summary of the system's thermodynamic properties is provided by equations of state. However, there is currently a lack of successful methods to predict the thermodynamic properties of confined fluids by use of equations of state, since their thermodynamic state depends on additional parameters introduced by the enclosing surface. In this work, we present a consistent thermodynamic framework that represents an equation of state for pure, confined fluids. The total system is decomposed into a bulk phase in equilibrium with a surface phase. The equation of state is based on an existing, accurate description of the bulk fluid and uses Gibbs' framework for surface excess properties to consistently incorporate contributions from the surface. We apply the equation of state to a Lennard-Jones spline fluid confined by a spherical surface with a Weeks–Chandler–Andersen wall-potential. The pressure and internal energy predicted from the equation of state are in good agreement with the properties obtained directly from molecular dynamics simulations. We find that when the location of the dividing surface is chosen appropriately, the properties of highly curved surfaces can be predicted from those of a planar surface. The choice of the dividing surface affects the magnitude of the surface excess properties and its curvature dependence, but the properties of the total system remain unchanged. The framework can predict the properties of confined systems with a wide range of geometries, sizes, interparticle interactions, and wall–particle interactions, and it is independent of ensemble. A targeted area of use is the prediction of thermodynamic properties in porous media, for which a possible application of the framework is elaborated.

I. INTRODUCTION

The behavior of fluids is known to change when they are confined in small geometries. In porous materials, for instance, a liquid phase can form through capillary condensation at pressures below the saturation pressure.[1–4] A popular example in the literature is confined water, where changes in both the dynamic behavior and phase transitions have been observed.[5–7] Molecular dynamics (MD) and Monte Carlo simulations, as well as density functional theory, are popular tools that have been used with great success to gain insight into how the fluid behavior is influenced by confinement.[8–13] There is, however, a need for a compact and predictive thermodynamic description of confined fluids that can be used to shed further light on the intriguing results obtained from simulations and experiments.

Equations of state (EoSs) provide a summary of a system's thermodynamic properties. For homogeneous fluids in macroscopic systems, the temperature, mass density, and composition are usually sufficient to characterize the thermodynamic state of the fluid. In confined systems, additional knowledge about features such as the system's geometry and wall–fluid interactions are needed since this can lead to wall-adsorption, layering, and disjoining effects.[8–11] For simple systems, such as ideal gas systems[14] or systems containing a small number of particles,[15] the effects of confinement can be included in exact expressions for the thermodynamic properties. For fluids with interacting particles, cubic EoSs are popular tools

that have been used extensively in process simulations, optimization studies, and solubility predictions.[16,17] There have been efforts to develop cubic EoSs for confined systems. Zarragoicoechea and Kuz[18] derived the van der Waals (vdW) EoS for a square-section nano-pore of infinite length[18] that predicted a shift in the critical point.[19] Travalloni *et al.* later introduced wall–fluid interactions to the vdW EoS.[20,21]

One major challenge in the development of cubic EoSs for confined systems is that the experimental characterization of fluids in nano-geometries is difficult. Challenges associated with the validation of the EoS is an issue for all types of EoSs that depend on parameters obtained from experiments.[22] Instead of parametrizing the experimental properties of confined fluids, it can, therefore, be advantageous to base the EoSs on fluids described by interaction potentials. This makes it possible to test the EoS predictions by comparing them with properties computed directly from molecular simulations in well-defined geometries. For instance, the thermodynamic properties of the hard-sphere fluid in random porous media have been successfully represented by scaled particle theory.[23] This description has later been applied in investigations of the properties of various fluids confined in random porous media, such as the Lennard-Jones (LJ) fluid,[24] polydisperse square-well chain fluids,[25] and fluids with particles interacting through a hard-sphere Morse potential.[26]

In this work, we formulate a general thermodynamic description that applies to fluids with a wide variety of interparticle interactions confined in systems with a wide range of wall–fluid interactions, geometries, and sizes. Since the EoS should return to the bulk description when the system is large enough, we base the EoS on an existing bulk description and show how surface contributions can be incorporated. The surface contributions arise from interactions between the fluid and the enclosing surface, which become increasingly relevant as the number of particles and volume decrease. A consequence of this is that, for sufficiently small systems, properties that are extensive in macroscopic systems are no longer Euler homogeneous of degree one.[27] The nanothermodynamic framework developed by Hill[28] is a consistent extension of classical thermodynamics that can be applied to such systems. Nanothermodynamics has been used in various studies to understand the behavior of small systems, like stretching and breaking of polymer chains[29,30] and transport in porous media.[31–33] In addition, nanothermodynamics has supported the analysis of size-scaling of thermodynamic properties, which is crucial for the computation of macroscopic properties from sub-sampling techniques.[34–36] In order to use the framework of Hill[28] to gain insight into the behavior of small systems, the underlying physical description of the system is required. In this work, we derive such a physical description by employing the framework of excess variables developed by Gibbs.[37] We split the thermodynamic description of a small system into a bulk phase and an excess, small-size contribution. The leading order small-size contribution usually comes from the system's surface area. We emphasize that line- and edge-contributions can also be relevant,[38,39] but such a discussion is beyond the scope of the present work. For system sizes where the total confined system can be described as a bulk phase and an excess surface phase, the formalism presented here provides a consistent framework that represents an EoS for confined systems. In particular, we show that the EoS reproduces results from molecular simulations of confined fluids that are nearly within the simulation accuracy.

II. THEORETICAL FRAMEWORK

In this section, we present a thermodynamic framework to describe confined fluids. The thermodynamic description of the system is split into a bulk phase and an excess surface phase. We consider the case where there is local equilibrium in both the bulk phase and the surface phase. In the following, properties with no subscript refer to the total system, properties with subscript "b" refer to the bulk phase, while properties with subscript "s" refer to the excess surface phase. We formulate the internal energy, U, as a function of the entropy, S, number of particles, N, and volume, V, for the bulk phase or area, Ω, for the surface phase. The volume of the total system is defined as the bulk volume, $V = V_\mathrm{b}$, and the area of the total system is defined as the surface phase area, $\Omega = \Omega_\mathrm{s}$. The entropy, number of particles, and internal energy are split into a bulk contribution and an excess surface contribution as follows:

$$N = N_\mathrm{b} + N_\mathrm{s} = N_\mathrm{b} + \Gamma\Omega, \tag{1}$$

$$S = S_\mathrm{b} + S_\mathrm{s} = S_\mathrm{b} + \eta\Omega, \tag{2}$$

$$U(N, V, S) = U_\mathrm{b}(N_\mathrm{b}, V, S_\mathrm{b}) + U_\mathrm{s}(N_\mathrm{s}, \Omega, S_\mathrm{s}), \tag{3}$$

where Γ is the excess number of particles per area, which is also referred to as the adsorption, and η is the excess entropy per area. The surface phase described by the excess variables is an autonomous thermodynamic system. This means that the surface phase has its own temperature, T_s, and chemical potential, μ_s. When the bulk phase is not in equilibrium with the surface phase, the bulk temperature, T_b, and the bulk chemical potential, μ_b, can differ from those of the surface phase. This leads to the following expressions for the internal energy of the bulk phase:

$$U_\mathrm{b} = T_\mathrm{b}S_\mathrm{b} - p_\mathrm{b}V + \mu_\mathrm{b}N_\mathrm{b}, \tag{4}$$

and the internal energy of the surface phase:

$$U_\mathrm{s} = T_\mathrm{s}S_\mathrm{s} + \gamma\Omega + \mu_\mathrm{s}N_\mathrm{s}, \tag{5}$$

where p is the pressure and γ is the surface energy.

In the following, we consider the situation where the bulk phase is in equilibrium with the surface phase, meaning that $T_\mathrm{b} = T_\mathrm{s}$ and $\mu_\mathrm{b} = \mu_\mathrm{s}$. Under these circumstances, we define the pressure and chemical potential in the system as follows:

$$p \equiv p_\mathrm{b} = -\left(\frac{\partial U_\mathrm{b}}{\partial V}\right)_{N_\mathrm{b}, S_\mathrm{b}}, \tag{6}$$

$$\mu \equiv \mu_\mathrm{b} = \left(\frac{\partial U_\mathrm{b}}{\partial N_\mathrm{b}}\right)_{V, S_\mathrm{b}}, \tag{7}$$

and the internal energy of the total confined system becomes

$$U = TS - pV + \mu N + \gamma\Omega. \tag{8}$$

A central quantity in the framework presented in this work is the bulk density,

$$\rho_b = \frac{N_b}{V} = \frac{N - \Gamma\Omega}{V}, \tag{9}$$

which for confined systems usually differs from the total density, $\rho = N/V$.

A key advantage with the above formulation is that intensive properties of the total confined system can be determined by considering the properties of the bulk phase as a function of T and ρ_b. In the formalism presented in this work, the bulk density can be computed from Eq. (9) when the total number of particles, the adsorption, and the system's geometry are known. To determine the total entropy and the total internal energy of the confined fluid, one also needs the excess entropy and the surface energy.

We shall hereby refer to the framework for computation of the properties of confined fluids as the "Nano-EoS." In Sec. II A, we explain how the properties of the bulk phase of the confined fluid can be computed from a bulk-EoS. In Sec. II B, we explain how the properties of the surface phase of a confined fluid in equilibrium can be computed when the adsorption is known. All thermodynamic properties computed from either the Nano-EoS or the bulk-EoS have superscript "EoS."

The Nano-EoS presented in this work is independent of the ensemble since $U_b(N_b, V, S_b)$ and $U_s(N_s, \Omega, S_s)$ are both Euler homogeneous of degree one. The energy state functions for various ensembles are, therefore, accessible from Legendre transformations of the internal energy of each phase. Ensemble dependence has been observed for both the pressure and the chemical potential in small systems.[14] However, we do not consider ensemble effects here since, for the system types we investigate, the Nano-EoS is expected to break down at system sizes larger than those where ensemble effects are relevant. See Bråten *et al.*[14] for a detailed discussion of when ensemble dependence becomes relevant.

A. Bulk properties

For a given bulk density, the properties of the bulk phase can be extracted from a bulk-EoS. The bulk internal energy is, therefore,

$$U_b^{EoS} = U_b^{EoS}(N_b, V, T). \tag{10}$$

Other properties of the bulk phase, such as energy state functions or entropy, can be computed from equivalent relations. Note that the internal energy extracted from a bulk-EoS is often normalized by the number of particles as follows: $U_b^{EoS}(N_b, V, T)/N_b$. The bulk internal energy of the confined system is, therefore, computed by multiplying the bulk prediction with N_b.

B. Surface excess properties

A prerequisite for computing surface excess properties is to define the location of the dividing surface. There are many different choices available, and for the system types we consider, the location of the dividing surface determines the value of V, and for curved surfaces, it also affects Ω. The choice of the dividing surface influences the decomposition into bulk and surface contributions. Some properties are invariant regardless of the choice of the dividing surface, such as the total internal energy of the confined fluid. Details on how the surface excess properties for different choices of the dividing surface are related to each other are presented in Sec. II B 2.

The surface phase is the excess with respect to a bulk phase at ρ_b and T. For equilibrium systems, the surface excess properties are, therefore, considered as functions of these two variables. Our starting point for the computation of surface excess properties is the adsorption, which is computed from the following relation:

$$\Gamma = \frac{N - \rho_b V}{\Omega}. \tag{11}$$

Adsorption is related to the other surface excess properties and the intensive properties of the total system through the Gibbs adsorption equation.[37] For a given choice of the dividing surface at a fixed position relative to the total volume, the Gibbs adsorption equation is given by

$$d\gamma = -\Gamma d\mu - \eta dT. \tag{12}$$

At constant temperature, Eq. (12) becomes

$$d\gamma = -\Gamma d\mu. \tag{13}$$

When the adsorption and the chemical potential are known for a range of bulk densities, Eq. (13) can be used to compute the differential surface energy. By using the fact that the surface energy is zero at zero density, the absolute value of the surface energy can be computed.

At constant chemical potential, Eq. (12) can be rewritten as an expression for the excess entropy per area as follows:

$$\eta = -\left.\frac{\partial\gamma}{\partial T}\right|_{\mu}. \tag{14}$$

From Eq. (14), it is apparent that η as a function of the bulk density can be readily computed from the temperature dependence of the surface energy when one knows how the chemical potential depends on the bulk density and the temperature.

The excess internal energy becomes

$$U_s^{EoS} = T\eta\Omega + \gamma\Omega + \mu\Gamma\Omega. \tag{15}$$

1. Curvature dependence of surface properties

The surface excess properties depend on the geometry of the surface. For nonplanar surfaces, the surface properties can be expressed as the surface properties of a planar wall plus additional curvature corrections.[38,39] The adsorption for a spherical surface with radius R is expressed as follows:

$$\Gamma(R) = \Gamma_0 + \frac{\Gamma_1}{R} + \mathcal{O}\left(\frac{1}{R^2}\right), \tag{16}$$

where Γ_0 refers to the adsorption at a planar wall, Γ_1 is the first-order curvature correction to the adsorption, and $\mathcal{O}(1/R^2)$ refers to the higher-order terms. Both the surface energy and the excess entropy per area can be expressed by equations similar to Eq. (16) and become

$$\gamma(R) = \gamma_0 + \frac{\gamma_1}{R} + \mathcal{O}\left(\frac{1}{R^2}\right), \tag{17}$$

$$\eta(R) = \eta_0 + \frac{\eta_1}{R} + \mathcal{O}\left(\frac{1}{R^2}\right). \tag{18}$$

In this work, we only investigate the first-order corrections, but higher-order corrections are also possible.[40,41] For the systems considered here, R is independent of T and μ. This means that γ_0 and γ_1 can be computed from Eq. (13) when Γ_0 and Γ_1 are known, and that η_0 and η_1 can be computed from Eq. (14) when γ_0 and γ_1 are known.

The capillary approximation (CA) states that the surface properties of a curved surface are equal to those of a planar surface. When the curvature corrections are small compared to the planar-wall contribution, the capillary approximation may provide a satisfactory description of the surface excess properties. In Sec. V, we discuss when the capillary approximation holds for confined fluids.

2. Shifting the location of the dividing surface

For the system types we consider, the volume of the system depends on the location of the dividing surface. Consequently, Γ, η, and γ will also depend on the location of the dividing surface.[40,42] In this section, we show how the surface properties of one dividing surface are related to those of another dividing surface.

In simulations, the fluid particles are confined by a wall. For spherical systems, this wall is located at the enclosing surface, $\widetilde{\Omega}$, at a distance $\widetilde{R}$ from the center of the sphere. This enclosing surface corresponds to the volume $\widetilde{V}$. For a box-shaped system, with a wall located at one of the sides, the surface area of this wall is independent of the dividing surface, $\widetilde{\Omega} = \Omega$, and the volume defined by the location of the wall is $\widetilde{V} = \widetilde{L}\Omega$. The location of the dividing surface can be specified as the distance from the enclosing wall, d_{wall}, which will be called the wall-thickness. Its sign is positive when $V < \widetilde{V}$, cf. Fig. 1. For a wall-thickness $d_{\text{wall}} = 0$, the volume and area corresponding to the dividing surface are $\widetilde{V}$ and $\widetilde{\Omega}$, respectively. Surface excess properties computed for this choice of dividing surface are marked by a tilde.

In some expressions for surface excess properties, a dividing surface located at $d_{\text{wall}} = 0$ is implicit for the system types investigated in this work. These are the excess functions for adsorption and the excess entropy, and the surface energy computed from the Kirkwood–Buff[13] (KB) equation. The respective excess functions for adsorption and the excess entropy are as follows:

$$\widetilde{\Gamma} = \frac{1}{\widetilde{\Omega}} \int_{\widetilde{V}} [\rho(\xi) - \rho_{\text{b}}] \mathrm{d}\widetilde{V}, \tag{19}$$

$$\widetilde{\eta} = \frac{1}{\widetilde{\Omega}} \int_{\widetilde{V}} [s(\xi) - s_{\text{b}}] \mathrm{d}\widetilde{V}, \tag{20}$$

where ξ is the coordinate normal to the wall, $\rho(\xi)$ is the number density profile, $s(\xi)$ is the entropy density profile, and s_{b} is the bulk entropy density. The KB equation utilizes the pressure anisotropy close to the surface and relates the surface energy to the pressure tensor profiles. For a box-shaped system, the surface energy can be computed from the KB equation as follows:

$$\widetilde{\gamma} = \int_0^{\widetilde{L}} [p_N(\xi) - p_T(\xi)] \mathrm{d}\xi, \tag{21}$$

where p_N and p_T are the normal and tangential components of the pressure tensor, respectively. The normal component of the pressure tensor is equal to the bulk pressure, $p_N(\xi) = p_{\text{b}}$.[32] The KB equation can also be defined for curved surfaces, but accurate computation of pressure tensors in the vicinity of curved surfaces remains an unresolved topic.[11,44–47]

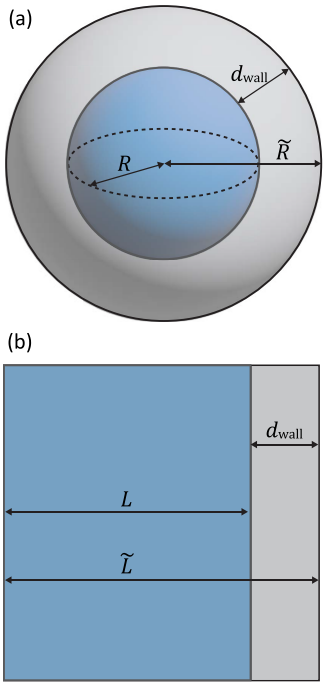

FIG. 1. Illustrations of (a) the spherical system and (b) a cross section of the planar-wall system investigated in this work. The dividing surface is located at R for the spherical system and at L for the planar-wall system, while the WCA-wall is located at $\widetilde{R}$ for the spherical system and at $\widetilde{L}$ for the planar-wall system. The wall-thickness, d_{wall}, is the distance between the dividing surface and the wall. (b) illustrates the section between $\widetilde{L}_x/2$ and $\widetilde{L}_x$ of the system investigated by MD simulations, which means that $\widetilde{L}$ in the figure corresponds to $\widetilde{L}_x/2$ in the simulations.

The surface properties for $d_{\text{wall}} = 0$ are related to the surface properties for a dividing surface located at $d_{\text{wall}} \neq 0$. For a planar wall, these relations are

$$\widetilde{\Gamma}_0 - \Gamma_0 = -\rho_{\text{b}} d_{\text{wall}}, \tag{22}$$

$$\widetilde{\gamma}_0 - \gamma_0 = p_{\text{b}} d_{\text{wall}}, \tag{23}$$

$$\widetilde{\eta}_0 - \eta_0 = -s_{\text{b}} d_{\text{wall}}, \tag{24}$$

and the relations for the curvature corrections of a spherical surface are

$$\widetilde{\Gamma}_1 - \Gamma_1 = \rho_{\text{b}} d_{\text{wall}}^2 - 2 d_{\text{wall}} \Gamma_0, \tag{25}$$

$$\widetilde{\gamma}_1 - \gamma_1 = -p_{\text{b}} d_{\text{wall}}^2 - 2 d_{\text{wall}} \gamma_0, \tag{26}$$

$$\widetilde{\eta}_1 - \eta_1 = s_{\text{b}} d_{\text{wall}}^2 - 2 d_{\text{wall}} \eta_0. \tag{27}$$

Equations (22)–(26) provide general relations between the surface excess properties for two dividing surfaces separated by a distance d_{wall}. In this work, we apply them to the specific case where $\widetilde{\Gamma}$, $\widetilde{\gamma}$, and $\widetilde{\eta}$ correspond to a dividing surface located at $d_{\text{wall}} = 0$. Further details about the derivation of Eqs. (22)–(26) are given in the supplementary material.

3. Surface properties in the low-density limit

For low-density systems, the calculation of statistical averages from molecular simulations requires considerable computational effort. Exact analytical expressions that provide a consistent description of the system's properties at low densities are, therefore, useful. In the low-density limit, the properties of fluids with interacting particles can be approximated by the properties of an ideal gas. In this section, we show how the surface excess properties of a confined ideal gas can be computed analytically.

The ideal gas particles do not interact with each other, but they do interact with the enclosing wall. The interaction energy between the particles and the wall is given by the wall-potential $W(\xi)$. In the region where the wall-potential is zero, the potential energy of the system is zero, and the density is equal to the bulk density. The density profile for the coordinate normal to the wall is[48]

$$\rho_{\text{IG}}(\xi) = \rho_{\text{b}} \exp\left(-\frac{W(\xi)}{k_{\text{B}}T}\right). \tag{28}$$

Combining Eq. (28) with Eq. (19) yields the expression for the adsorption of an ideal gas,

$$\begin{aligned}\widetilde{\Gamma}_{\text{IG}} &= \frac{1}{\widetilde{\Omega}}\int_{\widetilde{V}}[\rho_{\text{IG}}(\xi) - \rho_{\text{b}}]\mathrm{d}\widetilde{V} \\ &= \rho_{\text{b}}\frac{1}{\widetilde{\Omega}}\int_{\widetilde{V}}\left[\exp\left(-\frac{W(\xi)}{k_{\text{B}}T}\right) - 1\right]\mathrm{d}\widetilde{V}.\end{aligned} \tag{29}$$

Since the integral in the above expression is independent of density, the adsorption becomes a first-order linear function of the bulk density, where the slope is

$$\widetilde{\alpha} = \frac{1}{\widetilde{\Omega}}\int_{\widetilde{V}}\left[\exp\left(-\frac{W(\xi)}{k_{\text{B}}T}\right) - 1\right]\mathrm{d}\widetilde{V}. \tag{30}$$

This slope depends on the temperature and the geometry of the system, but it is independent of the bulk density. The differential of $\widetilde{\alpha}$ with respect to temperature is

$$\frac{\mathrm{d}\widetilde{\alpha}}{\mathrm{d}T} = \frac{1}{\widetilde{\Omega}}\int_{\widetilde{V}}\exp\left(-\frac{W(\xi)}{k_{\text{B}}T}\right)\frac{W(\xi)}{k_{\text{B}}T^2}\mathrm{d}\widetilde{V}. \tag{31}$$

Further details about the computation of α for different choices of the dividing surface are presented in the supplementary material.

The following equations are valid for any choice of the dividing surface and we, therefore, omit the tilde. The adsorption of the confined ideal gas is given by

$$\Gamma_{\text{IG}} = \alpha\rho_{\text{b}}, \tag{32}$$

and the surface energy can be obtained from Gibbs adsorption equation at constant temperature as follows:

$$\mathrm{d}\gamma_{\text{IG}} = -\Gamma_{\text{IG}}\mathrm{d}\mu_{\text{IG}}. \tag{33}$$

The integration variable μ_{IG} can be substituted for ρ_{b} through the expression for the chemical potential of an ideal gas as follows:

$$\mu_{\text{IG}} = k_{\text{B}}T\ln\left(\frac{\rho_{\text{b}}k_{\text{B}}T}{p_0}\right) + \mu_0(T), \tag{34}$$

where p_0 is the pressure of the standard state and μ_0 is the reference chemical potential. More details on the choice of the reference state are presented in the supplementary material. The differential chemical potential at constant temperature becomes $\mathrm{d}\mu_{\text{IG}} = k_{\text{B}}T\rho_{\text{b}}^{-1}\mathrm{d}\rho_{\text{b}}$, and since the surface energy is zero at zero density, integration of Eq. (33) yields

$$\gamma_{\text{IG}} = -k_{\text{B}}T\alpha\rho_{\text{b}}. \tag{35}$$

Similar to the expression for adsorption, the surface energy of the ideal gas is a first-order linear function of ρ_{b}. This implies the following simple relationship: $\gamma_{\text{IG}} = -k_{\text{B}}T\Gamma_{\text{IG}}$.

The excess entropy of the confined ideal gas is computed from the Gibbs adsorption equation at constant chemical potential, presented in Eq. (14). Differentiating the surface energy of the ideal gas with respect to temperature at constant chemical potential yields

$$\eta_{\text{IG}} = -\left.\frac{\partial\gamma_{\text{IG}}}{\partial T}\right|_{\mu_{\text{IG}}} = \rho_{\text{b}}\left(k_{\text{B}}T\frac{\mathrm{d}\alpha}{\mathrm{d}T} - \alpha\frac{\mathrm{d}\mu_0}{\mathrm{d}T}\right) - k_{\text{B}}\alpha\rho_{\text{b}}\ln\left(\frac{\rho_{\text{b}}k_{\text{B}}T}{p_0}\right). \tag{36}$$

In contrast to the adsorption and the surface energy, the excess entropy is not a first-order linear function of the bulk density. The excess entropy for a confined ideal gas consists of one term that is linear in ρ_{b} and one term that contains the nonlinearity $\rho_{\text{b}}\ln(\rho_{\text{b}}k_{\text{B}}T/p_0)$. The last term comes from the nonlinear relation between the density and the chemical potential.

III. COMPUTATIONAL DETAILS

We compute the thermodynamic properties of a confined fluid directly from MD simulations. This includes the properties of the total system, the bulk phase, and the surface phase. To investigate the impact of curvature on the surface excess properties, we compute the values for systems with a planar wall and in spherical systems. In the following, all the values and results presented are in reduced LJ units.

A. Simulation details

The MD simulations are performed with the simulation package Large-scale Atomic/Molecular Massively Parallel Simulator (LAMMPS).[49] The LAMMPS simulation input files are openly available, with the download details provided in the data availability statement. For the interparticle interactions, we employ the Lennard-Jones spline (LJs) potential.[50] See Hafskjold *et al.*[51] for a detailed discussion on the properties of systems containing particles interacting via the LJs potential. The interactions between the fluid and the wall are described by the Weeks–Chandler–Andersen (WCA) potential.[52] The WCA potential is a purely repulsive potential that is equal to the LJ potential truncated and shifted at $r_c = 2^{1/6}\sigma_{\text{wall}}$, where we use $\sigma_{\text{wall}} = 1$. The volume of the simulation box is $\widetilde{V}$, which is defined by the location of the walls. We consider one system with planar walls with dimensions $\widetilde{V} = \widetilde{L}_x L_y L_z$, where $\widetilde{L}_x = 40$ and $L_y = L_z = 20$, and three differently sized spherical

systems with radius $\widetilde{R} = 5, 10, 15$. The spherical systems have a WCA-wall located at $\widetilde{R}$. The system with planar walls has a WCA-wall located at each end of $\widetilde{L}_x$ and periodic boundary conditions in the other directions. Both system types are illustrated in Fig. 1. For all systems, we investigate values of $N/\widetilde{V}$ ranging from 0.05 to 0.80. The simulations are run in five parallels, which consist of 20×10^6 time steps each for $N/\widetilde{V} \leq 0.45$, and 2×10^6 time steps each for $N/\widetilde{V} > 0.45$. The size of a time step is $\Delta t = 0.002$ and the properties are sampled every hundred time step. All densities, geometries, and sizes are investigated for five different temperatures: $T = 1.90, 1.95, 2.00, 2.05, 2.10$. The pressure is computed from the virial expression.

B. Bulk equation of state

The bulk-EoS for the LJs fluid used in this work is obtained from the *uv*-theory of van Westen and Gross,[53] accessed through the open-source thermodynamic software Thermopack.[53] More details about the bulk-EoS based on *uv*-theory for LJs can be found in Ref. 54.

C. Application of the Nano-EoS

The flowchart presented in Fig. 2 explains the procedure for computing the thermodynamic properties of a confined fluid when N, T, the fluid's bulk properties and the surface excess properties, are known. The procedure shown in the figure can be used to predict the properties of confined fluids at equilibrium.

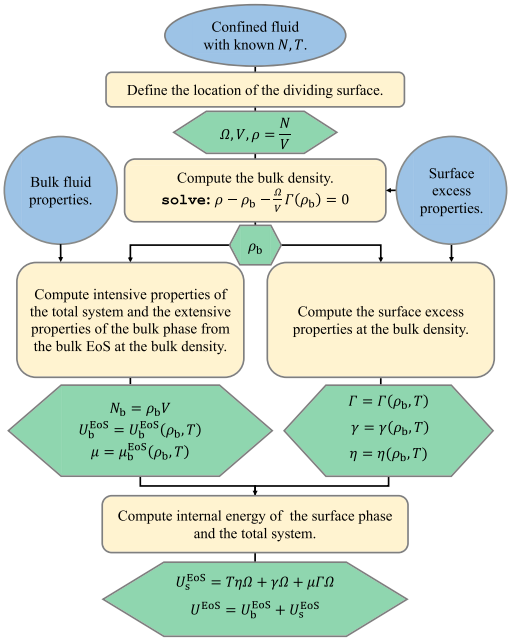

FIG. 2. Flowchart for computing thermodynamic properties of a confined fluid when N, T, the fluid's bulk properties and the surface excess, properties are known. The initial input is shown in the blue circles, explanations for each computation step are presented in the yellow boxes, and the computed properties are shown in the green hexagons.

IV. RESULTS—MOLECULAR SIMULATIONS OF CONFINED FLUIDS

In this section, we present the step-by-step procedure used for the computation and parametrization of the surface excess properties. This represents the "developer perspective" of the Nano-EoS. When the surface excess properties are computed and parameterized, they can be utilized to predict the thermodynamic properties of systems of any density within the range of validity of the Nano-EoS by following the procedure presented in Fig. 2. This represents the "user perspective" of the Nano-EoS, which is demonstrated in Sec. V. The presented results have been computed using a wall-thickness $d_{\text{wall}} = 1$. In the presentation of the results, the sphere sizes are referred to by the radius given by the location of the wall, $\widetilde{R}$. In Sec. VI A, we discuss how the choice of dividing surface impacts the computation of thermodynamic properties from the Nano-EoS. Error bars corresponding to two standard deviations are included in Figs. 4, 5, 8, and 13–16.

A. Computation of the bulk properties from simulations

To compute bulk properties from molecular simulations, one needs the location of the bulk region. The *bulk region* is here defined as the region of the system where the local contributions from the wall are negligible, e.g., that thermodynamic properties such as the density and the pressure are locally isotropic. When the location of the bulk region is known, the bulk number density, bulk internal energy density, and bulk pressure are easily computed from molecular simulations. Note that the *bulk region* in the simulations is not the same as the *bulk phase* in the Nano-EoS framework. The properties of the bulk phase in the Nano-EoS framework are equal to the properties in the bulk region extrapolated to the entire system volume.

The limits of the bulk region are identified from the system's density profiles. Figure 3 shows the density profiles in the x-direction for the system with planar walls and in the r-direction for the spherical systems. All systems show oscillatory profiles close to the wall that become more distinct with increasing density. The oscillatory behavior is due to structural changes close to the wall, which depend on the type of confinement, the type of fluid, and the size of the system.[33,56,57]

For the system with planar walls, the density profiles are all uniform for $20 < x < 30$, which makes it possible to identify one common bulk region for all the total densities. This is not possible for the spherical systems, since they do not always have a well-defined bulk region. For the spherical systems, the limits of the bulk region are, therefore, defined individually for each of the total densities investigated. The limits of the bulk regions are represented by dashed lines in Fig. 3. In the computation of the bulk density, bulk pressure, and bulk energy density, the data points in the region $r \leq 1$ are discarded due to a large degree of noise. While a validation of the Nano-EoS framework requires a bulk region, we will show in Sec. V that its predictions extrapolate very well beyond this regime. The parametrization of the surface excess properties presented

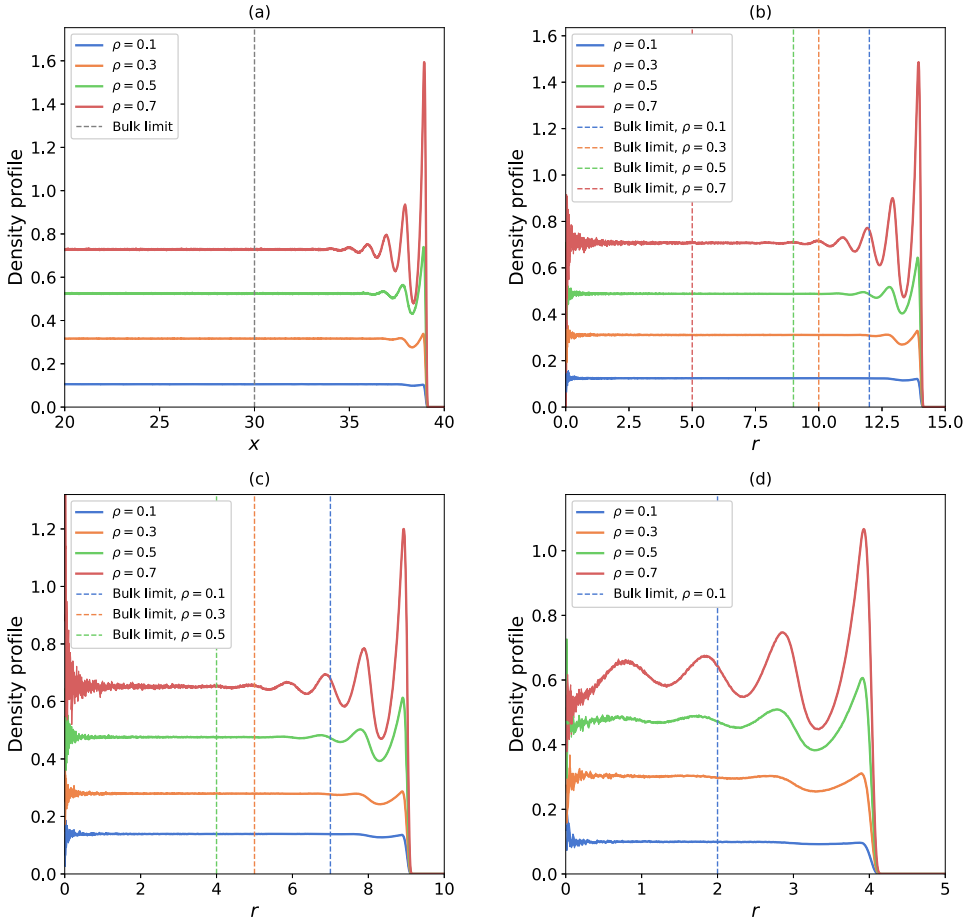

FIG. 3. Density profiles for a few selected total densities for (a) a planar wall and spherical systems with (b) $\widetilde{R}$ = 15, (c) $\widetilde{R}$ = 10, and (d) $\widetilde{R}$ = 5, for T = 2.0. Since the planar-wall system is symmetrical around the center of the simulation box, the figure shows the average of the two symmetrical parts. The left side of the profiles of the spherical systems corresponds to the smallest spherical bins in the center of the simulation box.

in Sec. IV B thereby allows us to compute the bulk and surface properties of systems that do not have well-defined bulk regions.

B. Computation of the surface excess properties from simulations

Surface properties are computed using the formalism presented in Sec. II B. For better readability, the surface properties are only presented for $T = 1.9, 2.0, 2.1$. Equations (32), (35), and (36) show that the adsorption and the surface energy do not depend on the reference state while the excess entropy does depend on the reference state.

In order to extract the surface excess properties at arbitrary densities, all the surface excess properties must be parameterized. For the adsorption and the surface energy, we use fifth- and ninth-degree polynomials, respectively. For the excess entropy, we use a ninth-degree polynomial plus the nonlinear term $\rho_b \ln(\rho_b k_B T/p_0)$ multiplied with a constant coefficient. The constant term is set to zero for all polynomials in order to ensure that all surface excess properties are zero at zero density. At low densities, the first-order coefficients of the polynomials will dominate, such that the surface properties of the LJs fluid can be approximated by those of the ideal gas presented in Sec. II B 3. In the fitting process, the first-order coefficients are, therefore, set to the predictions provided by the ideal gas

model. The first-order coefficients of the adsorption and the surface energy curves are given by Eqs. (32) and (35), respectively. For the excess entropy curve, both the first-order coefficient and the coefficient of the nonlinear term are given by Eq. (36). The coefficients for the parameterized curves of all the surface excess properties are available in the supplementary material.

1. Surface properties of a planar wall

The adsorption is computed from Eq. (11) by combining the bulk densities identified in Sec. IV A and the total densities computed using the volume defined by the dividing surface. Figure 4 shows the adsorption as a function of bulk density, where the fitted curves are represented by solid lines. The adsorption for purely repulsive walls in contact with fluids interacting through potentials containing both attractive and repulsive parts have previously been studied in detail.[8,11,56] For such systems, the adsorption at low densities is governed by the attractive interparticle interactions, which favor accumulation of the particles in the bulk region. At higher densities, the repulsive interactions dominate, which favor accumulation of the particles at the wall since this minimizes each particle's excluded volume. We emphasize that the values of the surface excess properties depend on the location of the dividing surface. Whether the computed adsorption curves reflect the above-described behavior, therefore, depends on the choice of dividing surface. Figure 4 shows that a dividing surface at $d_{\text{wall}} = 1$ reflects this behavior since the adsorption is negative at low densities and positive at higher densities for all the investigated temperatures.

When the parameterized adsorption is known as a function of the bulk density, the surface energy can be computed from the Gibbs adsorption equation [Eq. (13)]. The surface energy is also computed from the KB equation [Eq. (21)], combined with Eq. (23) in order to extract the surface energy for a dividing surface at $d_{\text{wall}} = 1$. Figure 5 shows the surface energies computed from the Gibbs adsorption equation and from the KB equation. The black dotted lines show the curves fitted to the surface energies computed from the Gibbs adsorption equation. In the Nano-EoS, we use the surface energies computed from the Gibbs adsorption equation, since computing all the surface excess properties with the adsorption as a starting point results in a more consistent framework. A comparison with the surface energies computed from the KB equation works as a quality check for the surface energies computed from the Gibbs adsorption equation. With the exception of the data points at the two highest densities, the prediction of the surface energy from the Gibbs adsorption equation is within two standard deviations of the values

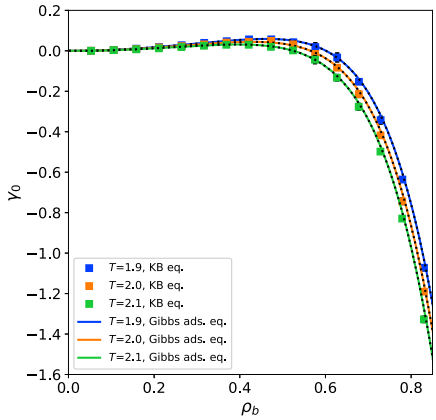

FIG. 5. Surface energy as a function of bulk density for the LJs fluid in contact with a planar wall with a WCA wall-potential. The curves fitted to the surface energy computed from the Gibbs adsorption equation are represented by black dotted lines. The dividing surface is located at $d_{\text{wall}} = 1$.

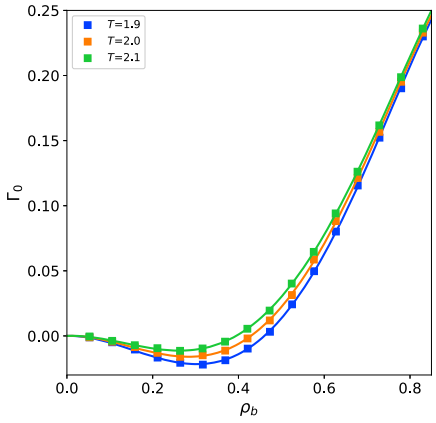

FIG. 4. Adsorption as a function of bulk density for the LJs fluid in contact with a planar wall with a WCA wall-potential. The fitted curves are represented by solid lines. The dividing surface is located at $d_{\text{wall}} = 1$.

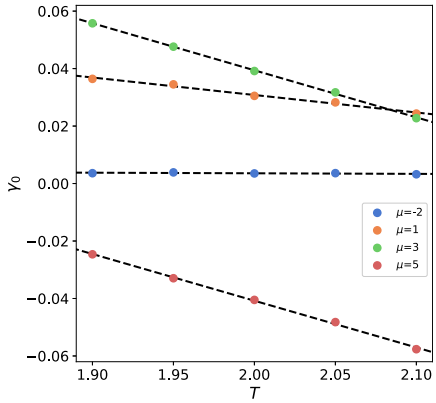

FIG. 6. Surface energy of the LJs fluid in contact with a planar wall with a WCA wall-potential, as a function of temperature. The surface energies at constant chemical potential are computed from the fitted curves in Fig. 5. The dividing surface is located at $d_{\text{wall}} = 1$.

computed using the KB equation. The increased deviation between the two methods observed at higher densities probably comes from the numerical integration of the Gibbs adsorption equation. This can be due to inaccuracies in the parameterized adsorption or the bulk chemical potential predicted from the bulk-EoS.

As shown in Eq. (14), the excess entropy is related to the temperature dependence of the surface energy at constant chemical potential. For most fluids, the relation between the chemical potential and density is temperature dependent. We, therefore, use the bulk-EoS to extract the bulk densities at different temperatures corresponding to a constant chemical potential. The surface energies at these densities are extracted from the surface energy polynomial, since these states are not represented by the discrete data points computed directly from simulations. Figure 6 shows the surface energies as functions of the temperature for a few selected chemical potentials. For the small temperature range considered here, the surface energy can be approximated as a first-order linear function of the temperature. This means that the excess entropy at $T = 2.0$ can be extracted from the negative slope of the dashed lines in Fig. 6. The resulting excess entropy as a function of bulk density is shown in Fig. 7 where the dotted black line is the fitted curve.

2. Curvature dependence of surface properties

We will next investigate the magnitude of the curvature dependence of the adsorption, surface energy, and excess entropy. Figure 8 shows the adsorption in the spherical systems and the parameterized planar-wall adsorption curve for $T = 2.0$. The data points show no observable deviation from the planar-wall curve, which suggests that the curvature dependence of the surface excess properties is very small. This is convenient, since it means that the surface properties of a planar wall can be used to describe properties of fluids confined by highly curved surfaces. The curves fitted to the adsorption of the small systems are also shown in Fig. 8, but the deviation from the planar-wall adsorption is barely visible. Since only the two lowest densities for the spherical system with $\widetilde{R} = 5$ have well-defined bulk regions, we do not parameterize the adsorption for this size.

The first-order curvature correction of the adsorption, Γ_1, can be extracted from the adsorption as a function of $1/R$. Figure 9 shows the adsorption, extracted from the fitted curves, for a few selected densities as a function of the inverse radius. The adsorptions for each system are extracted from the fitted curves since they must be compared at constant density, which is not represented by the discrete data points obtained directly from the simulations. The system with planar walls has an infinitely large radius, which corresponds

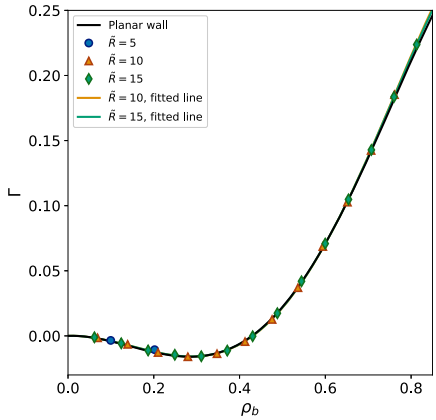

FIG. 8. Adsorption as a function of bulk density for the LJs fluid confined in small spherical systems with a WCA wall-potential. The fitted curves are represented by solid lines. The temperature is $T = 2.0$ and the dividing surface is located at $d_{\text{wall}} = 1$.

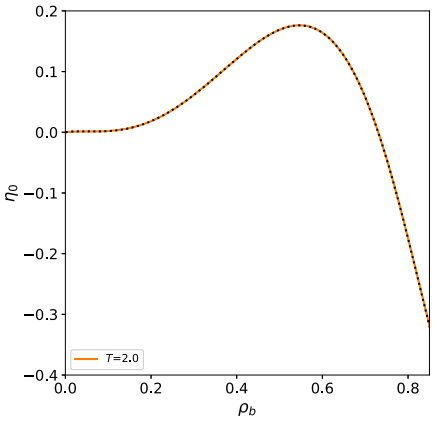

FIG. 7. Excess entropy as a function of bulk density for the LJs fluid in contact with a planar wall with a WCA wall-potential. The fitted curve is represented by a black dotted line. The dividing surface is located at $d_{\text{wall}} = 1$.

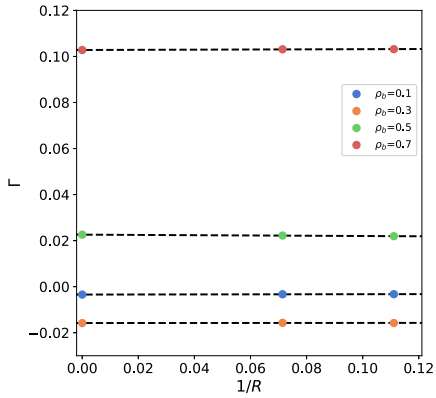

FIG. 9. Adsorption for the LJs fluid in contact with a wall with a WCA wall-potential, as a function of the inverse radius. The adsorption for the differently curved surfaces are extracted from the fitted curves in Fig. 8. The temperature is $T = 2.0$ and the dividing surface is located at $d_{\text{wall}} = 1$.

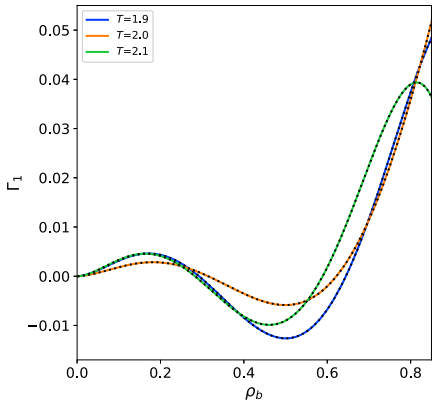

FIG. 10. First-order curvature correction of the adsorption as a function of bulk density for the LJs fluid in contact with a wall with a WCA wall-potential. The fitted curves are represented by black dotted lines. The dividing surface is located at $d_{\text{wall}} = 1$.

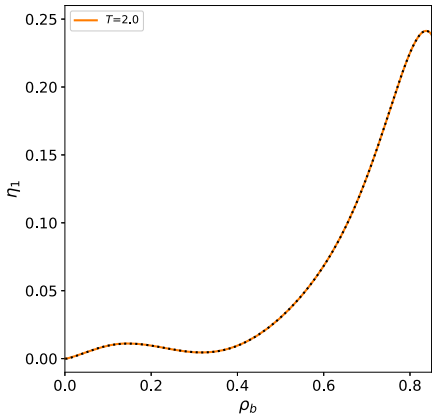

FIG. 12. First-order curvature correction of the excess entropy as a function of bulk density for the LJs fluid in contact with a wall with a WCA wall-potential. The fitted curve is represented by black dotted line. The dividing surface is located at $d_{\text{wall}} = 1$.

to $1/R = 0$. Figure 9 shows that the adsorption can be approximated as a first-order linear function of $1/R$, which means that a first-order correction sufficiently describes the curvature dependence of the adsorption for the spherical systems investigated in this work. The first-order curvature corrections, extracted from the slopes of the dashed lines in Fig. 9, are shown in Fig. 10 as functions of the bulk density.

All surface excess properties can be split into the planar-wall contribution and the curvature corrections. This means that γ_1 can be computed from Eq. (13), i.e., $d\gamma_1 = -\Gamma_1 d\mu$, and η_1 can be computed from Eq. (14), i.e., $\eta_1 = -\partial\gamma_1/\partial T|_\mu$. The first-order curvature corrections of the surface energy and excess entropy are displayed as functions of bulk density in Figs. 11 and 12, respectively. For bulk densities below $\rho_b = 0.4$, the first-order curvature corrections to all the surface excess properties have absolute values <0.01, which indicates that the capillary approximation is excellent in this density range. The curvature corrections of the surface excess properties are parameterized with the same functions as those used for the planar-wall properties. We do not include predictions from the ideal gas in the parametrization of the curvature corrections of the surface excess properties.

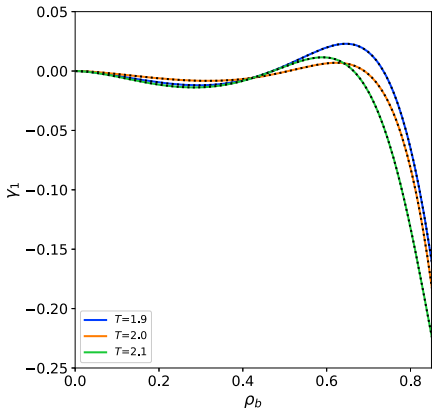

FIG. 11. First-order curvature correction of the surface energy as a function of bulk density for the LJs fluid in contact with a wall with a WCA wall-potential. The fitted curves are represented by black dotted lines. The dividing surface is located at $d_{\text{wall}} = 1$.

V. RESULTS—VALIDATION OF THE NANO-EOS

We will next present the predictions of the Nano-EoS and compare these to the values computed directly from the MD simulations. Emphasis is placed on the internal energy and the pressure. The surface internal energy, U_s, is a combination of all the surface excess properties, which means that it provides insight into the effect of confinement on the state of the fluid. Accurate pressure predictions are key in analyzing the driving forces of transport in porous media.[31–33] The superscript "sim" refers to properties computed directly from simulations.

A. Pressure

The pressure computed from simulations and the predictions of the Nano-EoS are presented in Fig. 13 as functions of the total density. The large degree of overlap between the predictions from the Nano-EoS and the simulation data confirms that the pressure of the confined system can be determined as a function of T and ρ_b. The accuracy of the pressure prediction, therefore, mainly depends on the accuracy of the predicted bulk density. The absolute error

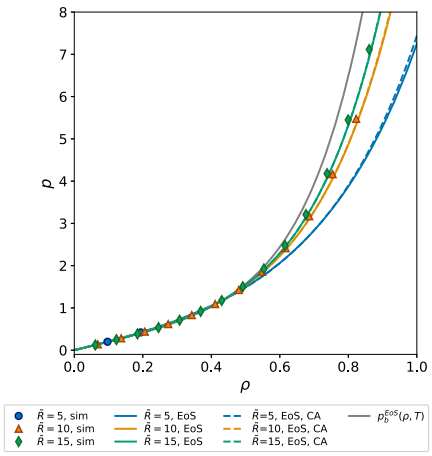

FIG. 13. Pressure as a function of the total density for the LJs fluid confined in a small spherical cavity with a WCA wall-potential. The colored solid lines represent the Nano-EoS predictions including curvature corrections while the dashed lines represent the predictions using the capillary approximation. The gray line shows the pressure for a bulk system with density ρ. The temperature is $T = 2.0$ and the dividing surface is located at $d_{\text{wall}} = 1$.

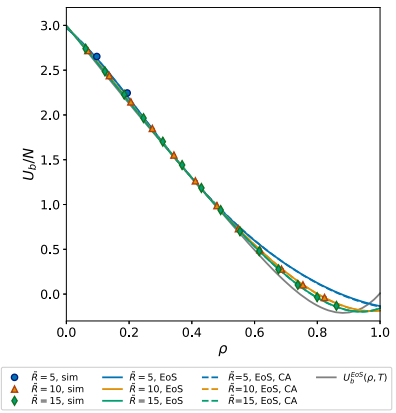

FIG. 14. Bulk internal energy [Eq. (4)] per number of particles as a function of total density for the LJs fluid confined in a small spherical cavity with a WCA wall-potential. The colored solid lines represent the Nano-EoS predictions including curvature corrections while the dashed lines represent the predictions using the capillary approximation. The gray line shows the internal energy per number of particles for a bulk system with density ρ. The temperature is $T = 2.0$ and the dividing surface is located at $d_{\text{wall}} = 1$.

of the bulk density is the difference between predictions from the Nano-EoS and the simulation results, $\Delta\rho_b = |\rho_b^{EoS} - \rho_b^{sim}|$. For all system sizes and the whole range of densities considered in this work, $\Delta\rho_b < 0.001$.

B. Internal energy

The bulk internal energy, U_b^{sim}, is computed by multiplying the value of V with the internal energy density in the bulk region, which can only be computed for systems with well-defined bulk regions. Figure 14 shows the bulk internal energy normalized by the number of particles as a function of the total density. Similar to the pressure, the Nano-EoS predictions of the bulk internal energy mainly depends on the accuracy of the predicted bulk density. The accuracy of the predictions of both the pressure and the bulk internal energy, therefore, indicates that the parameterized adsorption presented in Sec. IV B gives an accurate representation of the adsorption in the small systems. However, the results presented in Figs. 13 and 14 give no validation of whether the curvature correction is valid beyond the range of bulk densities available from simulations.

The surface internal energy, $U_s^{sim} = U^{sim} - U_b^{sim}$, is also only accessible for systems with a well-defined bulk region. Figure 15 shows the surface internal energy per number of particles as a function of the total density. Since the surface internal energy is normalized by the number of particles, the curves approach zero abruptly at very low densities. The large degree of overlap between the Nano-EoS predictions and the simulation results indicates that the Nano-EoS framework correctly represents the small-size contributions of the confined fluid. For the two largest spherical systems at total densities below $\rho = 0.5$, the predictions of U_s^{EoS}/N using the capillary approximation are almost indistinguishable from the predictions including curvature corrections. For $\widetilde{R} = 5$, the prediction using the capillary approximation is closer to the simulation results than the prediction of the Nano-EoS including the curvature

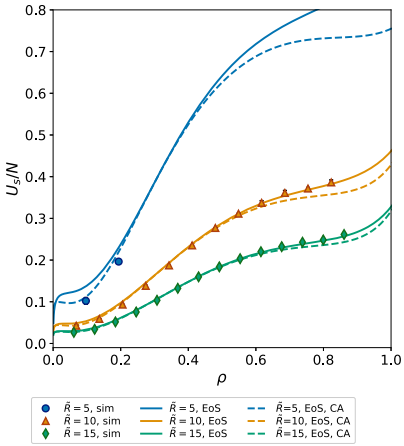

FIG. 15. Surface internal energy [Eq. (5)] per number of particles as a function of the total density for the LJs fluid confined in a small spherical cavity with a WCA wall-potential. The colored solid lines represent the Nano-EoS predictions including curvature corrections while the dashed lines represent the predictions using the capillary approximation. The temperature is $T = 2.0$ and the dividing surface is located at $d_{\text{wall}} = 1$.

corrections. This could be due to an overestimation of the curvature correction of the surface excess properties. One factor that could lead to this overestimation is that ideal gas predictions are not included in the parametrization of the curvature corrections. The fitting procedure is, therefore, more sensitive to the inaccuracies of the curvature corrections computed at low densities. One likely source of these inaccuracies is the excess entropy. Figures 5 and 11 show that the surface energy and its curvature dependence have very small temperature dependencies at low densities. This means that accurate computation of the excess entropy from $\eta = -\partial\gamma/\partial T|_{\mu}$ becomes challenging at low densities. It is also possible that higher-order curvature corrections are needed to accurately describe the surface excess properties for a system this small.

The total internal energy, U^{sim}, is accessible for all system sizes. Figure 16 shows the internal energy per number of particles as a function of the total density. The absolute error of U/N is the difference between the Nano-EoS prediction and the simulation results, $\Delta(U/N) = |(U/N)^{\mathrm{EoS}} - (U/N)^{\mathrm{sim}}|$. For the whole range of densities considered in this work, the absolute error is $\Delta(U/N) < 0.02$ for all system sizes. This shows that the parameterized surface excess properties and their curvature corrections extrapolate well beyond the regime of systems with well-defined bulk regions. The overlap is surprisingly good for $\widetilde{R} = 5$, given that no simulation data from this system are included in the parametrization of the surface excess properties. Similar to the predictions of the surface internal energy, the capillary approximation remains a good approximation for U^{EoS}/N for the two largest systems at total densities below $\rho = 0.5$.

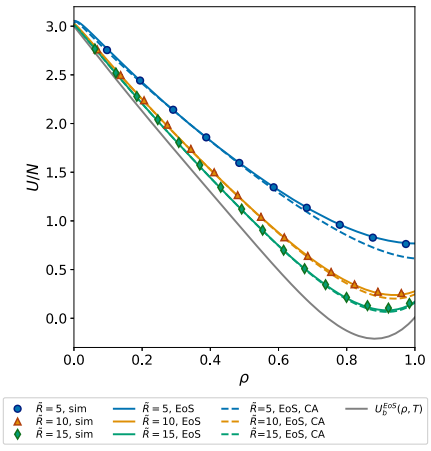

FIG. 16. Internal energy [Eq. (8)] per number of particles as a function of total density for the LJs fluid confined in a small spherical cavity with a WCA wall-potential. The colored solid lines represent the Nano-EoS predictions including curvature corrections while the dashed lines represent the predictions using the capillary approximation. The gray line shows the internal energy per number of particles for a bulk system with density ρ. The temperature is $T = 2.0$ and the dividing surface is located at $d_{\mathrm{wall}} = 1$.

VI. DISCUSSION—USE AND RANGE OF VALIDITY OF THE NANO-EOS

In the following, we discuss how the choice of the dividing surface influences the applicability of the framework (Sec. VI A), the expected range of validity of the Nano-EoS (Sec. VI B), and its application to porous media (Sec. VI C).

A. Impact of choice of the dividing surface

The magnitude of both the planar-wall values and the curvature corrections of the surface excess properties depends on the choice of the dividing surface.[58,59] To get more insight on this, we investigate how the choice of the dividing surface impacts the accuracy of the Nano-EoS. The adsorption computed from one choice of the dividing surface can easily be converted to another, arbitrary choice. We use Eqs. (22)–(26) presented in Sec. II B 2 to compute the surface excess properties for a dividing surface at $d_{\mathrm{wall}} = 0$. This definition of system volume includes a region close to the walls with very low probability of being occupied by particles. This is clearly visible from the density profiles in Fig. 3, which are zero close to the wall for all system shapes and sizes. As a consequence, the adsorption becomes negative for the whole density range when $d_{\mathrm{wall}} = 0$. From Eqs. (22)–(26), it is also clear that the absolute values of the planar wall contribution and the curvature correction of all surface excess properties are larger for $d_{\mathrm{wall}} = 0$ than for $d_{\mathrm{wall}} = 1$. This means that the capillary approximation no longer provides a satisfactory description of the surface excess properties.

The total density is also affected by the choice of dividing surface. Using $d_{\mathrm{wall}} = 1$ is a more convenient choice since it provides a more realistic representation of the actual region that the particles are most likely to occupy. This provides more intuitive results for the adsorption and the total density, e.g., a density that is closer to the actual density in the volume occupied by particles. The bulk density, pressure, and total internal energy predicted by the Nano-EoS, however, are not affected by the location of the dividing surface. Figures showing all surface excess properties, their curvature corrections, the different internal energy contributions, and the pressure for $d_{\mathrm{wall}} = 0$ at $T = 2.0$ are presented in the supplementary material. Many other choices for the dividing surface exist, probably including more optimal choices than $d_{\mathrm{wall}} = 1$, but we do not investigate the choice of the dividing surface further here.

B. Expected accuracy and range of validity

In the Nano-EoS framework, the effect of confinement is included in the confined fluid's internal energy. For ensemble equivalent systems, the energy state functions for various ensembles are accessible from Legendre transformations of the internal energy. When the energy state function of a system is known, the full thermodynamic description of that system is accessible. We, therefore, expect the accuracy of the predictions of the entropy, enthalpy, and energy state functions such as Helmholtz energy or Gibbs energy to be comparable to the accuracy of the internal energy predictions presented in this work. The intensive properties of the confined fluid depend on the bulk density and the temperature. The accuracy of the predictions of intensive properties, such as the chemical potential and compressibility, is, therefore, expected to be comparable to the accuracy of the pressure predictions presented in this work.

In this work, we consider pure fluids, but extension to mixtures is also possible. The framework can also be extended to other geometries by including the appropriate curvature corrections, line contributions, and edge contributions.[39] However, if the interactions between the wall and the particles cannot be approximated by a smooth potential, more complex shape effects, e.g., inaccessible regions or energetically favored hotspots, can arise, which are not so easily captured by size and shape corrections.[13] Such complex shape effects only come into play when the confined system is small enough. This lower size limit depends on both the interparticle interactions and the wall–particle interactions. Other effects that can occur for very small systems are surface–surface interactions, which lead to disjoining pressure effects.[60] We expect that further modifications of the framework and methodology are necessary for the Nano-EoS to extrapolate well to these situations.

An alternative framework for describing the thermodynamics of small systems is the nanothermodynamics developed by Hill.[28] Instead of introducing specific contributions from, e.g., the surface or the curvature, Hill's formalism provides a general framework for the thermodynamics of a system influenced by small size effects. For confined fluids, the thermodynamic functions suggested by Hill, therefore, provide descriptions of the whole system, with the bulk and surface combined. A key part of the derivation of Hill's nanothermodynamics is that each thermodynamic ensemble is considered separately. As a consequence, new ensemble-specific properties that are unique to small systems arise. Hill showed how his framework can be applied to spherical droplets in vapor in a way that does not require a dividing surface. By introducing a dividing surface, Hill claims that his formalism is equivalent to Gibbs' description.[28] A possibility for future work is, therefore, to compare Hill's formalism with the framework presented here. This can provide further insight into the ensemble-specific properties introduced by Hill.

C. Use of the Nano-EoS in porous media

For systems with LJs particles in contact with a spherical surface with a WCA wall-potential at $T = 2.0$, the functions for the surface excess properties provided in the supplementary material can be used directly to predict properties of systems in equilibrium. A possible application of the Nano-EoS is to predict thermodynamic properties in porous media. To explain how the Nano-EoS can be used for this purpose, we use the porous medium depicted in Fig. 17 as an example. This example represents a single-component system with a gradient in thermodynamic properties such as T and ρ in the z-direction but not in the x- and y-directions.

We consider a slab of width Δz_i, which we refer to as a representative elementary volume (REV), denoted with subscript i. Across the REV, the gradients in thermodynamic properties are sufficiently small to invoke the assumption of *local equilibrium*. Local equilibrium in this context means that the thermodynamic properties of the fluid in the slab can be described by the equations elaborated in Sec. II. This includes thermal and chemical equilibrium between the fluid, the solid, and the surface between these two phases within the slab. Discussions of the criteria for defining an REV in a porous medium can be found in Refs. 61 and 62.

We assume that the average number of particles, N_i, and the temperature, T_i, inside the slab are available, which is usually the case for porous media examined by molecular simulations. After defining the dividing surface between the fluid and solid, the volume, V_i, and the area, Ω_i within the slab as well as the average curvature can be computed. With these variables available, combined with the assumption of local equilibrium in the REV, thermodynamic properties such as the local pressure and chemical potential can be computed by using the algorithm described in Fig. 2. This requires as necessary inputs the bulk-EoS and a function for the adsorption. The use of the framework as presented in Sec. II assumes that line and edge contributions to the internal energy can be neglected. The results shown in Sec. V indicate that at least for some types of wall–particle interactions, the capillary approximation works well such that the influence of curvature can be neglected.

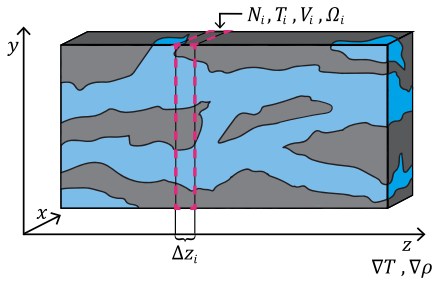

FIG. 17. Illustration of a fluid (blue) in a porous medium (gray). When local equilibrium is assumed in the REV (red dash), the Nano-EoS can be used to compute the state of the fluid for the number of particles, N_i, and temperature T_i, where subscript i refers to control volume i. In the control volume, the volume of the confined fluid is the blue region. The surface region is the interface between the blue and gray region. The exact values of V_i and Ω_i depend on the dividing surface.

VII. CONCLUSIONS

Equations of state (EoSs) provide a compact way to describe the thermodynamic state of a fluid. For bulk systems, the thermodynamic state of a fluid can be predicted from an EoS when the temperature, mass density, and composition are provided. When a fluid is confined in a small enough space, its properties will deviate from the bulk behavior due to the interactions between the fluid particles and the wall. Hence, for fluids under confinement, the impact of the enclosing surface on the fluid properties must be included in the EoS. In this work, we have presented a theoretical framework that describes the thermodynamic state of a confined fluid at equilibrium. The framework applies to a wide variety of interparticle interactions, wall–fluid interactions, and system geometries, and it is independent of the system's ensemble. When the underlying physical description of the fluid is provided, the framework presented represents an EoS for confined fluids. We refer to the proposed EoS for confined fluids as the "Nano-EoS." In the Nano-EoS, the description of the total confined system is split into a bulk phase and an excess surface phase. The properties of the bulk phase are described by a bulk-EoS and the properties of the surface phase are described by Gibbs' framework for excess variables. For equilibrium systems, these two phases have the same temperature and chemical potential.

Intensive properties of the total system such as chemical potential and pressure are, therefore, accessible from the properties of the bulk phase at ρ_b and T.

We have demonstrated the application of the Nano-EoS for a LJs fluid in contact with spherical surfaces with a WCA wall-potential. For this system, the Nano-EoS predicts values for the internal energy and pressure that are in good agreement with the values computed directly from MD simulations. Since the framework is ensemble independent, the energy state functions for any ensemble can be computed from Legendre transformations of the internal energy. Potential applications, therefore, include the prediction of the properties in control volumes at local equilibrium in a larger, nonequilibrium system.

The location of the dividing surface determines the volume of the system, and for curved surfaces, it also determines the surface area. The magnitude of the surface excess properties are, therefore, highly dependent on the choice of the dividing surface. We have investigated two choices for the dividing surface: one located at the origin of the wall potential, i.e., $d_{wall} = 0$, and one located a distance $d_{wall} = 1$ from the origin of the wall potential. We found that a dividing surface located at $d_{wall} = 1$ returns lower absolute values for the surface excess properties and their curvature dependence than $d_{wall} = 0$. Choosing a dividing surface that gives a small curvature dependence is convenient since it means that properties of highly curved surfaces can be accurately described by the properties of a planar surface. In other words, the so-called capillary approximation becomes increasingly valid.

In the low-density limit, the thermodynamic properties of a confined fluid with interacting particles approach those of a confined ideal gas. We have, therefore, derived exact analytical expressions for the surface excess properties of a confined ideal gas. The surface properties of the ideal gas are included in the Nano-EoS in order to ensure consistent extrapolation to the low-density limit. However, for confined fluids at low densities, the ideal gas predictions can also be used as an independent EoS to predict fluid properties.

SUPPLEMENTARY MATERIAL

The supplementary material contains the coefficients for the parameterized curves of the surface excess properties and details about reference states for the thermodynamic properties and about the impact of the choice of the dividing surface, including the derivation of equations presented in Sec. II B 2 and extra figures showing the results for a dividing surface located at $d_{wall} = 0$.

ACKNOWLEDGMENTS

This work was supported by the Research Council of Norway (Grant No. 275754). The authors acknowledge the Center of Excellence funding scheme of the Research Council of Norway (Grant No. 262644), PoreLab. Computational resources are provided by UNINETT Sigma2—The National Infrastructure for High Performance Computing and Data Storage in Norway (Grant No. NN9414k). The authors greatly appreciate discussions with Michael Rauter, Dick Bedeaux, Signe Kjelstrup, and Bjørn Hafskjold.

AUTHOR DECLARATIONS

Conflict of Interest

The authors have no conflicts to disclose.

Author Contributions

Vilde Bråten: Conceptualization (equal); Data curation (equal); Formal analysis (equal); Methodology (equal); Visualization (lead); Writing – original draft (lead); Writing – review & editing (equal). **Daniel Tianhou Zhang:** Conceptualization (equal); Investigation (equal); Methodology (equal); Writing – review & editing (supporting). **Morten Hammer:** Conceptualization (supporting); Methodology (supporting); Supervision (supporting); Writing – review & editing (supporting). **Ailo Aasen:** Conceptualization (equal); Investigation (equal); Methodology (equal); Supervision (equal); Writing – review & editing (equal). **Sondre Kvalvåg Schnell:** Conceptualization (equal); Formal analysis (equal); Methodology (equal); Supervision (equal); Writing – review & editing (equal). **Øivind Wilhelmsen:** Conceptualization (lead); Formal analysis (equal); Investigation (equal); Methodology (equal); Project administration (lead); Supervision (equal); Writing – review & editing (equal).

DATA AVAILABILITY

The LAMMPS simulation input files and text files containing the coefficients for the parameterized curves of the surface excess properties are openly available in Zenodo at https://doi.org/10.5281/zenodo.6478153.

REFERENCES

[1] A. V. Neimark and K. G. Kornev, "Classification of equilibrium configurations of wetting films on planar substrates," Langmuir **16**, 5526–5529 (2000).
[2] A. V. Neimark, P. I. Ravikovitch, and A. Vishnyakov, "Inside the hysteresis loop: Multiplicity of internal states in confined fluids," Phys. Rev. E **65**, 031505 (2002).
[3] T. Horikawa, D. D. Do, and D. Nicholson, "Capillary condensation of adsorbates in porous materials," Adv. Colloid Interface Sci. **169**, 40–58 (2011).
[4] T. Hiratsuka, H. Tanaka, and M. T. Miyahara, "Comprehensive modeling of capillary condensation in open-ended nanopores: Equilibrium, metastability, and spinodal," J. Phys. Chem. C **121**, 26877–26886 (2017).
[5] L. Liu, S.-H. Chen, A. Faraone, C.-W. Yen, and C.-Y. Mou, "Pressure dependence of fragile-to-strong transition and a possible second critical point in supercooled confined water," Phys. Rev. Lett. **95**, 117802 (2005).
[6] J. K. Brennan, T. J. Bandosz, K. T. Thomson, and K. E. Gubbins, "Water in porous carbons," Colloids Surf. **187-188**, 539–568 (2001).
[7] X.-Q. Chu, K.-H. Liu, M. S. Tyagi, C.-Y. Mou, and S.-H. Chen, "Low-temperature dynamics of water confined in a hydrophobic mesoporous material," Phys. Rev. E **82**, 020501 (2010).
[8] Y.-X. Yu, F.-Q. You, Y. Tang, G.-H. Gao, and Y.-G. Li, "Structure and adsorption of a hard-core multi-Yukawa fluid confined in a slitlike pore: Grand canonical Monte Carlo simulation and density functional study," J. Phys. Chem. B **110**, 334–341 (2006).
[9] B. Peng and Y.-X. Yu, "A density functional theory for Lennard-Jones fluids in cylindrical pores and its applications to adsorption of nitrogen on MCM-41 materials," Langmuir **24**, 12431–12439 (2008).
[10] Y.-X. Yu, "A novel weighted density functional theory for adsorption, fluid-solid interfacial tension, and disjoining properties of simple liquid films on planar solid surfaces," J. Chem. Phys. **131**, 024704 (2009).

[11] L.-Y. Wang, F. Gu, H.-J. Wang, and Z.-L. Sun, "Pressure profile for an associating Lennard-Jones fluid confined in a spherical cavity," J. Phys. Chem. B **121**, 2142–2152 (2017).
[12] B. R. Didar and I. Y. Akkutlu, "Pore-size dependence of fluid phase behavior and properties in organic-rich shale reservoirs," in *SPE International Symposium on Oilfield Chemistry* (2013); available at https://onepetro.org/SPEOCC/proceedings-pdf/13OCS/All-13OCS/SPE-164099-MS/1583712/spe-164099-ms.pdf.
[13] H. Cárdenas and E. A. Müller, "How does the shape and surface energy of pores affect the adsorption of nanoconfined fluids?," AIChE J. **67**, e17011 (2021).
[14] V. Bråten, D. Bedeaux, Ø. Wilhelmsen, and S. K. Schnell, "Small size effects in open and closed systems: What can we learn from ideal gases about systems with interacting particles?," J. Chem. Phys. **155**, 244504 (2021).
[15] I. Urrutia, "Three hard spheres in a spherical cavity," J. Chem. Phys. **135**, 024511 (2011).
[16] A. Aasen, M. Hammer, G. Skaugen, J. P. Jakobsen, and Ø. Wilhelmsen, "Thermodynamic models to accurately describe the PVTxy-behavior of water/carbon dioxide mixtures," Fluid Phase Equilib. **442**, 125–139 (2017).
[17] V. Koulocheris, V. Louli, E. Panteli, S. Skouras, and E. Voutsas, "Modelling of elemental mercury solubility in natural gas components," Fuel **233**, 558–564 (2018).
[18] G. J. Zarragoicoechea and V. A. Kuz, "van der Waals equation of state for a fluid in a nanopore," Phys. Rev. E **65**, 021110 (2002).
[19] G. J. Zarragoicoechea and V. A. Kuz, "Critical shift of a confined fluid in a nanopore," Fluid Phase Equilib. **220**, 7–9 (2004).
[20] L. Travalloni, M. Castier, F. W. Tavares, and S. I. Sandler, "Thermodynamic modeling of confined fluids using an extension of the generalized van der Waals theory," Chem. Eng. Sci. **65**, 3088–3099 (2010).
[21] L. Travalloni, M. Castier, F. W. Tavares, and S. I. Sandler, "Critical behavior of pure confined fluids from an extension of the van der Waals equation of state," J. Supercrit. Fluids **55**, 455–461 (2010).
[22] Ø. Wilhelmsen, A. Aasen, G. Skaugen, P. Aursand, A. Austegard, E. Aursand, M. A. Gjennestad, H. Lund, G. Linga, and M. Hammer, "Thermodynamic modeling with equations of state: Present challenges with established methods," Ind. Eng. Chem. Res. **56**, 3503–3515 (2017).
[23] M. Holovko, T. Patsahan, and W. Dong, "Fluids in random porous media: Scaled particle theory," Pure Appl. Chem. **85**, 115–133 (2012).
[24] M. F. Holovko, T. M. Patsahan, and V. I. Shmotolokha, "What is liquid in random porous media: The Barker-Henderson perturbation theory," Condens. Matter Phys. **18**, 13607 (2015).
[25] T. V. Hvozd, Y. V. Kalyuzhnyi, and P. T. Cummings, "Phase equilibria of polydisperse square-well chain fluid confined in random porous media: TPT of Wertheim and scaled particle theory," J. Phys. Chem. B **122**, 5458–5465 (2018).
[26] A. K. Nelson, Y. V. Kalyuzhnyi, T. Patsahan, and C. McCabe, "Liquid-vapor phase equilibrium of a simple liquid confined in a random porous media: Second-order Barker-Henderson perturbation theory and scaled particle theory," J. Mol. Liq. **300**, 112348 (2020).
[27] D. Bedeaux, S. Kjelstrup, and S. K. Schnell, *Nanothermodynamics. General Theory* (PoreLab Publisher, 2020).
[28] T. L. Hill, *Thermodynamics of Small Systems* (Dover Publications, New York, 1994).
[29] E. Bering, S. Kjelstrup, D. Bedeaux, J. M. Rubi, and A. S. de Wijn, "Entropy production beyond the thermodynamic limit from single-molecule stretching simulations," J. Phys. Chem. B **124**, 8909–8917 (2020).
[30] E. Bering, D. Bedeaux, S. Kjelstrup, A. S. de Wijn, I. Latella, and J. M. Rubi, "A Legendre–Fenchel transform for molecular stretching energies," Nanomaterials **10**, 2355 (2020).
[31] O. Galteland, D. Bedeaux, B. Hafskjold, and S. Kjelstrup, "Pressures inside a nano-porous medium. The case of a single phase fluid," Front. Phys. **7**, 60 (2019).
[32] M. T. Rauter, O. Galteland, M. Erdős, O. A. Moultos, T. J. H. Vlugt, S. K. Schnell, D. Bedeaux, and S. Kjelstrup, "Two-phase equilibrium conditions in nanopores," Nanomaterials **10**, 608 (2020).
[33] O. Galteland, D. Bedeaux, and S. Kjelstrup, "Nanothermodynamic description and molecular simulation of a single-phase fluid in a slit pore," Nanomaterials **11**, 165 (2021).
[34] S. K. Schnell, T. J. H. Vlugt, J.-M. Simon, D. Bedeaux, and S. Kjelstrup, "Thermodynamics of small systems embedded in a reservoir: A detailed analysis of finite size effects," Mol. Phys. **110**, 1069–1079 (2012).
[35] B. A. Strøm, J.-M. Simon, S. K. Schnell, S. Kjelstrup, J. He, and D. Bedeaux, "Size and shape effects on the thermodynamic properties of nanoscale volumes of water," Phys. Chem. Chem. Phys. **19**, 9016–9027 (2017).
[36] V. Bråten, Ø. Wilhelmsen, and S. K. Schnell, "Chemical potential differences in the macroscopic limit from fluctuations in small systems," J. Chem. Inf. Model. **61**, 840–855 (2021).
[37] J. W. Gibbs, *The Scientific Papers of J. Willard Gibbs* (Ox Bow Press, London, 1993).
[38] R. C. Tolman, "The effect of droplet size on surface tension," J. Chem. Phys. **17**, 333–337 (1949).
[39] W. Helfrich, "Elastic properties of lipid bilayers: Theory and possible experiments," Z. Naturforsch., C **28**, 693–703 (1973).
[40] A. Aasen, E. M. Blokhuis, and Ø. Wilhelmsen, "Tolman lengths and rigidity constants of multicomponent fluids: Fundamental theory and numerical examples," J. Chem. Phys. **148**, 204702 (2018).
[41] A. Aasen, D. Reguera, and Ø. Wilhelmsen, "Curvature corrections remove the inconsistencies of binary classical nucleation theory," Phys. Rev. Lett. **124**, 045701 (2020).
[42] I. E. Paganini, R. L. Davidchack, B. B. Laird, and I. Urrutia, "Properties of the hard-sphere fluid at a planar wall using virial series and molecular-dynamics simulation," J. Chem. Phys. **149**, 014704 (2018).
[43] J. G. Kirkwood and F. P. Buff, "The statistical mechanical theory of surface tension," J. Chem. Phys. **17**, 338–343 (1949).
[44] T. Ikeshoji, B. Hafskjold, and H. Furuholt, "Molecular-level calculation scheme for pressure in inhomogeneous systems of flat and spherical layers," Mol. Simul. **29**, 101–109 (2003).
[45] Y. Long, M. Śliwińska-Bartkowiak, H. Drozdowski, M. Kempiński, K. A. Phillips, J. C. Palmer, and K. E. Gubbins, "High pressure effect in nanoporous carbon materials: Effects of pore geometry," Colloids Surf., A **437**, 33–41 (2013).
[46] Z. Sun, Y. Kang, and J. Zhang, "Density functional study of pressure profile for hard-sphere fluids confined in a nano-cavity," AIP Adv. **4**, 031308 (2014).
[47] K. Shi, E. E. Santiso, and K. E. Gubbins, "Can we define a unique microscopic pressure in inhomogeneous fluids?," J. Chem. Phys. **154**, 084502 (2021).
[48] J.-P. Hansen and I. R. McDonald, *Theory of Simple Liquids: With Applications to Soft Matter* (Academic Press, 2013).
[49] S. Plimpton, "Fast parallel algorithms for short-range molecular dynamics," J. Comput. Phys. **117**, 1–19 (1995).
[50] B. L. Holian and D. J. Evans, "Shear viscosities away from the melting line: A comparison of equilibrium and nonequilibrium molecular dynamics," J. Chem. Phys. **78**, 5147–5150 (1983).
[51] B. Hafskjold, K. P. Travis, A. B. Hass, M. Hammer, A. Aasen, and Ø. Wilhelmsen, "Thermodynamic properties of the 3D Lennard-Jones/spline model," Mol. Phys. **117**, 3754–3769 (2019).
[52] J. D. Weeks, D. Chandler, and H. C. Andersen, "Role of repulsive forces in determining the equilibrium structure of simple liquids," J. Chem. Phys. **54**, 5237–5247 (1971).
[53] T. van Westen and J. Gross, "Accurate thermodynamics of simple fluids and chain fluids based on first-order perturbation theory and second virial coefficients: UV-theory," J. Chem. Phys. **155**, 244501 (2021).
[54] T. van Westen, M. Hammer, B. Hafskjold, A. Aasen, J. Gross, and Ø. Wilhelmsen, "Perturbation theories for fluids with short-ranged attractive forces: A case study of the Lennard-Jones spline fluid," J. Chem. Phys. **156**, 104504 (2022).
[55] See https://github.com/SINTEF/thermopack, Thermopack (2022).
[56] F. Heidari, T. Keshavarzi, and G. A. Mansoori, "Attractive energy contribution to nanoconfined fluids behavior: The normal pressure tensor," Microfluid. Nanofluid. **10**, 899–906 (2011).
[57] A. Helmi and E. Keshavarzi, "The role of concavo-convex walls of a nanopore on the density profile, adsorption, solvation force, and capillary condensation of confined fluids: A DFT study," Chem. Phys. **433**, 67–75 (2014).
[58] I. Urrutia, "Bending rigidity and higher-order curvature terms for the hard-sphere fluid near a curved wall," Phys. Rev. E **89**, 032122 (2014).

[59]A. Reindl, M. Bier, and S. Dietrich, "Implications of interface conventions for morphometric thermodynamics," Phys. Rev. E **91**, 022406 (2015).
[60]M. A. Gjennestad and Ø. Wilhelmsen, "Thermodynamic stability of volatile droplets and thin films governed by the disjoining pressure in open and closed containers," Langmuir **36**, 7879 (2020).
[61] S. Whitaker, "Flow in porous media I: A theoretical derivation of Darcy's law," Transp. Porous Media **1**, 3–25 (1986).
[62]O. Galteland, M. T. Rauter, M. S. Bratvold, T. T. Trinh, D. Bedeaux, and S. Kjelstrup, "Local thermodynamic description of isothermal single-phase flow in porous media," arXiv:2203.02334 (2022).

Supplementary Material for "Equation of state for confined fluids"

Vilde Bråten,[1] Daniel Tianhou Zhang,[2] Morten Hammer,[3,4] Ailo Aasen,[4] Sondre Kvalvåg Schnell,[1] and Øivind Wilhelmsen[3,4,a)]

[1)]*Department of Materials Science and Engineering, Norwegian University of Science and Technology, NTNU, Trondheim, NO-7491, Norway*

[2)]*Department of Chemistry, Norwegian University of Science and Technology, NTNU, Trondheim, NO-7491, Norway*

[3)]*Porelab, Department of Chemistry, Norwegian University of Science and Technology, NTNU, Trondheim, NO-7491, Norway*

[4)]*PoreLab, SINTEF Energy Research, Gas Technology, Trondheim, NO-7465, Norway*

(Dated: 22 April 2022)

[a)]Electronic mail: oivind.wilhelmsen@ntnu.no

I. COEFFICIENTS FOR THE FITTED CURVES OF THE SURFACE EXCESS PROPERTIES

The text files containing the coefficients for the parametrized curves of the surface excess properties are openly available in Zenodo at https://doi.org/10.5281/zenodo.6478153.

The coefficients for the fitted curves for the planar-wall values and the first order curvature correction of the adsorption are presented in Tabs. I-II, the surface energy are presented in Tabs. III-IV and the excess entropy are presented in Tabs. V-VI.

TABLE I. Adsorption at a planar wall for $d_{\text{wall}} = 1$. $\Gamma_0(\rho_\text{b}) = a + b\rho_\text{b} + c\rho_\text{b}^2 + d\rho_\text{b}^3 + e\rho_\text{b}^4 + f\rho_\text{b}^5$.

Coefficient	$T = 1.90$	$T = 1.95$	$T = 2.00$	$T = 2.05$	$T = 2.10$
a	0.00000	0.00000	0.00000	0.00000	0.00000
b	0.00953	0.01061	0.01167	0.01271	0.01373
c	-0.77594	-0.77913	-0.68662	-0.67603	-0.61297
d	1.58877	1.85142	1.52426	1.67399	1.52440
e	0.65174	0.01663	0.45928	0.03662	0.14695
f	-1.17268	-0.78121	-0.99936	-0.72281	-0.74751

TABLE II. Curvature correction of adsorption for $d_{\text{wall}} = 1$. $\Gamma_1(\rho_\text{b}) = a + b\rho_\text{b} + c\rho_\text{b}^2 + d\rho_\text{b}^3 + e\rho_\text{b}^4 + f\rho_\text{b}^5$.

Coefficient	$T = 1.90$	$T = 1.95$	$T = 2.00$	$T = 2.05$	$T = 2.10$
a	-0.00000	0.00000	0.00000	0.00000	-0.00000
b	0.00234	0.00252	0.00243	0.00264	0.00240
c	0.59258	1.01846	0.30837	0.91722	0.65325
d	-3.57623	-6.20226	-1.76525	-5.72320	-4.19085
e	6.11202	11.13465	2.81099	10.56513	7.76629
f	-3.10120	-6.15928	-1.25426	-5.95611	-4.32248

TABLE III. Surface energy at a planar wall for $d_{\mathrm{wall}} = 1$.

$\gamma_0(\rho_\mathrm{b}) = a + b\rho_\mathrm{b} + c\rho_\mathrm{b}^2 + d\rho_\mathrm{b}^3 + e\rho_\mathrm{b}^4 + f\rho_\mathrm{b}^5 + g\rho_\mathrm{b}^6 + h\rho_\mathrm{b}^7 + i\rho_\mathrm{b}^8 + j\rho_\mathrm{b}^9$.

Coefficient	$T = 1.90$	$T = 1.95$	$T = 2.00$	$T = 2.05$	$T = 2.10$
a	-0.00000	-0.00000	-0.00000	-0.00000	-0.00000
b	-0.01810	-0.02069	-0.02335	-0.02606	-0.02884
c	0.79764	0.82444	0.74374	0.75345	0.69847
d	-2.46990	-2.71141	-2.29608	-2.44545	-2.22945
e	9.01100	10.27818	8.48987	9.26126	8.37120
f	-19.13788	-25.17417	-19.77913	-23.65633	-21.57274
g	7.89549	24.70527	13.67004	24.72495	21.71918
h	37.60841	10.04141	23.73384	5.09139	6.85787
i	-68.82404	-44.94288	-54.89324	-38.29630	-38.26827
j	31.14794	22.83272	26.11509	20.17619	19.92676

TABLE IV. Curvature correction of surface energy for $d_{\mathrm{wall}} = 1$.

$\gamma_1(\rho_\mathrm{b}) = a + b\rho_\mathrm{b} + c\rho_\mathrm{b}^2 + d\rho_\mathrm{b}^3 + e\rho_\mathrm{b}^4 + f\rho_\mathrm{b}^5 + g\rho_\mathrm{b}^6 + h\rho_\mathrm{b}^7 + i\rho_\mathrm{b}^8 + j\rho_\mathrm{b}^9$.

Coefficient	$T = 1.90$	$T = 1.95$	$T = 2.00$	$T = 2.05$	$T = 2.10$
a	-0.00000	-0.00000	-0.00000	-0.00000	-0.00000
b	0.00122	0.00199	-0.00089	0.00062	0.00029
c	-0.74878	-1.22507	-0.43169	-1.14014	-0.85168
d	5.15959	7.89918	2.90677	7.15125	5.45051
e	-24.66515	-36.52158	-13.78938	-32.33381	-24.62024
f	87.37120	131.62091	47.50878	117.36194	89.14947
g	-197.24404	-308.73075	-102.86574	-279.40818	-210.81669
h	270.57019	443.51280	134.33716	407.52302	304.95926
i	-204.38948	-354.61489	-95.59716	-332.06190	-246.42347
j	63.32314	118.73029	26.96516	113.34687	83.05037

TABLE V. Excess entropy at a planar wall for $d_{\mathrm{wall}} = 1$.

$\eta_0(\rho_\mathrm{b}) = a_0\rho_\mathrm{b}\ln(\rho_\mathrm{b}k_\mathrm{B}T/p_0) + a + b\rho_\mathrm{b} + c\rho_\mathrm{b}^2 + d\rho_\mathrm{b}^3 + e\rho_\mathrm{b}^4 + f\rho_\mathrm{b}^5 + g\rho_\mathrm{b}^6 + h\rho_\mathrm{b}^7 + i\rho_\mathrm{b}^8 + j\rho_\mathrm{b}^9$.

Coefficient	$T = 2.00$
$a0$	-0.01167
a	-0.00000
b	0.06227
c	-1.97010
d	18.57721
e	-63.59549
f	157.14109
g	-287.74132
h	334.86606
i	-225.36134
j	67.78789

TABLE VI. Curvature correction of excess entropy for $d_{\mathrm{wall}} = 1$.

$\eta_1(\rho_\mathrm{b}) = a_0\rho_\mathrm{b}\ln(\rho_\mathrm{b}k_\mathrm{B}T/p_0) + a + b\rho_\mathrm{b} + c\rho_\mathrm{b}^2 + d\rho_\mathrm{b}^3 + e\rho_\mathrm{b}^4 + f\rho_\mathrm{b}^5 + g\rho_\mathrm{b}^6 + h\rho_\mathrm{b}^7 + i\rho_\mathrm{b}^8 + j\rho_\mathrm{b}^9$.

Coefficient	$T = 2.00$
$a0$	0.04696
a	0.00000
b	0.21944
c	-0.00220
d	-6.87929
e	23.51825
f	-32.80236
g	58.07848
h	-143.46949
i	181.16751
j	-80.92004

II. REFERENCE STATES FOR THERMODYNAMIC PROPERTIES FROM EQUATIONS OF STATE

In our work we use the following expressions for the ideal gas contribution to the energy, entropy and chemical potential

$$U_{\mathrm{IG}} = N u_0(T), \tag{S.1}$$

$$S_{\mathrm{IG}} = N k_{\mathrm{B}} \ln\left(\frac{V}{N}\frac{p_0}{k_{\mathrm{B}}T}\right) + N s_0(T), \tag{S.2}$$

$$F_{\mathrm{IG}} = -N k_{\mathrm{B}} T \ln\left(\frac{V}{N}\frac{p_0}{k_{\mathrm{B}}T}\right) + N f_0(T), \tag{S.3}$$

$$H_{\mathrm{IG}} = pV + N h_0(T), \tag{S.4}$$

$$\mu_{\mathrm{IG}} = k_{\mathrm{B}} T \ln\left(\frac{N}{V}\frac{k_{\mathrm{B}}T}{p_0}\right) + \mu_0(T) \tag{S.5}$$

where the subscript 0 signifies the reference state of the thermodynamic properties. The expressions for the reference state of the internal energy and the entropy are

$$\begin{aligned} u_0(T) &= u_0^0 + \int_{T_0}^{T} C_V \mathrm{d}T \\ &= u_0^0 - \frac{3}{2}k_{\mathrm{B}}T_0 + \frac{3}{2}k_{\mathrm{B}}T, \end{aligned} \tag{S.6}$$

and

$$\begin{aligned} s_0(T) &= s_0^0 + \int_{T_0}^{T} \frac{C_V}{T}\mathrm{d}T + k_{\mathrm{B}} \ln\frac{T}{T_0} \\ &= s_0^0 + \frac{5}{2}k_{\mathrm{B}} \ln\frac{T}{T_0}. \end{aligned} \tag{S.7}$$

The reference states of the Helmholtz energy, enthalpy and chemical potential are expressed as functions of $u_0(T)$ and $s_0(T)$. The reference state for the Helmholtz energy is

$$\begin{aligned} f_0(T) &= u_0(T) - T s_0(T) \\ &= u_0^0 - \frac{3}{2}k_{\mathrm{B}}T_0 + \frac{3}{2}k_{\mathrm{B}}T - T s_0^0 - \frac{5}{2}k_{\mathrm{B}}T \ln\frac{T}{T_0}, \end{aligned} \tag{S.8}$$

the reference state for the enthalpy is

$$\begin{aligned} h_0(T) &= u_0(T) \\ &= u_0^0 - \frac{3}{2}k_{\mathrm{B}}T_0 + \frac{3}{2}k_{\mathrm{B}}T, \end{aligned} \tag{S.9}$$

and the reference state for the chemical potential is

$$\begin{aligned} \mu_0(T) &= k_{\mathrm{B}}T + u_0(T) - T s_0(T) \\ &= \frac{5}{2}k_{\mathrm{B}}T + u_0^0 - \frac{3}{2}k_{\mathrm{B}}T_0 - T s_0^0 - \frac{5}{2}k_{\mathrm{B}}T \ln\frac{T}{T_0}. \end{aligned} \tag{S.10}$$

The differential of the reference chemical potential with respect to temperature is

$$\frac{\mathrm{d}\mu_0}{\mathrm{d}T} = \frac{5}{2} k_\mathrm{B} \ln \frac{T_0}{T} - s_0^0. \tag{S.11}$$

This differential occurs in the expression for the excess entropy of the confined ideal gas. In this work we use reduced LJ units, where $T_0 = 1[-]$, $p_0 = 1[-]$, $u_0^0 = (3/2) k_\mathrm{B} T_0[-]$ and $s_0^0 = 0[-]$.

III. SHIFTING THE LOCATION OF THE DIVIDING SURFACE

We show how the surface properties of a spherical dividing surface located at $\tilde{R} = R + \sigma$ are related to the surface properties of a dividing surface located at R. We investigate the relations for the *adsorption* by first deriving those of a planar wall, and then deriving the relations for the curvature corrections. The formulas presented here are general for two dividing surfaces separated by a distance σ. In the paper, we apply it to the case where $\sigma = d_{\text{wall}}$ such that $\tilde{R}$ represents the case where $d_{\text{wall}} = 0$.

In the following we use that the bulk number density, ρ_{b}, and the total number of particles $N = \rho_{\text{b}} V + \Gamma \Omega$, are independent of the dividing surface

$$\rho_{\text{b}} \tilde{V} + \tilde{\Gamma} \tilde{\Omega} = \rho_{\text{b}} V + \Gamma \Omega. \tag{S.12}$$

A. Planar wall

For a planar surface located at L we have

$$V = L^3, \quad \tilde{\Omega} = L^2, \quad \Gamma = \Gamma_0. \tag{S.13}$$

For a planar surface located at $\tilde{L} = L + \sigma$ we have

$$\tilde{V} = L^2(L + \sigma), \quad \tilde{\Omega} = L^2, \quad \tilde{\Gamma} = \tilde{\Gamma_0}. \tag{S.14}$$

For a planar wall, the surface area does not depend on the location of the dividing surface, $\Omega = \tilde{\Omega}$, such that Eq. (S.12) becomes

$$\tilde{\Gamma_0} - \Gamma_0 = \frac{1}{\Omega} \rho_{\text{b}} (V - \tilde{V}) = -\rho_{\text{b}} \sigma. \tag{S.15}$$

B. Spherical wall

For a spherical surface located at R we have

$$V = \frac{4}{3} \pi R^3, \quad \Omega = 4\pi R^2, \tag{S.16}$$

and the adsorption is

$$\Gamma = \Gamma_0 + \frac{\Gamma_1}{R}. \tag{S.17}$$

For a spherical surface located at $\tilde{R} = R + \sigma$ we have

$$\tilde{V} = \frac{4}{3}\pi(R+\sigma)^3, \quad \tilde{\Omega} = 4\pi(R+\sigma)^2, \tag{S.18}$$

and the adsorption is

$$\tilde{\Gamma} = \tilde{\Gamma_0} + \frac{\tilde{\Gamma_1}}{R+\sigma}. \tag{S.19}$$

For a spherical system, Eq. (S.12) becomes

$$\rho_\mathrm{b}\frac{4}{3}\pi(R+\sigma)^3 + \tilde{\Gamma}4\pi(R+\sigma)^2 = \rho_\mathrm{b}\frac{4}{3}\pi R^3 + \Gamma 4\pi R^2, \tag{S.20}$$

which can be simplified to

$$\frac{\rho_\mathrm{b}}{3}\left((R+\sigma)^3 - R^3\right) = \Gamma R^2 - \tilde{\Gamma}\,(R+\sigma)^2\,. \tag{S.21}$$

Expanding the adsorption into the planar-wall contribution and the curvature correction according to Eqs. (S.17) and (S.19), and using the relation for the planar-wall contribution in Eq. (S.15) results in the following:

$$-\rho_\mathrm{b}\left(R\sigma + \frac{2}{3}\sigma^2\right) = -\Gamma_0\left(R\sigma + \sigma^2\right) + \Gamma_1 R - \tilde{\Gamma_1}\,(R+\sigma)\,, \tag{S.22}$$

which can be rewritten to

$$\tilde{\Gamma_1} - \Gamma_1 = \rho_\mathrm{b}\sigma^2 - 2\sigma\Gamma_0 + \frac{1}{R}\left(\rho_\mathrm{b}\frac{2}{3}\sigma^3 - \Gamma_0\sigma^2 - \tilde{\Gamma_1}\sigma\right). \tag{S.23}$$

Since terms proportional to R^{-1} do not occur in the first order curvature correction, the relation for the curvature corrections of the adsorption becomes

$$\tilde{\Gamma_1} - \Gamma_1 = \rho_\mathrm{b}\sigma^2 - 2\sigma\Gamma_0. \tag{S.24}$$

C. Surface energy and excess entropy

Equivalent relations for the planar-wall contribution and the curvature correction of the *surface energy* can be derived by using that the bulk pressure, p_b, and the total grand free energy, $U - TS - \mu N = -pV + \gamma\Omega$, are independent of the dividing surface. For a planar wall, the relation for the surface energy is

$$\tilde{\gamma_0} - \gamma_0 = p_\mathrm{b}\sigma, \tag{S.25}$$

while the relation for the curvature correction is

$$\tilde{\gamma}_1 - \gamma_1 = -p_\mathrm{b}\sigma^2 - 2\sigma\gamma_0. \tag{S.26}$$

Equivalent relations for the planar-wall contribution and the curvature correction of the *excess entropy* can be derived by using that the bulk entropy density, s_b, and the total entropy, $S = s_\mathrm{b}V + \eta\Omega$, are independent of the dividing surface. The relation for the excess entropy of a planar wall is

$$\tilde{\eta}_0 - \eta_0 = -s_\mathrm{b}\sigma, \tag{S.27}$$

where s_b is the bulk entropy density. The relation for the curvature correction is

$$\tilde{\eta}_1 - \eta_1 = s_\mathrm{b}\sigma^2 - 2\sigma\eta_0. \tag{S.28}$$

D. Ideal gas

For a confined ideal gas, the adsorption for a dividing surface corresponding to $\widetilde{\Omega}$ and $\widetilde{V}$ is $\widetilde{\Gamma_\mathrm{IG}} = \widetilde{\alpha}\rho_\mathrm{b}$, where

$$\widetilde{\alpha} = \frac{1}{\widetilde{\Omega}} \int \left[\exp\left(-\frac{W(\xi)}{k_\mathrm{B}T} \right) - 1 \right] \mathrm{d}\widetilde{V}. \tag{S.29}$$

The slope α can be computed for other choices of dividing surface through Eq. (S.12). For a planar wall, the relation is

$$\widetilde{\alpha_0} - \alpha_0 = -\sigma, \tag{S.30}$$

and for a spherical wall, the relation is

$$\alpha = \widetilde{\alpha} + \sigma + \frac{1}{R}\left(\sigma^2 + 2\sigma\widetilde{\alpha}\right) + \frac{1}{R^2}\left(\frac{\sigma^3}{3} + \sigma\widetilde{\alpha}\right) \tag{S.31}$$

We do not approximate α for a spherical surface as the planar wall contribution plus curvature corrections.

IV. EXTRA FIGURES

A. Surface excess properties of a planar wall at $d_{\mathbf{wall}} = 0$

Figures S1-S3 show the planar-wall contributions to the adsorption, surface energy and excess entropy computed for a dividing surface located at $d_{\mathrm{wall}} = 0$. In Figs. S1-S3, the square markers and the full lines are computed directly from the simulation data, while the dashed lines are computed by utilizing the surface excess properties of a dividing surface located at $d_{\mathrm{wall}} = 1$ combined with Eqs. (S.15), (S.25) and (S.27). The deviations between the properties computed by these two approaches arise from uncertainties occurring in the different terms in Eqs. (S.15), (S.25) and (S.27), such as the prediction of ρ_{b}, p_{b} and s_{b}, as well as the surface excess properties extracted from the curve fitting.

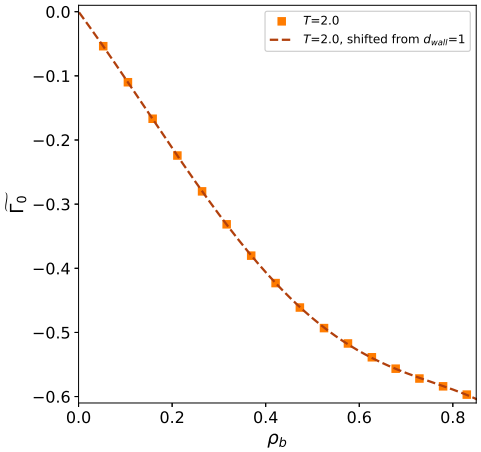

FIG. S1. Adsorption as a function of bulk density for the LJs fluid in contact with a planar wall with a WCA wall-potential. The dividing surface is located at $d_{\mathrm{wall}} = 0$. The dashed line is computed from Eq. (S.15).

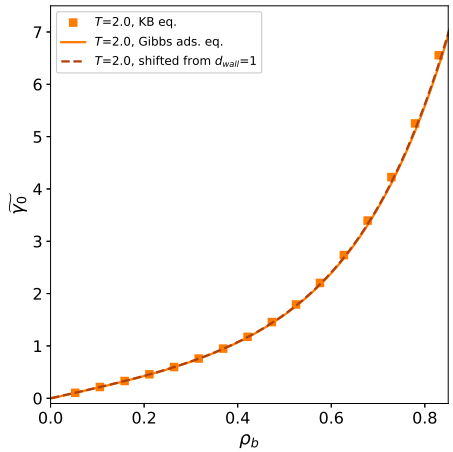

FIG. S2. Surface energy as a function of bulk density for the LJs fluid in contact with a planar wall with a WCA wall-potential. The dividing surface is located at $d_{\text{wall}} = 0$. The dashed line is computed from Eq. (S.25).

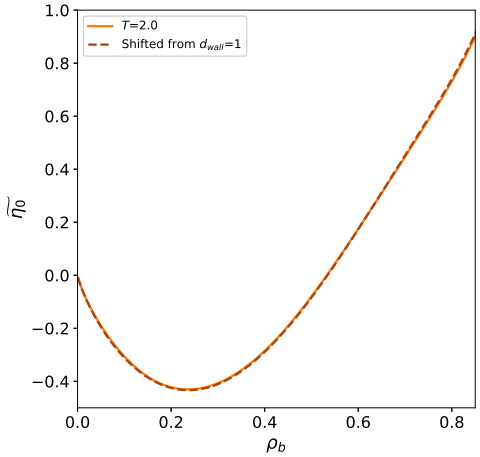

FIG. S3. Excess entropy as a function of bulk density for the LJs fluid in contact with a planar wall with a WCA wall-potential. The dividing surface is located at $d_{\text{wall}} = 0$. The dashed line is computed from Eq. (S.27).

B. Curvature corrections of the surface excess properties of a surface at $d_{\mathbf{wall}} = 0$

In Figs. S4-S6, the curvature correction of the adsorption, surface energy and excess entropy computed for a dividing surface located at $d_{\text{wall}} = 0$ are displayed. In Figs. S4-S6, the full lines are computed directly from the simulation data, while the dashed lines are computed by utilizing the curvature corrections of the surface excess properties of a dividing surface located at $d_{\text{wall}} = 1$ combined with Eqs. (S.24), (S.26) and (S.28).

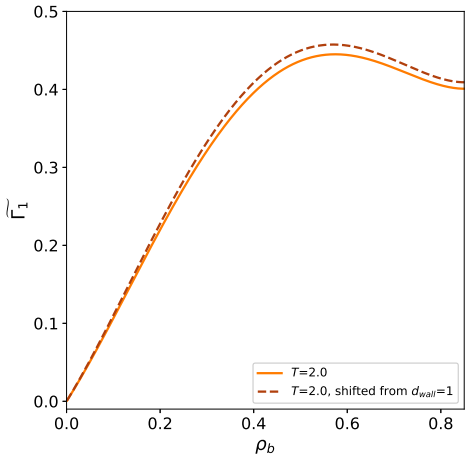

FIG. S4. Curvature correction for the adsorption of the LJs fluid in contact with a wall with a WCA wall-potential, as a function of bulk density. The dividing surface is located at $d_{\text{wall}} = 0$. The dashed line is computed from Eq. (S.24).

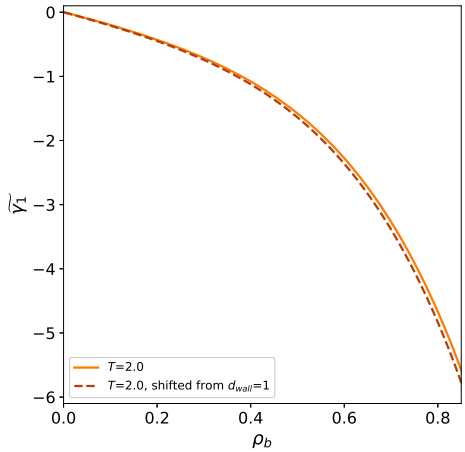

FIG. S5. Curvature correction for the surface energy of the LJs fluid in contact with a wall with a WCA wall-potential, as a function of bulk density. The dividing surface is located at $d_{\text{wall}} = 0$. The dashed line is computed from Eq. (S.26).

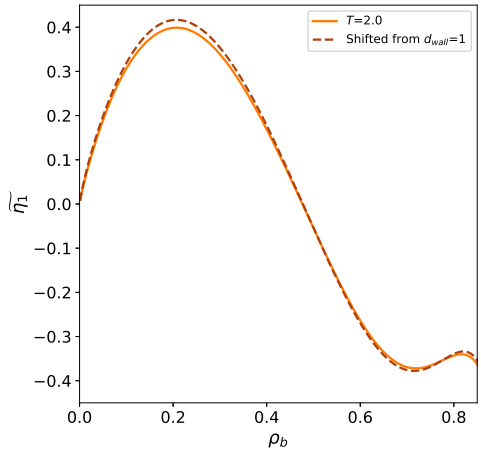

FIG. S6. Curvature correction for the excess entropy of the LJs fluid in contact with a wall with a WCA wall-potential, as a function of bulk density. The dividing surface is located at $d_{\text{wall}} = 0$. The dashed line is computed from Eq. (S.28).

C. Nano-EoS predictions for $d_{\text{wall}} = 0$

Figures S7-S11 shows the adsorption, pressure, bulk internal energy, surface internal energy and total internal energy. The markers represent properties computed directly from simulations, while the lines shows the Nano-EoS predictions. In the Nano-EoS predictions, the surface excess properties of a dividing surface located at $d_{\text{wall}} = 0$ are computed from the surface excess properties of a dividing surface located at $d_{\text{wall}} = 1$ combined with Eqs. (S.15), (S.25), (S.27), (S.24), (S.26) and (S.28).

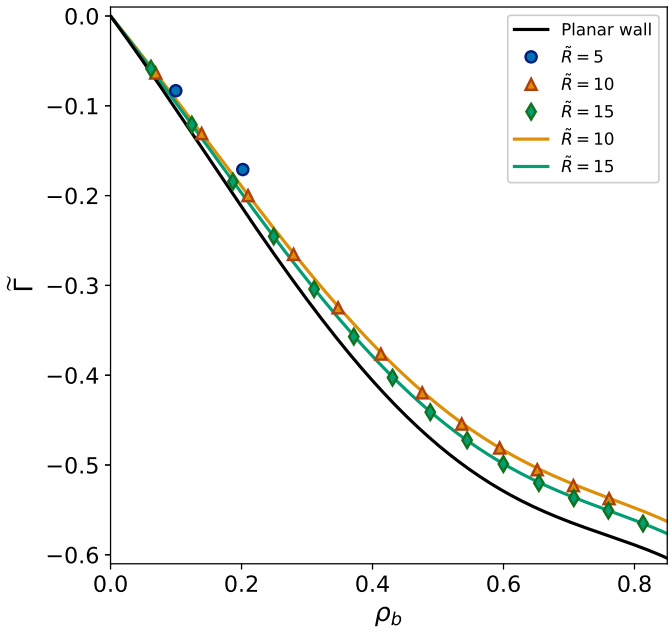

FIG. S7. Adsorption as a function of bulk density for the LJs fluid confined in small spherical systems with a WCA wall-potential. The temperature is $T = 2.0$ and the dividing surface is located at $d_{\text{wall}} = 0$.

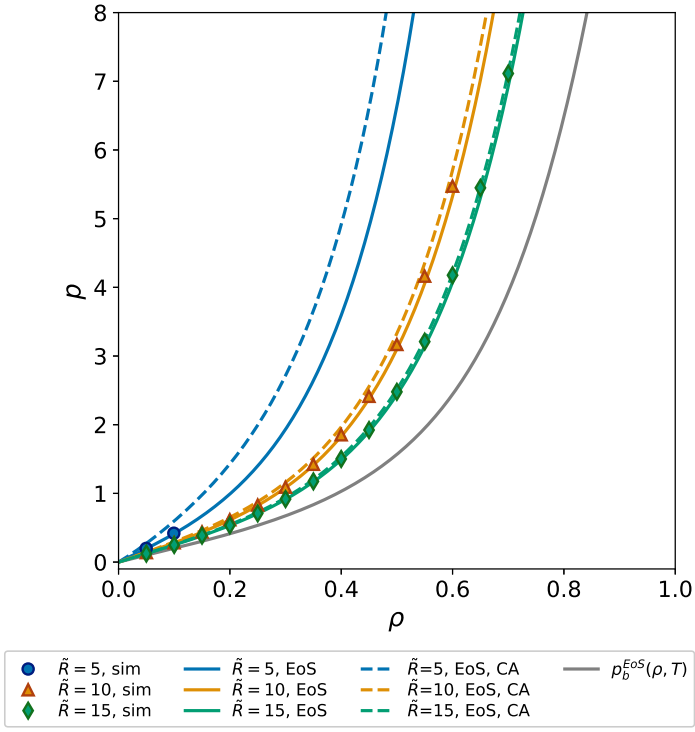

FIG. S8. Pressure as a function of the total density for the LJs fluid confined in a small spherical cavity with a WCA wall-potential. The full lines represent the Nano-EoS predictions including curvature corrections while the dashed lines represent the predictions of the capillary approximation. The gray full line shows the pressure for a bulk system with density ρ. The temperature is $T = 2.0$ and the dividing surface is located at $d_{\text{wall}} = 0$.

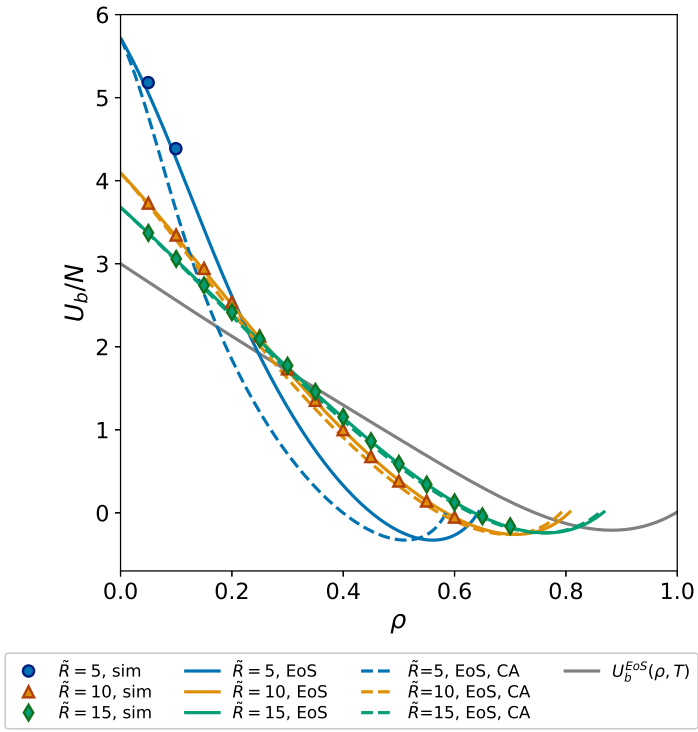

FIG. S9. Bulk internal energy per number of particles as a function of total density for the LJs fluid confined in a small spherical cavity with a WCA wall-potential. The colored full lines represent the Nano-EoS predictions including curvature corrections while the dashed lines represent the predictions of the capillary approximation. The gray full line shows the internal energy per number of particles for a bulk system with density ρ. The temperature is $T = 2.0$ and the dividing surface is located at $d_{\text{wall}} = 0$.

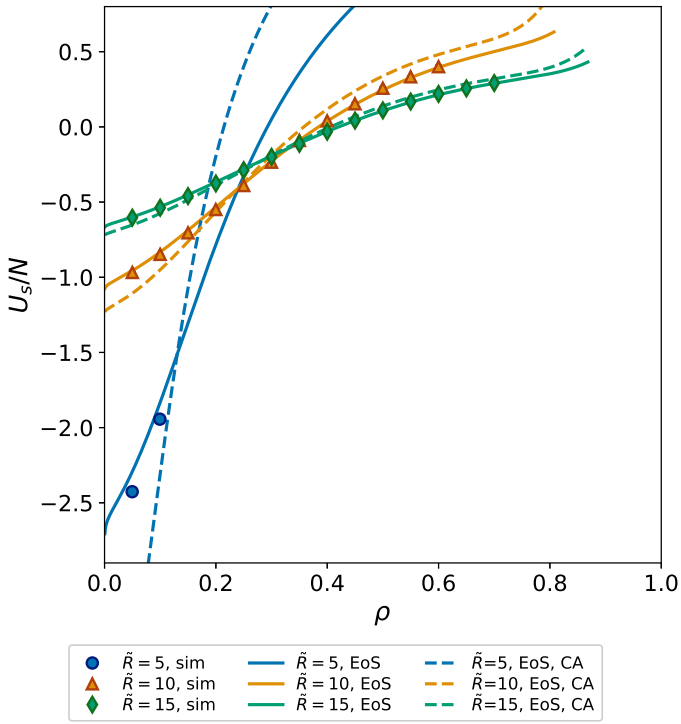

FIG. S10. Surface excess internal energy per number of particles as a function of total density for the LJs fluid confined in a small spherical cavity with a WCA wall-potential. The colored full lines represent the Nano-EoS predictions including curvature corrections while the dashed lines represent the predictions of the capillary approximation. The temperature is $T = 2.0$ and the dividing surface is located at $d_{\text{wall}} = 0$.

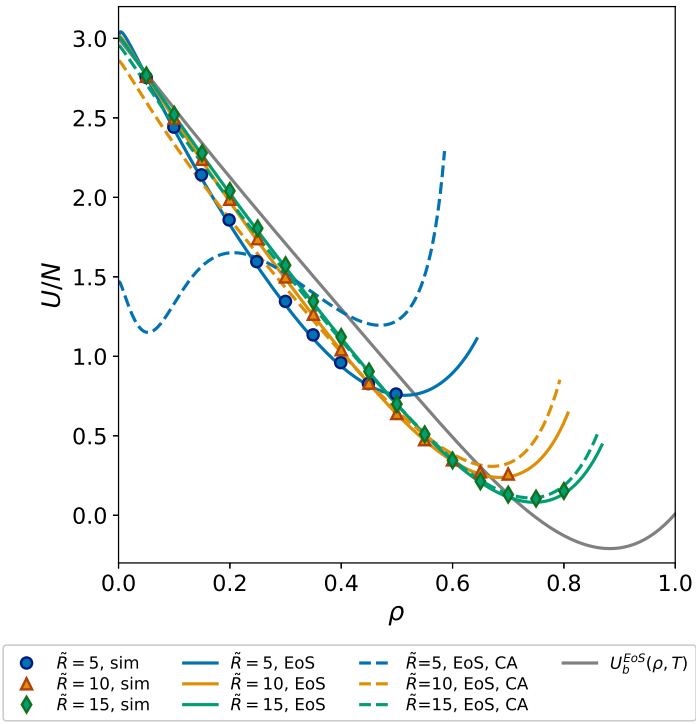

FIG. S11. Internal energy per number of particles as a function of total density for the LJs fluid confined in a small spherical cavity with a WCA wall-potential. The full lines represent the Nano-EoS predictions including curvature corrections while the dashed lines represent the predictions of the capillary approximation. The gray full line shows the internal energy per number of particles for a bulk system with density ρ. The temperature is $T = 2.0$ and the dividing surface is located at $d_{\text{wall}} = 0$.

ISBN 978-82-326-5357-7 (printed ver.)
ISBN 978-82-326-6749-9 (electronic ver.)
ISSN 1503-8181 (printed ver.)
ISSN 2703-8084 (online ver.)

NTNU

Norwegian University of
Science and Technology